Alternative DNA Repair During Meiosis in the Budding Yeast *S. cerevisiae*

By: Ryan Reeves

Supervisor: Dr Stephen Gray

Thesis submitted to the University of Nottingham for the degree of Doctor of Philosophy.

Date submitted October 2024

Abstract

In order for meiosis to occur, DNA double-strand breaks (DSBs) must be induced and subsequently repaired in a homology-directed manner; this process is called meiotic recombination. As unrepaired DSBs can have catastrophic consequences for cells, meiotic recombination must be tightly regulated. Despite being studied for decades, new evidence suggests that novel repair pathways and mechanisms are at play during meiosis. By using the budding yeast *S. cerevisiae*, two alternative DSB repair mechanisms were investigated to readdress our understanding of meiotic DSB processing. The first involves an uncharacterised way of removing the DSB-inducing enzyme Spo11 from DNA. The second seeks to understand which DSB repair pathway is leading to gross chromosomal rearrangements during meiosis.

Meiotic DSBs are initiated by Spo11, which cuts DNA but remains covalently attached. The Spo11 'roadblock' must be removed from the DNA for meiosis to progress. This action is undertaken nucleolytically by the MRX complex, which cleaves the DNA which the Spo11 is bound to (Neale et al., 2005). Whilst this method of Spo11 release via MRX-induced cleavage has long been demonstrated, an alternative mechanism has been overlooked. A recent study showed that when the MRX complex is compromised, recombinant DNA products can be produced (Yun and Kim, 2019), indicating that the Spo11 has somehow been removed independently of the MRX complex. We hypothesised that Spo11 is being removed from DNA by the phosphodiesterase Tdp1, which is upregulated in meiotic prophase (Kugou et al., 2007) and has been shown to remove similar protein adducts from DNA (Nitiss et al., 2006). By investigating this mechanism through fluorescent reporter strains, western blotting, PFGEs and Southern blotting, it was determined that Tdp1 isn't responsible for the alternative Spo11 removal mechanism.

The second part of this project seeks to define a homology-directed annealing pathway which is utilised to repair meiotic DSBs. This pathway is repairing DNA at non-allelic loci, a process referred to as ectopic recombination, which can generate gross chromosomal

rearrangements (Grushcow et al., 1999). Ectopic recombination occurs around 1 % of the time during meiosis in wildtype *S. cerevisiae* and is upregulated in strains lacking the checkpoint protein Rad24 (Grushcow et al., 1999, Shinohara and Shinohara, 2013). It was recently shown that whilst short regions of homology are utilised, this pathway is independent of the RecA recombinase homologs Rad51 and Dmc1 (Allison et al., 2023), indicating a pathway which doesn't utilise strand-invasion. The single strand annealing pathway (SSA) utilises Rad52-Rad59 to anneal ssDNA together with 60-200 bp of homology, with the nuclease complex Rad1-Rad10 required to trim non-homologous trails (Sugawara et al., 2000, Fishman-Lobell et al., 1992). This study shows that the SSA proteins Rad1, Rad10, Rad52, and Rad59 are all present during meiosis in wildtype and *rad24Δ* backgrounds, and that Rad59 is more abundant in a *rad24Δ* background when compared to wildtype.

Abbreviations

A	Alanine/Adenine (context dependent)
Amp	Ampicillin
APS	Ammonium Persulfate
ATP	Adenosine Triphosphate
BER	Base Excision Repair
BIR	Break Induced Replication
bp	Base Pairs
C	Cytosine/Cysteine (context dependent)
CO	Crossover
D	Aspartic Acid
DDC	DNA Damage Checkpoint
ddH_2O	Distilled Water
D-loop	Displacement Loop
dHJ	Double Holliday Junction
DNA	Deoxyribonucleic Acid
dsDNA	Double-stranded DNA
E	Glutamic Acid
EDTA	Ethyleneiaminetetraacetic acid
G	Glycine/Guanine (context dependent)
G418	Genetecin
HJ	Holliday Junction
HR	Homologous Recombination
hrs	Hours
Hyg	Hygromycin
KAc	Potassium Acetate
Kan	Kanamycin
kDa	Kilo Dalton
LB	Lysogeny Broth
MMEJ	Microhomology Mediated End Joining
MMR	Mismatch Repair
NCO	Non-Crossover

NER	Nucleotide Excision Repair
NHEJ	Non-Homologous End Joining
nt	Nucleotides
OD_{600}	Optical Density 600nm
P	Proline
PCR	Polymerase Chain Reaction
Q	Glutamine
RNA	Ribonucleic Acid
s	Seconds
S	Serine
SDM	Site Directed Mutagenesis
SDS-PAGE	Sodium Dodecyl Sulfate Polyacrylamide Gel Electrophoresis
SDW	Sterile Distilled Water
SSA	Single Strand Annealing Pathway
ssDNA	Single-stranded DNA
T	Threonine/Thymine (context dependent)
TAE	Tris-Acetate-EDTA
TBE	Tris-Borate-EDTA
TCE	2,2,2-Trichloroethanol
TEMED	Tris(hydroxymethyl) aminomethane
TOPcc	Topoisomerase cleavage complex
U	Uracil
UV	Ultraviolet light
v / v	Volume / volume
V	Volts
wt	Wildtype
w / v	Weight / volume
x g	Centrifugal force (x gravity)
Y	Tyrosine
YPA	Yeast, Peptone, potassium Acetate broth
YPD	Yeast, Peptone, Dextrose broth

Contents

Chapter 1: Introduction

1.1 DNA Repair

1.1.1 DNA Structure and Function

Deoxyribonucleic acid (DNA) is a polymer found in all living organisms. It is made up of monomers called nucleotides. These nucleotides are made up of a sugar-phosphate group attached to one of four different nucleobases (bases): Adenine (A), Thymine (T), Cytosine (C), and Guanine (G). The sugar-phosphate groups can be covalently linked together to form strands, with the 3′-hydroxyl group of one nucleotide being ligated to the 5′-phosphate group of another nucleotide. The covalently linked sugar-phosphate groups are referred to as the 'sugar phosphate backbone', with the un-bound 3′ and 5′ ends conferring the directionality/polarity of the strand. DNA is made up of two polynucleotide chains, called a 'duplex', which is held together by hydrogen bonds between the nucleobases; with A-T pairing with 2 hydrogen bonds, and C-G pairing with 3 hydrogen bonds, whilst the sugar-phosphate backbone also forms hydrogen-bonds with water molecules. These strands of DNA wind around one another to form a double helix, with a major and a minor groove (Watson and Crick, 1953, Olby, 1974, Alberts et al., 2002). The general structure of DNA is shown in **Figure 1-1**.

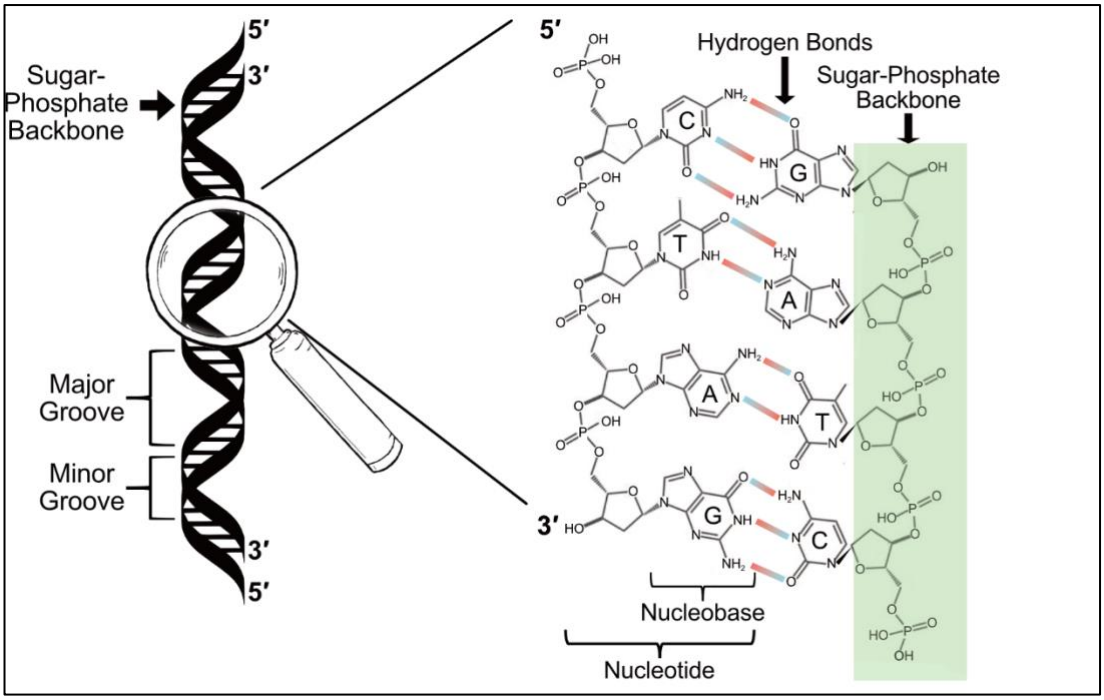

Figure 1-1 The Structure of DNA. Two strands of DNA form a helix with a major and minor groove. The individual nucleotides are joined together to form a sugar phosphate backbone. Hydrogen bonding is possible between the different bases, with C and G forming 3 bonds, A and T forming 2. Negative region of the hydrogen bonds are shown in blue, positive regions shown in red.

In Eukaryotic organisms, such as the budding yeast *Saccharomyces cerevisiae*, the DNA is packaged around special proteins called histones. Histones are octameric proteins, made up of two H2A-H2B dimers, with two H3 and two H4 monomers, to form a core. 145-147 base pairs (bp) of DNA are wrapped around each of these histones to form a 'nucleosome' particle, which can be linked together by H1 histones so the DNA is packed densely as a chromosome (Williamson and Pinto, 2012). In *S. cerevisiae*, there are over 12 megabases of DNA, which are divided across 16 chromosomes and a 2 micron plasmid which fit inside the nucleus of the cell (Goffeau et al., 1996, Rizvi et al., 2018). Chromosomes have a specific structure which has telomeres at each end and a centromere within the chromosome structure. The telomeres are non-coding G-C-rich repetitive sequences which cap the chromosomes (Auriche et al., 2008). In *S. cerevisiae* telomeres are around 350 bp long and have an irregular sequence of $T(G_{1-3})$ (Kupiec, 2014). The

centromeres contain a special H3 Histone called Cse4 which allows kinetochore microtubules to bind for cell division as well as linking sister chromatids together when in a diploid state (Bloom and Costanzo, 2017)

The genetic information within the sequence of DNA acts as a blueprint for the synthesis of proteins. The ‘central dogma’ of molecular biology is that DNA is transcribed to messenger RNA (mRNA), which is then translated into proteins with the aid of transfer RNA (tRNA) (Crick, 1958). The DNA sequence which codes for a protein is known as a gene, which has a ‘reading frame’ made up of triple-base-sequences known as codons. These codons code for individual amino acids as well as start/stop sequences, which are used to make full proteins (Fitch, 1964).

1.1.2 DNA Damage and Repair Pathways

DNA is prone to damage from exogenous sources such as UV light, pH variations, oxidative stress from reactive oxygen species, alkylating agents; as well as endogenous sources such as stalled replication forks and trapped topoisomerases. In order for the genetic integrity to be maintained and passed on to progeny, the damage is repaired by specific DNA repair pathways. During mitotic growth and vegetative states, there are several pathways which can be relied upon to repair DNA. An overview of the different types of damage and pathways on-hand to repair them is shown in **Figure 1-2**.

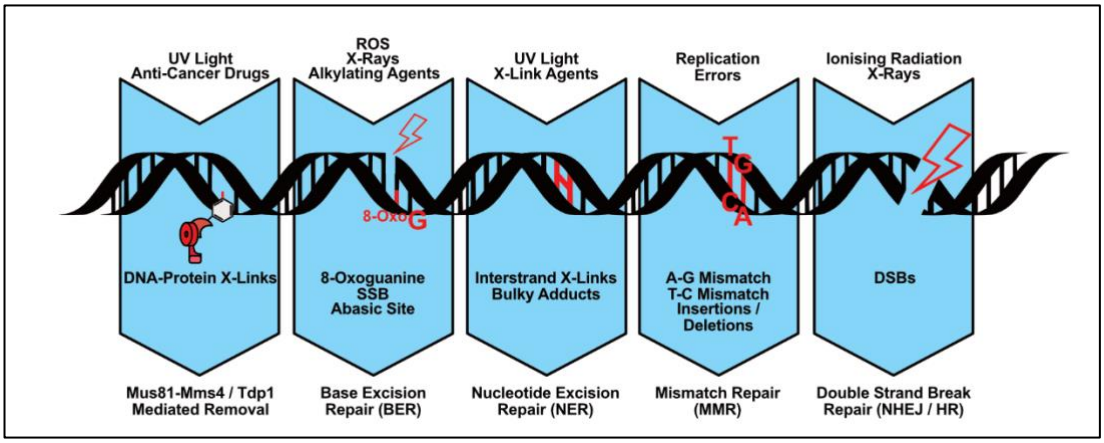

Figure 1-2 DNA repair pathways active during mitotically growing *S. cerevisiae.* Sources of DNA are shown at the top, with a visual representation of how these DNA damages look on a dsDNA helix, with which pathway could be used to repair said damage shown underneath.

Base excision repair (BER) is used to repair oxidised bases such as 8-oxoguanine, as well as abasic sites like 7-methylguanosine, and single strand breaks (SSBs). Here the base is 'flipped out' by a glycosylase, cut from the backbone by an endonuclease, with the gap filled by a polymerase and the backbone re-sealed by a ligase (Krokan and Bjoras, 2013).

Nucleotide excision repair (NER) is used to repair lesions which can disrupt the helical structure of DNA, such as thymidine dimers induced by UV and interstrand-crosslinks (ICLs) brought-on by nitrogen mustard. NER centres around the recruitment of the transcription factor II (TFIIH) complex, which unwinds the DNA with helicase action so that

endonucleases can cut out the damaged DNA fragment. Once again, a polymerase fills in the DNA sequence-gap and a ligase repairs the sugar-phosphate backbone (Kuper and Kisker, 2023).

Mismatch Repair (MMR) is responsible for replacing incorrectly-paired bases which can be generated by oxidative stress. MMR is reliant on the MutSα and MutLα complexes, which are heterodimers made up of Msh2-Msh6 and Mlh1-Pms1 respectively. The MutSα complex recognises the mismatch and then recruits the nucleolytic MutLα complex to nick the DNA to the 5′ of the mismatch. Then exonucleases like Exo1 are recruited to degrade one strand partially, which is then resynthesised by a polymerase and sealed by a ligase (Chalissery et al., 2017).

Proteins can become bound to DNA to form DNA-protein crosslinks (DPCs). These can occur when endogenous sources such as UV light bind a protein to DNA, but they can also happen exogenously when an enzyme gets stuck in an intermediate form on the DNA, remaining covalently bound. An example of this is when topoisomerases cleave DNA, but then remain bound as a ‘cleavage complex’. These can act as roadblocks for replication or transcription machinery, so they need to be removed, which can be brought on by nucleases such as Mus81-Mms4, or by phosphodiesterases such as Tdp1, which can remove the topoisomerase from the DNA without nuclease activity (Section **1.4.1**) (Marini et al., 2023).

Sometimes, DNA can be broken on both strands simultaneously, this is called a double strand break (DSB). A single unrepaired DSB is enough to induce apoptosis in *S. cerevisiae* (Rich et al., 2000). As such, there are several pathways which can be employed to repair DSBs, which are discussed in detail later (section **1.2**)

1.1.3 Post-Translational Modifications

The function of particular proteins can fluctuate depending on whether they are needed to be active, inactive, signalling, or degraded. Regulation of a protein's function can be achieved with the covalent attachment of a specific molecule; this is called post-translational modification (PTM). PTMs are reversible additions which can cause conformational changes in a protein's structure, thereby altering its function. The most common PTM in *S. cerevisiae* is phosphorylation, with phosphosites being located on 59 % of the whole yeast proteome (Leutert et al., 2023). Phosphorylation can occur on serine, threonine, and tyrosine residues, with the phosphate donated from ATP molecules. These phosphorylation events are regulated by 159 known kinases and phosphatases which add phosphates and subsequently remove the PTM respectively (Bodenmiller et al., 2008, Bodenmiller et al., 2010, Leutert et al., 2023). This phosphorylation allows for proteins to respond dynamically to stress, with 18 % of the yeast proteome acquiring a phosphorylation PTM within 5 minutes of a stress exposure such as heat, alcohol, oxidising agents, and pH (Leutert et al., 2023).

Another essential PTM is Ubiquitylation, which is the addition of the 8.5 kDa protein Ubiquitin onto lysine, serine, threonine, or cysteine residues (Goldstein et al., 1975). Ubiquitin is bound to proteins three enzymes working sequentially: ubiquitin-activating E1 enzymes, ubiquitin-conjugating E2 enzymes, and finally E3 ubiquitin ligase enzymes. Ubiquitin can be added as a monomer or linked as poly-ubiquitin chains via one-of-seven ubiquitin-ubiquitin conjugating lysine residues and the G-76 residue of another ubiquitin molecule (Finley et al., 2012). The mono/polyubiquitin chain formed determines the function of the PTM. For example: K-48 linked ubiquitin chains target proteins for degradation by the 26S proteasome (Pickart, 1997); monomeric K-63 ubiquitin is associated with protein trafficking (Lauwers et al., 2009); whereas poly-K63-ubiquitin can directly bind to DNA to facilitate repair in higher Eukaryotes (Liu et al., 2018). As well as ubiquitin, *S. cerevisiae* proteins can be modified with the addition of Smt3 (SUMO, Small ubiquitin-like modifier), Atg8, Atg12, Hub1, Rub1 (NEDDylation), and Urm1 (Sengupta and Pick, 2023).

PTMs are vital for the regulation of chromatin structure via histone modifications. There are many types of histone modifications, including methylation, acetylation, phosphorylation, and acylation. PTMs are usually added to the N-terminal tails of histones on lysine, serine, threonine, and arginine residues (Imhof and Becker, 2001). PTMs can alter nucleosome structure to allow for chromatin condensation, DNA repair/replication, and transcription; this sequence-independent regulation of DNA is called epigenetics (Chou et al., 2023). For example, histone H3 can be trimethylated (H3K4me3) to ‘open up’ promoter regions for transcription, whilst demethylation (H3K4me2) can repress nucleosome remodelling (Kim and Buratowski, 2009). Another example is the phosphorylation of H2A by Mec1 and Tel1 to form γ-H2A which helps to recruit DNA repair proteins in response to DSBs (Lee and Russell, 2013).

1.2 DSB Repair in *S. cerevisiae*

The budding yeast *S. cerevisiae* is a useful model organism as it has many conserved proteins and pathways compared to more complex Eukaryotes, yet is less biologically complex. For example, studies on yeast glucose repression led to the discoveries of the Warburg and Crabtree effects in human cancers (Diaz-Ruiz et al., 2011). In the field of DNA repair, *S. cerevisiae* was used to characterise the RAD52 epistasis group which are vital for homologous recombination (HR) during both mitosis and meiosis (San Filippo et al., 2008). The HR pathway is well conserved between humans and *S. cerevisiae,* which is demonstrated in table **Table 1-1**. As well as HR, *S. cerevisiae* is used as a model organism to investigate many pathways of DSB repair, which shall be discussed in this chapter.

Table 1-1 Homologous recombination factors in humans and budding yeast. Adapted from (San Filippo et al., 2008)

Human	***S. cerevisiae***	**Function**
Rad51	Rad51	Main mitotic and secondary meiotic recombinase
Dmc1	Dmc1	Meiotic recombinase
MRN complex: Mre11 Rad50 Nbs1	MRX complex: Mre11 Rad50 Xrs2	DNA binding and nuclease activities
CtIP	Sae2	Promotes MRN/MRX nuclease function
BRCA2	None	ssDNA binding and recombination mediation
Rad52	Rad52	ssDNA binding and annealing
None	Rad59	ssDNA binding and annealing
Rad54	Rad54	Stimulates D-loop formation
Rad54B	Rdh54	Stimulates D-loop formation
Rad51B-Rad51C Rad51D-XRCC2 Rad51C-XRCC3	Rad55 Rad57	ssDNA binding, recombination mediation
Hop2 Mnd1	Hop2 Mnd1	Interacts with Rad51 and Dmc1

1.2.1 Homologous Recombination: SDSA and dHJ Repair

Homologous recombination (HR) is a way of repairing a DSB which utilises a donor template on another chromosome for repair. As this is the case, HR is only an option during the S and G_2 phases of the cell cycle, when there is a sister chromatid available. As it uses a template to make a copy, rather than simply annealing or ligating strands together, HR is considered error free (Mathiasen and Lisby, 2014). HR is also utilised to repair meiotic DSBs, this process is different to the mitotic HR described below and it detailed extensively later (section **1.3.2** to **1.3.9**).

The first stage of HR is the resection of the DNA to generate a 3′-ssDNA tail. It is this resected end which will be used to invade the template duplex strand for repair. This process is started by the MRX complex. The MRX complex binds to the DSB and gets activated by the accessory protein Sae2. This then stimulates the nuclease function of the MRX complex, which resects DNA in a 3′-5′ direction, commencing the generation of a 3′-ssDNA substrate (Gobbini et al., 2018). Then long-range resection is activated by Exo1 and Sgs1-Dna2. This long-range resection generates a 3′-ssDNA tail which is around 3 kb long (Zhu et al., 2008). As soon as the ssDNA is exposed, RPA binds to it (Kim et al., 1992).

Rad51 is the recombinase which conducts the homology search and aids the formation of a displacement loop (D-loop) for repair. Rad51 is loaded onto the resected 3′-ssDNA tail with the help of Rad52, which helps displace RPA to form the nucleoprotein filament / presynaptic complex (Sugiyama and Kowalczykowski, 2002). The Rad51-DNA filaments formed are dynamic and are modulated by Srs2 and Rad55-Rad57 (Liu et al., 2023). Rad51 can be antagonised by the helicase Srs2, which removes Rad51 from DNA strands. This anti-recombinase action is counteracted by the Rad55-Rad57 heterodimer, which stabilises Rad51-DNA interaction to protect from Srs2 (Srs2 prevents hyper-recombination) (Liu et al., 2011). Once loaded onto the DNA, Rad51 is ready to invade the template strand.

Strand invasion consists of Rad51 annealing the resected DNA from the DSB to the template strand. This creates a 3-stranded ssDNA-Rad51-dsDNA intermediate which can go on to form a D-loop. Rad52 also has some strand annealing activity, which helps Rad51 to

capture the template strand (Shi et al., 2009). The translocase Rdh54 also helps Rad51-strand exchange by engaging in chromatin remodelling. Rdh54 is able to reposition nucleosomes which facilitates Rad51 strand invasion activity (Kwon et al., 2008). Rad51 stabilises strand exchange by using triplet recognition; Rad51 is able to 'step over' mismatches, but cannot stabilise them, hence its preference for using sister sequences rather than homologous sequences (Lee et al., 2015). Rad51 requires ATP (though not hydrolysis) and at least 8 nucleotides of homology for strand exchange to take place (Sung and Stratton, 1996, Qi et al., 2015). Rad54 helps to turn the three-stranded intermediate synaptic complex (ssDNA:Rad51:dsDNA) into heteroduplex DNA/D-loop (Spies et al., 2016, Tavares et al., 2019). This is due to Rad54's ATPase activity which is stimulated by Rad51 (Petukhova et al., 1999).

Once strand exchange has taken place and a D-loop has formed, the invasive ssDNA strand acts as a primer for DNA synthesis using the template strand.v Polδ and Polε are required for synthesising DNA and extending the D-loop in a 5′-3′ direction (Wang et al., 2004). Polδ D-loops can be unwound by the 3′-5′ translocases such as the Sgs1-Top3-Rmi1 (STR) complex, Srs2, and Mph1 (Fasching et al., 2015, Liu et al., 2017, Prakash et al., 2009). Once the D-loop has been extended by the synthesis of new DNA on the repair strand, there are two possible repair options: synthesis dependent strand annealing (SDSA) or the formation and resolution/decatenation of a nicked HJ or a double Holliday junction (dHJ).

In mitotically dividing cells, SDSA is the preferred repair mechanism. Furthermore, only a small number of joint molecules (JMs, when two chromatids physically link via a dHJ) are detected, though at a 10 x lower abundance than in meiosis. These mitotic dHJs show a preference for sister chromatids as a repair template as opposed to the homolog (Bzymek et al., 2010). The dissociation of the newly-synthesised strand from the template strand and re-annealing to the opposite DSB resected end is facilitated by Rad52 (Sugiyama et al., 2006). If the newly-synthesised strand is too long to re-anneal, the 3′ flaps can be trimmed by the Rad1-Rad10 nuclease complex working in conjunction with Rad51 and Msh2-Msh3 (Karlin and Fischhaber, 2013). SDSA results in a short 'gene conversion' event where the

homologous template was used, this is also referred to as a non-crossover (NCO). When Rad52 is bound to ssDNA without RPA present, Rad51 is able to inhibit Rad52-mediated DNA annealing, possibly to prevent SSA occurring (Wu et al., 2008).

If SDSA is not utilised for repair, an additional process called ‘second end capture’ is required. Here the remaining DSB resected 3′-ssDNA end is able to invade the repair template duplex DNA (Szostak et al., 1983). Second-end capture is facilitated by the annealing activity of Rad52 as the second ssDNA strand is coated with RPA. It helps Rad51 to displace the complementary strand to form the second Holliday junction. As with the initial strand invasion, Rad54 is also required for the second-end capture (Sugiyama et al., 2006, Nimonkar et al., 2008). Second end capture usually results in forming a second D-loop which can migrate to form two nicked HJs and a JM. Then there are three options for resolving the JM. The first involves resolution by the nuclease complex Mus81-Mms4 as the nicked HJs can act as an ideal substrate as Mus81-Mms4 has a preference for 3′-flap structures and D-loops, whilst it has low affinity for processing dHJs (Constantinou et al., 2002, Ehmsen and Heyer, 2008). This can result in a crossover or non-crossover product. The other two options involve the nicked Holliday junctions being ligated (right) to form a double Holliday Junction (dHJ). This dHJ can then be ‘dissolved’ by the STR complex. The STR complex is made up of the RecQ-like 3′-5′ helicase Sgs1, the type IA topoisomerase Top3, and the fold-accessory factor Rmi1, which together form a dHJ dissolution complex or ‘dissolvasome’. With dHJ dissolution, Top3 decatenates the DNA, allowing the strands to pass between one another; this process is facilitated by the helicase activity of Sgs1. When a dHJ is dissolved, it results in non-crossover products (Bizard and Hickson, 2014). The final option is to nucleolytically resolve the dHJ with SSNs such as Slx1-Slx4 and Yen1 to produce either crossover or non-crossover products (Xu et al., 2021, Carreira et al., 2022, Schwartz and Heyer, 2011, Ip et al., 2008). An overview of DSB repair via HR/SDSA is shown in **Figure 1-3**.

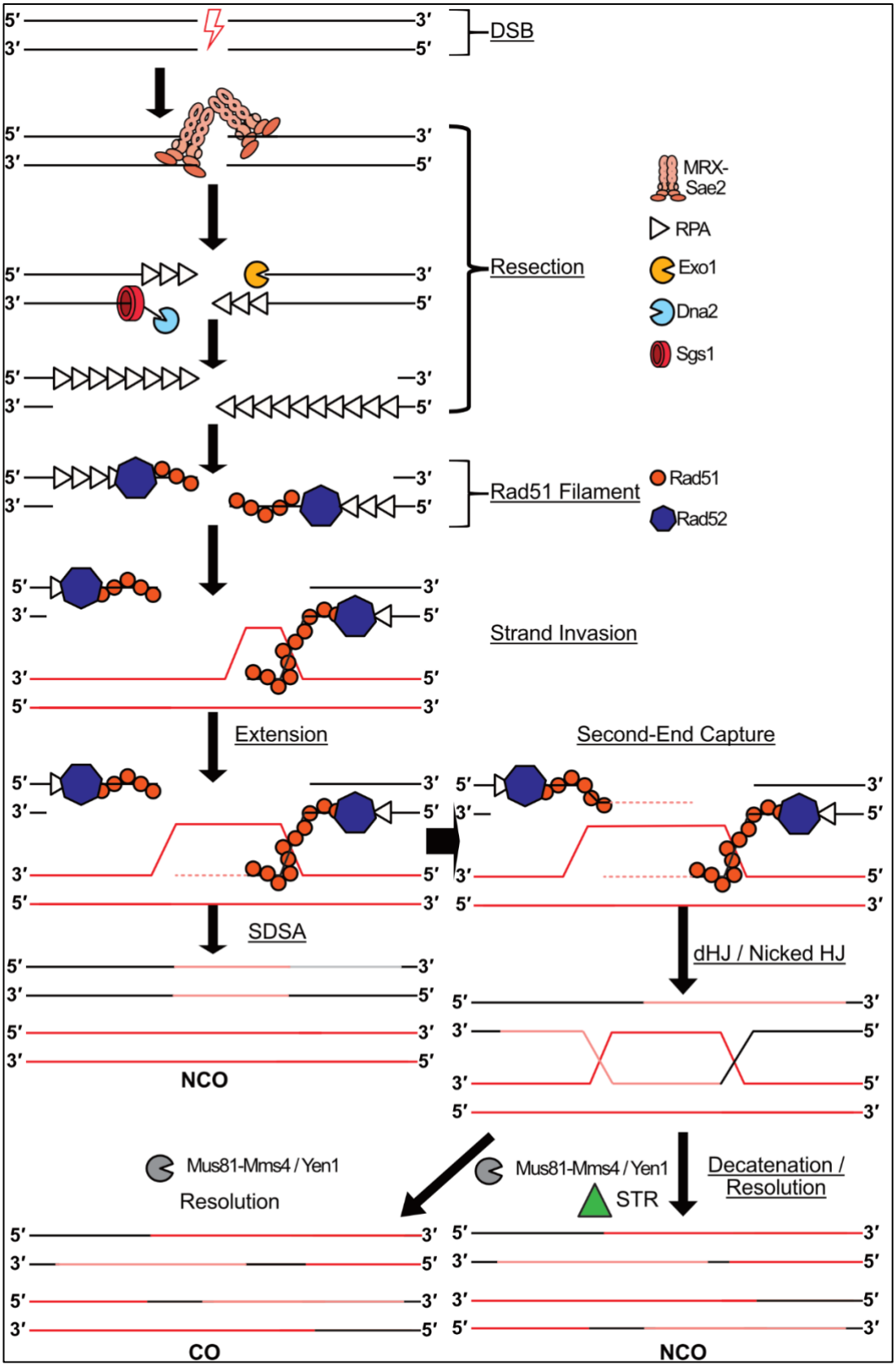

Figure 1-3 Overview of HR and SDSA in mitotically growing *S. cerevisiae.* A DSB is formed at the top. Then 2 MRX-Sae2 complexes bind to the ends 5′-ends of the DSB and

span the gap via Rad50 coiled-coils. Then 5′-3′ long-range ssDNA resection takes place courtesy of Exo1 and Sgs1-Dna2, allowing RPA to bind to the single-strands. Then Rad51 is loaded onto the ssDNA with the help of Rad52 to form the Rad51 filament. Then the recombinase Rad51 performs a homology search and displaces a strand to bind to the repair template, forming a D-loop. This is then used as a primer for repair, and the D-loop migrates. If the strand then dissociates and re-anneals over the other side of the DSB, this is SDSA. Then the annealing activity of Rad52 allows for second-end capture and a second D-loop is formed. These converge on one-another to form either a nicked dHJ which can be processed by Mus81-Mms4 nuclease action, or proceed to form a full dHJ which can be decatenated by STR. SDSA and decatenation produce NCOs, whilst nuclease resolution by Mus81-Mms4 or Yen1 can produce CO or NCO.

1.2.2 The DNA Damage Response Checkpoint

In *S. cerevisiae*, the DNA Damage Response Checkpoint (DDC) a response to damaged DNA which prevents cells dividing during mitosis, thereby maintaining genomic integrity (the cell cycle is outlined in section **1.2.6**). The DDC is mediated by two phosphatidylinositol-3-kinase-related protein kinase (PIKK) family proteins: Tel1 and Mec1 (reviewed here (Colombo et al., 2020)). Tel1 is the *S. cerevisiae* homolog of the mammalian ATM (Ataxia-Telangiectasia-Mutated) whilst Mec1 is homologous to ATR (ATM-and-Rad3-Related). These kinases target S/TQ motifs on proteins in order to phosphorylate them. Tel1 has also been shown to phosphorylate D/E-S/T motifs (Comstock et al., 2024). Tel1 is recruited to DSBs, whilst Mec1 requires a resected end to be activated.

Tel1 usually exists as a homodimer and is only active when as in its monomeric form (Xin et al., 2019) and is recruited to DSBs by the MRX complex (Fukunaga et al., 2011). This interaction stabilises the MRX complex on the DNA and can be counteracted by Rif2 (Cassani et al., 2016). Tel1 is then able to activate MRX nuclease activity by phosphorylating its cofactor, Sae2 (Terasawa et al., 2008). This nuclease activity creates a 3′-ssDNA end which is spontaneously bound by RPA to protect the DNA from forming secondary structures and being bound by interfering proteins (Kim et al., 1992). As the DSB now has a resected end with RPA attached, the ‘911 clamp’ can be loaded onto the DSB.

The 911 clamp is a heterotrimer made up of Ddc1, Mec3, and Rad17. This trimer forms a ring around the DSB, and is loaded onto the DNA by the clamp loader Rad24 along with RFC2-5 (Replication factor C) (Majka et al., 2006).The 911 clamp is able to inhibit short-range resection of the MRX complex to prevent excess DNA cleavage when multiple MRX complexes are loaded (Gobbini et al., 2020). Once the clamp is loaded, Mec1 can be recruited.

Mec1, along with its cofactor Ddc2, is recruited to DSBs with RPA-coated ssDNA, (Dubrana et al., 2007, Deshpande et al., 2017). This alone, however, is not enough to fully activate Mec1. Mec1 needs to interact with the ‘911 clamp’ and the accessory protein Dpb11 before it is fully active (Puddu et al., 2008). Mec1 facilitates interaction between the 911 clamp and Dpb11 by phosphorylating T602 of Ddc1, which allows Dpb11 binding and

therefore full Mec1 activation (Majka et al., 2006). Mec1 and Tel1 are also able to phosphorylate the histone H2A to form γ-H2A, which helps to recruit Rad9 (Grenon et al., 2007) (Toh et al., 2006).

Rad9 is partially activated by interacting with H3K79me, which is stabilised by the γ-H2A histone medication provided by Mec1/Tel1 (Lee et al., 2013). Rad9 is fully activated when bound to Dpb11. Mec1-Dpb11-Rad9 signalling doesn't efficiently occur in G_1 when CDK is present, instead phosphorylating Rad9 and interacting during S, G2, and M phases (Pfander and Diffley, 2011).

Once fully active, Rad9 which then is able to inhibit the Sgs1 helicase, preventing end resection by the Sgs1-Dna2 complex (Bonetti et al., 2015). End resection is further inhibited by Rad9 activating Rad53. Rad53 is able to phosphorylate Exo1 to prevent long-range resection (Morin et al., 2008). This Rad9 end-resection-inhibition function is countered by Fun30. Fun30 has helicase and ATPase domains, which allow nucleosome remodelling. This remodelling facilitates end resection by Exo1 and Sgs1-Dna2 by increasing access to DNA, bypassing the nucleosome-bound Rad9 which inhibits both Exo1 and Sgs1-Dna2 (Chen et al., 2012). Fun30 can also bind to Dpb11 in a competitive manner to prevent Rad9 activation (Bantele et al., 2017). This Dpb11 competitive-binding is also exhibited by Slx4-Rtt107 (Dibitetto et al., 2016).

Tel1 signalling is gradually lost once DNA ends are resected, indicating that once Mec1 is activated by the generation of ssDNA, Tel1 signalling is no longer needed, there is a switch from Tel1 to Mec1 signalling (Mantiero et al., 2007). As well as reducing Tel1 activity, Mec1 can attenuate its own signal via Rad53 signalling to prevent excessive end resection (Clerici et al., 2014).

As well as ensuring end-resection is under control, Rad9 activation of Rad53 can pause the cell cycle. Rad53 can phosphorylate Dun1 to activate it, which prevents entry into anaphase, preventing cell division. Similarly, Rad9 can activate Chk1, which activates Pds1 which also prevents anaphase entry (Jia et al., 2004). An overview of the DDC is shown below in **Figure 1-4**.

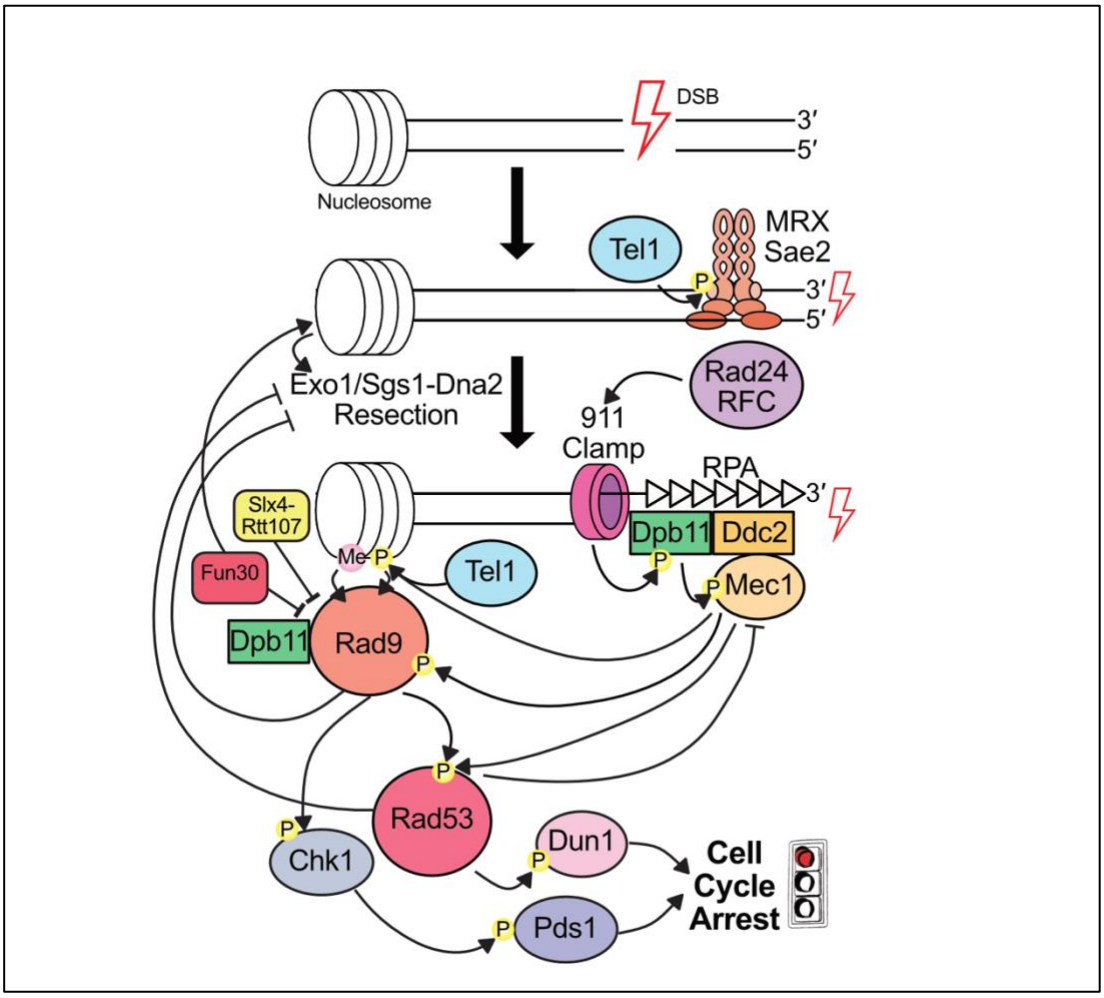

Figure 1-4 The DDC in *S. cerevisiae.* The DDC is shown acting on one side of a DSB. P = phosphorylation. Me = methylation. A DSB occurs, then MRX binds. Tel1 phosphorylates Sae2, allowing MRX-Sae2 to commence end resection and load Exo1/Sgs1-Dna2 for long-range 5′-3′ end resection. Then the 911 clamp is loaded by Rad24-RFC, which activates Dpb11 which activates Mec1-Ddc2. Then Mec1 and Tel1 can regulate Rad53 signalling via Rad9 (or Mec1-Rad53 directly). Fun30 and Slx4-Ree107 prevent Rad9 activation by Dpb11 binding. Fun30 aids nucleosome rearrangement to help Exo1/Sgs1-Dna2 perform end resection.

1.2.3 Break-Induced Replication

Break Induced Replication (BIR) is an HR pathway which is independent of the recombinase Rad51. This form of repair is used to repair one-sided DSBs such as stalled replication forks and at telomeres (Signon et al., 2001, Mehta and Haber, 2014). BIR involves a single-end invasion, followed by replication using the homologous chromosome as a template. Rad51 is shown to bind during BIR, but it is removed by the helicase Srs2 to prevent the formation of JMs (Elango et al., 2017).

As with the other HR pathways described, BIR begins with 5′-3′ end resection to generate a 3′-ssDNA tail. Rad52 and Rad54 are required for BIR to take place, but Rad51 is not essential as around 5 % of wt levels of BIR are seen in a *rad51Δ* background (Davis and Symington, 2023). Rad51-independent BIR is a less efficient pathway, this pathway depends on Rad59 as well as on Mre11–Rad50–Xrs2 complex and on the Swi2/Snf2 chromatin remodeller complex. The Rad51-dependent pathway meanwhile requires Rad55-Rad57 (Signon et al., 2001, Malkova et al., 2005).

Following the SEI, the broken strand is repaired using a migrating replication bubble. Here a D-loop migrates to allow conservative DNA synthesis, coupled with lagging-strand synthesis using the newly-formed strand as a template (Donnianni and Symington, 2013). This replication bubble is driven forward by the 5′-3′ helicase Pif1 with the polymerase Polδ (Saini et al., 2013). Pif1 is activated by Mec1-Rad9-Rad53 phosphorylation (Vasianovich et al., 2014).This repair can take place from the break site all the way to the telomeres, spanning over 100 kb which can lead to the incorporation of mismatches as there is no separate second-strand synthesis like in other dHJ or SDSA repair, meaning that mismatches are not detected and fixed by MMR (Saini et al., 2013). Lagging-strand synthesis requires the Polα-Primase complex (Lydeard et al., 2007).

In *S. cerevisiae,* BIR is used to repair DSBs which arise in repetitive microsatellite regions, which can often form hairpin or G quadruplex secondary structures. This repair is aided by the SSN Mus81 (Gadgil et al., 2020). An overview of BIR is shown in **Figure 1-5**.

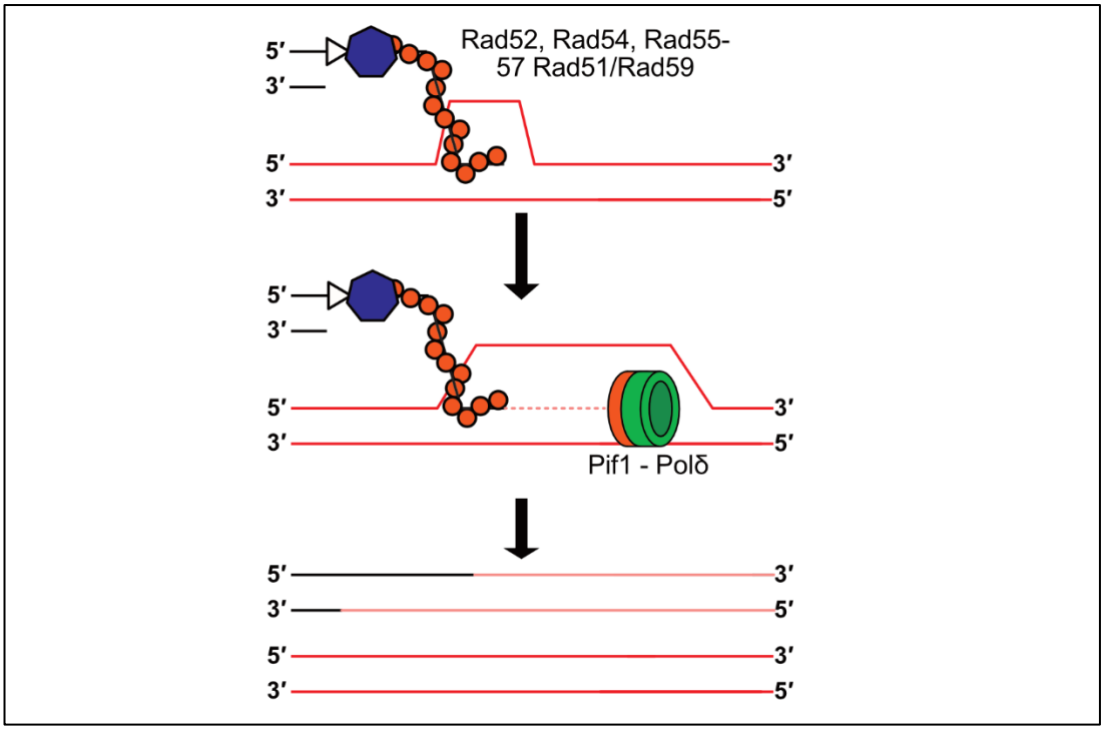

Figure 1-5 Break Induced Replication in *S. cerevisiae.* A single-ended DSB occurs and end-resection takes place. Then Rad52, Rad54, Rad55-57 and either Rad51 or Rad59 perform a homology search to form a D-loop. This is used as a primer for replication by Pif1 helicase with Polδ.

As well as classical BIR as previously described homology-mediated BIR, the repair process can switch from homology-driven BIR to microhomology-mediated BIR (MMBIR). The switch from BIR to MMBIR is driven by a lack of Pif1 helicase causing a collapse of the replication fork, and results in a template switch for the repairing strand. MMBIR is also known as fork stalling and template switching (FoSTeS) (Zhang et al., 2009). This template needs up to 6nt of microhomology on a nearby single-stranded DNA molecule to proceed, which results in GCRs. In *S. cerevisiae* MMBIR is driven by the translesion polymerases Rev1 and Pol ζ which are responsible for the DNA synthesis. (Sakofsky et al., 2015) MMBIR can result in duplication of genes as well as ‘exon shuffling’ where two or more exons from different genes can be combined ectopically to create novel genes (Zhang et al., 2009). MMBIR also requires the NHEJ protein Dnl4 (Payen et al., 2008). MMBIR has been attributed to copy number variation (CNV) and low copy repeat (LCR) regions in the human genome (Hastings et al., 2009).

1.2.4 C-NHEJ

Classical/canonical Non-Homologous End Joining (c-NHEJ, reviewed here (Emerson and Bertuch, 2016)) is a way of repairing blunt-ended DSBs. It is most active during the G_1 phase of the cell cycle (Aylon et al., 2004). There are three main stages of c-NHEJ. Firstly, the Ku complex with the MRX complex bind to the ends of the DNA and physically link them together. Then the other NHEJ factors bind: Nej1 loads Dnl4-Lif1; whilst Rad27 and Pol4 are also recruited. Finally, ends are processed to eliminate overhangs and the gap is filled by ligation (Ferguson et al., 2000, Ira et al., 2004). The checkpoint proteins Rad9, Rad24, Rad17, Mec1, Mec3, and Rad53 are all needed for efficient NHEJ to take place (de la Torre-Ruiz and Lowndes, 2000)

NHEJ begins when the Ku complex binds to a DSB with minimal overhangs. The Ku complex is a heterodimer comprising of the Ku70 and Ku80 proteins. When these subunits combine, they form a β-barrel structure which encircles a full turn of duplex DNA. The Ku complex doesn't contact specific bases, but instead interacts with the sugar-phosphate backbone, slotting into the major and minor grooves of the DNA. As it binds to the groove rather than specific bases, it means it binds to blunt-ended duplex DNA in a sequence-independent manner (Walker et al., 2001). Whilst the Ku80 subunit is catalytically essential for telomeric heterochromatin formation, it is the Ku70 subunit which is essential for repair of DSBs by NHEJ owing to it's protruding α-5 helix (Ribes-Zamora et al., 2007) . The Ku serves three main purposes. The first is to sterically protect DNA ends. The other two functions are the recruitment of the MRX complex and the Dnl4 ligase.

The MRX complex is required for both NHEJ as well as HR. In NHEJ, it is needed to span the gap in the DNA thanks to the Rad50 coiled-coil domains interacting with one another. In HR, the MRX complex recruits Exo1 for 5′-3′ end-resection, however in NHEJ the Ku complex physically inhibits Exo1 loading, thereby driving repair towards NHEJ (Mimitou and Symington, 2010, Hohl et al., 2011). This Ku-MRX interplay is complicated by the MRX being able to eventually remove the Ku complex from unrepaired DNA ends to drive repair towards HR (Balestrini et al., 2013)

The Ku complex is vital for recruiting the ligase Dnl4 via the mediator-protein Nej1 (Wilson et al., 1997, Chen and Tomkinson, 2011). Dnl4 does not act alone, and forms a heterotrimer with two Lif1 molecules; without the Lif1 binding, Dnl4 is unstable and cannot efficiently ligate DNA (Deshpande and Wilson, 2007). This type IV ligase utilises a catalytic lysine residue, K282, with ATP and NAD^+ to form a phosphodiester bond between the broken DNA ends (Ellenberger and Tomkinson, 2008, Ramos et al., 1998, Teo and Jackson, 1997). Any remaining gaps are repaired by Pol4 (Bebenek et al., 2005). The efficiency of NHEJ is increased by the presence of Fen1 (AKA Rad27) which helps to remove overhangs for blunt-end ligation to occur (Daley and Wilson, 2008).

As this repair doesn't utilise a template like HR, it can lead to small deletions/insertions being incorporated. Despite being considered 'error-prone', *in vivo* assays utilising continually-active endonucleases have shown that NHEJ can repair blunt-ended DSBs with at least 99.8 % precision (Lee et al., 1999). An overview of NHEJ is shown in **Figure 1-6**.

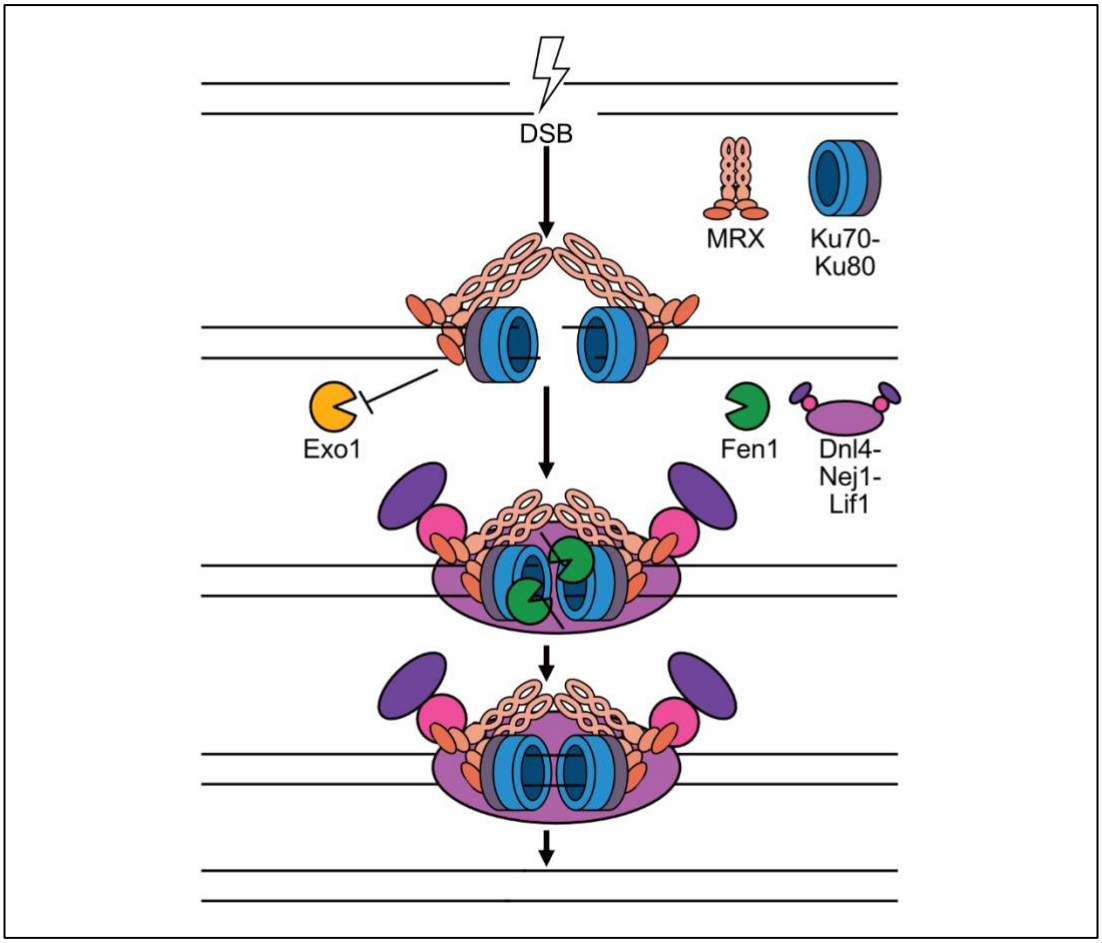

Figure 1-6 Overview of NHEJ in *S. cerevisiae.* A DSB occurs. The MXR complex binds and spans the DSB Ku70-Ku80 also bind on the ends of the DSB, preventing Exo1 end resection. The ends are processed to blunt ends by Fen1. Then Dnl4 is loaded with the help of Nej1 and Lif1. Dnl4 ligates the ends.

1.2.5 Annealing-Based Repair

1.2.5.1 MMEJ

Microhomology mediated end joining (MMEJ, also called Alternative End Joining) is another form of DSB repair in yeast. This pathway is comparable to the Polθ mediated end-joining pathway seen in higher Eukaryotes (Sfeir and Symington, 2015). Here, short ssDNA flanking regions are annealed together due to short regions of homology. MMEJ is inhibited by RPA and is independent of both the Ku complex and Rad52, but requires several other factors utilised in NHEJ and SSA (Lee et al., 2019, Ma et al., 2003). A region of homology between 8-20 base pairs with at least 80 % homology is the ideal substrate for MMEJ (Lee

et al., 2019). As such small regions of imperfect homology are used, MMEJ can lead to chromosomal rearrangements and deletions (Lee and Lee, 2007). Long range resection is required to uncover the required regions of homology, and in *exo1Δ* and *sgs1Δ* backgrounds, MMEJ doesn't proceed (McVey, 2014).

The MRX complex is required to process the ends of the DSB, without its nuclease function, MMEJ is reduced, though not abolished. This is because much like the SSA pathway, MMEJ needs 5′-resected DNA ends to anneal together. Tel1 promotes this by phosphorylating Sae2 which activates the MRX complex and also inhibits NHEJ (Lee et al., 2019). In the absence of MRX nuclease function or in a *tel1Δ* background, Exo1 overexpression can recover 5′-end resection to allow MMEJ to take place (Lee and Lee, 2007). Srs2 is required to prevent Rad51 binding to the resected ends, thereby preventing repair via HR and driving repair towards MMEJ (Lee and Lee, 2007). Despite end resection taking place, RPA binding prevents MMEJ. This indicates that the annealing of homologous regions may be spontaneous between uncovered DNA strands which have sufficient homologies (Deng et al., 2014).

Once the microhomologies are annealed, there are 3′-ssDNA flaps which flank the annealed region which must be removed. It was initially thought that Rad1-Rad10 SSNs are responsible for this flap-trimming, but it has been since shown that MMEJ can occur in *rad1Δ*, *mus81Δ*, and *slx4Δ* backgrounds, meaning the SSN responsible for flap trimming in MMEJ remains elusive (Shaltz and Jinks-Robertson, 2023). Following the flap-trimming, polymerases are needed to fill-in the gaps between the annealed-section and the break. The most active MMEJ polymerase is Polδ, though Rad30 (aka Polη), Polζ, and the mismatch-tolerant Pol4 have also been implicated (Lee and Lee, 2007). As with NHEJ, Dnl4 is required for MMEJ. It is presumed to be the ligase responsible, along with Cdc9, for sealing the DNA ends in MMEJ (Ma et al., 2003, Shaltz and Jinks-Robertson, 2023). MMEJ is shown in **Figure 1-7**.

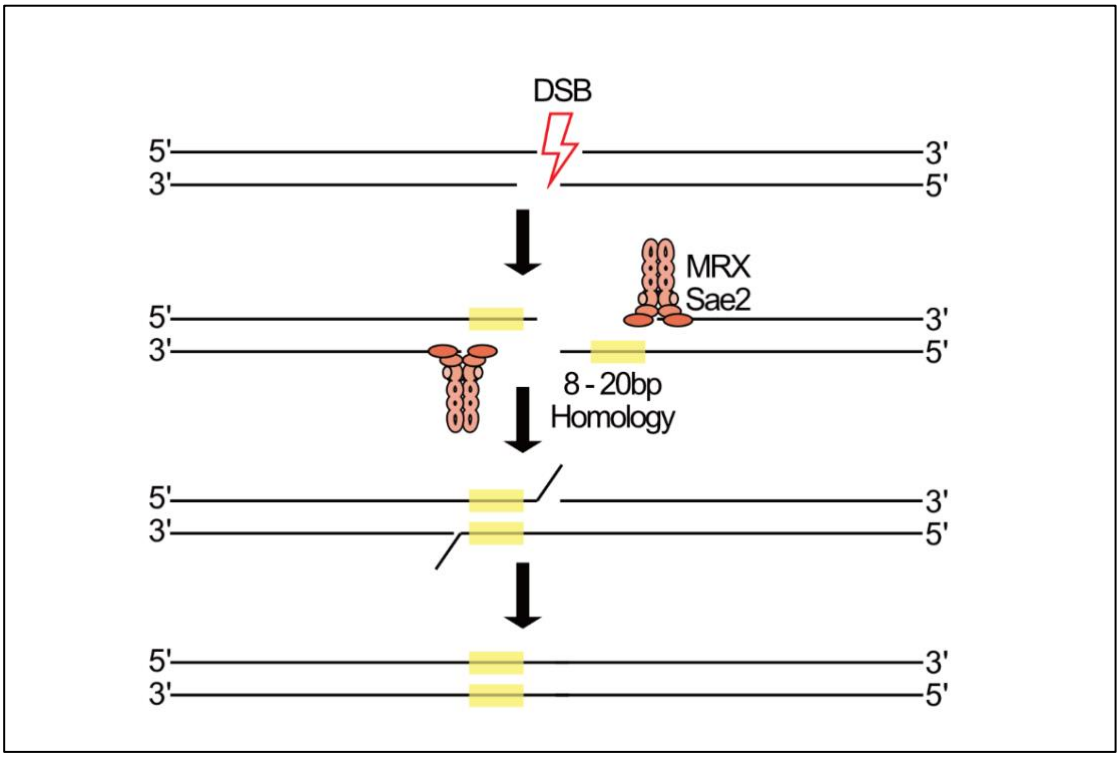

Figure 1-7 MMEJ in *S. cerevisiae.* A DSB occurs, then the MRX complex binds, with minimal resection taking place. A short region of homology allows the strands to anneal. The overhangs are trimmed and the ends are ligated together.

1.2.5.2 SSA

The SSA pathway (reviewed here (Bhargava et al., 2016)) is a DSB repair pathway which involves annealing short homologous sequences of resected 3′ ssDNA which flank a DSB (Maryon and Carroll, 1991). Despite being reliant on partial homology, SSA is independent of Rad51, Rad54, and Rad55-Rad57 (Ivanov et al., 1996). SSA is most efficient using regions of homology 63-205bp long, thought it can utilise homology sequences less than 30bp long; this means that SSA is error prone, often leading to deletions, unwanted insertions, and chromosomal rearrangements (Sugawara et al., 2000, Fishman-Lobell et al., 1992). SSA repair begins with a homology search; this time Rad52 and Rad59 perform the role. As SSA involved annealing two sequences of ssDNA together, a true 'recombinase' isn't needed as there is no need for strand-displacement. Therefore, Rad52's RPA-displacing and strand-annealing activity, aided by Rad59, is enough to join the complimentary strands together (Shinohara et al., 1998, Bai and Symington, 1996, Davis and Symington, 2001). The Rad52-Rad59 annealing activity can be reduced by the binding of the Smt3 (SUMO) as well as by Rad51, indicating that the SSA pathway is only active when other HR pathways have been compromised (Wu et al., 2008, Burgess et al., 2007, Altmannova et al., 2010).

Once complementary sequences have been annealed, the remaining 3′-ssDNA form overhanging tails. These tails must be removed so the DNA can be properly re-sealed. This tail-removal is catalysed by the Rad1-Rad10 nuclease complex. Rad1 is an XPF homolog, whilst Rad10 is an ERCC1 homolog; these proteins work together to cleave 3′-ssDNA junctions (Bardwell et al., 1994). The Rad1-Rad10 complex is reliant on other proteins for efficient nuclease activity, such as Slx4. Slx4 is phosphorylated by Mec1/Tel1, and it interacts directly with Rad1-Rad10 to aid non-homologous tail cleavage (Flott et al., 2007, Toh et al., 2010). This nuclease complex is also aided by Saw1, which recognises 3′-tails and recruits Rad1-Rad10 to remove the flaps (Li et al., 2013). Msh2 and Msh3 have also been demonstrated to help Rad1 with cutting non-homologous tails, but only when they are over 30nt long (Pâques and Haber, 1997). When the homologous tails are very short, Polδ can remove them with proofreading activity (Toh et al., 2010). The SSA pathway is summarised in **Figure 1-8**.

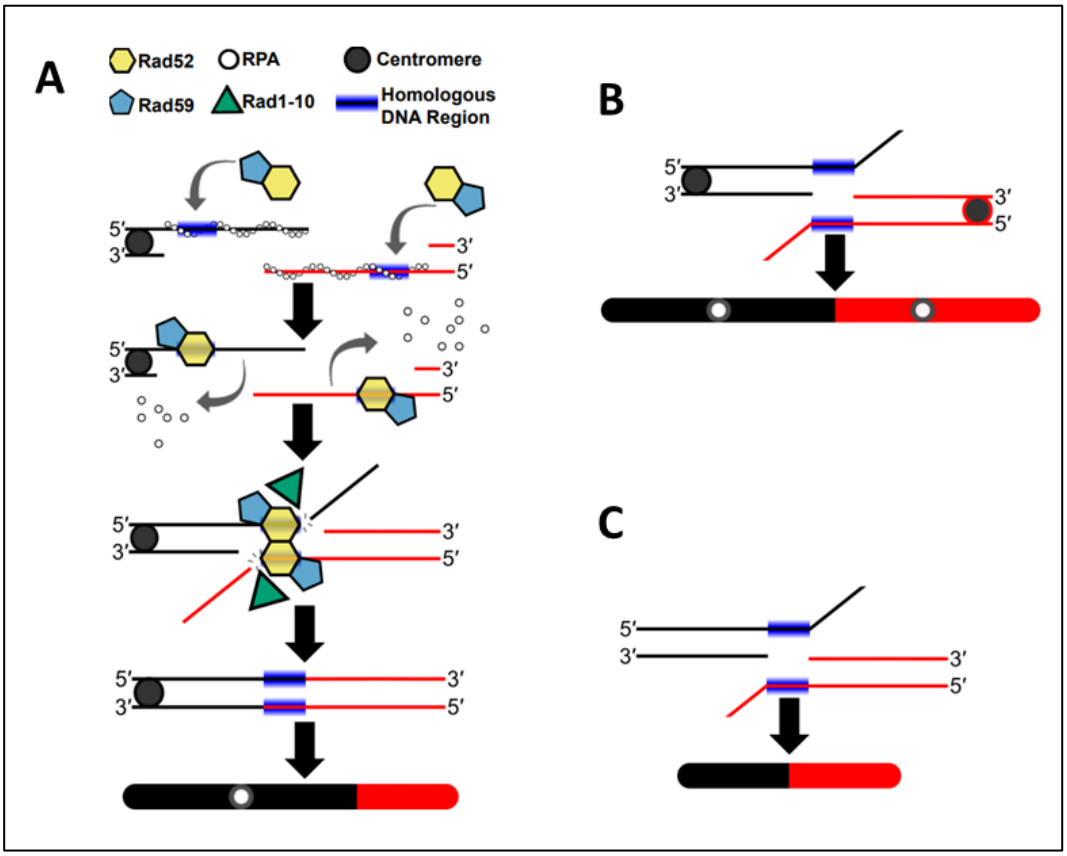

Figure 1-8 The SSA Pathway in *S. cerevisiae.* A) A DSB occurs and end resection takes place, uncovering a region of homology and allowing RPA to bind. Rad52 with Rad59 displace the RPA and anneal the homologous regions together. Then the overhangs are trimmed by the Rad1-Rad10 nuclease complex. **B)** Shows a dicentric chromosome made as a result of SSA at non-allelic loci (ectopic recombination). **C)** also shows ectopic recombination as a result of SSA, this time making an acentric chromosome.

1.2.6 DSB repair choice and the cell cycle

The cell cycle is a sequence of events which occur to allow a cell to divide properly. The stage of the cell cycle the organism is in will determine which DSB repair pathway is utilised. In *S. cerevisiae*, non homologous end joining (NHEJ, section **1.2.4**) is the preferred pathway during G_1, whilst homologous recombination (HR, section **1.2.1**) is the preferred pathway for haploid strains in the S / G_2 stages as there is a template available due to the replication of DNA forming sister chromatids, though diploids can use the homolog (Mathiasen and Lisby, 2014).

There are four stages to the cell cycle: Gap 1 (G_1), Synthesis (S), Gap 2 (G_2) and Mitosis (M). During G_1, the cells grow and either entering S phase and commit to cell division, or instead enter G_0 (quiescence) where they don't divide. During S phase, the DNA is replicated to make sister chromosomes, the cells begin budding, and the spindle pole body (SPB) assembles which allows microtubules to bind. G_2 is the second 'gap' phase, where the mitotic spindle assembles to pull the nucleus towards the bud 'neck'. M phase is when the cells divide, and where the Prophase, Metaphase, Anaphase, and Telophase stages of mitosis occur. Here the microtubules attached to the SPB pull the sister chromatids apart to segregate the chromosomes equally, the SPB then disassembles and the daughter cell 'buds' off (Pizzul et al., 2022). The cell cycle is summarised in **Figure 1-9**.

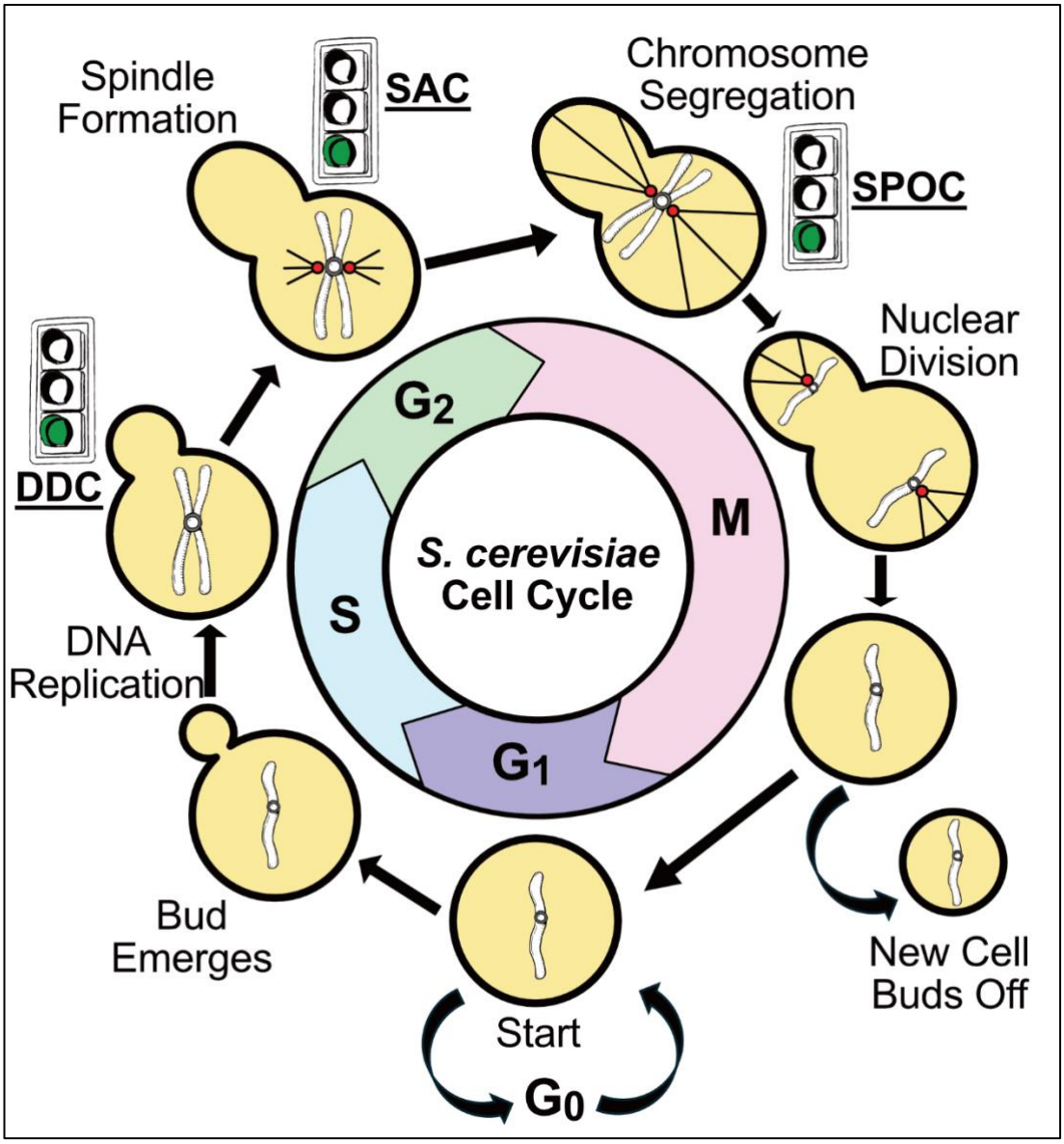

Figure 1-9 Overview of the cell cycle in *S. cerevisiae*. The bud emerges at the start of S-phase, and DNA is replicated. Any DNA damage here halts the cycle due to the DDC being activated. In G_2 the spindle assembles and microtubules bind, with the spindle-assembly checkpoint ensuring this takes place correctly. Then during M phase, the chromosomes line up to be separated, checked by the SPOC, then the chromatids are pulled apart and the daughter cell buds off.

The cell cycle is regulated by cyclin-dependent kinases (CDK, phosphorylation described in section **1.1.3**), In budding yeast there are four minor kinase and the master regulator Cdc28 (Cdk1) (Mathiasen and Lisby, 2014). Cdc28 is present throughout the cell cycle, but its activity is regulated by unstable proteins called cyclins. Cdc28 is activated by

nine different cyclins which are active at different points of the cell cycle: Cln1-3 are active in G_1, Clb5/6 are active in S phase, Clb1/2 are active during G_2 / M phase; whilst Clb3/4 from S phase to early M phase. When activated, Cdc28 acts as a proline-directed kinase which can phosphorylate over 300 protein targets involved in DNA replication, chromosome segregation, transcription, and cell morphogenesis. Cdc28 targets these proteins for phosphorylation on target sequences S/T*-P or S/T*-P-x-K/R (* is the phosphorylated residue, x is any amino acid) (Holt et al., 2009, Enserink and Kolodner, 2010, Malumbres, 2014).

To ensure that cells divide accurately, thereby preserving genomic integrity and ploidy, there are cell cycle 'checkpoints' which can halt the cell cycle if needs be. There are three main checkpoints: the DNA damage checkpoint (DDC, section **1.2.2**) which is triggered by lesions in DNA; the spindle assembly checkpoint (SAC) which becomes active when kinetochores aren't correctly attached to microtubules; and the spindle position checkpoint (SPOC) which ensures chromosomes are correctly distributed when the cells divide. Whilst these checkpoints are all activated in different ways, are all able to inactivate Cdc28 via the anaphase-promoting complex/cyclosome (APC/C). The APC/C targets cyclins for degradation by the proteasome via interactions with the accessory proteins Cdc20 and Cdh1. When active, the APC/C prevents the cell cycle progressing from metaphase to anaphase, therefore pausing the cell cycle until the DNA is repaired/aligned correctly. Furthermore, checkpoint proteins can halt the cell cycle independently of the APC/C. For example, the DDR proteins Rad53 and Chk1 can pause mitotic progression by directly inactivating the chromosome segregation protein Pds1, thereby blocking entry into anaphase (Matellan and Monje-Casas, 2020, Peters, 2006).

1.3 Meiosis in *S. cerevisiae*

1.3.1 Meiosis Overview

Meiosis is a type of cell division which occurs in sexually-reproducing organisms. Derived from the Greek word for 'lessening', meiosis produces haploid 'gamete' cells from a diploid parental cell. This differs from mitosis which produces two identical diploid cells from a diploid parent. The process of meiosis consists of a round of DNA replication, followed by two meiotic cell divisions (MI and MII) to produce four genetically distinct gametes. This is summarised below in **Figure 1-10**.

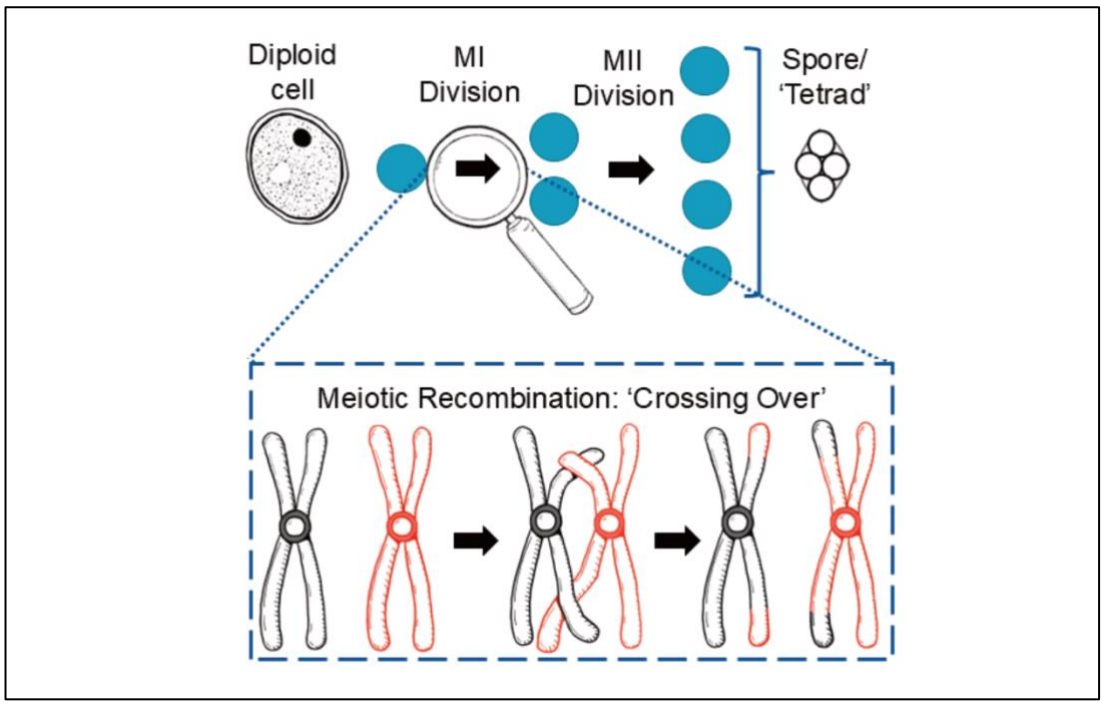

Figure 1-10 Overview of meiosis in *S. cerevisiae*. The diploid parent cell undergoes 2 rounds of division to form four genetically distinct gametes, in *S. cerevisiae* they're called tetrads/spores. During the first meiotic division, 'crossing over' occurs, shown as black and red homologous chromosomes exchanging genetic information.

The first stage of meiosis is the replication of the homologous chromatids (homologs) to produce sister chromosomes. Following the DNA replication is prophase I, which is further split into leptotene, zygotene, pachytene, diplotene, and diakinesis stages, defined by the status of the synaptonemal complex (section **1.3.4**). During leptotene the four

chromatids pair up via nucleoprotein filaments. These stages are defined by how the chromosomes look under a microscope. Leptotene is also the stage where programmed DSBs occur. During zygotene, the DSBs begin to be repaired with the help of the homologous chromosome. This pairing is aided by the formation of the synaptonemal complex (SC) nucleoprotein structure. The SC is fully formed at pachytene, which allows full repair via homologous recombination mechanisms. Some of these are repaired in such a way that the homologous chromatids physically link together to form a joint molecule (JM). When viewed via microscopy, these individual links between the chromosomes are called chiasma. These JMs links serve the dual purpose of ensuring accurate chromosome segregation as meiosis proceeds, whilst also permitting the swap of genetic material between homologous chromosomes. If no crossovers occurred, the meiotic division could lead to aneuploidy, so it is essential that at least one crossover event occurs between homologs, this is called the ‘obligate crossover rule’ (Jones, 1984, Martini et al., 2006). During diplotene, the synaptonemal complex begins to disassemble. By diakinesis, the SC has fully disassembled leaving chromatids which are now visibly connected via chiasmata. Following prophase I is metaphase I; here the joined-up chromatids assemble on the ‘metaphase plate’. During anaphase, the homologs are separated from each-other, moving to opposite ends of the cell allowing the MI division to occur. A subsequent second meiotic division (MII) follows this, where the sister chromatids are separated; now four genetically unique haploid cells have been produced (Hunter, 2015).

1.3.2 Meiotic Recombination

For meiotic recombination to occur DNA must first be replicated, producing sister chromatids. The replication must happen before DSBs can occur; so these events must be tightly coordinated as DSBs can be lethal to a cell (Borde et al., 2000, Rich et al., 2000). To ensure crossing over occurs in *S. cerevisiae*, over 100 DSBs are effected during meiotic prophase I (Pan et al., 2011). The severing of the DNA is handled by the meiosis-specific archaeal Topo VI-like enzyme Spo11, which works as part of a 'core complex', working as a team with the 'RMM' complex (Atcheson et al., 1987, Cao et al., 1990b, Bergerat et al., 1997, Keeney et al., 1997, Claeys Bouuaert et al., 2021b) (reviewed here (Lam and Keeney, 2014, Yadav and Claeys Bouuaert, 2021)). Following the Spo11 DNA nicking, the Spo11 protein then remains bound to the 5′-end of the DNA and needs to be removed. The DNA is subsequently cleaved downstream and resected in a 3′-5′ direction by the MRX complex (Garcia et al., 2011a), releasing the Spo11-oligonucleotide complex (Neale et al., 2005). Following short-range resection by MRX, the 5′ strand is resected further by Exo1 to leave a long 3′ ssDNA flap (Zhu et al., 2008). This 3′ ssDNA flap is the perfect substrate for repair the of the DSB via homologous recombination as it can invade duplex DNA to form a D-loop which provides a repair template. In meiosis, this strand invasion is controlled by the recombinases Rad51 and Dmc1 (Bishop et al., 1992, Bishop, 1994). The final stage of meiotic recombination involves either repair via a double Holliday Junction (dHJ), which results in genetic crossover (CO); or synthesis dependent strand annealing (SDSA), which results in genetic non-crossover (NCO) (Schwacha and Kleckner, 1995, Allers and Lichten, 2001).

1.3.3 DSB Hotspots

Whilst meiotic DSBs occur throughout the chromosome, there are regions where they are more likely to form; these are designated ‘hotspots’. The corresponding regions where little DSB activity is seen are dubbed ‘coldspots’ (Baudat and Nicolas, 1997). As DSBs are more likely to be seen at hotspots, they are widely utilised in meiotic research. For example, the His4::Leu2 hotspot on CHR III is often probed for Southern blotting to look at meiotic CO/NCO formation *in vivo* (Cao et al., 1990a).

Hotspots are usually 50-250bp in length, though they can be well over 1kb long (Pan et al., 2011). Hotspots are usually separated out by coldspots which can be 50-200kb long, ensuring hotspots are distributed along chromosomes (Pan et al., 2011). Hotspots themselves don’t have a specific sequence, but they do have several common characteristics which increase the chances of a DSB occurring within their boundaries. In budding yeast, hotspots tend to be found in promoter regions and are repressed near telomeres, centromeres, and repetitive regions (Buhler et al., 2007). With regards to chromatin structure, hotspots tend to occur in regions of open chromatin and often correlate (perhaps coincidentally (Tischfield and Keeney, 2012)) with trimethylated histone lysine residue 4 (H3K4me3) (Berchowitz et al., 2009). These regions may provide an easier place for DSB-machinery to cut, free from nucleosome occlusion. Whilst hotspots are found throughout chromosomes, not all hotspots are created equally, with the strongest 33% of hotspots having >75% of the total DSB activity. Furthermore, small chromosomes have higher levels of DSBs per kb than large chromosomes; this helps to ensure crossing-over can occur on all chromosomes, regardless of size. As well as measuring CO distances in kb, they can be measured in centimorgans (cM), with 1 cM being equal to a 1 % chance that two markers on the same chromosome will be separated during recombination (Haldane, 1919). Overall this point to hotspots representing windows of opportunity for DSBs to occur, rather than guaranteed DSB-causing regions (Pan et al., 2011).

1.3.4 DNA-Protein Scaffolds During Meiotic Recombination

In Prophase I, the chromosomes are arranged into 'loops' bound to proteinaceous 'axes'. (reviewed here (Kleckner, 2006), and shown in **Figure 1-11**). The axes are made of Red1, Hop1, and Rec8; these form a scaffold for the chromatids to condense themselves onto, with protruding 10-50kb chromatin loops. Red1 is a coiled-coil protein which can form homotetramers. These Red1 units extend into oligomeric filaments, which form the axis core (West et al., 2019). Hop1 is a HORMAD protein (HORMAD = Hop1, Rev7, Mad2) which is recruited to the chromosome axis by Red1 (Aravind and Koonin, 1998). Without Hop1, chromosomes cannot be compacted to form the loop-axis structure (Schalbetter et al., 2019). Rec8 is a meiosis-specific homolog of the Mcd1/Scc1/Rad21 kleisin cohesin (Klein et al., 1999). Rec8 helps hold the chromosomes in place; the gaps between Rec8 form the loops, the DNA held by Rec8 form the axial element (Muller et al., 2018, Ito et al., 2014). Rec8 also binds the cohesin complex (Smc1, Smc3, and Scc3) which form a ring structure which physically encircles sister chromatids. This means that the sister chromatids are physically on top of one another, arranged into loops and axes (Ivanov and Nasmyth, 2005). These cohesin rings manage to compact the DNA at the axial elements, but allow DNA to move into loops if required for transcription (Sun et al., 2015). Rec8 is negatively regulated by phosphorylation, which helps to remove the protein/cohesins so meiotic divisions can occur (Yoon et al., 2016). DSBs primarily occur in the loop sections, with Rec8 levels positively correlating with coldspots (Pan et al., 2011). As an additional layer of complexity, Red1 promotes DSBs, so the DSBs occur in loop sections which are physically brought to the axis; this is called the 'tethered loop-axis' model (Blat et al., 2002). At the leptotene-zygotene transition, the sister axes come together, pairing up with the homologous chromosomes. These then form a zipper-like structure which is completed at pachytene called the synaptonemal complex (SC, reviewed here (Gao and Colaiacovo, 2018)).

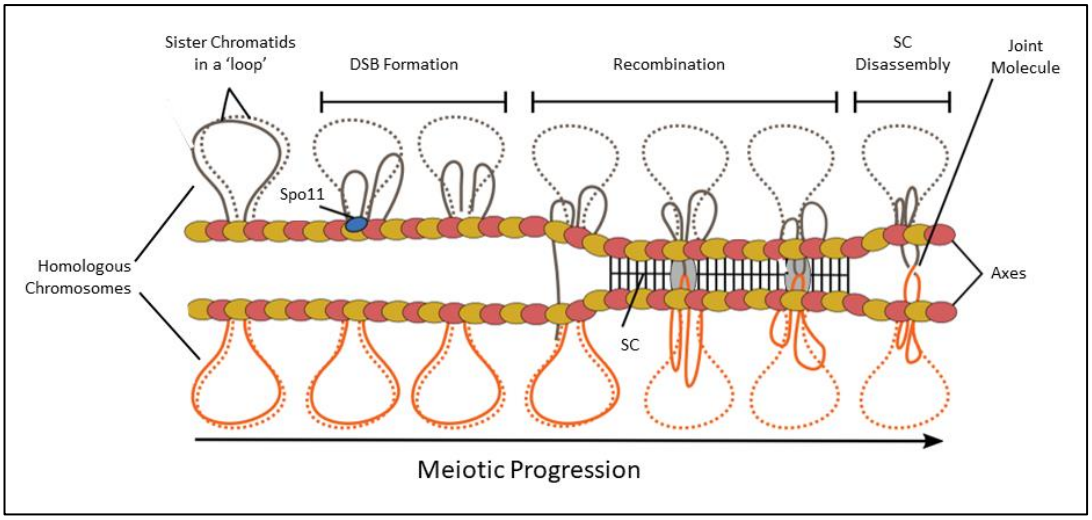

Figure 1-11 The tethered loop axis model of DSB formation during meiosis in *S. cerevisiae.* The homologous chromosomes are aligned together with the help of proteinaceous axes formed of Hop1-Red1 and Rec8. These allow the DNA to form 'loops' which is where DSBs occur. During recombination, the SC forms, then disassembles revealing joint molecules. Adapted from (Yadav and Claeys Bouuaert, 2021).

The SC is a tripartite DNA-protein scaffold structure formed of the two lateral elements (the Hop1-Red1 axes) held together by a central region. The purpose of the SC is to bring the homologs into close proximity so that COs can occur, as well as promoting 'Class I' COs (section **1.3.9**) (Grey and de Massy, 2022). The central element of the SC is formed of ZMM proteins (Zip1-4, Msh4-5, Mer3, Spo16). Zip1 is a coiled-coil protein which forms a major part of the central element. the C-terminus OF Zip1 helps bind it to the chromosomes at the lateral elements (Sym et al., 1993, Tung and Roeder, 1998). Zip1 needed for SC formation along with Ecm11 and Gmc2, which together down-regulate Spo11-mediated DSB formation (Lee et al., 2021) . Zip4 helps to recruit Zip2 and Spo16, referred to as the ZZS complex, to help bind and stabilise D-loops formed during meiotic recombination (Pyatnitskaya et al., 2022). Zip3 is an E3 Smt3 (SUMO) ligase which can act to bridge Zip1 and the ZZS complexes to bring them all into close proximity (Voelkel-Meiman et al., 2024). Mer3 is a SF2 helicase with 3′-5′ directionality which is able to work with Dmc1 to protect D-loops. This is achieved by binding to Top3-Rmi1 of the STR complex, thereby out-competing Sgs1, which prevents the anti-CO STR complex from being active (Altmannova et al., 2023). Msh4-5 form the heterodimeric Mutsγ complex. Mutsγ is activated

by SUMOylation (Smt3) and helps stabilise and resolve double Holliday junctions (He et al., 2021, Dash et al., 2024).

Within the SC, crossover designation occurs, which can result in the physical linking of the homologous chromosomes to form a joint molecule (JM). When Ndt80 is transcribed for pachytene exit, it reinscribes Cdc5 which promotes the disassembly of the SC (Sourirajan and Lichten, 2008, Xu et al., 1995). when the SC disassembles at diplotene, the JMs are still tethered together. These JMs allow for proper chromosomal alignment and separation at the MI division.

1.3.5 Spo11 and DSB Formation

The way that DSBs are produced mechanistically during leptotene is centred around a key protein called Spo11. Spo11 doesn't act alone, but rather in a 'core complex' which, in turn, acts with several other proteins/complexes to create highly controlled DSB events. Spo11 teams up with Ski8, Rec102, and Rec104 to form a heterotetramer with 1:1:1:1 stoichiometry. Overall the Spo11 core complex very closely resembles the archaeal Topo VI (a type II topoisomerase), with Ski8-Spo11 forming the A subunit, Rec102-Rec104 forming the B subunit (Corbett et al., 2007, Graille et al., 2008, Claeys Bouuaert et al., 2021b). Spo11 is the catalytic unit of the core complex, with its Y-135 residue being used to cut a single strand of DNA via a transesterification reaction (Bergerat et al., 1997, Keeney et al., 1997). Spo11 is bound directly to Ski8, which is a WD-domain β-propeller protein (Madrona and Wilson, 2004, Halbach et al., 2013). Ski8 (originally called Rec103) is involved in mRNA degradation in vegetative cells, but is expressed 15x more during meiosis (Anderson and Parker, 1998, Gardiner et al., 1997). Ski8 is essential for meiotic recombination where it relocalises from the cytoplasm to the nucleus to help mediate/stabilise Spo11's interaction with chromatin (Arora et al., 2004). Rec102 is a homolog of the Topo VI B transducer domain and also binds directly to Spo11, but at the opposite end to Ski8 (Vrielynck et al., 2016). Rec102 is known to associate with chromatin loops in early prophase, with rec102/4Δ strains showing reduced Spo11 foci on chromatin (Kee et al., 2004). Rec102 binds to Rec104 to form a chromatin binding complex which can bind to DNA, mediating the interaction of Spo11 with the RMM proteins Mei4/Rec114, and possibly aiding Spo11 with nuclear localisation (Salem et al., 1999, Maleki et al., 2007, Prieler et al., 2005).

The core complex is recruited to DSB sites, where two Spo11 complexes work in tandem to form a single DSB. Each Spo11 cuts one DNA phosphodiester backbone via a transesterification reaction, overlapping by 2nt so that both strands are cut (Pan et al., 2011) . After the DNA has been cut, Spo11 remains covalently bound to the 5′-end of the cleaved DNA via a phospho-tyrosyl link between the DNA backbone and the catalytic Y135 of Spo11. Multiple Spo11 core complexes can cut at a single hotspot region, creating 'double cuts' which are usually separated by 33 to >100nt (Johnson et al., 2021). These

‘double cuts’ make up around 20% of all Spo11 DSBs (Prieler et al., 2021). Spo11 seems to cut at bent DNA regions similar to the Top2 topoisomerase; Spo11 may be inducing the bends itself or may even be trapping two strands of DNA at once (Claeys Bouuaert et al., 2021b, Prieler et al., 2021). This is shown below in **Figure 1-12**.

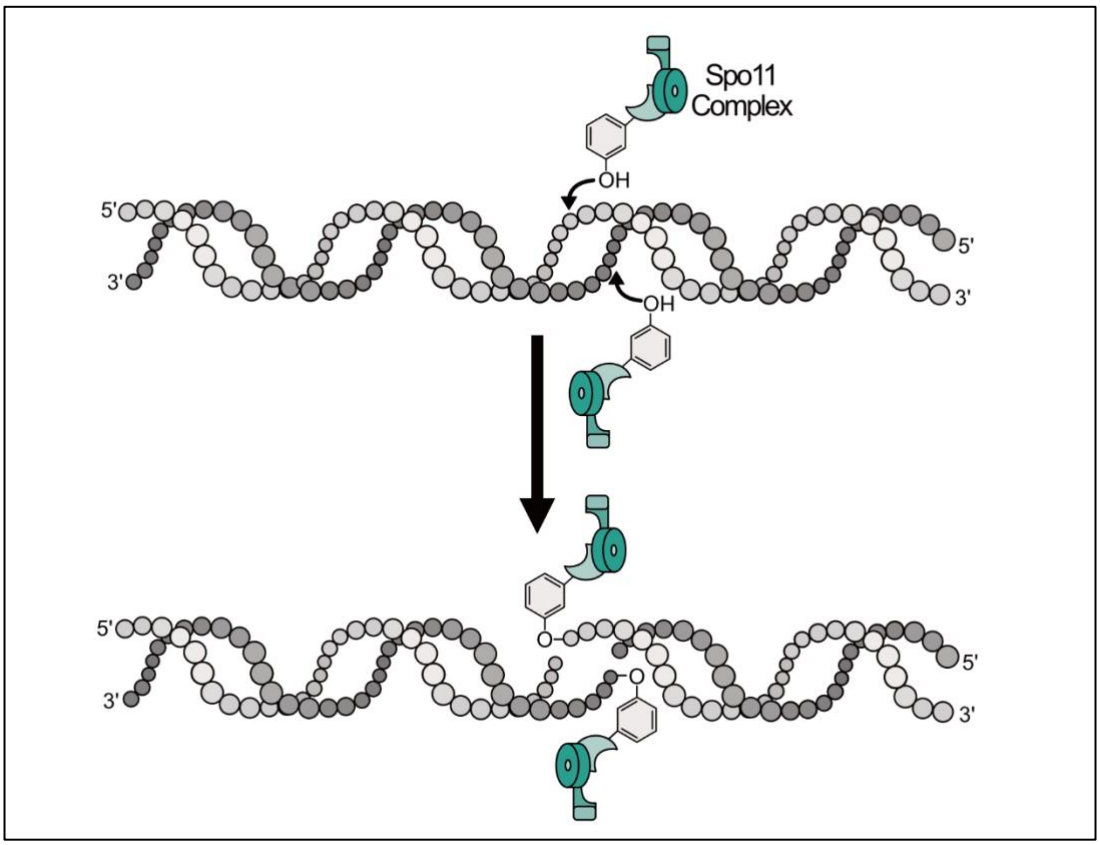

Figure 1-12 Spo11 induced DSBs during meiosis. Two Spo11 complexes work to form a DSB, and remain covalently attached to the 5′-end of the DNA.

The Spo11 core complex is guided to recombination sites with the help of the RMM complex: Rec114, Mei4, and Mer2 (Li et al., 2006). These proteins exist at Rec114-Mei4 and Mer2 units, which come together on chromatin to form the RMM complex. Mer2 (previously Rec107) is a homotetramer with coiled-coil and simple shared motifs (SSM) (Claeys Bouuaert et al., 2021a). It is spliced by Mer1 during early meiosis and phosphorylated by CDK and DDK to acquire its function (Engebrecht et al., 1991, Wan et al., 2008). Mer2 interacts with Spp1 (which is part of the H3K4 methylation COMPASS complex (Sollier et al., 2004)), Rec114-Mei4, Xrs2 (Henderson et al., 2006), and Hop1 (Rousova et al., 2021) as

well as interacting with DNA which could help bring the DSB machinery from the loop to the chromosome axis (Acquaviva et al., 2013). Rec114 and Mei4 are meiosis-specific proteins which exist as a 2-Rec114 : 1-Mei4 heterotrimer (Pittman et al., 1993, Menees et al., 1992, Claeys Bouuaert et al., 2021a). Rec114 is needed for Spo11 to reach hotspots as it can localise on chromosomes (Maleki et al., 2007). These RMM proteins also have to compete with other DNA-bound proteins, which could help to regulate their function (Claeys Bouuaert et al., 2021a).

1.3.6 Spo11 Removal by the MRX Complex

Once the DSB has been initiated, Spo11 is covalently bound to the 5′ end of the DNA and must be removed for DNA repair and meiotic progression. This is catalysed by the MRX-Sae2 complex, which cleaves downstream of the Spo11, allowing the Spo11 to be released with an oligo attached. This also prevents the Ku complex (section **1.2.4**) binding and paves the way for the resection of the 5′ ends, both of which drive repair towards HR (Foster et al., 2011) (section **1.2.1**). The resection is controlled by the MRX complex (reviewed here (Gobbini et al., 2016)). Mre11 has five N-terminal phosphoesterase motifs which confer both ssDNA endonuclease activity as well as 3′ to 5′ exonuclease activity that is increased in the presence of Rad50 and ATP (Sharples and Leach, 1995, Paull and Gellert, 1998, Trujillo and Sung, 2001). Mre11 is able to dimerise, which facilitates binding to DNA and Rad50 (Williams et al., 2008). Rad50 has a nucleotide binding ‘head’ domain which can bind to around 18nt at the MRX-dimer interface in an ATP-dependent manner (Seifert et al., 2016). As well as a head domain, Rad50 has a long coiled-coil ‘hook’ domain which extends away from the MRe11/Xrs2 subunits. This allows Rad50 to dimerise with another Rad50 coiled-coil as the Zn^{2+} hook domains physically tether one-another (Hopfner et al., 2002). Thanks to Rad50 and Mre11 dimerisation, 4 MRX complexes can be connected. The Xrs2 subunit binds to the Mre11 subunits and is essential for nuclear localisation, Tel1 interaction, and stabilising the complex/tethering to DNA (Tsukamoto et al., 2005, Nakada et al., 2003, Oh et al., 2018). Whilst not a permanent part of the MRX complex, phosphorylated Sae2 binds to the MRX complex to promote endonuclease and

resection activity (Cannavo and Cejka, 2014, Huertas et al., 2008). Sae2 doesn't bind to Xrs2 as previously thought (Oh et al., 2016), but in fact binds to Rad50 (the commonly used *rad50S* mutant stops this interaction, hence the phenotype of poor end resection (Alani et al., 1990)) (Cannavo et al., 2018).

Rad50 has ATPase activity which causes a conformational change which drives Mre11 nuclease activity (Hopfner et al., 2001). When MRX is bound to ATP and DNA, the Rad50 head domains dimerise, blocking Mre11's nuclease activity; the complex is in a 'closed' state. When ATP is hydrolysed, the nucleotide binding domains (NBDs) rotate outwards, 'opening' up the complex. This not only allows Mre11 access to the DNA, but it also partially melts the DNA duplex allowing Mre11 nuclease activity for 3′-5′ end resection (Mockel et al., 2012, Liu et al., 2016). Rif2 has been demonstrated to promote ATP hydrolysis and decreased DNA tethering which aids resection, whilst Tel1 can stabilise MRX on the DNA, decreasing resection (Cassani et al., 2016). MRX resection accounts for the short-range end resection, which is around 300nts (Garcia et al., 2011a). The long-range 5′-3′ resection is taken care of by Exo1, which is recruited by the MRX complex (Gobbini et al., 2018).

Exo1 is a Rad2/XPG family exonuclease which resects DNA in a 5′-3′ direction, leaving a long 3′ ssDNA tail (Tran et al., 2002). The average resection length in meiotic recombination is around 800nts, which is far shorter than mitotic resection lengths (~3kb) (Zhu et al., 2008) . The process of Spo11 removal is summarised in **Figure 1-13**.

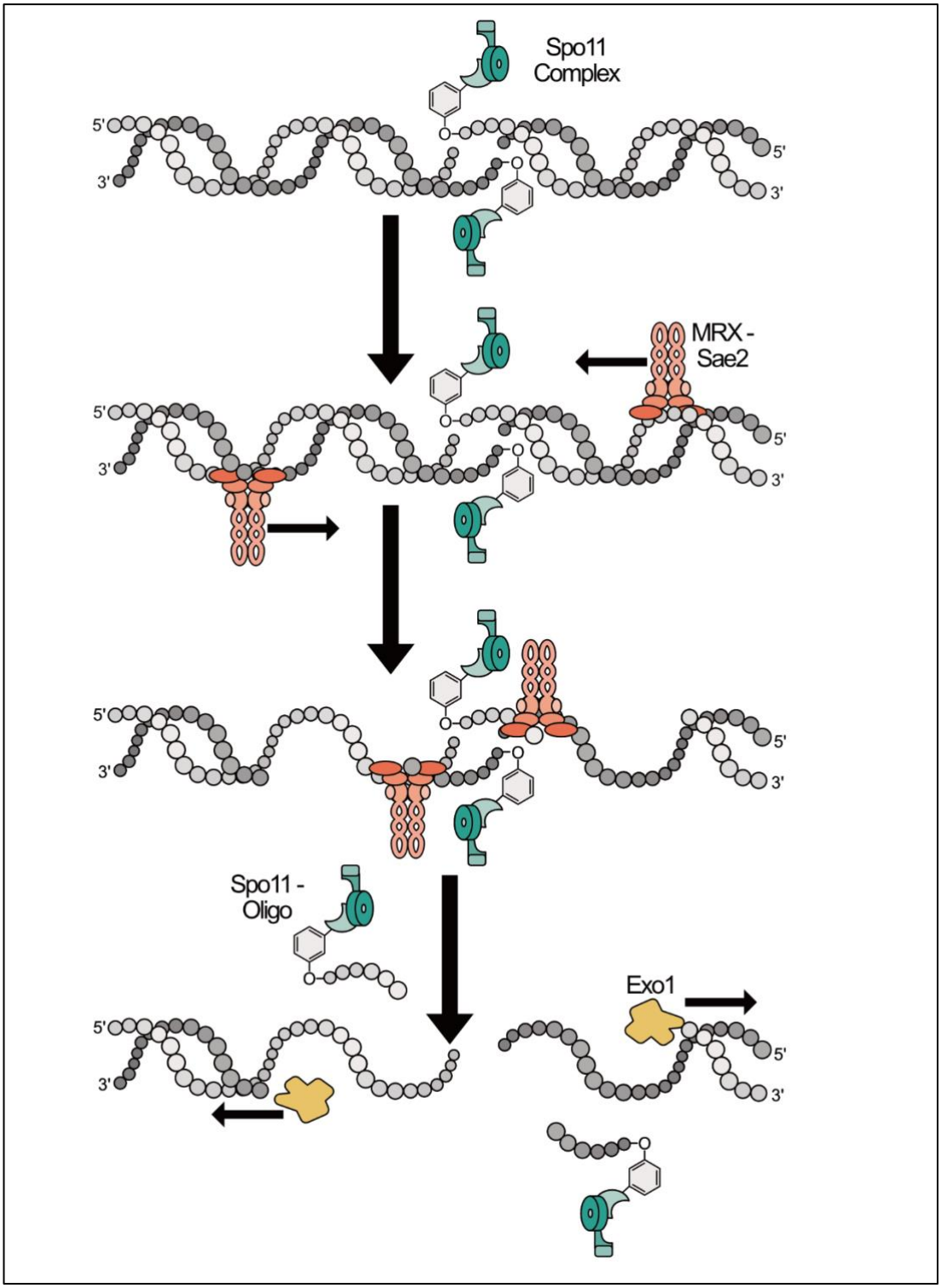

Figure 1-13 Spo11 removal and 5′-end resection during meiosis. Spo11 complexes are bound to the DNA. Then the MRX-Sae2 complex binds and resects the DNA in a 3′-5′ direction towards the Spo11. This releases the Spo11 and allows Exo1 to be loaded for long-range 5′-3′ end resection, generating a 3′-ssDNa tail.

1.3.7 Checkpoint Proteins in Meiosis

As with vegetative cell, the DSB checkpoint proteins Mec1 and Tel1 play an active role to repair Spo11-induced DSBs. Unlike with vegetative cells, Rad9 is insensitive to Spo11 induced breaks, meaning that Rad53 signalling isn't active during meiosis (Usui and Shinohara, 2021). Without Mec1, the frequency of meiotic recombination is reduced, highlighting the important role played by these kinases during meiosis (Kato and H., 1994). As described earlier (section **1.2.2**), Mec1 helps to load the 911 clamp to DSB sites, which prevents prophase I exit until the DSBs have been repaired (Majka and Burgers, 2003). Interestingly, when the 911 clamp is disrupted with *rad17Δ* along with the recombinase deficient *dmc1Δ*, the cellular arrest can be bypassed to allow MI division regardless of DNA recombination status (Hepworth et al., 1998).

An early target for Mec1/Tel1 is Rec114. Phosphorylated Rec114 has a weaker interaction to DNA at DSB hotspots. This means that it isn't able to recruit Spo11 to make DSBs, meaning that Mec1/Tel1 prevent excessive DSB formation and localisation (Carballo et al., 2013). Mec1 and Tel1 are also able to phosphorylate Sae2, which is required for MRX nuclease function during meiosis. Without this phosphorylation event, end resection does not occur (Terasawa et al., 2008). Another essential Mec1/Tel1 phosphorylation target is the axial element protein Hop1. In phosphorylating Hop1, Mek1 subsequently dimerises and becomes activated (Terasawa et al., 2008, Niu et al., 2005). Mek1 is a paralogue of Rad53 and is considered the 'master regulator' of promoting homolog repair bias during meiosis (Hollingsworth, 2016). The SC protein Zip1 is able to be phosphorylated by Mec1 in order to weaken centromeric pairing between non-homologous chromosomes, thus aiding the homology search. This ties together chromosome dynamics with DSB repair in meiosis (Falk et al., 2010). Mec1 is also able to inhibit Ndt80 as a way to promote DSBs being generated without exiting Prophase I prematurely (Gray et al., 2013).

As well as Mec1/Tel1, the Cdc28 and Cdc7-Dbf4 kinase (DDK) are both kinases with an important meiotic role. Cdc28, when activated by the cyclin Clb5, phosphorylates Mer2. This is then followed-up by DDK also phosphorylating Mer2, which allows Mer2 to

interact with Spp1 to help the RMM complex bring the DSB machinery to the axes (Wan et al., 2008).

1.3.8 Meiotic Recombinases: Rad51 and Dmc1

As the DSB now has now been fully resected leaving a long 3′ ssDNA tail, recombination can occur with the help of the RecA recombinase homologs Rad51 and Dmc1 (reviewed here (Brown and Bishop, 2014)). These proteins use the single strand to match the sequence to a homologous sequence (homology search) which then invades the homologous sequence in a process called single end invasion (SEI) to form a displacement loop (D-loop) (Hunter and Kleckner, 2001). Before the recombinases can act, the ssDNA is coated with the heterotrimeric Replication Protein A (RPA) to form an nucleoprotein filament (Brill and Stillman, 1991). This stage protects the ssDNA from forming secondary structure as well as preventing unwanted protein-DNA interactions (Kim et al., 1992).

Rad51 can bind to both ssDNA and dsDNA. Although it has ATPase activity it doesn't need to hydrolyse ATP for D-loop formation (Sung and Stratton, 1996). It displaces RPA on ssDNA more efficiently with the help of Rad52 (Sugiyama and Kowalczykowski, 2002, Shi et al., 2009). The Rad55-Rad57 heterodimer can help Rad51 to displace RPA too, whilst also protecting the Rad51-ssDNA nucleoprotein filament from anti-recombination helicases such as Srs2 (Sung, 1997, Liu et al., 2011). Rad54 helps Rad51 to form D-loops, though it shows a preference for forming crossovers with sister chromatids rather than homologs (Niu et al., 2009). Whilst Rad51 is essential for mitotic recombination, Rad51 is not the active meiotic recombinase; instead it plays a Dmc1-supporting role during meiotic recombination (Cloud et al., 2012). Rad52 has also been implicated in aiding homology pairing during meiotic recombination (Joo et al., 2024).

Dmc1 is the meiosis specific recombinase which is essential for recombination between homologs to occur (Bishop et al., 1992). Unlike Rad51 which can only stabilise complementary strands, Dmc1 is able to stabilise mismatched triplets. This enables Dmc1 to form a D-loop between homologs which have similar, though not identical, sequences rather than sisters which are identical (Lee et al., 2015). Without Dmc1, the cells arrest in prophase I with accumulated DSBs due in part to the inactivation of the pachytene-exit transcription

factor Ndt80 (Tung and Roeder, 1998). Much like Rad51, Dmc1 can bind ssDNA and dsDNA with ATP-binding, not hydrolysis, being essential for strand exchange (Hong et al., 2001). Dmc1 has been demonstrated to co-occupy ssDNA ends with Rad51, highlighting Rad51's supporting role in meiotic recombination (Brown et al., 2015). The Mei5-Sae3 complex help mediate the displacement of RPA by Dmc1 on ssDNA, which improves Dmc1 loading onto ssDNA by up to 9-fold (Ferrari et al., 2009, Hayase et al., 2004). The Hop2-Mnd1 dimer helps to facilitate Dmc1's homology search and D-loop formation by up to 30-fold; this is accomplished by binding to dsDNA, condensing it, then binding to Dmc1 to bring them together (Pezza et al., 2010, Chan et al., 2014). Rdh54 (also called Tid1) is an ATP-dependent translocase which can help Dmc1 to form JMs between homologs, therefore promoting crossovers. Rdh54 achieves this by catalysing strand pairing whilst also stabilising D-loops (Prasad et al., 2007, Nimonkar et al., 2012, Chan et al., 2019). Furthermore, *rdh54Δ* strains show defects in CO formation (Shinohara et al., 2003b). Dmc1-catalysed strand invasion is shown in **Figure 1-14**.

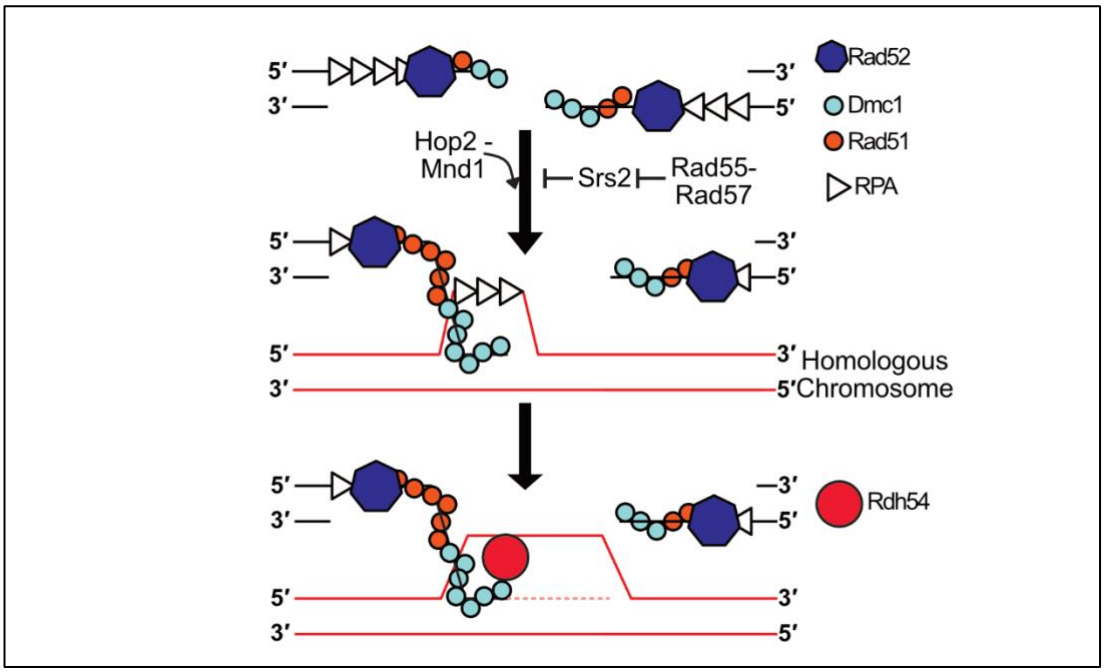

Figure 1-14 Dmc1-catalysed strand invasion. Dmc1 and Rad51 bind to the resected DNA end with the help of Rad52. Dmc1 performs the homology search and strand invasion into the homologous chromosome. Then Rad54 helps to stabilise the D-loop.

1.3.9 Crossover/Non-Crossover Formation

Once SEI has led to the formation of a D-loop, recombination can be resolved as crossover (CO) or non-crossover (NCO) products (reviewed here (Gray and Cohen, 2016)). It is important to balance COs with NCOs, as without crossovers, the JMs won't form which are essential for genetic variability and for accurate meiotic division; however, too many crossovers could sacrifice genomic integrity. NCOs use a short section of the homologous chromosome as a repair template, resulting in gene conversion (GC). Via this method the homologs are only transiently connected and the exchange of genetic material is minimal (Palmer et al., 2003). NCOs are formed by the synthesis dependent strand annealing pathway or the dissolution of a JM (Allers and Lichten, 2001, Cejka et al., 2010). With SDSA, the 3′ ssDNA from the break is repaired using the homologous strand as a template. When the newly synthesised strand matches the sequence of the ssDNA from the opposite end of the DSB, the invasive strand leaves the D-loop and re-anneals to the original strand, repairing the break (Merker et al., 2003).

A CO uses the homologous template for repair, physically linking the chromosomes to form a JM, leading to a recombinant chromosome which is different from either parental strand. COs are formed via a four-way joint DNA molecule called a double Holliday Junction (dHJ) (Allers and Lichten, 2001). To form a dHJ, the second resected end from the DSB also invades the homologous strand, this in a process called second end capture. As the invasive strands are repaired, the HJs move closer to each other until the DSB has been repaired and the dHJ structure is formed. The majority of COs are produced by the 'Type (aka class) I' pathway. Type I COs form dHJs which are stabilised by the ZMM and are evenly spaced out along the chromosome, which is called 'Crossover Interference' (Börner et al., 2004, Wang et al., 2015). The ZMM complex (reviewed here (Pyatnitskaya et al., 2019)) mutants show defects in SC assembly and CO formation (Ross-Macdonald and Roeder, 1994, Shinohara et al., 2008). The ZMM complex is important for stabilising D-loops whilst protecting them from disruptive helicases (discussed below) (Mazina et al., 2004, Duroc et al., 2017), which allows the dHJ structure to form. In order to resolve the dHJ and form recombinant chromatids, the pachytene-exit transcription Ndt80 factor must transcribe Cdc5,

which in-turn helps to promote JM resolution (Sourirajan and Lichten, 2008). In order to resolve JMs and produce COs, the strands must be asymmetrically processed by the MutLγ nuclease homolog (Mlh1-Mlh3) working with Msh4-Msh5 and Exo1 (Zakharyevich et al., 2012, Nishant et al., 2008). Here, Exo1 is only playing a structural role and the MutLγ-Exo1 complex may also be working with Chd1, Rtk1, and Caf120 to efficiently resolve COs (Wild et al., 2019).

Alternatively, 'Type II' COs can form in a ZMM-independent manner by the recruitment of nucleases Mus81-Mms4 (de Los Santos et al., 2003). Here the nucleases can nick the dHJ-intermediate, or a single D-loop, so it is resolved without forming a true dHJ. These COs are minor compared to ZMM mediated 'Type I', though unlike Type I COs they are not subject to CO interference distribution (De Muyt et al., 2012, Zakharyevich et al., 2012) . Other structure selective nucleases, such as Yen1 and Slx1-4 have also been implicated in resolving JMs (De Muyt et al., 2012).

There are a number of different proteins which can promote/prevent the formation of JMs (thereby promoting CO/NCO resolution respectively), as well as whether these JMs are formed as inter sister chromatids (IS-JMs), or as homolog joint molecules (IH-JMs). One such regulator is the STR complex. The STR complex is a heterotrimer formed of Sgs1, the topoisomerase Top3 (De Muyt et al., 2012), and DNA-binding protein Rmi1 (Mullen et al., 2005). The STR complex is able to unwind and decatenate Holliday Junctions which are unprotected by the ZMM complex, this drives the recombination away from dHJ/CO towards dissolution/NCO (Oh et al., 2007, Cejka and Kowalczykowski, 2010, Tang et al., 2015). Sgs1's activity is increased by CDK phosphorylation, decreased by Cdc5 hyperphosphorylation, and may be regulated by the structural maintenance proteins Smc5/6 (Grigaitis et al., 2020, Agashe et al., 2021). Another helicase which can attenuate JM formation is the UvrD-like Srs2 (Veaute et al., 2003). Unlike the STR complex which can unwind and decatenate Holliday Junctions, Srs2 instead prevents JM formation by disrupting Rad51-ssDNA filaments. Srs2 achieves this by triggering Rad51 ATPase activity, causing it to dissociate, which makes them less stable for Dmc1 to utilise effectively (Krejci et al., 2003, Antony et al., 2009). The Rad51-antagonising activity of Srs2 can in-turn be countered

by Rad55-Rad57 dimer or the Shu complex (Shu1, Shu2, Psy3, and Csm2) preventing Srs2-Rad51 binding, thus restoring JM formation (Liu et al., 2011, Bernstein et al., 2011, Sasanuma et al., 2013). Hed1 is a protein which binds to Rad51 and downregulates its recombinase activity by disrupting Rad51-Rad54 binding (Callender et al., 2016). Hed1 activity therefore reduces Rad51's IS-JM formation, shifting the JM bias towards IH-JM via Dmc1 activity (Tsubouchi and Roeder, 2006, Lao et al., 2013). Mek1 (aka Mre4) is a meiosis-specific kinase which has been described as a 'master regulator' of meiosis (Hollingsworth, 2016). Mek1 is able to promote IH-JM bias in a number of different ways. One method Mek1 employs is phosphorylating Rad54; this prevents Rad54 binding to Rad51, which prevents Rad51 IS-JM recombinase activity, moving the bias towards Dmc1's IH-JM formation (Niu et al., 2009). As a belt-and-braces approach to preventing Rad54 aiding Rad51, Mek1 also stabilises Hed1 via phosphorylation, which allows Hed1 to interfere with Rad54-Rad51 binding (Callender et al., 2016) . The formation of meiotic CO/NCOs is shown in **Figure 1-15**.

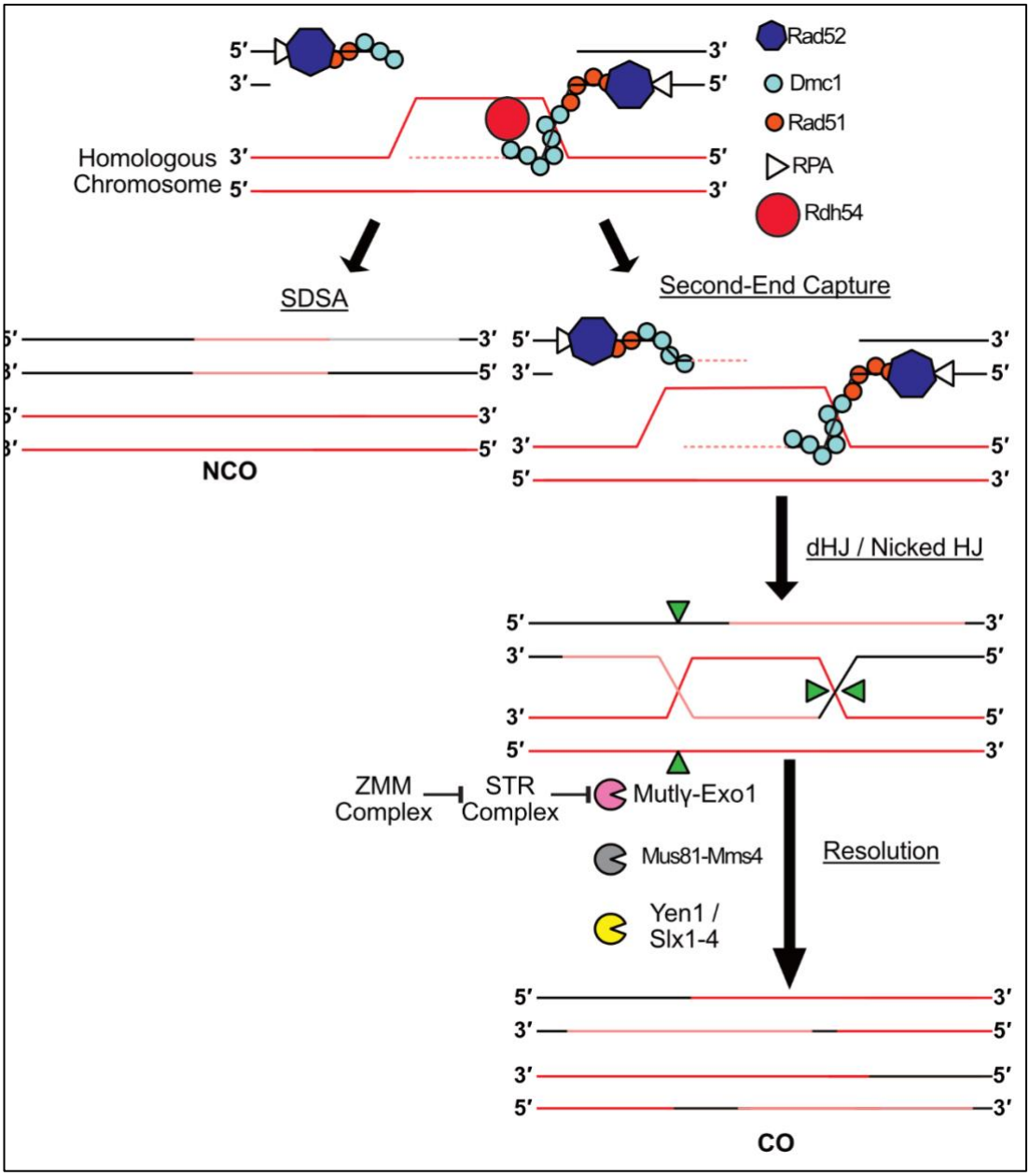

Figure 1-15 Formation of CO / NCO products during meiosis. The D-loop formed by Dmc1 extends as DNA is replicated. This strand can then be displaced and re-join the other-side of the DSB, this is called SDSA. Alternatively, second-end capture can be performed by Dmc1 on the opposite side of the DSB. The D-loops converge to form either a nicked dHJ which can be processed by Mus81-Mms4, or they can form a dHJ which is processed by Mutlγ-Exo1 or Yen1/Slx1/4 to form crossovers. The green arrows represent where strands are asymmetrically processed.

1.4 Aims of the Project

1.4.1 Alternative Removal of Spo11 by Tdp1

When Spo11 catalyses DNA breaks, it remains covalently attached to the 5′ end of the DNA via a phosphotyrosyl bond. As discussed earlier (sections **1.3.5** and **1.3.6**), the MRX-Sae2 complex is responsible for removing Spo11 via nuclease activity, thereby releasing Spo11 with DNA still attached. This pathway has been characterised and understood for decades (Neale et al., 2005). However, there may be alternative pathways which can remove Spo11.

In *C. elegans*, when NHEJ is compromised via *com-1* mutation, meiotic DSBs are formed but remain unrepaired or undergo improper repair. This indicates that NHEJ may be repairing meiotic DSBs but relies on an alternate way of removing Spo11 in order to ligate the ends together (Penkner et al., 2007). Evidence for alternative pathways processing Spo11 has also been seen in *S. cerevisiae.* In 2019, a paper was published which showed that in a *rad50S ku70Δ* background, meiotic recombination products are formed (Yun and Kim, 2019), shown in **Figure 1-16**. This means that when the MRX complex is compromised and NHEJ is also inviable, Spo11 is somehow removed and CO/NCO products are generated. One of the aims of this project is to investigate how Spo11 is removed.

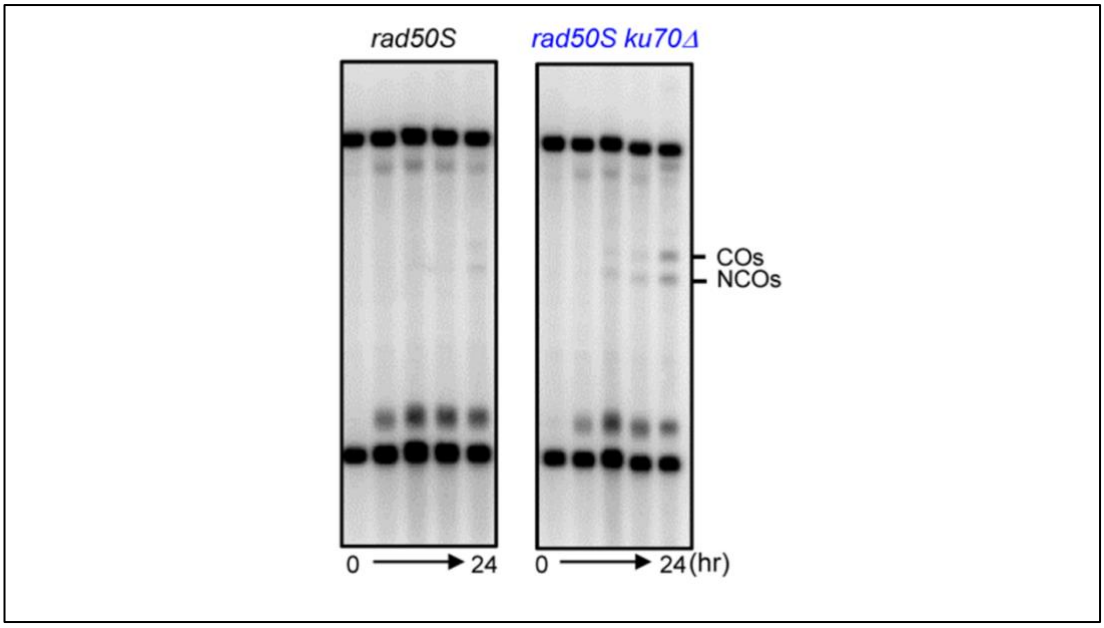

Figure 1-16 CO and NCO products are formed in MRX/NHEJ null mutant strains of *S. cerevisiae.* A restriction digest and Southern blot shows that intermediate-sized bands corresponding to CO/NCO products can be formed when the MRX complex is compromised via *rad50S* and the NHEJ pathway is null due to *ku70Δ*. Figure 4A from Yun and Kim, 2019.

When Spo11 function was first characterised, it was hypothesised that it could be removed nucleolytically or the Spo11 could be removed via hydrolysis (Keeney et al., 1997). Whilst there is ample evidence for the former, it could be possible that Spo11 can be removed by hydrolysis, but that the resulting 2nt-overhang DSB can be bound by the Ku complex for NHEJ repair. Furthermore, this repair pathway wouldn't generate a Spo11-oligo as the tyrosine would be directly released from the phosphate of the DNA backbone. As Spo11 bound to DNA resembles a topoisomerase cleavage complex (TOPcc) (Claeys Bouuaert et al., 2021b), perhaps the phosphodiesterase Tdp1 could be responsible for Spo11 processing.

Topoisomerases exist to alleviate torsional stresses on DNA. This arises when DNA is replicated, transcribed and separated, which can lead to spontaneous breaks. To alleviate this, Topoisomerases can break DNA in a controlled manner by transesterification of the phosphate backbone of DNA using a catalytic tyrosine residue. This allows the relaxation/formation of supercoils, DNA decatenation, and even allow DNA strands to pass

through one another (Pommier et al., 2016). Whilst these DNA breakages are usually transient, sometimes the topoisomerases can get stuck and form a TOPcc. These TOPcc can act as roadblocks to DNA repair/replication machinery, and as such they can be stabilised by anticancer drugs such as camptothecins to help kill cancerous cells (Bjornsti and Kaufmann, 2019). In *S. cerevisiae*, TOPcc complexes can be removed by the protein Tdp1 (Yang et al., 1996).

Tyrosyl DNA phosphodiesterase 1 (Tdp1) is a phospholipase D superfamily protein which is able to remove both 3′-phosphotyrosyl and 5′-phosphotyrosyl links made by type-I and type-II topoisomerases respectively (Pouliot et al., 1999, Nitiss et al., 2006). Tdp1 requires two catalytic histidine residues to hydrolyse phosphotyrosyl-bonds. The first active Histidine is H182, which is required for the initial nucleophilic attack on the phosphotyrosine, whilst the second histidine residue, H432, then acts as a general acid-base to remove Tdp1 from the DNA (Comeaux et al., 2015, Liu et al., 2004, He et al., 2007). This indicates that Tdp1 may be able to remove Spo11 from DNA as it does with 5′-TOPccs. Additionally a study looking at transcription during meiosis showed that *tdp1* is upregulated in an *mre11Δ* background, indicating that Tdp1 can remove Spo11 when the MRX-Sae2 complex is unable to fulfil its duties (Kugou et al., 2007).

This hypothesis is strengthened by recent evidence that human Tdp2 is able to remove *S. cerevisiae*-derived Spo11 oligos *in vitro*, though not *in vivo*. In fact this phosphotyrosyl-link removal by a phosphodiesterase is utilised in ‘closed complex sequencing’ (CC-Seq), which is used to remove Spo11 from oligos so the DNA can be sequenced (Cortes Ledesma et al., 2009, Johnson et al., 2024, Brown et al., 2024).

The first aim of this project is to see whether the phosphodiesterase Tdp1 can remove Spo11 from DNA, thereby allowing CO/NCO products to form during meiosis.

1.4.2 Is the SSA Pathway Generating Ectopic Repair Products During Meiosis?

The second aim of this project addresses how ectopic repair products are generated during meiosis. Ectopic recombination is where recombination occurs at a non-allelic site, which often leads to gross chromosomal rearrangements (GCRs). These ectopic products are seen around 1 % of the time during meiosis, and studies have shown that Mec1, Rad17, and Rad24 all play a role in supressing ectopic-repair formation (Grushcow et al., 1999). Although ectopic recombination has been studied for many years, the exact pathway responsible for generating these products remains elusive. However, a recent study has posited that the single-strand annealing pathway (section **1.2.5.2**) may be generating these ectopic repair products (Allison et al., 2023).

The study in question utilised the *HIS4::LEU2* and *leu2::hisG* loci on CHR III to monitor ectopic repair product formation. The *HIS4::LEU2* sequence is a known hotspot (Cao et al., 1990a) which shares homology with *leu2::hisG*, as such ectopic products can form between the two. These products can be visualised via Southern blotting as they generate acentric/dicentric products with a different molecular weight to the parental strand. They found that in a recombinase-defective strain, i.e. *rad51Δ and dmc1Δ*, these homology-driven ectopic products form. As such, a homology-driven strand-invasion-independent pathway must be responsible. They also saw that in *rad24Δ* strains that more ectopic products are formed. Rad24 plays an essential role in loading the 911 clamp for the DDC pathway to become active. Without Rad24, Mec1 signalling is affected, which disrupts the inter-homolog bias required for meiotic recombination (Carballo et al., 2008). Also, *rad24Δ* strains are associated with increased resection lengths (Shinohara et al., 2003a). Put together, this indicates that a strand-annealing, homology-driven pathway is responsible: perhaps the SSA pathway (Allison et al., 2023).

The second aim of this project centres around investigating whether the SSA pathway is active during meiosis, specifically monitoring the SSA-essential proteins Rad1, Rad10, Rad52, and Rad59 via western blotting.

Chapter 2: Materials and Methods

2.1 Chemicals

2.1.1 Buffers, Solutions, Reagents, and Microbiological Media

Table 2-1 Buffers, solutions, reagents, and microbiological media used in this study. All chemicals from Sigma or Fisher unless otherwise stated.

Media Name	**Composition (in dH_2O unless stated otherwise)**
100 x AAHLTU	1 mg/ml Adenine 1 mg/ml Arginine 1 mg/ml Histidine 1 mg/ml Tryptophan 1 mg/ml Uracil 3mg/ml Leucine
1.5% Agar Plates	1.5 g Agar per 100 ml LB/YPD Media
100 x Denhardt's solution	2% Ficoll 400 2% polyvinyl pyrrolidone (PVP) 360 2% BSA (Fraction V).
gDNA Lysis Buffer	3 % w/v SDS 100 mM EDTA pH 8.1 1 mg/ml Proteinase K
Hyb Solution	5 % w / v Dextran Sulfate 6 x SSPE 1 % SDS
Hyb Wash 1	2 x SSPE 0.2 % SDS
Hyb Wash 2	0.2 x SSPE

	0.2 % SDS
LB Media	10 g/L tryptone 5 g/L (w/v) yeast extract 10 g/L NaCl NaOH to pH 7
PFGE/SB Denaturing Buffer	3 M NaCl 0.4 M NaOH
PFGE LMP agarose mix	1% w / v low-melt-point agarose 125 mM EDTA pH 8 Boil then keep incubated at 55 °C to remain molten.
5 X PFGE/SB Neutralisation Buffer	0.56 M Na_2HPO_4 0.44 M $NaH_2PO_4 \cdot H_2O$
PFGE Solution 1	37.7 mM EDTA pH 8 20 % v / v SCE Buffer 2 % v / v 2-mercaptoethanol 1 mg / ml Zymolyase 20T
PFGE Solution 2	0.45 M EDTA pH 8 20mM Tris pH 8 1 % v / v 2-mercaptoethanol 10 µg / ml RNAse A
PFGE Solution 3	0.25 M EDTA pH 8 20 mM Tris pH 8 1 % Sodium Sarcosyl 1 mg / ml Proteinase K
PFGE Storage Buffer	50 mM EDTA pH 8 50 % v / v Glycerol
PFGE/SB Transfer Buffer	3 M NaCl 8 mM NaOH

Pre-Hyb Solution	6 x SSPE 1 % SDS 5 x Denhardt's Solution
SCE Buffer	1 M Sorbitol 0.1 M Sodium Citrate 60 mM EDTA pH 8 HCl to adjust to pH 7
•2 X SDS Loading Buffer	4% w / v SDS 100mM Tris HCl pH6.8 20% v / v Glycerol 1mM EDTA pH 8 10 % v / v saturated Bromophenol Blue *5 % v / v 2-mercaptoethanol added fresh before each use.
5 x SDS Running Buffer	125 mM Tris base 1.04 M Glycine 1 % w/v SDS
4 X SDS Stacking Mix	0.5 M Tris pH 6.8 0.4 % w / v SDS
Spheroplasting Buffer	1 M Sorbitol 100mM EDTA pH 8.1 100mM Tris HCL pH 7.5
Sporulation Media	2 % w/v Potassium Acetate 1 x AAHLTU
20 X SSPE	3M NaCl 230mM NaH_2PO_4 32mM EDTA NaOH added to reach pH 7.4

STE buffer	0.5 M Tris HCl pH 8.1 10 mM EDTA 2% w / v SDS 1% w / v saturated Bromophenol Blue
5 X TBE	0.9 M Trizma Base 0.9 M Boric Acid 10 mM EDTA pH 8
10 x TBS	200 mM Tris base 1.5 M NaCl HCl to pH 7.6
1 x TBST	10 % v/v 10 x TBS 0.1 % v/v Tween-20
TE Buffer	1 mM EDTA pH 8.0 10mM Tris pH 8.0
1 x Turbo-Blot Transfer Buffer	20 % v/v Turbo-Blot 5 x Transfer Buffer (BioRad) 20 % v/v Ethanol
Yeast Transformation Mix	33 % v/v PEG 3350 100 mM lithium acetate 280 ng/µl ssDNA 2-5 µg/µl insert DNA
YPD + ALU Media	10 g/L yeast extract 20 g/L peptone 20 g/l dextrose 500 µM adenine sulfate 800 µM uracil 1 mM Leucine

2.1.2 Antimicrobials used in this study

Table 2-2 Antimicrobials used in this study. All dissolved in sterile distilled water (SDW).

Antibiotic	**Stock Concentration**	**Working Concentration**
Ampicillin	100 mg/ml	100 µg/ml
G418 (Geneticin)	200 mg/ml	200 µg/ml
Hygromycin	200 mg/ml	200 µg/ml
Kanamycin	10 mg/ml	50 µg/ml
Nourseothricin (Nat)	100 mg/ml	100 µg/ml

2.2 Biological Strains

2.2.1 Yeast strains used in this study

Table 2-3 Strains of *S. cerevisiae* used in this study. All strains are SK1-based unless stated otherwise. All strains marked with † were made for this study; strains labelled SG made by Dr Stephen Gray; strains labelled JB made by Joe Brealey.

Name (YSG 'X')	Strain	Mating Type	Genotype	Source or Reference
3	Wildtype	a	*ho::LYS2, lys2, ura3, arg4-nsp, leu2::hisG, his4X::LEU2, nuc1::LEU2*	SG
4	Wildtype	α	*ho::LYS2, lys2, ura3, arg4-nsp, leu2::hisG, his4X::LEU2, nuc1::LEU2*	SG
5	Wildtype	a/α	*ho::LYS2/', lys2/', ura3/', arg4-nsp/', leu2::hisG/', his4X::LEU2/', nuc1::LEU2/'*	SG
10	*rad24Δ*	a	*ho::LYS2, lys2, ura3, arg4-nsp, leu2::hisG, his4X::LEU2, nuc1::LEU2, rad24Δ::Hyg*	SG
12	*dmc1Δ-rad24Δ*	a	*ho::LYS2, lys2, ura3, arg4-nsp, leu2::hisG, his4X::LEU2, nuc1::LEU2, dmc1Δ::LEU2, rad24Δ::Hyg*	SG
16	Wildtype Nuclease	α	*ho::LYS2, lys2, ura3, arg4-nsp, leu2::hisG, his4X::LEU2-(NgoMIV;+ori)--URA3*	SG
17	Wildtype Nuclease	a	*ho::LYS2, lys2, ura3, arg4-nsp, leu2::hisG, HIS4::LEU2-(BamHI;+ori)*	SG
18	Wildtype Nuclease	α	*ho::LYS2, lys2, ura3, arg4-nsp, leu2::hisG, HIS4::LEU2-(BamHI;+ori)*	SG
19	Wildtype Nuclease	a	*ho::LYS2, lys2, ura3, arg4-nsp, leu2::hisG, his4X::LEU2-(NgoMIV;+ori)--URA3*	SG
29	Wildtype Fluorescent	a	*ho::LYS2, lys2, ura3, leu2::hisG, trp1::hisG, THR1::mCerulean-TRP1*	SG
33	Wildtype Fluorescent	α	*ho::LYS2, lys2, ura3, leu2::hisG, trp1::hisG, THR1::mCerulean-TRP1*	SG
102	*rad24Δ*	α	*ho::LYS2, lys2, ura3, arg4-nsp, leu2::hisG, his4X::LEU2, nuc1::LEU2, rad24Δ::Hyg*	SG
190 / 191	Rad1-His_6-HA_3	a	*ho::LYS2, lys2, ura3, arg4-nsp, leu2::hisG, his4X::LEU2, nuc1::LEU2, RAD1-6xHis-3xHA-KanMX*	†
192 / 193	Rad1-His_6-HA_3	α	*ho::LYS2, lys2, ura3, arg4-nsp, leu2::hisG, his4X::LEU2, nuc1::LEU2, RAD1-6xHis-3xHA-KanMX*	†

Name (YSG 'X')	Strain	Mating Type	Genotype	Source or Reference
194 / 195	Rad1-His_6-HA_3, *rad24Δ*	a	*ho::LYS2, lys2, ura3, arg4-nsp, leu2::hisG, his4X::LEU2, nuc1::LEU2, rad24Δ::Hyg, RAD1-6xHis-3xHA-KanMX*	†
196 / 197	Rad1-His_6-HA_3, *rad24Δ*	α	*ho::LYS2, lys2, ura3, arg4-nsp, leu2::hisG, his4X::LEU2, nuc1::LEU2, rad24Δ::Hyg, RAD1-6xHis-3xHA-KanMX*	†
198 / 199	Rad10-His_6-HA_3	a	*ho::LYS2, lys2, ura3, arg4-nsp, leu2::hisG, his4X::LEU2, nuc1::LEU2, RAD10-6xHis-3xHA-KanMX*	†
200 / 201	Rad10-His_6-HA_3	α	*ho::LYS2, lys2, ura3, arg4-nsp, leu2::hisG, his4X::LEU2, nuc1::LEU2, RAD10-6xHis-3xHA-KanMX*	†
202 / 203	Rad10-His_6-HA_3, *rad24Δ*	a	*ho::LYS2, lys2, ura3, arg4-nsp, leu2::hisG, his4X::LEU2, nuc1::LEU2, rad24Δ::Hyg, RAD10-6xHis-3xHA-KanMX*	†
204 / 205	Rad59-His_6-HA_3	a	*ho::LYS2, lys2, ura3, arg4-nsp, leu2::hisG, his4X::LEU2, nuc1::LEU2, RAD59-6xHis-3xHA-KanMX*	†
206 / 207	Rad59-His_6-HA_3	α	*ho::LYS2, lys2, ura3, arg4-nsp, leu2::hisG, his4X::LEU2, nuc1::LEU2, RAD59-6xHis-3xHA-KanMX*	†
208 / 209	Rad59-His_6-HA_3, *rad24Δ*	a	*ho::LYS2, lys2, ura3, arg4-nsp, leu2::hisG, his4X::LEU2, nuc1::LEU2, rad24Δ::Hyg, RAD59-6xHis-3xHA-KanMX*	†
216	*rad1Δ*	a	*ho::LYS2, lys2, ura3, arg4-nsp, leu2::hisG, his4X::LEU2, nuc1::LEU2, rad1Δ::KanMX*	SG
217	*rad1Δ*	α	*ho::LYS2, lys2, ura3, arg4-nsp, leu2::hisG, his4X::LEU2, nuc1::LEU2, rad1Δ::KanMX*	SG
218	*rad10Δ*	a	*ho::LYS2, lys2, ura3, arg4-nsp, leu2::hisG, his4X::LEU2, nuc1::LEU2, rad10Δ::KanMX*	SG
219	*rad10Δ*	α	*ho::LYS2, lys2, ura3, arg4-nsp, leu2::hisG, his4X::LEU2, nuc1::LEU2, rad10Δ::KanMX*	SG
220 / 221	*rad1Δ*	a / α	*ho::LYS2/', lys2/', ura3/', arg4-nsp/', leu2::hisG/', his4X::LEU2/', nuc1::LEU2/', rad1Δ::KanMX/'*	SG
222	*rad10Δ*	a / α	*ho::LYS2/', lys2/', ura3/', arg4-nsp/', leu2::hisG/', his4X::LEU2/', nuc1::LEU2/', rad10Δ::KanMX/'*	SG
236	Wildtype Fluorescent	a/α	*ho::LYS2/', lys2/', ura3/', leu2::hisG/', trp1::hisG/', THR1::mCerulean-TRP1/THR1, CEN8::tdTomato-LEU2/CEN8*	SG
237	*mlh1Δ* Fluorescent	a/α	*ho::LYS2/', lys2/', ura3/', leu2::hisG/', trp1::hisG/', THR1::mCerulean-TRP1/THR1, CEN8::tdTomato-LEU2/CEN8, mlh1Δ::KanMX/'*	SG
266 / 267	Rad59-His_6-HA_3, *rad24Δ*	α	*ho::LYS2, lys2, ura3, arg4-nsp, leu2::hisG, his4X::LEU2, nuc1::LEU2, rad24Δ::Hyg, RAD59-6xHis-3xHA-KanMX*	†

Name (YSG 'X')	Strain	Mating Type	Genotype	Source or Reference
294 / 295	Rad52-His_6-HA_3	a	*ho::LYS2, lys2, ura3, arg4-nsp, leu2::hisG, his4X::LEU2, nuc1::LEU2, RAD52-6xHis-3xHA-KanMX*	†
296 / 297	Rad52-His_6-HA_3	α	*ho::LYS2, lys2, ura3, arg4-nsp, leu2::hisG, his4X::LEU2, nuc1::LEU2, RAD52-6xHis-3xHA-KanMX*	†
298 / 299	*rad52Δ rad24Δ*	a	*ho::LYS2, lys2, ura3, arg4-nsp, leu2::hisG, his4X::LEU2, nuc1::LEU2, rad24Δ::Hyg, RAD52-6xHis-3xHA-KanMX*	†
300 / 301	Rad52-His_6-HA_3, *rad24Δ*	α	*ho::LYS2, lys2, ura3, arg4-nsp, leu2::hisG, his4X::LEU2, nuc1::LEU2, rad24Δ::Hyg, RAD52-6xHis-3xHA-KanMX*	†
302 / 303	*rad52Δ*	a	*ho::LYS2, lys2, ura3, arg4-nsp, leu2::hisG, his4X::LEU2, nuc1::LEU2, rad52Δ::KanMX*	†
304 / 305	*rad52Δ*	α	*ho::LYS2, lys2, ura3, arg4-nsp, leu2::hisG, his4X::LEU2, nuc1::LEU2, rad52Δ::KanMX*	†
306 / 307	*rad52Δ, rad24Δ*	a	*ho::LYS2, lys2, ura3, arg4-nsp, leu2::hisG, his4X::LEU2, nuc1::LEU2, rad24Δ::Hyg, rad52Δ::KanMX*	†
308	Rad52(R37K)-His_6-HA_3	a	*ho::LYS2, lys2, ura3, arg4-nsp, leu2::hisG, his4X::LEU2, nuc1::LEU2, RAD52 (R37K)-6xHis-3xHA-KanMX*	†
309	Rad59(F180A)-His_6-HA_3	a	*ho::LYS2, lys2, ura3, arg4-nsp, leu2::hisG, his4X::LEU2, nuc1::LEU2, RAD59 (F180A)-6xHis-3xHA-KanMX*	†
310	Rad59(F180A)-His_6-HA_3	α	*ho::LYS2, lys2, ura3, arg4-nsp, leu2::hisG, his4X::LEU2, nuc1::LEU2, RAD59 (F180A)-6xHis-3xHA-KanMX*	†
311	Rad59(F180A)-His_6-HA_3, *rad24Δ*	a	*ho::LYS2, lys2, ura3, arg4-nsp, leu2::hisG, his4X::LEU2, nuc1::LEU2, rad24Δ::Hyg, RAD59 (F180A)-6xHis-3xHA-KanMX*	†
312	Rad1(D825A)-His_6-HA_3	α	*ho::LYS2, lys2, ura3, arg4-nsp, leu2::hisG, his4X::LEU2, nuc1::LEU2, RAD1 (D825A)-6xHis-3xHA-KanMX*	†
313	Rad1(D825A)-His_6-HA_3, *rad24Δ*	a	*ho::LYS2, lys2, ura3, arg4-nsp, leu2::hisG, his4X::LEU2, nuc1::LEU2, rad24Δ::Hyg, RAD1 (D825A)-6xHis-3xHA-KanMX*	†
314	Rad1(S1071A)-His_6-HA_3	a	*ho::LYS2, lys2, ura3, arg4-nsp, leu2::hisG, his4X::LEU2, nuc1::LEU2, RAD1 (S1071A)-6xHis-3xHA-KanMX*	†
315	Rad1(S1071A)-His_6-HA_3	α	*ho::LYS2, lys2, ura3, arg4-nsp, leu2::hisG, his4X::LEU2, nuc1::LEU2, RAD1 (S1071A)-6xHis-3xHA-KanMX*	†
316	Rad1(S1071A)-His_6- HA_3, *rad24Δ*	a	*ho::LYS2, lys2, ura3, arg4-nsp, leu2::hisG, his4X::LEU2, nuc1::LEU2, rad24Δ::Hyg, RAD1 (S1071A)-6xHis-3xHA-KanMX*	†

Name (YSG 'X')	Strain	Mating Type	Genotype	Source or Reference
317	Rad1(S1071D)-His_6-HA_3	a	*ho::LYS2, lys2, ura3, arg4-nsp, leu2::hisG, his4X::LEU2, nuc1::LEU2, RAD1 (S1071D)-6xHis-3xHA-KanMX*	†
318	Rad1(S1071D)-His_6-HA_3	α	*ho::LYS2, lys2, ura3, arg4-nsp, leu2::hisG, his4X::LEU2, nuc1::LEU2, RAD1 (S1071D)-6xHis-3xHA-KanMX*	†
319	Rad1(S1071D)-His_6- HA_3, *rad24Δ*	a	*ho::LYS2, lys2, ura3, arg4-nsp, leu2::hisG, his4X::LEU2, nuc1::LEU2, rad24Δ::Hyg, RAD1 (S1071D)-6xHis-3xHA-KanMX*	†
320	Rad1(S1071D)-His_6- HA_3, *rad24Δ*	a	*ho::LYS2, lys2, ura3, arg4-nsp, leu2::hisG, his4X::LEU2, nuc1::LEU2, RAD1 (T1072A)-6xHis-3xHA-KanMX*	†
321	Rad1(T1072A)-His_6- HA_3, *rad24Δ*	a	*ho::LYS2, lys2, ura3, arg4-nsp, leu2::hisG, his4X::LEU2, nuc1::LEU2, rad24Δ::Hyg, RAD1 (T1072A)-6xHis-3xHA-KanMX*	†
322	Rad1(T1072D)-His_6- HA_3	a	*ho::LYS2, lys2, ura3, arg4-nsp, leu2::hisG, his4X::LEU2, nuc1::LEU2, RAD1 (T1072D)-6xHis-3xHA-KanMX*	†
323	Rad1(T1072D)-His_6- HA_3	α	*ho::LYS2, lys2, ura3, arg4-nsp, leu2::hisG, his4X::LEU2, nuc1::LEU2, RAD1 (T1072D)-6xHis-3xHA-KanMX*	†
324	Rad1(T1072D)-His_6- HA_3, *rad24Δ*	a	*ho::LYS2, lys2, ura3, arg4-nsp, leu2::hisG, his4X::LEU2, nuc1::LEU2, rad24Δ::Hyg, RAD1 (T1072D)-6xHis-3xHA-KanMX*	†
325 - 327	Rad1-His_6-HA_3, *rad24Δ, dmc1Δ*	α	*ho::LYS2, lys2, ura3, arg4-nsp, leu2::hisG, his4X::LEU2, nuc1::LEU2, dmc1Δ::LEU2, rad24Δ::Hyg RAD1-6xHis-3xHA-KanMX*	†
328 / 329	Rad10-His_6-HA_3, *rad24Δ, dmc1Δ*	α	*ho::LYS2, lys2, ura3, arg4-nsp, leu2::hisG, his4X::LEU2, nuc1::LEU2, dmc1Δ::LEU2, rad24Δ::Hyg RAD10-6xHis-3xHA-KanMX*	†
330 / 331	*rad24Δ*	a / α	*ho::LYS2/', lys2/', ura3/', arg4-nsp/', leu2::hisG/', his4X::LEU2/', nuc1::LEU2/', rad24Δ::HYG/'*	†
472	Rad1-His_6-HA_3, *rad24Δ, dmc1Δ*	a	*ho::LYS2, lys2, ura3, arg4-nsp, leu2::hisG, his4X::LEU2, nuc1::LEU2, dmc1Δ::LEU2, rad24Δ::Hyg RAD1-6xHis-3xHA-KanMX*	†
473 - 475	Rad10-His_6-HA_3, *rad24Δ, dmc1Δ*	a	*ho::LYS2, lys2, ura3, arg4-nsp, leu2::hisG, his4X::LEU2, nuc1::LEU2, dmc1Δ::LEU2, rad24Δ::Hyg RAD10-6xHis-3xHA-KanMX*	†
476 - 478	Rad52-His_6-HA_3, *rad24Δ, dmc1Δ*	α	*ho::LYS2, lys2, ura3, arg4-nsp, leu2::hisG, his4X::LEU2, nuc1::LEU2, dmc1Δ::LEU2, rad24Δ::Hyg RAD52-6xHis-3xHA-KanMX*	†
479 / 480	Rad52-His_6-HA_3, *rad24Δ, dmc1Δ*	a	*ho::LYS2, lys2, ura3, arg4-nsp, leu2::hisG, his4X::LEU2, nuc1::LEU2, dmc1Δ::LEU2, rad24Δ::Hyg RAD52-6xHis-3xHA-KanMX*	†
481 - 483	Rad59-His_6-HA_3, *rad24Δ, dmc1Δ*	α	*ho::LYS2, lys2, ura3, arg4-nsp, leu2::hisG, his4X::LEU2, nuc1::LEU2, dmc1Δ::LEU2, rad24Δ::Hyg RAD59-6xHis-3xHA-KanMX*	†

Name (YSG 'X')	Strain	Mating Type	Genotype	Source or Reference
484 / 485	Rad59-His_6-HA_3, *rad24Δ, dmc1Δ*	a	*ho::LYS2, lys2, ura3, arg4-nsp, leu2::hisG, his4X::LEU2, nuc1::LEU2, dmc1Δ::LEU2, rad24Δ::Hyg RAD59-6xHis-3xHA-KanMX*	†
486 / 487	Rad10-His_6-HA_3, *rad24Δ*	α	*ho::LYS2, lys2, ura3, arg4-nsp, leu2::hisG, his4X::LEU2, nuc1::LEU2, rad24Δ::Hyg, RAD10-6xHis-3xHA-KanMX*	†
488 / 489	*rad52Δ, rad24Δ*	α	*ho::LYS2, lys2, ura3, arg4-nsp, leu2::hisG, his4X::LEU2, nuc1::LEU2, rad24Δ::Hyg, rad52Δ::KanMX*	†
490 / 491	*rad1Δ, rad24Δ*	a	*ho::LYS2, lys2, ura3, arg4-nsp, leu2::hisG, his4X::LEU2, nuc1::LEU2, rad24Δ::Hyg, rad1Δ::KanMX*	†
492 / 493	*rad1Δ, rad24Δ*	a	*ho::LYS2, lys2, ura3, arg4-nsp, leu2::hisG, his4X::LEU2, nuc1::LEU2, rad24Δ::Hyg, rad1Δ::KanMX*	†
494 / 495	*rad10Δ, rad24Δ*	a	*ho::LYS2, lys2, ura3, arg4-nsp, leu2::hisG, his4X::LEU2, nuc1::LEU2, rad24Δ::Hyg, rad10Δ::KanMX*	†
496 / 497	*rad10Δ, rad24Δ*	α	*ho::LYS2, lys2, ura3, arg4-nsp, leu2::hisG, his4X::LEU2, nuc1::LEU2, rad24Δ::Hyg, rad10Δ::KanMX*	†
505 - 508	*rad24Δ*	a / α	*ho::LYS2/', lys2/', ura3/', arg4-nsp/', leu2::hisG/', his4X::LEU2/', nuc1::LEU2/', rad24Δ::Hyg/'*	†
536	*mus81Δ* Fluorescent	a	*ho::LYS2, lys2, ura3, leu2::hisG, trp1::hisG, THR1::mCerulean-TRP1, mus81Δ::KanMX*	JB / SG
537 - 538	*pms1Δ* Fluorescent	a	*ho::LYS2, lys2, ura3, leu2::hisG, trp1::hisG, THR1::mCerulean-TRP1, pms1Δ::KanMX*	JB / SG
540	*slx4Δ* Fluorescent	a	*ho::LYS2, lys2, ura3, leu2::hisG, trp1::hisG, THR1::mCerulean-TRP1, slx4Δ::KanMX*	JB / SG
541	*tdp1Δ* Fluorescent	a	*ho::LYS2, lys2, ura3, leu2::hisG, trp1::hisG, THR1::mCerulean-TRP1, tdp1Δ::KanMX*	JB / SG
542	*yen1Δ* Fluorescent	a	*ho::LYS2, lys2, ura3, leu2::hisG, trp1::hisG, THR1::mCerulean-TRP1, yen1Δ::KanMX*	JB / SG
543 / 544	*ku70Δ* Fluorescent	α	*ho::LYS2, lys2, ura3, leu2::hisG, trp1::hisG, CEN8::tdTomato-LEU2, ku70Δ::NatMX*	JB / SG
545	*ku70Δ, sae2Δ* Fluorescent	α	*ho::LYS2, lys2, ura3, leu2::hisG, trp1::hisG, CEN8::tdTomato-LEU2, ku70Δ::NatMX, sae2Δ::KanMX*	JB / SG
546 / 547	Tdp1-His_6-HA_3	a	*ho::LYS2, lys2, ura3, arg4-nsp, leu2::hisG, his4X::LEU2, nuc1::LEU2, 6xHis-3xHA-TDP1::KanMX*	JB / SG
548 / 549	Tdp1-His_6-HA_3	α	*ho::LYS2, lys2, ura3, arg4-nsp, leu2::hisG, his4X::LEU2, nuc1::LEU2, 6xHis-3xHA-TDP1::KanMX*	JB / SG
550 / 551	Tdp1-His_6-HA_3 Fluorescent	a	*ho::LYS2, lys2, ura3, leu2::hisG, trp1::hisG, THR1::mCerulean-TRP1, 6xHis-3xHA-TDP1::KanMX*	JB / SG

Name (YSG 'X')	Strain	Mating Type	Genotype	Source or Reference
552 / 553	Tdp1-His_6-HA_3 Fluorescent	α	*ho::LYS2, lys2, ura3, leu2::hisG, trp1::hisG, THR1::mCerulean-TRP1, 6xHis-3xHA-TDP1::KanMX*	JB / SG
554 - 557	*ku70Δ, sae2Δ, tdp1Δ* Fluorescent	a / α	*ho::LYS2/', lys2/', ura3/', leu2::hisG/', trp1::hisG/', THR1::mCerulean-TRP1/THR1, CEN8::tdTomato-LEU2/CEN8, ku70Δ::NatXM/', sae2Δ::KanMX/', tdp1Δ::KanMX/'*	JB / SG
558	*ku70Δ, sae2Δ, tdp1Δ* Fluorescent	α	*ho::LYS2, lys2, ura3, leu2::hisG, trp1::hisG, THR1::mCerulean-TRP1, ku70Δ::NatXM, sae2Δ::KanMX, tdp1Δ::KanMX*	JB / SG
559	*ku70Δ, sae2Δ, tdp1Δ* Fluorescent	a	*ho::LYS2, lys2, ura3, leu2::hisG, trp1::hisG, THR1::mCerulean-TRP1, ku70Δ::NatXM, sae2Δ::KanMX, tdp1Δ::KanMX*	JB / SG
564	*ku70Δ* Fluorescent	a	*ho::LYS2, lys2, ura3, leu2::hisG, trp1::hisG, CEN8::tdTomato-LEU2, ku70Δ::NatXM*	JB / SG
565	*ku70Δ* Fluorescent	α	*ho::LYS2, lys2, ura3, leu2::hisG, trp1::hisG, THR1::mCerulean-TRP1, ku70Δ::NatXM*	JB / SG
566 - 568	*ku70Δ* Fluorescent	a / α	*ho::LYS2/', lys2/', ura3/', leu2::hisG/', trp1::hisG/', THR1::mCerulean-TRP1/THR1, CEN8::tdTomato-LEU2/CEN8, ku70Δ::NatXM/'*	JB / SG
569	*sae2Δ* Fluorescent	a	*ho::LYS2, lys2, ura3, leu2::hisG, trp1::hisG, THR1::mCerulean-TRP1, sae2Δ::KanMX*	JB / SG
570	*sae2Δ* Fluorescent	α	*ho::LYS2, lys2, ura3, leu2::hisG, trp1::hisG, CEN8::tdTomato-LEU2, sae2Δ::KanMX*	JB / SG
571	*sae2Δ* Fluorescent	a / α	*ho::LYS2/', lys2/', ura3/', leu2::hisG/', trp1::hisG/', THR1::mCerulean-TRP1/THR1, CEN8::tdTomato-LEU2/CEN8, sae2Δ::KanMX/'*	JB / SG
572	*ku70Δ, sae2Δ* Fluorescent	a	*ho::LYS2, lys2, ura3, leu2::hisG, trp1::hisG, CEN8::tdTomato-LEU2, ku70Δ::NatXM, sae2Δ::KanMX*	JB / SG
573	*ku70Δ, sae2Δ* Fluorescent	α	*ho::LYS2, lys2, ura3, leu2::hisG, trp1::hisG, THR1::mCerulean-TRP1, ku70Δ::NatXM, sae2Δ::KanMX*	JB / SG
574 - 576	*ku70Δ, sae2Δ* Fluorescent	a / α	*ho::LYS2/', lys2/', ura3/', leu2::hisG/', trp1::hisG/', THR1::mCerulean-TRP1/THR1, CEN8::tdTomato-LEU2/CEN8, ku70Δ::NatXM/', sae2Δ::KanMX/'*	JB / SG
577	*tdp1Δ* Fluorescent	a	*ho::LYS2, lys2, ura3, leu2::hisG, trp1::hisG, THR1::mCerulean-TRP1, tdp1Δ::KanMX*	JB / SG
578	*tdp1Δ* Fluorescent	α	*ho::LYS2, lys2, ura3, leu2::hisG, trp1::hisG, CEN8::tdTomato-LEU2, tdp1Δ::KanMX*	JB / SG
579 / 580	*tdp1Δ* Fluorescent	a / α	*ho::LYS2/', lys2/', ura3/', leu2::hisG/', trp1::hisG/', THR1::mCerulean-TRP1/THR1, CEN8::tdTomato-LEU2/CEN8, tdp1Δ::KanMX/'*	JB / SG
589	*mlh1Δ, ku70Δ, sae2Δ* Fluorescent	a	*ho::LYS2, lys2, ura3, leu2::hisG, trp1::hisG, CEN8::tdTomato-LEU2, ku70Δ::NatXM, sae2Δ::KanMX, mlh1Δ::KanMX*	JB / SG
590	*mus81Δ, ku70Δ, sae2Δ* Fluorescent	a	*ho::LYS2, lys2, ura3, leu2::hisG, trp1::hisG, CEN8::tdTomato-LEU2, ku70Δ::NatXM, sae2Δ::KanMX, mus81Δ::KanMX*	JB / SG

Name (YSG 'X')	Strain	Mating Type	Genotype	Source or Reference
591	*mus81Δ, ku70Δ, sae2Δ* Fluorescent	α	*ho::LYS2, lys2, ura3, leu2::hisG, trp1::hisG, THR1::mCerulean-TRP1, ku70Δ::NatXM, sae2Δ::KanMX, mus81Δ::KanMX*	JB / SG
592	*slx4Δ, ku70Δ, sae2Δ* Fluorescent	a	*ho::LYS2, lys2, ura3, leu2::hisG, trp1::hisG, THR1::mCerulean-TRP1, ku70Δ::NatXM, sae2Δ::KanMX, slx4Δ::KanMX*	JB / SG
599 / 600	*rad59Δ*	a	*ho::LYS2, lys2, ura3, arg4-nsp, leu2::hisG, his4X::LEU2, nuc1::LEU2, rad59Δ::KanMX*	†
601 / 602	*rad59Δ*	α	*ho::LYS2, lys2, ura3, arg4-nsp, leu2::hisG, his4X::LEU2, nuc1::LEU2, rad59Δ::KanMX*	†
603 / 604	*rad59Δ, rad24Δ*	a	*ho::LYS2, lys2, ura3, arg4-nsp, leu2::hisG, his4X::LEU2, nuc1::LEU2, rad24Δ::Hyg, rad59Δ::KanMX*	†
605 / 606	*rad59Δ, rad24Δ*	α	*ho::LYS2, lys2, ura3, arg4-nsp, leu2::hisG, his4X::LEU2, nuc1::LEU2, rad24Δ::Hyg, rad59Δ::KanMX*	†
607 / 608	Rad10-His_6-HA_3	a / α	*ho::LYS2/', lys2/', ura3/', arg4-nsp/', leu2::hisG/', his4X::LEU2/', nuc1::LEU2/', RAD10-6xHis-3xHA-KanMX/'*	†
609 / 610	*rad59Δ*	a / α	*ho::LYS2/', lys2/', ura3/', arg4-nsp/', leu2::hisG/', his4X::LEU2/', nuc1::LEU2/', rad59Δ::KanMX/'*	†
611	*rad52Δ*	a / α	*ho::LYS2/', lys2/', ura3/', arg4-nsp/', leu2::hisG/', his4X::LEU2/', nuc1::LEU2/', rad52Δ::KanMX/'*	†
612 - 614	*rad10Δ, rad24Δ*	a / α	*ho::LYS2/', lys2/', ura3/', arg4-nsp/', leu2::hisG/', his4X::LEU2/', nuc1::LEU2/', rad24Δ::Hyg/', rad10Δ::KanMX/'*	†
615 - 617	Rad1-His_6-HA_3, *rad24Δ*	a / α	*ho::LYS2/', lys2/', ura3/', arg4-nsp/', leu2::hisG/', his4X::LEU2/', nuc1::LEU2/', rad24Δ::Hyg/', RAD1-6xHis-3xHA-KanMX/'*	†
618 - 620	Rad59-His_6-HA_3, *rad24Δ*	a / α	*ho::LYS2/', lys2/', ura3/', arg4-nsp/', leu2::hisG/', his4X::LEU2/', nuc1::LEU2/', rad24Δ::Hyg/', RAD59-6xHis-3xHA-KanMX/'*	†
621 / 622	Rad52-His_6-HA_3, *rad24Δ*	a / α	*ho::LYS2/', lys2/', ura3/', arg4-nsp/', leu2::hisG/', his4X::LEU2/', nuc1::LEU2/', rad24Δ::Hyg/', RAD52-6xHis-3xHA-KanMX/'*	†
623 - 625	*rad1Δ, rad24Δ*	a / α	*ho::LYS2/', lys2/', ura3/', arg4-nsp/', leu2::hisG/', his4X::LEU2/', nuc1::LEU2/', rad24Δ::Hyg/', rad1Δ::KanMX/'*	†
626	*rad52Δ, rad24Δ*	a / α	*ho::LYS2/', lys2/', ura3/', arg4-nsp/', leu2::hisG/', his4X::LEU2/', nuc1::LEU2/', rad24Δ::Hyg/', rad52Δ::KanMX/'*	†
627 - 629	*rad59Δ, rad24Δ*	a / α	*ho::LYS2/', lys2/', ura3/', arg4-nsp/', leu2::hisG/', his4X::LEU2/', nuc1::LEU2/', rad24Δ::Hyg/', rad59Δ::KanMX/'*	†
630 - 632	Rad1-His_6-HA_3	a / α	*ho::LYS2/', lys2/', ura3/', arg4-nsp/', leu2::hisG/', his4X::LEU2/', nuc1::LEU2/', RAD1-6xHis-3xHA-KanMX/'*	†

Name (YSG 'X')	Strain	Mating Type	Genotype	Source or Reference
633 - 635	Rad10-His_6-HA_3, *rad24Δ*	a / α	*ho::LYS2/', lys2/', ura3/', arg4-nsp/', leu2::hisG/', his4X::LEU2/', nuc1::LEU2/', rad24Δ::Hyg/', RAD10-6xHis-3xHA-KanMX/'*	†
636 - 638	Rad59-His_6-HA_3	a / α	*ho::LYS2/', lys2/', ura3/', arg4-nsp/', leu2::hisG/', his4X::LEU2/', nuc1::LEU2/', RAD59-6xHis-3xHA-KanMX/'*	†
639 / 640	*ku70Δ* Nuclease	α	*ho::LYS2, lys2, ura3, arg4-nsp, leu2::hisG, his4X::LEU2-(NgoMIV;+ori)--URA3, ku70Δ::NatMX*	†
641 / 642	*ku70Δ* Nuclease	a	*ho::LYS2, lys2, ura3, arg4-nsp, leu2::hisG, HIS4::LEU2-(BamHI;+ori), ku70Δ::NatMX*	†
643 / 644	*sae2Δ* Nuclease	α	*ho::LYS2, lys2, ura3, arg4-nsp, leu2::hisG, his4X::LEU2-(NgoMIV;+ori)--URA3, sae2Δ::KanMX*	†
645 / 646	*sae2Δ* Nuclease	a	*ho::LYS2, lys2, ura3, arg4-nsp, leu2::hisG, HIS4::LEU2-(BamHI;+ori), sae2Δ::KanMX*	†
689 / 690 / 712	*ku70Δ* Nuclease	a / α	*ho::LYS2/', lys2/', ura3/', arg4-nsp/', leu2::hisG/',HIS4::LEU2-(BamHI;+ori), his4X::LEU2-(NgoMIV;+ori)--URA3, ku70Δ::NatMX/'*	†
691 - 693	*sae2Δ* Nuclease	a / α	*ho::LYS2/', lys2/', ura3/', arg4-nsp/', leu2::hisG/',HIS4::LEU2-(BamHI;+ori), his4X::LEU2-(NgoMIV;+ori)--URA3, sae2Δ::KanMX/'*	†
694 / 695	*ku70Δ* Nuclease	α	*ho::LYS2, lys2, ura3, arg4-nsp, leu2::hisG, HIS4::LEU2-(BamHI;+ori), ku70Δ::NatMX*	†
696 / 697	*ku70Δ* Nuclease	a	*ho::LYS2, lys2, ura3, arg4-nsp, leu2::hisG, his4X::LEU2-(NgoMIV;+ori)--URA3, ku70Δ::NatMX*	†
698 / 699	*sae2Δ* Nuclease	α	*ho::LYS2, lys2, ura3, arg4-nsp, leu2::hisG, HIS4::LEU2-(BamHI;+ori), sae2Δ::kanMX*	†
700 / 701	*sae2Δ* Nuclease	a	*ho::LYS2, lys2, ura3, arg4-nsp, leu2::hisG, his4X::LEU2-(NgoMIV;+ori)--URA3, sae2Δ::kanMX*	†
702 / 703	*tdp1Δ* Nuclease	α	*ho::LYS2, lys2, ura3, arg4-nsp, leu2::hisG, HIS4::LEU2-(BamHI;+ori), tdp1Δ::kanMX*	†
704 / 705	*tdp1Δ* Nuclease	a	*ho::LYS2, lys2, ura3, arg4-nsp, leu2::hisG, his4X::LEU2-(NgoMIV;+ori)--URA3, tdp1Δ::kanMX*	†
706 - 708	Wildtype Nuclease	a / α	*ho::LYS2/', lys2/', ura3/', arg4-nsp/', leu2::hisG/',HIS4::LEU2-(BamHI;+ori), his4X::LEU2-(NgoMIV;+ori)--URA3*	†
709 / 716 / 717	*ku70Δ, sae2Δ* Nuclease	a / α	*ho::LYS2/', lys2/', ura3/', arg4-nsp/', leu2::hisG/',HIS4::LEU2-(BamHI;+ori), his4X::LEU2-(NgoMIV;+ori)--URA3, ku70Δ::NatMX/', sae2Δ::KanMX/'*	†
710 / 711	Tdp1-His_6-HA_3 Fluorescent	a / α	*ho::LYS2/', lys2/', ura3/', leu2::hisG/', trp1::hisG/', THR1::mCerulean-TRP1, CEN8::tdTomato-LEU2, 6xHis-3xHA-TDP1::KanMX/'*	†
713	*ku70Δ, sae2Δ* Nuclease	α	*ho::LYS2, lys2, ura3, arg4-nsp, leu2::hisG, his4X::LEU2-(NgoMIV;+ori)--URA3, ku70Δ::NatMX, sae2Δ::KanMX*	†
714 / 715	*ku70Δ, sae2Δ* Nuclease	a	*ho::LYS2, lys2, ura3, arg4-nsp, leu2::hisG, HIS4::LEU2-(BamHI;+ori), ku70Δ::NatMX, sae2Δ::KanMX*	†
716 / 717	*ku70Δ, sae2Δ* Nuclease	a / α	*ho::LYS2/', lys2/', ura3/', arg4-nsp/', leu2::hisG/',HIS4::LEU2-(BamHI;+ori), his4X::LEU2-(NgoMIV;+ori)--URA3, ku70Δ::NatMX/', sae2Δ::KanMX/'*	†

Name (YSG 'X')	Strain	Mating Type	Genotype	Source or Reference
718	*mus81Δ* Fluorescent	α	*ho::LYS2, lys2, ura3, leu2::hisG, trp1::hisG, THR1::mCerulean-TRP1, mus81Δ::KanMX*	†
719	*pms1Δ* Fluorescent	a	*ho::LYS2, lys2, ura3, leu2::hisG, trp1::hisG, THR1::mCerulean-TRP1, pms1Δ::KanMX*	†
720	*pms1Δ* Fluorescent	α	*ho::LYS2, lys2, ura3, leu2::hisG, trp1::hisG, CEN8::tdTomato-LEU2, pms1∆::KanMX*	†
721	*slx4Δ* Fluorescent	a	*ho::LYS2, lys2, ura3, leu2::hisG, trp1::hisG, THR1::mCerulean-TRP1, slx4Δ::KanMX*	†
722	*slx4Δ* Fluorescent	α	*ho::LYS2, lys2, ura3, leu2::hisG, trp1::hisG, THR1::mCerulean-TRP1, slx4Δ::KanMX*	†
723	*yen1Δ* Fluorescent	a	*ho::LYS2, lys2, ura3, leu2::hisG, trp1::hisG, THR1::mCerulean-TRP1, yen1Δ::KanMX*	†
724	*yen1Δ* Fluorescent	α	*ho::LYS2, lys2, ura3, leu2::hisG, trp1::hisG, CEN8::tdTomato-LEU2, yen1∆::KanMX*	†
725 - 727	*mus81Δ* Fluorescent	a / α	*ho::LYS2/', lys2/', ura3/', leu2::hisG/', trp1::hisG/', THR1::mCerulean-TRP1, CEN8::tdTomato-LEU2, mus81∆::KanMX/'*	†
728 / 729	*pms1Δ* Fluorescent	a / α	*ho::LYS2/', lys2/', ura3/', leu2::hisG/', trp1::hisG/', THR1::mCerulean-TRP1, CEN8::tdTomato-LEU2, pms1∆::KanMX/'*	†
730 - 732	*slx4Δ* Fluorescent	a / α	*ho::LYS2/', lys2/', ura3/', leu2::hisG/', trp1::hisG/', THR1::mCerulean-TRP1, CEN8::tdTomato-LEU2, slx4∆::KanMX/'*	†
733 - 735	*yen1Δ* Fluorescent	a / α	*ho::LYS2/', lys2/', ura3/', leu2::hisG/', trp1::hisG/', THR1::mCerulean-TRP1, CEN8::tdTomato-LEU2, yen1∆::KanMX/'*	†
736	Tdp1-His_6-HA_3, *ku70Δ* Fluorescent	a	*ho::LYS2, lys2, ura3, leu2::hisG, trp1::hisG, CEN8::tdTomato-LEU2, ku70∆::NatMX, 6xHis-3xHA-TDP1::KanMX*	†
737	Tdp1-His_6-HA_3, *ku70Δ* Fluorescent	α	*ho::LYS2, lys2, ura3, leu2::hisG, trp1::hisG, THR1::mCerulean-TRP1, ku70∆::NatMX, 6xHis-3xHA-TDP1::KanMX*	†
738	Tdp1-His_6-HA_3, *sae2Δ* Fluorescent	a	*ho::LYS2, lys2, ura3, leu2::hisG, trp1::hisG, THR1::mCerulean-TRP1, sae2Δ::KanMX, 6xHis-3xHA-TDP1::KanMX*	†
739	Tdp1-His_6-HA_3, *sae2Δ* Fluorescent	α	*ho::LYS2, lys2, ura3, leu2::hisG, trp1::hisG, CEN8::tdTomato-LEU2, sae2Δ::KanMX, 6xHis-3xHA-TDP1::KanMX*	†
740 - 742	Tdp1-His_6-HA_3, *ku70Δ* Fluorescent	a / α	*ho::LYS2/', lys2/', ura3/', leu2::hisG/', trp1::hisG/', THR1::mCerulean-TRP1, CEN8::tdTomato-LEU2, ku70∆::NatMX/', 6xHis-3xHA-TDP1::KanMX/'*	†
743 - 745	Tdp1-His_6-HA_3, *sae2Δ* Fluorescent	a / α	*ho::LYS2/', lys2/', ura3/', leu2::hisG/', trp1::hisG/', THR1::mCerulean-TRP1, CEN8::tdTomato-LEU2, sae2∆::KanMX/', 6xHis-3xHA-TDP1::KanMX/'*	†
745	*mlh1Δ, ku70Δ, sae2Δ* Fluorescent	a	*ho::LYS2, lys2, ura3, leu2::hisG, trp1::hisG, THR1::mCerulean-TRP1, ku70∆::NatMX, sae2∆::KanMX, mlh1∆::KanMX*	†

Name (YSG 'X')	Strain	Mating Type	Genotype	Source or Reference
747	*mlh1Δ, ku70Δ, sae2Δ* Fluorescent	α	*ho::LYS2, lys2, ura3, leu2::hisG, trp1::hisG, CEN8::tdTomato-LEU2, ku70Δ::NatMX, sae2Δ::KanMX, mlh1Δ::KanMX*	†
748	*mus81Δ, ku70Δ, sae2Δ* Fluorescent	a	*ho::LYS2, lys2, ura3, leu2::hisG, trp1::hisG, CEN8::tdTomato-LEU2, ku70Δ::NatMX, sae2Δ::KanMX, mus81Δ::KanMX*	†
749	*mus81Δ, ku70Δ, sae2Δ* Fluorescent	α	*ho::LYS2, lys2, ura3, leu2::hisG, trp1::hisG, THR1::mCerulean-TRP1, ku70Δ::NatMX, sae2Δ::KanMX, mus81Δ::KanMX*	†
750 - 752	*mlh1Δ, ku70Δ, sae2Δ* Fluorescent	a / α	*ho::LYS2/', lys2/', ura3/', leu2::hisG/', trp1::hisG/', THR1::mCerulean-TRP1, CEN8::tdTomato-LEU2, ku70Δ::NatMX/', sae2Δ::KanMX/', mlh1Δ::KanMX/'*	†
753 / 754	*mus81Δ, ku70Δ, sae2Δ* Fluorescent	a / α	*ho::LYS2/', lys2/', ura3/', leu2::hisG/', trp1::hisG/', THR1::mCerulean-TRP1, CEN8::tdTomato-LEU2, ku70Δ::NatMX/', sae2Δ::KanMX/', mus81Δ::KanMX/'*	†
799	*mus81Δ* Fluorescent	a	*ho::LYS2, lys2, ura3, leu2::hisG, trp1::hisG, CEN8::tdTomato-LEU2, mus81Δ::KanMX*	†
800	P^{CUP1}-Tdp1-His_6-HA_3 Nuclease	α	*ho::LYS2, lys2, ura3, arg4-nsp, leu2::hisG, HIS4::LEU2-(BamHI;+ori), PCUP1-6xHis-3xHA-TDP1::KanMX*	†
801 / 802	P^{CUP1}-Tdp1-His_6-HA_3 Nuclease	a	*ho::LYS2, lys2, ura3, arg4-nsp, leu2::hisG, his4X::LEU2-(NgoMIV;+ori)--URA3, PCUP1-6xHis-3xHA-TDP1::KanMX*	†
803	P^{CUP1}-Tdp1-His_6-HA_3 Fluorescent	α	*ho::LYS2, lys2, ura3, leu2::hisG, trp1::hisG, CEN8::tdTomato-LEU2, PCUP1-6xHis-3xHA-TDP1::KanMX*	†
804	*tdp1Δ, ku70Δ* Fluorescent	a	*ho::LYS2, lys2, ura3, leu2::hisG, trp1::hisG, CEN8::tdTomato-LEU2, ku70Δ::NatMX, tdp1Δ::KanMX*	†
805	*tdp1Δ, ku70Δ* Fluorescent	α	*ho::LYS2, lys2, ura3, leu2::hisG, trp1::hisG, THR1::mCerulean-TRP1, ku70Δ::NatMX, tdp1Δ::KanMX*	†
806 - 808	*tdp1Δ, ku70Δ* Fluorescent	a / α	*ho::LYS2/', lys2/', ura3/', leu2::hisG/', trp1::hisG/', THR1::mCerulean-TRP1, CEN8::tdTomato-LEU2, ku70Δ::NatMX/', tdp1Δ::KanMX/'*	†
809	*tdp1Δ, sae2Δ* Fluorescent	α	*ho::LYS2, lys2, ura3, leu2::hisG, trp1::hisG, CEN8::tdTomato-LEU2, sae2Δ::KanMX, tdp1Δ::KanMX*	†
810	*tdp1Δ, sae2Δ* Fluorescent	a	*ho::LYS2, lys2, ura3, leu2::hisG, trp1::hisG, THR1::mCerulean-TRP1, sae2Δ::KanMX, tdp1Δ::KanMX*	†
811 - 813	*tdp1Δ, sae2Δ* Fluorescent	a / α	*ho::LYS2/', lys2/', ura3/', leu2::hisG/', trp1::hisG/', THR1::mCerulean-TRP1, CEN8::tdTomato-LEU2, sae2Δ::KanMX/', tdp1Δ::KanMX/'*	†

Name (YSG 'X')	Strain	Mating Type	Genotype	Source or Reference
814	*slx4Δ, ku70Δ, sae2Δ* Fluorescent	α	*ho::LYS2, lys2, ura3, leu2::hisG, trp1::hisG, CEN8::tdTomato-LEU2, ku70Δ::NatMX, sae2Δ::KanMX, slx4Δ::KanMX*	†
815	*slx4Δ, ku70Δ, sae2Δ* Fluorescent	a	*ho::LYS2, lys2, ura3, leu2::hisG, trp1::hisG, THR1::mCerulean-TRP1, ku70Δ::NatMX, sae2Δ::KanMX, slx4Δ::KanMX*	†
816 - 818	*slx4Δ, ku70Δ, sae2Δ* Fluorescent	a / α	*ho::LYS2/', lys2/', ura3/', leu2::hisG/', trp1::hisG/', THR1::mCerulean-TRP1, CEN8::tdTomato-LEU2, ku70Δ::NatMX/', sae2Δ::KanMX/', slx4Δ::KanMX/'*	†
819	*yen1Δ, ku70Δ, sae2Δ* Fluorescent	α	*ho::LYS2, lys2, ura3, leu2::hisG, trp1::hisG, CEN8::tdTomato-LEU2, ku70Δ::NatMX, sae2Δ::KanMX, yen1Δ::KanMX*	†
820	*yen1Δ, ku70Δ, sae2Δ* Fluorescent	a	*ho::LYS2, lys2, ura3, leu2::hisG, trp1::hisG, THR1::mCerulean-TRP1, ku70Δ::NatMX, sae2Δ::KanMX, yen1Δ::KanMX*	†
821 - 823	*yen1Δ, ku70Δ, sae2Δ* Fluorescent	a / α	*ho::LYS2/', lys2/', ura3/', leu2::hisG/', trp1::hisG/', THR1::mCerulean-TRP1, CEN8::tdTomato-LEU2, ku70Δ::NatMX/', sae2Δ::KanMX/', yen1Δ::KanMX/'*	†
824	Tdp1-His_6-HA_3, *ku70Δ, sae2Δ* Fluorescent	α	*ho::LYS2, lys2, ura3, leu2::hisG, trp1::hisG, CEN8::tdTomato-LEU2, ku70Δ::NatMX, sae2Δ::KanMX, 6xHis-3xHA-TDP1::KanMX*	†
825	Tdp1-His_6-HA_3, *ku70Δ, sae2Δ* Fluorescent	a	*ho::LYS2, lys2, ura3, leu2::hisG, trp1::hisG, THR1::mCerulean-TRP1, ku70Δ::NatMX, sae2Δ::KanMX, 6xHis-3xHA-TDP1::KanMX*	†
826 - 828	Tdp1-His_6-HA_3, *ku70Δ, sae2Δ* Fluorescent	a / α	*ho::LYS2/', lys2/', ura3/', leu2::hisG/', trp1::hisG/', THR1::mCerulean-TRP1, CEN8::tdTomato-LEU2, ku70Δ::NatMX/', sae2Δ::KanMX/', 6xHis-3xHA-TDP1::KanMX/'*	†
831	*pms1Δ, ku70Δ, sae2Δ* Fluorescent	α	*ho::LYS2, lys2, ura3, leu2::hisG, trp1::hisG, CEN8::tdTomato-LEU2, ku70Δ::NatMX, sae2Δ::KanMX, pms1Δ::KanMX*	†
832	*pms1Δ, ku70Δ, sae2Δ* Fluorescent	a	*ho::LYS2, lys2, ura3, leu2::hisG, trp1::hisG, THR1::mCerulean-TRP1, ku70Δ::NatMX, sae2Δ::KanMX, pms1Δ::KanMX*	†
833 - 835	*pms1Δ, ku70Δ, sae2Δ* Fluorescent	a / α	*ho::LYS2/', lys2/', ura3/', leu2::hisG/', trp1::hisG/', THR1::mCerulean-TRP1, CEN8::tdTomato-LEU2, ku70Δ::NatMX/', sae2Δ::KanMX/', pms1Δ::KanMX/'*	†
836	*tdp1Δ, ku70Δ* Nuclease	α	*ho::LYS2, lys2, ura3, arg4-nsp, leu2::hisG, HIS4::LEU2-(BamHI;+ori), tdp1Δ::kanMX, ku70Δ::NatMX*	†
837	*tdp1Δ, ku70Δ* Nuclease	a	*ho::LYS2, lys2, ura3, arg4-nsp, leu2::hisG, his4X::LEU2-(NgoMIV;+ori)--URA3, tdp1Δ::kanMX, ku70Δ::NatMX*	†

Name (YSG 'X')	Strain	Mating Type	Genotype	Source or Reference
838 - 840	*tdp1Δ, ku70Δ* Nuclease	a / α	*ho::LYS2/', lys2/', ura3/', arg4-nsp/', leu2::hisG/',HIS4::LEU2-(BamHI;+ori), his4X::LEU2-(NgoMIV;+ori)--URA3, tdp1Δ::KanMX/', ku70Δ::NatMX/'*	†
841	*tdp1Δ, sae2Δ* Nuclease	α	*ho::LYS2, lys2, ura3, arg4-nsp, leu2::hisG, HIS4::LEU2-(BamHI;+ori), tdp1Δ::kanMX, sae2Δ::KanMX*	†
842	*tdp1Δ, sae2Δ* Nuclease	a	*ho::LYS2, lys2, ura3, arg4-nsp, leu2::hisG, his4X::LEU2-(NgoMIV;+ori)--URA3, tdp1Δ::kanMX, sae2Δ::KanMX*	†
843 - 845	*tdp1Δ, sae2Δ* Nuclease	a / α	*ho::LYS2/', lys2/', ura3/', arg4-nsp/', leu2::hisG/',HIS4::LEU2-(BamHI;+ori), his4X::LEU2-(NgoMIV;+ori)--URA3, tdp1Δ::KanMX/', sae2Δ::kanMX/'*	†
846	*tdp1Δ, ku70Δ, sae2Δ* Nuclease	α	*ho::LYS2, lys2, ura3, arg4-nsp, leu2::hisG, HIS4::LEU2-(BamHI;+ori), tdp1Δ::kanMX, sae2Δ::KanMX, ku70Δ::NatMX*	†
847	*tdp1Δ, ku70Δ, sae2Δ* Nuclease	a	*ho::LYS2, lys2, ura3, arg4-nsp, leu2::hisG, his4X::LEU2-(NgoMIV;+ori)--URA3, tdp1Δ::kanMX, sae2Δ::KanMX, ku70Δ::NatMX*	†
848 - 850	*tdp1Δ, ku70Δ, sae2Δ* Nuclease	a / α	*ho::LYS2/', lys2/', ura3/', arg4-nsp/', leu2::hisG/',HIS4::LEU2-(BamHI;+ori), his4X::LEU2-(NgoMIV;+ori)--URA3, tdp1Δ::KanMX/', sae2Δ::kanMX/', ku70Δ::NatMX/'*	†
851 - 853	t*dp1Δ* Nuclease	a / α	*ho::LYS2/', lys2/', ura3/', arg4-nsp/', leu2::hisG/',HIS4::LEU2-(BamHI;+ori), his4X::LEU2-(NgoMIV;+ori)--URA3, tdp1Δ::KanMX/'*	†
897 - 899	P^{CUP1}-Tdp1-His_6-HA_3 Nuclease	a / α	*ho::LYS2/', lys2/', ura3/', arg4-nsp/', leu2::hisG/', HIS4::LEU2-(BamHI;+ori), his4X::LEU2-(NgoMIV;+ori)--URA3, PCUP1-6xHis-3xHA-TDP1::KanMX/'*	†
906	P^{CUP1}-Tdp1-His_6-HA_3 Fluorescent	a	*ho::LYS2, lys2, ura3, leu2::hisG, trp1::hisG, THR1::mCerulean-TRP1, PCUP1-6xHis-3xHA-TDP1::KanMX*	†
907	P^{CUP1}-Tdp1-His_6-HA_3, *ku70Δ* Nuclease	a	*ho::LYS2, lys2, ura3, arg4-nsp, leu2::hisG, his4X::LEU2-(NgoMIV;+ori)--URA3, PCUP1-6xHis-3xHA-TDP1::KanMX, ku70Δ::NatMX*	†
908	P^{CUP1}-Tdp1-His_6-HA_3, *ku70Δ* Nuclease	α	*ho::LYS2, lys2, ura3, arg4-nsp, leu2::hisG, HIS4::LEU2-(BamHI;+ori), PCUP1-6xHis-3xHA-TDP1::KanMX, ku70Δ::NatMX*	†
909	P^{CUP1}-Tdp1-His_6-HA_3, *sae2Δ* Nuclease	a	*ho::LYS2, lys2, ura3, arg4-nsp, leu2::hisG, his4X::LEU2-(NgoMIV;+ori)--URA3, PCUP1-6xHis-3xHA-TDP1::KanMX, sae2Δ::KanMX*	†

Name (YSG 'X')	Strain	Mating Type	Genotype	Source or Reference
910	P^{CUP1}-Tdp1-His_6-HA_3, *sae2Δ* Nuclease	α	*ho::LYS2, lys2, ura3, arg4-nsp, leu2::hisG, HIS4::LEU2-(BamHI;+ori), PCUP1-6xHis-3xHA-TDP1::KanMX, sae2Δ::KanMX*	†
911	P^{CUP1}-Tdp1-His_6-HA_3, *ku70Δ, sae2Δ* Nuclease	a	*ho::LYS2, lys2, ura3, arg4-nsp, leu2::hisG, his4X::LEU2-(NgoMIV;+ori)--URA3, PCUP1-6xHis-3xHA-TDP1::KanMX, ku70Δ::NatMX, sae2Δ::KanMX*	†
912	P^{CUP1}-Tdp1-His_6-HA_3, *ku70Δ, sae2Δ* Nuclease	α	*ho::LYS2, lys2, ura3, arg4-nsp, leu2::hisG, HIS4::LEU2-(BamHI;+ori), PCUP1-6xHis-3xHA-TDP1::KanMX, ku70Δ::NatMX, sae2Δ::KanMX*	†
913 - 915	P^{CUP1}-Tdp1-His_6-HA_3 Fluorescent	a / α	*ho::LYS2/', lys2/', ura3/', leu2::hisG/', trp1::hisG/', THR1::mCerulean-TRP1, CEN8::tdTomato-LEU2, PCUP1-6xHis-3xHA-TDP1::KanMX/'*	†
916 – 918	P^{CUP1}-Tdp1-His_6-HA_3, *ku70Δ* Nuclease	a / α	*ho::LYS2/', lys2/', ura3/', arg4-nsp/', leu2::hisG/', HIS4::LEU2-(BamHI;+ori), his4X::LEU2-(NgoMIV;+ori)--URA3, PCUP1-6xHis-3xHA-TDP1::KanMX/', ku70Δ::NatMX/'*	†
919 – 921	P^{CUP1}-Tdp1-His_6-HA_3, *sae2Δ* Nuclease	a / α	*ho::LYS2/', lys2/', ura3/', arg4-nsp/', leu2::hisG/', HIS4::LEU2-(BamHI;+ori), his4X::LEU2-(NgoMIV;+ori)--URA3, PCUP1-6xHis-3xHA-TDP1::KanMX/', sae2Δ::KanMX/'*	†
922 - 924	P^{CUP1}-Tdp1-His_6-HA_3, *ku70Δ, sae2Δ* Nuclease	a / α	*ho::LYS2/', lys2/', ura3/', arg4-nsp/', leu2::hisG/', HIS4::LEU2-(BamHI;+ori), his4X::LEU2-(NgoMIV;+ori)--URA3, PCUP1-6xHis-3xHA-TDP1::KanMX/', ku70Δ::NatMX/', sae2Δ::KanMX/'*	†
925 - 927	P^{CUP1}-Tdp1-His_6-HA_3 S288C Background	α	*ade8, PCUP1-6xHis-3xHA-TDP1::KanMX*	†
952	*tdp1Δ, ku70Δ, sae2Δ* Fluorescent	a	*ho::LYS2, lys2, ura3, leu2::hisG, trp1::hisG, CEN8::tdTomato-LEU2, ku70Δ::NatXM, sae2Δ::KanMX, tdp1Δ::KanMX*	†
953	*tdp1Δ, ku70Δ, sae2Δ* Fluorescent	α	*ho::LYS2, lys2, ura3, leu2::hisG, trp1::hisG, THR1::mCerulean-TRP1, ku70Δ::NatXM, sae2Δ::KanMX, tdp1Δ::KanMX*	†
954 - 956	*tdp1Δ, ku70Δ, sae2Δ* Fluorescent	a / α	*ho::LYS2/', lys2/', ura3/', leu2::hisG/', trp1::hisG/', THR1::mCerulean-TRP1/THR1, CEN8::tdTomato-LEU2/CEN8, ku70Δ::NatXM/', sae2Δ::KanMX/', tdp1Δ::KanMX/'*	†

Name (YSG 'X')	Strain	Mating Type	Genotype	Source or Reference
957	P^{CUP1}-Tdp1-His_6-HA_3, *ku70Δ* Fluorescent	α	*ho::LYS2, lys2, ura3, leu2::hisG, trp1::hisG, CEN8::tdTomato-LEU2, ku70Δ::NatMX, PCUP1-6xHis-3xHA-TDP1::KanMX*	†
958	P^{CUP1}-Tdp1-His_6-HA_3, *ku70Δ* Fluorescent	a	*ho::LYS2, lys2, ura3, leu2::hisG, trp1::hisG, THR1::mCerulean-TRP1, ku70Δ::NatMX, PCUP1-6xHis-3xHA-TDP1::KanMX*	†
959	P^{CUP1}-Tdp1-His_6-HA_3, *ku70Δ, sae2Δ* Fluorescent	α	*ho::LYS2, lys2, ura3, leu2::hisG, trp1::hisG, CEN8::tdTomato-LEU2, ku70Δ::NatMX, sae2Δ::KanMX, PCUP1-6xHis-3xHA-TDP1::KanMX*	†
960	P^{CUP1}-Tdp1-His_6-HA_3, *ku70Δ, sae2Δ* Fluorescent	a	*ho::LYS2, lys2, ura3, leu2::hisG, trp1::hisG, THR1::mCerulean-TRP1, ku70Δ::NatMX, sae2Δ::KanMX, PCUP1-6xHis-3xHA-TDP1::KanMX*	†
961	P^{CUP1}-Tdp1-His_6-HA_3, *sae2Δ* Fluorescent	α	*ho::LYS2, lys2, ura3, leu2::hisG, trp1::hisG, CEN8::tdTomato-LEU2, sae2Δ::KanMX, PCUP1-6xHis-3xHA-TDP1::KanMX*	†
962	P^{CUP1}-Tdp1-His_6-HA_3, *sae2Δ* Fluorescent	a	*ho::LYS2, lys2, ura3, leu2::hisG, trp1::hisG, THR1::mCerulean-TRP1, sae2Δ::KanMX, PCUP1-6xHis-3xHA-TDP1::KanMX*	†
1172 / 1173	*rad1Δ, rad24Δ, dmc1Δ*	a	*ho::LYS2, lys2, ura3, arg4-nsp, leu2::hisG, his4X::LEU2, nuc1::LEU2, dmc1Δ::LEU2, rad24Δ::Hyg, rad1Δ::KanMX*	†
1174 / 1175	*rad1Δ, rad24Δ, dmc1Δ*	α	*ho::LYS2, lys2, ura3, arg4-nsp, leu2::hisG, his4X::LEU2, nuc1::LEU2, dmc1Δ::LEU2, rad24Δ::Hyg, rad1Δ::KanMX*	†
1176 / 1177	*rad10Δ, rad24Δ, dmc1Δ*	α	*ho::LYS2, lys2, ura3, arg4-nsp, leu2::hisG, his4X::LEU2, nuc1::LEU2, dmc1Δ::LEU2, rad24Δ::Hyg, rad10Δ::KanMX*	†
1178 / 1179	*rad10Δ, rad24Δ, dmc1Δ*	a	*ho::LYS2, lys2, ura3, arg4-nsp, leu2::hisG, his4X::LEU2, nuc1::LEU2, dmc1Δ::LEU2, rad24Δ::Hyg, rad10Δ::KanMX*	†
1180 /1182	*rad52Δ, rad24Δ, dmc1Δ*	a	*ho::LYS2, lys2, ura3, arg4-nsp, leu2::hisG, his4X::LEU2, nuc1::LEU2, dmc1Δ::LEU2, rad24Δ::Hyg, rad52Δ::KanMX*	†
1181 / 1182	*rad52Δ, rad24Δ, dmc1Δ*	α	*ho::LYS2, lys2, ura3, arg4-nsp, leu2::hisG, his4X::LEU2, nuc1::LEU2, dmc1Δ::LEU2, rad24Δ::Hyg, rad52Δ::KanMX*	†

Name (YSG 'X')	Strain	Mating Type	Genotype	Source or Reference
1184 / 1187	*rad59Δ, rad24Δ, dmc1Δ*	α	*ho::LYS2, lys2, ura3, arg4-nsp, leu2::hisG, his4X::LEU2, nuc1::LEU2, dmc1Δ::LEU2, rad24Δ::Hyg, rad59Δ::KanMX*	†
1185 / 1186	*rad59Δ, rad24Δ, dmc1Δ*	a	*ho::LYS2, lys2, ura3, arg4-nsp, leu2::hisG, his4X::LEU2, nuc1::LEU2, dmc1Δ::LEU2, rad24Δ::Hyg, rad59Δ::KanMX*	†
1197 - 1199	Rad1-His_6-HA_3, rad24Δ. *dmc1Δ*	a / α	*ho::LYS2/', lys2/', ura3/', arg4-nsp/', leu2::hisG/', his4X::LEU2/', nuc1::LEU2/', dmc1Δ::LEU2/', rad24Δ::Hyg/', RAD1-6xHis-3xHA-KanMX/'*	†
1200 – 1202	Rad10-His_6-HA_3, *rad24Δ. dmc1Δ*	a / α	*ho::LYS2/', lys2/', ura3/', arg4-nsp/', leu2::hisG/', his4X::LEU2/', nuc1::LEU2/', dmc1Δ::LEU2/', rad24Δ::Hyg/', RAD10-6xHis-3xHA-KanMX/'*	†
1203 – 1205	Rad52-His_6-HA_3, *rad24Δ. dmc1Δ*	a / α	*ho::LYS2/', lys2/', ura3/', arg4-nsp/', leu2::hisG/', his4X::LEU2/', nuc1::LEU2/', dmc1Δ::LEU2/', rad24Δ::Hyg/', RAD52-6xHis-3xHA-KanMX/'*	†
1206 – 1208	Rad59-His_6-HA_3, *rad24Δ. dmc1Δ*	a / α	*ho::LYS2/', lys2/', ura3/', arg4-nsp/', leu2::hisG/', his4X::LEU2/', nuc1::LEU2/', dmc1Δ::LEU2/', rad24Δ::Hyg/', RAD59-6xHis-3xHA-KanMX/'*	†
1209 - 1211	*rad24Δ*	a / α	*ho::LYS2/', lys2/', ura3/', arg4-nsp/', leu2::hisG/', his4X::LEU2/', nuc1::LEU2/', rad24Δ::HYG/'*	†
1212 / 1213	*rad10Δ*	a	*ho::LYS2, lys2, ura3, arg4-nsp, leu2::hisG, his4X::LEU2, nuc1::LEU2, rad10Δ::KanMX*	†
1214 / 1215	*rad10Δ*	α	*ho::LYS2, lys2, ura3, arg4-nsp, leu2::hisG, his4X::LEU2, nuc1::LEU2, rad10Δ::KanMX*	†
1216 – 1218	*rad1Δ, rad24Δ. dmc1Δ*	a / α	*ho::LYS2/', lys2/', ura3/', arg4-nsp/', leu2::hisG/', his4X::LEU2/', nuc1::LEU2/', dmc1Δ::LEU2/', rad24Δ::Hyg/', rad1Δ::KanMX'*	†
1219 / 1220	*rad10Δ, rad24Δ. dmc1Δ*	a / α	*ho::LYS2/', lys2/', ura3/', arg4-nsp/', leu2::hisG/', his4X::LEU2/', nuc1::LEU2/', dmc1Δ::LEU2/', rad24Δ::Hyg/', rad10Δ::KanMX'*	†
1221	*rad52Δ, rad24Δ. dmc1Δ*	a / α	*ho::LYS2/', lys2/', ura3/', arg4-nsp/', leu2::hisG/', his4X::LEU2/', nuc1::LEU2/', dmc1Δ::LEU2/', rad24Δ::Hyg/', rad52Δ::KanMX'*	†
1222 – 1224	*rad59Δ, rad24Δ. dmc1Δ*	a / α	*ho::LYS2/', lys2/', ura3/', arg4-nsp/', leu2::hisG/', his4X::LEU2/', nuc1::LEU2/', dmc1Δ::LEU2/', rad24Δ::Hyg/', rad59Δ::KanMX'*	†
1225 - 1227	Rad52-His_6-HA_3	a / α	*ho::LYS2/', lys2/', ura3/', arg4-nsp/', leu2::hisG/', his4X::LEU2/', nuc1::LEU2/', RAD52-6xHis-3xHA-KanMX/'*	†

2.3 DNA Substrates

2.3.1 Plasmids used in this study

Table 2-4 Plasmids used in this study. All plasmids marked with † were made for this study; plasmids labelled SG made by Dr Stephen Gray.

Plasmid Name	Vector Backbone	Origin	Resistance	Description	Source or Reference
pSG11	pFA6a	ColE1	Amp^R, KanMX	C-terminal His_6 and HA_3 tags	SG
pGADT7	n/a	pUC 2 μ	Amp^R	Yeast-2-Hybrid 'prey' vector with GAL4 activation domain. *LEU2* marker.	Clontech
pGBKT7	n/a	pUC 2 μ	Kan^R	Yeast-2-Hybrid 'bait' vector with GAL4 DNA binding domain. *TRP1* marker.	Clontech
pSG144	pSG11	ColE1	Amp^R, KanMX	*S. cerevisiae* RAD1 with C-terminal His_6 and HA_3 tags	†
pSG145	pSG11	ColE1	Amp^R, KanMX	*S. cerevisiae* RAD10 with C-terminal His_6 and HA_3 tags	†
pSG147	pSG11	ColE1	Amp^R, KanMX	*S. cerevisiae* RAD59 with C-terminal His_6 and HA_3 tags	†
pSG267	pSG11	ColE1	Amp^R, KanMX	*S. cerevisiae* RAD52 with C-terminal His_6 and HA_3 tags	†
pSG268	pSG11	ColE1	Amp^R, KanMX	*S. cerevisiae* RAD1 D825A C-terminal His_6 and HA_3 tags	†
pSG269	pSG11	ColE1	Amp^R, KanMX	*S. cerevisiae* RAD1 S613D C-terminal His_6 and HA_3 tags	†
pSG270	pSG11	ColE1	Amp^R, KanMX	*S. cerevisiae* RAD1 S1071A C-terminal His_6 and HA_3 tags	†

Plasmid Name	Vector Backbone	Origin	Resistance	Description	Source or Reference
pSG271	pSG11	ColE1	Amp^R, KanMX	*S. cerevisiae* RAD1 S1071D C-terminal His_6 and HA_3 tags	†
pSG272	pSG11	ColE1	Amp^R, KanMX	*S. cerevisiae* RAD1 T1072A C-terminal His_6 and HA_3 tags	†
pSG273	pSG11	ColE1	Amp^R, KanMX	*S. cerevisiae* RAD1 T1072D C-terminal His_6 and HA_3 tags	†
pSG274	pSG11	ColE1	Amp^R, KanMX	*S. cerevisiae* RAD52 R37 (70)K C-terminal His_6 and HA_3 tags	†
pSG275	pSG11	ColE1	Amp^R, KanMX	*S. cerevisiae* RAD52 R37(70)A C-terminal His_6 and HA_3 tags	†
pSG276	pSG11	ColE1	Amp^R, KanMX	*S. cerevisiae* RAD59 F180A C-terminal His_6 and HA_3 tags	†
pSG277 / pSG278	pGADT7	pUC 2 µ	Amp^R	RAD1 Yeast-2-Hybrid ‘prey’ vector.	†
pSG279 / pSG280	pGADT7	pUC 2 µ	Amp^R	RAD10 Yeast-2-Hybrid ‘prey’ vector.	†
pSG281 / pSG282	pGADT7	pUC 2 µ	Amp^R	RAD52 Yeast-2-Hybrid ‘prey’ vector.	†
pSG283 / pSG284	pGADT7	pUC 2 µ	Amp^R	RAD59 Yeast-2-Hybrid ‘prey’ vector.	†
pSG285	pGBKT7	pUC 2 µ	Kan^R	RAD1 Yeast-2-Hybrid ‘bait’ vector.	†
pSG286 / pSG287	pGBKT7	pUC 2 µ	Kan^R	RAD10 Yeast-2-Hybrid ‘bait’ vector.	†
pSG288 / pSG289	pGBKT7	pUC 2 µ	Kan^R	RAD52 Yeast-2-Hybrid ‘bait’ vector.	†
pSG290 / pSG291	pGBKT7	pUC 2 µ	Kan^R	RAD59 Yeast-2-Hybrid ‘bait’ vector.	†
pSG322	pSG11	ColE1	Amp^R, KanMX	pSG147 with *S. cerevisiae* rad59Δ::KanMX	†

2.3.2 Primers used in this study

Table 2-5 DNA primers used in this study. All Tm temperatures are specific for the polymerase Q5 unless otherwise stated. All primers marked with † were designed for this study; primers labelled SG designed by Dr Stephen Gray; primers labelled JB were designed by Joe Brealey; primers labelled KH were designed by Kate Hodson.

(№) Name	Sequence 5' - 3'	Description	Tm (°C)	Extension Time (s)	Source or Reference
(87) RAD24_F-1368	CTTCGCCAGTCGTATGCCCC	Checking rad24Δ::Hyg integration.	69	240	SG
(90) RAD24_R+3252	GTCACTAAGGAGGAGGCCGG				
(88) RAD24_F-1077	GTTTTCAATGTTTGGCAATGCCC	Checking rad24Δ::Hyg integration.	65	240	SG
(89) RAD24_R+3114	GTTTTAATTGGTGAAGCCTCGCG				
(99) RAD1_F-1141	TCCGATTGGATTTCTGGGGGG	Checking integration of rad1 deletion cassette	70	300	SG
(101) RAD1_R+4445	CTACTAGCGCCGCTTGTTCCC				
(100) RAD1_F-1016	ATCTTGCGAAATCCGTTCCCG	Amplifying rad1 deletion cassette	67	300	SG
(102) RAD1_R+2675	TAGAGGGGTTATGCAAAGGCCC				
(103) RAD10_F-1549	CATCTTCAGATATTTCGTCGAAGGG	Checking integration of rad10 deletion cassette	63	180	SG
(106) RAD10_R+1687	TAGTGTAACGGGGTCTGCTGGG				
(104) RAD10_F-1424	GCGTCTTCGTCATCATTGCCG	Amplifying rad10 deletion cassette	66	180	SG
(105) RAD10_R+1058	GAAAGAACGCCATATCAGCGCC				
(129) Nat_F	GGCTGGAGGTCACCAACGTCAACGC	Checking ku70Δ transformants.	69	240	SG
(404) KU70_R_+4525	AAAGGGCTAGCCGTAATTCGTCGAC				
(175) HIS4 R@+1102	CTTTGTCGGAAGCCTTCACCACGTCC	Making the Leu2 LH probe for Southern blotting.	70	30	(Gray et al., 2013)
(176) HIS4 F@+427	GTACGTACAGACCGTCCTGACGG				

(№) Name	Sequence 5' - 3'	Description	Tm (°C)	Extension Time (s)	Source or Reference
(227) pSG11 Backbone Rad1_fwd	TGCTGTTCAGTAGGATATCAGATCCACTAGTGGCCTATG	Making pSG144, backbone fragment	65	150	†
(228) pSG11 Backbone Rad1_rev	ATGCCTATTAACTTCGACCTGCAGCGTACGAAG				
(229) Rad1-1051 fwd	GCTGCAGGTCGAAGTTAATAGGCATCAACCC	Making pSG144, rad1 + upstream fragment	58	130	†
(230) Rad1+3300 rev	ATGATGAGAACCCACAGGTGCTTCAGGAAC				
(231) pSG11 Tags Rad1 fwd	TGAAGCACCTGTGGGTTCTCATCATCATCATC	Making pSG144, tags + marker fragment	56	60	†
(232) pSG11 Tags Rad1 rev	CTCAGACTCCACAATCGATGAATTCGAGCTC				
(233) Rad1+3587 fwd	GAATTCATCGATTGTGGAGTCTGAGCGTGG	Making pSG144, rad1 downstream fragment	62	30	†
(234) Rad1+4535 rev	GGATCTGATATCCTACTGAACAGCAATAATTGGGATTAG				
(235) pSG11 Backbone Rad10_fwd	CGTGAAAGGCTGCGATATCAGATCCACTAGTGGCCTATG	Making pSG145, backbone fragment	65	150	†
(236) pSG11 Backbone Rad10_rev	CAAGAGTTCCAGATCGACCTGCAGCGTACGAAG				
(237) Rad10-1018 fwd	GCTGCAGGTCGATCTGGAACTCTTGGATCTG	Making pSG145, rad10 + upstream fragment	56	50	†
(238) Rad10+630 rev	ATGATGAGAACCTAAATTCAAATATTCAATATATTTTGCAG				
(239) pSG11 Tags Rad10 fwd	ATATTTGAATTTAGGTTCTCATCATCATCATC	Making pSG145, tags + marker fragment	56	60	†
(240) pSG11 Tags Rad10 rev	GAATATCATCAGAATCGATGAATTCGAGCTC				
(241) Rad10+730 fwd	GAATTCATCGATTCTGATGATATTCCATCCAACTTC	Making pSG145, rad10 downstream fragment	62	40	†
(242) Rad10+1981 rev	GGATCTGATATCGCAGCCTTTCACGAAACAG				
(243) pSG11 Backbone Rad52_fwd	TGCTCTCTATACCGATATCAGATCCACTAGTGGCCTATG	Making pSG267, backbone fragment	65	150	†
(244) pSG11 Backbone Rad52_rev	AGGATTATGGAGATCGACCTGCAGCGTACGAAG				
(245) Rad52-826 fwd	GCTGCAGGTCGATCTCCATAATCCTCTTGACACG	Making pSG267, rad52 + upstream fragment	62	70	†
(246) Rad52+1413 rev	ATGATGAGAACCAGTAGGCTTGCGTGCATG				

(№) Name	Sequence 5' - 3'	Description	Tm (°C)	Extension Time (s)	Source or Reference
(247) pSG11 Tags Rad52 fwd	ACGCAAGCCTACTGGTTCTCATCATCATCATC	Making pSG267, tags + marker fragment	56	60	†
(248) pSG11 Tags Rad52 rev	GCCAGGAAGCGTTATCGATGAATTCGAGCTC				
(249) Rad52+1416 fwd	GAATTCATCGATAACGCTTCCTGGCCGAAAC	Making pSG267, rad52 downstream fragment	64	45	†
(250) Rad52+2985 rev	GGATCTGATATCGGTATAGAGAGCAAAGACTGCTC				
(251) pSG11 Backbone Rad59_fwd	TATTCTTCGTCGCGATATCAGATCCACTAGTGGCCTATG	Making pSG147, backbone fragment	65	150	†
(252) pSG11 Backbone Rad59_rev	ATGACGACTTAACTCGACCTGCAGCGTACGAAG				
(253) Rad59-1001 fwd	GCTGCAGGTCGAGTTAAGTCGTCATGGCCATC	Making pSG147, rad59 + upstream fragment.	59	52	†
(254) Rad59+714 rev	ATGATGAGAACCTTTGATATGCGTGCCTTTAG				
(255) pSG11 Tags Rad59 fwd	CACGCATATCAAAGGTTCTCATCATCATCATC	Making pSG147, tags + marker fragment.	56	60	†
(256) pSG11 Tags Rad59 rev	TTCCGTTCGCATCATCGATGAATTCGAGCTC				
(257) Rad59+828 fwd	GAATTCATCGATGATGCGAACGGAACAGGTATC	Making pSG147, rad59 downstream fragment.	62	40	†
(258) Rad59+1991 rev	GGATCTGATATCGCGACGAAGAATATGACATAGAG				
(259) Rad1-1309 fwd	ACGATATGGGATAAGACGGGAGATTGC	Checking rad1 tag cassette integration.	68	510	†
(260) Rad1+5868 rev	GCTATGAGTTTCGCTATACTGACTGACTTGC				
(261) Rad10-1365 fwd	GACAGTGGCATCAAATCTTCTTCATCAATGG	Checking rad10 tag cassette integration.	70	300	†
(262) Rad10+2232	CTTGAGCATCTGGCATTACTATGAGACATGTG				
(263) Rad52-2033 fwd	CTGTCTTGTTGTACTCTATCTTGGGC	Checking rad52 tag cassette integration.	63	450	†
(264) Rad52+3993 rev	ATACCGATGAAGTGGACGATGAAG				
(265) Rad59-1729 fwd	CAAGTCGCAACACAACCATTAATACGC	Checking rad59 tag cassette integration.	69	360	†
(266) Rad59+2814	GAATTTGGTGAGCAGATCATCCGTG				
(267) Rad1 pSG11 insert fwd	AGTTAATAGGCATCAACCCAGG	Making transformation cassette from pSG144.	61	420	†
(268) Rad1 pSG11 insert rev	CTACTGAACAGCAATAATTGGGATTAG				

(№) Name	Sequence 5' - 3'	Description	Tm (°C)	Extension Time (s)	Source or Reference
(269) Rad10 pSG11 insert fwd	TCTGGAACTCTTGGATCTGC	Making transformation cassette from pSG145.	60	240	†
(270) Rad10 pSG11 insert rev	GCAGCCTTTCACGAAACAG				
(271) Rad52 pSG11 insert fwd	TCTCCATAATCCTCTTGACAC	Making transformation cassette from pSG267.	56	300	†
(272) Rad52 pSG11 insert rev	GGTATAGAGAGCAAAGACTGC				
(273) Rad59 pSG11 insert fwd	GTTAAGTCGTCATGGCCATC	Making transformation cassette from pSG147.	60	240	†
(274) Rad59 pSG11 insert rev	GCGACGAAGAATATGACATAGAG				
(275) pSG11 back-marker fwd	CCTCCGATCGTTGTCAGAAG	Checking pSG144/145/147/267 HiFi assembly orientation (long fragment).	63	360	†
(276) pSG11 back-marker rev	CTGCCAGCGCATCAACAAT				
(277) pSG11 marker-back fwd	TCGATTCGATACTAACGC	Checking pSG144/145/147/267 HiFi assembly orientation (short fragment).	55	60	†
(278) pSG11 marker-back rev	ATACGACTCACTATAGGGAGAC				
(287) Spo11_F_Tag	AGCGCGACTACTCCTTAGCC	Amplifying the tagged spo11 fragment for transformation.	68	30	SG
(289) Spo11_R_Tag	ATGCTGTATTGGAGGGTGGG				
(288) Spo11_F2_Tag	TATTTACCGATGCGGACCCC	Checking spo11-tag integration.	64	60	SG
(290) Spo11_R2_Tag	GAAGCTGTTTTCGTAGAGCC				
(313) Rad52-946 fwd	TTTGTGACAGCTAGCACG	Amplifying rad52 deletion cassette.	55	210	†
(314) Rad52+2985 rev	GGTATAGAGAGCAAAGACTGC				
(315) Rad59-1001 fwd	GTTAAGTCGTCATGGCCATC	Amplifying rad59 deletion cassette.	57	210	†
(316) Rad59+1991 rev	GCGACGAAGAATATGACATAGAG				
(453) Rad1 SDM D825A F	CGTCATTGTGGCAACACGTGAGTTTAATG	SDM for pSG268 SDM for pSG268.	56 56	600 600	†
(454) Rad1 SDM D825A R	ACATCCTGAGTAAGATTATGG				

(№) Name	Sequence 5' - 3'	Description	Tm (°C)	Extension Time (s)	Source or Reference
(455) Rad1 SDM S613A F	TAAGAAGGGAGCCGGTGATGATTTG	Making S613A Rad1.	51	600	†
(456) Rad1 SDM S613A/D R	ATTTCTTCAGATAACTTATGATC	Making pSG269/S613A Rad1.	51/54	600	†
(457) Rad1 SDM S613D F	TAAGAAGGGAGATGGTGATGATTTGGATG	Making pSG269.	54	600	†
(458) Rad1 SDM S1071A F	AGAACAAGAGGCCACAGATGAAAATC	Making pSG270.	55	600	†
(459) Rad1 SDM S1071A/D R	TGTTCTTCTTTTTCTGTTCTC	Making pSG270/271.	55/57	600	†
(460) Rad1 SDM S1071D F	AGAACAAGAGGATACAGATGAAAATCTTG	Making pSG271.	57	600	†
(461) Rad1 SDM T1072A F	ACAAGAGTCAGCCGATGAAAATCTTG	Making pSG272.	58	600	†
(462) Rad1 SDM T1072A/D R	TCTTGTTCTTCTTTTTCTGTTC	Making pSG272/273.	58	600	†
(463) Rad1 SDM T1072D F	ACAAGAGTCAGATGATGAAAATCTTGAATCTC	Making pSG273.	58	600	†
(464) Rad52 R37K F	TATCTCCAAGAAGGTTGGGTTTGG	Making pSG274.	53	420	†
(465) Rad52 R37K/A R	TACTCAGGTCCTAATTTC	Making pSG274/275.	53	420	†
(466) Rad52 R37A F	TATCTCCAAGGCAGTTGGGTTTG	Making pSG275.	53	420	†
(467) Rad59 K166A F	CAGGTCGAAAGCAGAGGCTGTAG	Making K166A Rad59.	53	220	†
(468) Rad59 K166A R	TTATAACATTCGCCTCTC				
(469) Rad59 F180A F	GTTATTGAGCGCAGAAAAAATCATACTCGATTATG	Making pSG276.	61	220	†
(470) Rad59 F180A F	GCCTTCTTTAACGCATCG				
(474) Rad52 – 46 F	GTTGTCAAGAACTGCTGAAGG	Checking rad52 deletion cassette.	63	45	†
(475) Rad52 + 1392 R	GGGATTGATCTTTGGTCTTCC				†
(476) Rad59 - 290 F	GGATGTTATAGATGTTGAGGC	Checking rad59 deletion cassette.	60	30	†
(477) Rad59 + 674 R	GTCGGCTTGCTATTAGTCG				†
(502) Rad1+0 pGAD F	GACGTACCAGATTACGCTCA*T*ATGTCTCAGTTATTTTATCAGGG	Making pSG277.	58	180	†
(503) Rad1+3303 pGAD R	TCTGCAGCTCGAGCTCGATGTTACACAGGTGCTTCAGG				

(№) Name	Sequence 5' - 3'	Description	Tm (°C)	Extension Time (s)	Source or Reference
(504) Rad10+0 pGAD F	GACGTACCAGATTACGCTCA*T*ATGAACAATACTGATCCTAC	Making pSG279.	54	45	†
(505) Rad10+633 pGAD R	TCTGCAGCTCGAGCTCGATGTCATAAATTCAAATATTCAATATATTTTGC				
(506) Rad52+0 pGAD F	GACGTACCAGATTACGCTCA*T*ATGAATGAAATTATGGATATGGATGAGAAG	Making pSG281.	61	90	†
(507) Rad52+1416 pGAD R	TCTGCAGCTCGAGCTCGATGTCAAGTAGGCTTGCGTGC				
(508) Rad59+0 pGAD F	GACGTACCAGATTACGCTCA*T*ATGACGATTCAAGCGAAG	Making pSG283.	56	45	†
(509) Rad59+717 pGAD R	TCTGCAGCTCGAGCTCGATGTTATTTGATATGCGTGCC				
(510) Rad1+0 pGBK F	ATCTCAGAGGAGGACCTGCA*T*ATGTCTCAGTTATTTTATCAGGG	Making pSG285.	58	180	†
(511) Rad1+3303 pGBK R	GCGGCCGCTGCAGGTCGACGTTACACAGGTGCTTCAGG				
(512) Rad10+0 pGBK F	ATCTCAGAGGAGGACCTGCA*T*ATGAACAATACTGATCCTAC	Making pSG286.	54	45	†
(513) Rad10+633 pGBK R	GCGGCCGCTGCAGGTCGACGTCATAAATTCAAATATTCAATATATTTTGC				
(514) Rad52+0 pGBK F	ATCTCAGAGGAGGACCTGCA*T*ATGAATGAAATTATGGATATGGATGAGAAG	Making pSG288.	61	90	†
(515) Rad52+1416 pGBK R	GCGGCCGCTGCAGGTCGACGTCAAGTAGGCTTGCGTGC				
(516) Rad59+0 pGBK F	ATCTCAGAGGAGGACCTGCA*T*ATGACGATTCAAGCGAAG	Making pSG290.	56	45	†
(517) Rad59+717 pGBK R	GCGGCCGCTGCAGGTCGACGTTATTTGATATGCGTGCC				
(518) pGAD insert check F	TCGATGATGAAGATACCCC	Checking pSG277-283 HiFi assembly (Taq used).	48	210	†
(519) pGAD insert check R	AGTTGAAGTGAACTTGCGG				
(520) pGBK insert check F	AAGTGCGACATCATCATCG	Checking pSG285-291 HiFi assembly (Taq used).	45	210	†
(521) pGBK insert check R	CTATGACCATGATTACGCC				
(537) KanC_F	TGATTTTGATGACGAGCGTAAT	Amplifying from KanMX cassette forward.	61	180	†
(690) Sae2_F-1091	ACAAATGGGGATTGTCAAAGGG	Preparing sae2Δ::KanMX cassette.	64	210	†
(691) Sae2_R+2306	TTTCGACTTTCTGATGCCATACCG				

(№) Name	Sequence 5' - 3'	Description	Tm (°C)	Extension Time (s)	Source or Reference
(692) Sae2_F-1354	AGCAATGGTTCAACTATTGGGGG	Checking sae2Δ transformants.	66	240	†
(693) Sae2_R+2550	ACCATAAATGAAGTAGCGCCCG				
(714) Rad1_S613A_II_F	TAAGAAGGGAgccGGTGATGATTTGGATGAC	Making S613A mutation in rad1 in pSG144.	68	300	†
(715) Rad1_S613A_II_R	ATTTCTTCAGATAACTTATGATCCTCAAAAACCACCTCC				
(716) Rad59_K166A_II_F	AGGTCGAAAgcaGAGGCTGTAGGC	Making K166A mutation in rad59 in pSG147.	69	220	†
(717) Rad59_K166A_II_R	GTTATAACATTCGCCTCTCGAGGACAAAG				
(740) KU70_F_-1131	ATAGCGGCTATGCTAAGCTCCC	Making ku70::NatMX cassette.	70	240	SG / JB
(741) KU70_R_+3147	TTGGCGCAAGCTCTAATCCGC				
(746) MLH1_F_-1390	AGATTGGTAGACCGTCCGAAGGC	Checking mlh1Δ::KanMX transformants.	69	240	SG / JB
(747) MLH1_R_+3813	GTAGACGGCAAATACTGGGACGC				
(750) MUS81_F_-1383	TCGCTGTCGAAGTCAAGAACGC	Checking mus81Δ::KanMX transformants.	66	240	SG / JB
(751) MUS81_R_+3483	AACTTCCAGTACAAGCGTCGG				
(754) PMS1_F_-1596	GGGCGTTTCCAAAGAGAAAAGCC	Checking pms1Δ::KanMX transformants.	68	240	SG / JB
(755) PMS1_R_+4152	AAGTACTCTACTGTGGCCGCC				
(758) SLX4_F_-1406	ATTGCTGAAACCGGTACTTCCG	Checking slx4Δ::KanMX transformants.	67	240	SG / JB
(759) SLX4_R_+3851	CGCCCCTTCTATCCTGAATACCC				
(760) TDP1_F_-1590	TTGGTTCATCATACGCCAGCTGCC	Making tdp1Δ::KanMX cassette.	70	240	SG / JB
(761) TDP1_R_+2678	ACCCATGGACGTGGAAAAGAGGC				
(762) TDP1_F_-1909	GCGAATTGGTCGTTTAGAGGG	Checking tdp1 deletion cassette integration.	65	300	SG / JB
(763) TDP1_R_+3126	CCCAAAGTGACGTTTTCGCC				
(573) KanC_F	TGATTTTGATGACGAGCGTAAT	Checking tdp1Δ transformants.	63	120	SG / JB
(763) TDP1_R_+3126	CCCAAAGTGACGTTTTCGCC				
(764) YEN1_F_-1383	TAACTTCAACTCAGTCCCCTCCC	Checking yen1Δ::KanMX transformants.	67	240	SG
(765) YEN1_R_+3347	GAAGAAGGTCCATTCAAGGCCG				

(№) Name	Sequence 5' - 3'	Description	Tm (°C)	Extension Time (s)	Source or Reference
(770) FWD pDMC1 screen	TTCCCTGGAAGCGCCATTTT	Checking dmc1Δ::LEU2 integration	64	120	SG /†
(1326) DMC1_R+1385	GGATGATGATGAGGAGCTCC				
(843) pSG147_rad59KO_F	CAGGATAAACAGACAAAATAGCG	Making pSG322.	62	360	†
(844) pSG147_rad59KO_R	TATTTTGTCTGTTTATCCTGAAATATGCTC				
(888) TDP1_Upstream_fwd	ATTGTACTGAGAGTGCACCACAAATGTTGATTAAATTATGATTTCC	Checking P^{CUP1}-integration into pSG333.	63	300	SG / JB
(889) TDP1_Upstream_rev	GATGATGCATTAATAATCGGTTGAAAACACATTATC				
(933) pif1 -856 F	GTTAGCTCCTCACTTGTAGG	Making pif1 deletion cassette.	61	210	†
(934) pif1 +3518 R	GTAAGACGATACCTCCTGCC				
(935) pif1 -1354 F	GTACCAGTTGTAGTGCTACC	Checking pif1 deletion cassette integration.	61	300	†
(936) pif1 +3972 R	GTTTCCTGCTTGAGTGATCG				
(1005) pSG11-6His3HA-TDP1_fwd	ATGCATCATCATCATCATC	HiFi assembly of pSG334.	55	300s	†
(1006) pSG11-6His3HA-TDP1_rev	TAATAATCGGTTGAAAACACATTATC				
(1007) pCUP1_fwd	GTGTTTTCAACCGATTATTACTAGTTAGAAAAAGACATTTTTGC	HiFi Assmbly of pSG334.	57	15	†
(1008) pCUP1_rev	TGATGATGATGATGATGCATGATGACTTCTATATGATATTGCAC				
(1048) TDP1_-1514_F	ATGGATCCGATATTACTGGC	Checking P^{CUP1}-tdp1 integration.	60	90	†
(1049) TDP1_+113_R	GCCATATTCTCCATTTCAGC				
(1137) tdp1_H182A_F	CGCTTCCCACgctACGAAGCTGATC	SDM primers for making tdp1 H182A/H182F mutants.	61	420	†
(1138) tdp1_H182F_F	CGCTTCCCACtttACGAAGCTGATC				
(1139) tdp1_H182A/F_R	AATGGGGGCATCGTTATTTC				
(1140) tdp1_H432R_F	GACGCCCGCGcgcTCTAAGTTTT	SDM primers for making tdp1 H432R mutant.	68	420	†
(1141) tdp1_H432R_R	GTCCCTCGTCTTCTAGTAACCATAG				
(1197) RMD6_F@+13	CTTGCAACATCGTTATACTCCCAG	PFGE probe for chromosome V.	64	30	(Gray et al., 2013)
(1198) RMD6_R@+592	GAACTTTGAACCTTTGCACCTCTAC				

(№) Name	Sequence 5' - 3'	Description	Tm (°C)	Extension Time (s)	Source or Reference
(1199) CHA1_F@-9	ACCAGCGAGATGTCGATAGTCTAC	PFGE probe for chromosome III.	62	60	(Gray et al., 2013)
(1200) CHA1_R@+1052	TCTGGAAATATGAAATTGTCAGCG				
(1201) JEN1_F@-2	ATATGTCGTCGTCAATTACAGATGAG	PFGE probe for chromosome XI.	63	30	(Gray et al., 2013)
(1202) JEN1_R@+620	GGCCACTTTCTGGAAGACTTATC				
(1272) MXR2_F	CGTGAAGTGGAACGATGCCC	Making the MXR2 RH probe for Southern blotting.	68	20	(Gray et al., 2013)
(1273) MXR2_R	GCAACTGTTTCCAGCCTTCACC				
(1359) MAT-a	CAATGATTAAAATAGCATAGTCGG	Checking mating-type of strains via PCR.	55	30	KH
(1360) MAT-α	CAGCACGGAATATGGGAC				
(1361) MAT-R	GGTGCATTTGTCATCCGTC				
(1456) SB_MXR2_SEQ_F	AACAGGGATCTCAGTAGG	Sequencing the His4::Leu2 region for SB analysis.	59	840	†
(1457) SB_MXR2_SEQ_R	CTGGTGTAGACTTACTTGCC				

2.4 General Microbiology

2.4.1 PCR

Polymerase chain reaction (PCR) was used throughout this study to check yeast transformation success, prepare probes for SB/PFGEs, sequence genes, and make cassettes for making plasmids/yeast transformations. All reactions were run in a Techne 3Prime thermocycler. Unless otherwise stated, Q5® polymerase (NEB) was used. All primers used in this study are shown in **Table** 2-5. The A generic PCR reaction set-up is shown in **Table 2-6** with conditions shown in **Table 2-7**.

Table 2-6 Generic PCR set-up using Q5® polymerase

Component	**Final Concentration**
Q5® HF 2x Master Mix	1x
Forward Primer	500 nM
Reverse Primer	500 nM
Template DNA	< 50 µg / µl
Up to 20 µl with SDW	

Table 2-7 Generic PCR conditions for Q5® PCR reactions.

Temperature/°C	**Time/Seconds**	**Cycles**
98	120	1
98	30	25-30
51-72 (Tm of primer dependent)	30	
72	30-60 / kb	
72	300	1

2.4.2 PCR ‘Clean-up’

If PCR products (section **2.4.1**) were to be used in downstream applications such as yeast transformations, sequencing or making SB/PFGE probes the DNA had to be ‘cleaned-up’; this was achieved using the Macherey-Nagel™ NucleoSpin® Gel and PCR Clean-up Kit(Macherey-Nagel, 2021a).

The whole PCR reaction mix was added to 2-volumes of ‘NTI’ buffer in a 1.5 ml microfuge tube (Sarstedt). This was then loaded onto a NucleoSpin® column which was centrifuged at 11,000 *xg* (Sigma 1-15P Microcentrifuge) for 30 seconds to bind the DNA to the column; the flow-through was discarded. The bound-DNA was then washed by adding 700 µl ‘NT3’ to the column, spinning at 11,000 *xg*, discarding the flow through, then repeating this wash step again. After the two washes, the column was dried by spinning at 11,000 *xg* for 1 minute with the collection tube and flow-through being discarded. The column was then put into a new 1.5 ml microfuge tube and 30 µl ‘NE’ elution buffer was added. This was incubated at room temperature for 1 minute, then centrifuged at 11,000 *xg* for 1 minute to elute the DNA into the microfuge tube.

2.4.3 Agarose Gel Electrophoresis

Agarose gel electrophoresis was used to separate out fragments of DNA in order to check PCR products, plasmid products, and DNA digests.

Before loading onto a gel, 2 µl of 6 x Purple Loading Dye (NEB) was added to 10 µl of the DNA samples and gently mixed. Agarose powder was dissolved by heating 150 ml of 1 x TAE buffer in a 200 ml bottle (Simax); the % w/v of agarose added depended on the DNA being analysed, see **Table** 2-8. Once the dissolved agarose had cooled 0.2 µg/ml Ethidium Bromide was added to the gel before casting in an agarose gel tray with loading combs inserted. Once completely set, 10 µl of the DNA sample was loaded into the wells, with 10 µl pre-stained 1kb ladder (NEB) as a guide. Gels were run at 100-120v for 30-60 minutes using a BioRad Model 200/2.0 power supply, and imaged using a BioRad ChemiDoc™ MP UV transilluminator.

Table 2-8 Agarose Gel Percentages and their Effective DNA Separation Ranges. Table modified from Themo Scientific (Thermo-Scientific, 2012)

Agarose Gel (%)	DNA Separation Range (bp)
0.75	800-11,000
1	400-8,000
1.5	200-3,000
2	100-2,000

2.4.4 Transformation of Chemically Competent Cells

All bacterial work used NEB® 5-alpha competent cells (Genotype: *fhuA2 Δ(argF-lacZ)U169 phoA glnV44 Φ80 Δ(lacZ)M15 gyrA96 recA1 relA1 endA1 thi-1 hsdR17*) .A 50 µl aliquot of NEB® 5-alpha competent cells was thawed on ice, of which 10 µl was used per transformation. To this, 5-100 ng of the desired plasmid was added, and mixed by gently tapping the tube; this mixture was then left to incubate on ice for 20 minutes. After this initial incubation, the cells were subjected to a 45 second heat-shock at 42°C in a water bath (Grant) before being left on ice for a further 5 minutes. 100 µl LB media was then added to the cells, which were incubated for 1 hour at 37°C with gentle rotation (Cole Parmer). The whole transformation mix was then spread onto LB-agar plates (1.5% w/v agar) containing the appropriate antibiotic to select for the desired plasmid (see **Table 2-2**).

2.4.5 Isolation of Plasmid DNA

Plasmid DNA was extracted from cells (*E coli* NEB® 5-alpha cells) and purified using Machery-Nagel™ NucleoSpin® Plasmid Mini kit (Macherey-Nagel, 2021b).

An overnight culture was set up in a 15 ml round-bottom plastic tube (Falcon) using a single colony of the transformed *E. coli* strain (section **2.4.4**) in 3 ml of LB media supplemented with the appropriate antibiotic (**Table 2-2**). This culture was grown for 16 hours at 37 °C with shaking at 180 RPM (New Brunswick Scientific Innova™ 4330). From this culture, 1.5 ml was used for the plasmid purification, the rest was used to store the transformed strain as a glycerol stock (section **2.4.6**).

1.5 ml of the overnight culture was spun down at 11.000 *xg* for 1 minute (Sigma 1-15P Microcentrifuge) in a 1.5 ml microfuge tube (Sarstedt) and the supernatant was discarded. The pellet was resuspended in 250 µl 'A1' buffer supplemented with RNAse A. To this mix, 250 µl of 'A2' lysis buffer was added and mixed by inverting the tube 8 times; this was incubated at room temperature for 5 minutes. Once the cells were lysed, 300 µl of 'A3' neutralisation buffer was added and mixed by inverting the tube 8 times, which turned the lysate colourless. The lysate was then clarified by centrifugation at 11,000 *xg* for 5 minutes, with the supernatant then being loaded onto a NucleoSpin® column.

The plasmid DNA was bound to the column by spinning the lysate through the column for 1 minute at 11,000 *xg* and discarding the flow-through. Then the bound plasmid DNA was washed by adding 500 µl 'AW' wash buffer to the column, spinning at 11,000 *xg* for 1 minute, and discarding the flow-through. Then 600 µl 'A4' wash buffer, supplemented with ethanol, was added to the column, centrifuged at 11,000 *xg* for 1 minute, and the flow-through was once-again discarded. The silica membrane with the DNA bound to-it was then dried by centrifuging for 2 minutes at 11,000 *xg* before the collection tube with any flow-through was discarded. The NucleoSpin® column with bound DNA was then added to a 1.5 ml microfuge tube (Sarstedt) and 30 µl 'AE' elution buffer was added. This was incubated at room temperature for 1 minute, before eluting the plasmid DNA into the microfuge tube by centrifuging at 11,000 *xg* for 1 minute. The concentration of the plasmid DNA was measured using a Thermo NanoDrop™ 2000 Spectrophotometer.

2.4.6 Making Glycerol Stocks

For long-term storage of yeast strains and plasmid-containing *E. coli*, glycerol stocks were made. For storing yeast, single colony was inoculated into a 15 ml glass test tube (Kimble) containing 3 ml YPD + ALU broth which was grown with rotation at 20 RPM overnight at 30 °C (Cole Parmer). For *E. coli,* a single transformant was grown in a plastic tube (Falcon) containing 3 ml LB media + the appropriate antibiotic to maintain plasmid selection, which was grown at 37 °C overnight with 20 RPM rotation. The following day, 750 µl of overnight culture was added to a cryotube (Axygen Scientific) containing 750 µl 50 % glycerol, making the final concentration of glycerol in the stocks 25 %. The glycerol stocks were mixed thoroughly by inverting and stored at -80 °C. These stocks could be 'woken up' by streaking onto YPD/LB plates and incubating at 30/37 °C for 1-3 days.

2.4.7 Making Plasmids via HiFi Assembly

All plasmid cloning in this study was designed using NEBuilder® HiFi assembly (NEB) strategies. HiFi assembly fragments were designed using the NEBuilder® Assembly Tool(NEB, 2022). The individual fragments were generated separately using PCR (section **2.4.1**) and/or plasmid restriction digest (section **2.4.8**) To ensure each fragment was correct, fragments were run on an agarose-TAE gel (section **2.4.3**), which were then purified (section **2.4.2**). The clean fragments were measured on a NanoDrop™ 2000 Spectrophotometer (Thermo Fisher) to determine the concentration of DNA present. For the HiFi assembly, the fragments were added together according to **Table 2-9** and incubated at 50 °C for one hour. Following this incubation, 5 µl of the HiFi assembly mix was used to transform *E. Coli* (section **2.4.4**).

Table 2-9 NEBuilder® HiFi Assembly Set-Up.

Component	**2-3 Fragment Assembly**	**4-6 Fragment Assembly**
DNA Molar Ratio	Vector:Insert 1:2	Vector:Insert 1:1
Total amount of DNA	0.03-0.2 pmols	0.2-0.5 pmols
NEB HiFi DNA Master Mix	10 µl	10 µl
SDW	Up to 20 µl	Up to 20 µl

2.4.8 Restriction Digests

All restriction digests set up according to the Table 2-10 below and left for 1-16 hours at 37 °C. All restriction enzymes were from NEB and compatible with CutSmart® Buffer.

Table 2-10 Restriction Digest Mix

Component	**Concentration**
10 x CutSmart® Buffer	1 x
NEB-HF Restriction Enzyme(s)	1 Unit / µl
DNA	50-150 ng/µl
SDW	Up to 20 µl

2.4.9 SDM

Site Directed Mutagenesis strategy designed using the NEBasechanger® software (NEB, 2021). PCR performed as described in section **2.4.1** with 25 amplification cycles. The PCR product was then subjected to Kinase, Ligase, DpnI (KLD) treatment to join-up the plasmid and digest any starting plasmid. KLD reaction set up as described below in **Table** 2-11, incubated at room temperature for 5 minutes for optimal kinase/ligase reactions, followed by 30 minutes at 37 °C for optimal DpnI digestion. 5 µl of the KLD mix was used to transform *E. coli* as described earlier (section **2.4.4**).

Table 2-11 KLD reaction set-up.

Component	**Concentration**
PCR Product	5-15 ng/µl
2 x KLD Buffer (NEB)	1 x
10 x KLD Enzyme Mix (NEB)	1 x
SDW	Up to 20 µl

2.5 *S. cerevisiae* Methods

2.5.1 Yeast Genomic DNA Preparation

In order to amplify yeast genes by PCR, first the yeast genomic DNA (gDNA) must be isolated and purified. This is achieved by cell lysis, phenol choloroform extraction of DNA, and ethanol precipitation with RNAse digestion to purify the DNA.

A single yeast colony was inoculated in 3 ml YPD + ALU broth which was left to rotate at 20 RPM overnight at 30 °C (Cole Parmer). Following overnight growth, 1.5 ml of the culture was pelleted (Sigma 1-15P Microcentrifuge) at 15,500 *x g* and resuspended in 0.5 ml Spheroplasting buffer with 1 % 2-mercaptoethanol and 0.25 mg/ml Zymolyase 20T. This solution was then incubated at 30 °C for 30-60 minutes. Next, 100 µl gDNA lysis buffer was added to the solution, which was mixed by gentle inversion before being incubated at 55 °C for a further 30-60 minutes. After this incubation step, the lysis mix was removed from the incubator and allowed to cool to room temperature before adding 500 µl Phenol:Chloroform:Isoamyl Alcohol 25:24:1 (Acros organics) in a fume hood. The samples were shaken vigorously 30 times and then allowed to settle for 5 minutes. The samples were shaken vigorously 10 times more and then centrifuged at 15,500 *x g* for 5 minutes.

The centrifugation step separated the solution into two phases; 450 µl of the top (aqueous) phase was carefully removed with large-diameter tips and placed into a clean 1.5 ml microfuge tube, whilst the bottom (organic) phase was discarded. The DNA and RNA in the aqueous phase was then precipitated by the addition of 50 µl 3 M Sodium Acetate and 500 µl ice-cold 100 % Ethanol, with gentle inversion to aid the precipitation. The DNA-RNA could then be incubated on ice for 1 hour, or be immediately pelleted at 15,500 *x g* for 1-20 minutes at 4 °C (Eppendorf 5417R). The supernatant was then discarded. The pellet was then briefly pulsed in the centrifuge and the remaining supernatant was removed. The DNA-RNA pellet was then washed with 1 ml of ice-cold 70% Ethanol, centrifuged at 15,500 *x g* for 1-20 minutes at 4 °C. Again, the supernatant was poured off. The pellet was pulsed down and aspirated as before, then air dried for 5-10 minutes. Once the ethanol had evaporated completely, the DNA-RNA pellet was dissolved in 500 µl TE buffer, aided by incubation at

37 °C for 1 hour to overnight. The RNA was then digested by adding 1 mg/ml RNAse A and incubating the sample for 1 hour at 37 °C. Once the RNA was digested, the DNA was precipitated once more by the addition on 50 µl 3 M Sodium Acetate and 1 ml ice-cold 100% Ethanol. The solution was inverted several times to aid precipitation, followed by pelleting at 15,500 *x g* for 1-20 minutes at 4 °C. The supernatant was poured off, the tube pulsed down, and the remaining solution removed with a pipette. The pellet was then washed with 1 ml ice cold 70% ethanol which was spun down at 15,500 *x g* for 1-20 minutes, supernatant removed, pulsed down, aspirated, and finally air-dried for 5-10 minutes. The dry DNA pellet was then resuspended in TE buffer overnight at 4 °C. If the pellet didn't dissolve overnight, the DNA was incubated at 37 °C for 1 hour with occasional flicking to aid resuspension. This gDNA in TE was stored at -20 °C.

2.5.2 Yeast Transformation

For this study, many genes had to be mutated and deleted in *S. cerevisiae*. This was achieved by creating a 'cassette' of DNA via PCR (section **2.4.1**). This cassette contained sequences homologous to the upstream and downstream regions of the gene of interest, with a drug-resistance gene either replacing the gene or between the modified-gene-sequence and the downstream sequence. Many deletions were made using the Saccharomyces Genome Deletion Project Yeast Knockout Collection (YKO) (Giaever and Nislow, 2014). All transformations were accomplished using the 'Lithium Acetate' method, described below, modified from here(Gietz, 2014).

A single colony of yeast was inoculated in 20 ml YPD + ALU media in a 250 ml flask (Simax) and grown overnight at 30 °C with shaking at 250 RPM (New Brunswick Scientific Innova® 44). The overnight culture was then used to inoculate another flask containing 20 ml of fresh YPD + ALU media at a 1:20 dilution. This new culture was grown for 4 hours at 30 °C with shaking at 250 RPM to allow the yeast to reach log phase. Once they reached log phase, the cells were transferred to a 50 ml centrifuge tube (Sarstedt) and pelleted at 3,200 *x g* (Sigma 1-15P Microcentrifuge) for 5 minutes. The supernatant was removed and the cells were resuspended in 20 ml SDW. The cells were once again centrifuged at 3,200 *x g* for 5 minutes and this time the cells were transferred to a 1.5 ml microfuge tube (Sarstedt) and resuspended in 1 ml 100 mM lithium acetate. These were then centrifuged at 7,000 *x g* for 1 minute and resuspended in 500 µl 100 mM lithium acetate; 50 µl of this cell mix was used per transformation. Each 50 µl of cells was then pelleted at 7,000 *x g* for 30 seconds and resuspended in 360 µl of the transformation mix containing the insert DNA cassette.

To ensure total resuspension of the pellet, the cells and transformation mix were vortexed for a minute (SLS Lab Basics). Once adequately resuspended, the cells were incubated at 30 °C for 30 minutes (LEEC), then 42 °C for 20 minutes (Grant). The cells were then spun down at 7,000 *x g* for 30 seconds, the supernatant was removed, and the cells were resuspended in 1 ml YPD + ALU. Once resuspended, the cells were grown for 1 hour at 30 °C with rotation at 20 RPM (Cole Parmer). After this outgrowth stage, the cells were centrifuged at 7,000 *x g* for 30 seconds and the supernatant was removed. The cells were

resuspended in 100 µl of SDW and spread onto the appropriate YPD-agar selection plate (**Table 2-2**). The plates were grown at 30 °C for 3-5 days. Successful transformants were verified by re-streaking onto selection plates and grown at 30 °C for 2 days.

2.5.3 Mating Yeast Strains

A 10 µl drop of SDW was placed onto some clean Parafilm® M sealing film. To this, a single colony of the first of the strains to-be-mated was added and fully resuspended. Then an equal sized colony from the second strain was added and resuspended in the 10 µl of water. The two strains in water were then added to a YPD + ALU plate as a single patch, which was allowed to fully dry before incubating overnight at 30 °C. Following overnight incubation, the patch made up of the two strains was mixed together with a wooden toothpick. If mating haploids to get diploids, the mixed-patch was streaked-out to acquire single colonies. If the mating was to mate strains for generating new haploids, the patch was added to a 15 ml test tube containing 2 ml of 2 % KAc to allow sporulation; these spores could then be split into individual haploid strains either by random spore analysis (section **2.5.4**) or by tetrad dissection (section **2.5.6**).

2.5.4 Random Spore Analysis

In order to mate strains together to generate genetically-distinct new strains, the spores resulting from mating must be isolated into single colonies. In the absence of a dissection microscope, these spores can be split and isolated using random spore analysis. This technique was adapted from (Treco and Winston, 2008).

A mating patch was set up as previously described (section **2.5.3**). The whole patch was mixed with a wooden toothpick and then used to inoculate 2 ml of 2 % potassium acetate in a 15 ml test tube. This sporulation culture was then incubated at 30 °C for 3 days with 20 RPM rotation (Cole Parmer). Successful mating was determined by viewing 10 µl of the sporulation culture using a light microscope (Prior PX042); this presence of 'tetrads' indicating successful mating. If sporulation was successful, 1 ml of the sporulation culture was added to a 1.5 ml microfuge tube and centrifuged at 15,500 *x g* for 1 minute to form a pellet. The supernatant was removed, with 500 µl SDW being used to resuspend the pellet. The centrifugation and resuspension steps were repeated to ensure no remaining potassium acetate in the suspension. In order to lyse un-sporulated yeast cells, 1 % 2-mercaptoethanol and 0.25 mg/ml Zymolyase 20T were added to the washed sporulation mix, which was then incubated at 30 °C overnight with gentle rotation. After the overnight incubation, 200 µl of 1.5% Triton-X was added and mixed thoroughly. The tetrads were then separated by sonication at 10 % amplitude for 15 seconds using an MSE Soniprep 150. Once again a light microscope was used to check that the tetrads had been separated; any remaining tetrads could be separated by further sonication. Following sonication, the spores were centrifuged at 1,200 *x g* for 10 minutes. The supernatant was carefully removed, and the spores were resuspended in 500 µl SDW. These spores were then diluted 1:100 and 1:1000; 100 µl of each of these dilutions was streaked out onto YPG + AU plates supplemented with selection markers. The plates were incubated at 30 °C for 2 days, with successful colonies re-streaked onto selection plates to check resistance phenotypes.

2.5.5 Meiotic Timecourses

To get a clear picture of what is going on during meiosis, samples can be taken during a meiotic timecourse. Yeast cultures are first synchronised in YPA broth, before washing and putting into sporulation media. Samples are taken at the required timepoints, usually from 0-12 hours with additional 'after meiosis' samples at 48-72 hours.

The desired strain was inoculated into 20 ml YPD + ALU in a 250 ml flask (Simax) and grown overnight at 30 °C with shaking at 250 RPM (New Brunswick Scientific Innova® 44). The Optical Density (OD_{600}) was measured so that the overnight YPD + ALU cultures could be used to inoculate 200 ml of YPA culture to a final OD of 0.2. The YPA cultures were set up in 2 L flasks (Simax) which were incubated for 13 ½ hours at 30 °C with shaking at 250 RPM. If required, vegetative samples could also be collected at this stage from the overnight YPD + ALU samples.

After the 13 ½ hour YPA incubation to synchronise the yeast cultures, the cultures were added to a 250 ml centrifuge tube (Nalgene) and spun at 3,500 *xg* for 5 minutes (Sorvall® RC5B Plus) to pellet the yeast. The supernatant was then poured-away and replaced with 200 ml 30 °C to wash the pellets. These were resuspended with the aid of a strippette (Greiner Bio-One Cellstar®) before being re-pelleted at 3,500 *xg* for 5 minutes. These cultures were then centrifuged once more at 3,500 *xg* for 5 minutes and the supernatant was again poured off. The pellets were then resuspended in 200 ml sporulation media which was pre-warmed to 30 °C. The four 200 ml sporulation cultures were added to a 250 ml flask, and a 20 ml sample was taken as the first time-point (T_0). The flasks were grown for 8-72 hours at 30 °C shaking at 250 RPM, with 10-30 ml samples being taken at required time-points and pelleted in 50 ml centrifuge tubes (Sarstedt) at 3,500 *xg* (Eppendorf 5810R) . After the completion of the timecourse, usually 48-72 hours, samples could be taken for measuring spore efficiency or spore viability (sections **2.5.7** and **2.5.6**)

2.5.6 Tetrad Dissection

The preferred way to generate haploid strains from a mating patch is by tetrad dissection. This has the advantage of knowing exactly how many spores you'll plate without having to use multiple dilutions. It also allows you to follow segregation patterns; this allows you to mate two parental strains which use the same selection marker. For example, strain A has a KanMX cassette replacing *geneA* (*geneAΔ*::KanMX), whilst parent B has a KanMX cassette replacing *geneB* (*geneBΔ::*KanMX), you could mate, dissect and replica plate onto G418 to find 2:2 segregants which will have both *geneAΔ*::KanMX and *geneBΔ*::KanMX. Furthermore, tetrad dissection is used to measure spore viability of strains by simply counting how many spores grow once dissected.

Diploid/mated-haploid strains were inoculated into 2 ml sporulation media 24-72 hours. Alternatively, timecourse culture (section **2.5.5**) could also be used if dissecting tetrads to measure spore viability. If tetrads were successfully produced, 1 ml of the sporulation mix was pelleted at 15,500 *x g* for 1 minute and resuspended in 500 µl SDW. To this, 0.25 mg/ml Zymolyase 20T was added and incubated at 37 °C for 30 minutes. 1 µl of this tetrad mix was added to 9 µl SDW on a piece of Parafilm® M sealing film and added as a streak to the left-side of a YPD + ALU plate. Once dried, tetrads were dissected using a Singer Instruments MSM System. Dissected spores were then incubated at 30 °C for 2-3 days. Colonies were then replica-plated onto different selection markers/Synthetic Dropout plates to select for the correct genotype.

2.5.7 Sporulation Efficiency

As well as monitoring meiotic phenotypes by measuring spore viability via tetrad dissection (section **2.5.6**), how well the strains can sporulate is also a useful measure of meiotic effects. Samples were taken at the end of a meiotic timecourse (section **2.5.5**), usually after 48-72 hours in sporulation medium. 10 µl of this sample was taken, placed on a glass slide (Fisher), covered with a slip (SLS) and viewed under a light microscope (PriorPX042); sporulation efficiency was measured by comparing un-sporulated cells to tetrads with at least 300 cells counted per strain.

2.5.8 Fluorescence Microscopy

To assess the synchronicity of meiotic timecourse cultures, nuclei were counted using DAPI staining. 100 µl timecourse sample was taken and added to 500 µl methanol. 2 µl of 2.5 µg/ml DAPI stain was dropped onto a cover slip (SLS) which was then placed on a microscope slide (Fisher) with 8 µl of timecourse-methanol sample placed on it. These were imaged on a Zeiss Axiophot upright fluorescence microscope using the DAPI filter. Stained nuclei were counted to gauge divisions and therefore culture synchronicity.

2.6 Protein Detection Methods

2.6.1 Obtaining Protein pellets for SDS PAGE

10 – 20 ml of sample from a meiotic timecourse / vegetative culture were pelleted in 50 ml centrifuge tubes (Sarstedt) at 3,200 *xg* for 4 minutes. The pellet was resuspended in 1 ml SDW and transferred to a 2 ml screw-cap tube (Sarstedt) and re-pelleted at 15,500 *xg* for 1 minute (Sigma 1-15P Microcentrifuge). The supernatant was then discarded, and the pelleted samples were chilled on ice for 10 minutes. Around 100-200 µl pre-chilled glass beads were then added to each sample, along with 100-300 µl of ice-cold 10 % Trichloroacetic acid (TCA). The cells were then lysed by vortexing the samples (SLS Lab Basics) with the TCA/glass beads for 1 minute before returning the samples to ice.

Once the cells were lysed, the supernatant was removed from the 2 ml screw-cap tubes and added to a 1.5 ml microfuge tube (Sarstedt). This was then pelleted at 15,500 *xg* for 1 minute, and the supernatant was discarded. The pellet was then resuspended in 100-300 µl STE buffer, which was then boiled at 95 °C for 5 minutes. The samples were then re-centrifuged at 15,500 *xg* for 1 minute and the supernatant which contains the soluble proteins was added to a new 1.5 ml microfuge tube and stored at -20 °C.

2.6.2 SDS PAGE and Western Blotting

Proteins can be separated by size using SDS Poly-Acrylamide Gel Electrophoresis (SDS PAGE). For further specificity, affinity-tagged proteins can be viewed independently by transferring proteins from the SDS PAGE gel onto a membrane and probing with antibodies; this is called western Blotting. Ordinarily, proteins on an SDS PAGE gel are viewed by staining, meaning that an identical gel is required for the western Blotting. This also adds the need for loading controls where a 'housekeeping' protein is tagged to ensure the original SDS PAGE was loaded properly. The gels in this study were made using Trichloroethanol (TCE) which allows proteins to be viewed using UV light with no need to stain(Ladner et al., 2004). This saves time in making fewer gels, no staining/destaining time as well as negating the need to probe for a loading control.

The SDS PAGE gels were cast according to the recipes shown in Table 2-12 using BioRad mini PROTEAN® 1.5 mm plates. First the resolving layer was cast, covered in a thin layer of isopropyl alcohol, and left to set for around 30 minutes. Once set, the resolving layer was poured on top, the comb was added, and the gel left to set for a further 30 minutes. Once fully set, the cast gels were added to a BioRad mini PROTEAN® Tetra System tank filled with 1x SDS running buffer.

Table 2-12 SDS PAGE gel recipes. Each recipe shows enough for 1 SDS PAGE gel. Approximate protein resolving ranges are shown below the corresponding gel percentage.

Component	Resolving Layer					Stacking Layer
	7.5 % Gel (25-200 kDa)	**10 % Gel** (15-100 kDa)	**12 % Gel** (10-70 kDa)	**15 % Gel** (12-45 kDa)		
30 % Bis-Acrylamide (Biorad)	2.5 ml	3.3 ml	4 ml	5 ml		625 µl
1 M Tris-HCl pH8.8 + TCE	2.5 ml	2.5 ml	2.5 ml	2.5 ml		-
10 % SDS	100 µl	100 µl	100 µl	100 µl		-
4 x SDS Stacking Mix	-	-	-	-		1.25 ml
ddH_20	4.8 ml	4 ml	3.3 ml	2.3 ml		3.1 ml
10 % APS	100 µl	100 µl	100 µl	100 µl		25 µl
TEMED	10 µl	10 µl	10 µl	10 µl		10 µl
Total	10 ml	10 ml	10 ml	10 ml		5 ml

Once the gels were prepared, the protein samples were thawed and each sample had an equal volume of 2 X SDS Loading Buffer supplemented with 2-mercaptoethanol added to it. Between 20 – 40 µl of protein sample was added to each well alongside Precision Plus Protein Dual Colour Standard (BioRad) to act as a ladder. Any empty lanes were filled with 1 X SDS Loading Buffer to ensure the gel ran straight. The proteins were then separated via electrophoresis at 120 V for 2 – 3 hours (Consort EV243 Power Supply).

When the proteins had migrated sufficiently, the gels were disassembled and the proteins were viewed via excitation with UV (BioRad ChemiDoc™ MP imaging system). Prior to transferring the proteins to a PVDF membrane (BioRad), the membrane and filter stacks had to be prepared. The membrane was activated by submersion in 100 % ethanol, before being incubated in 1 x Trans-Blot Turbo Transfer Buffer (BioRad) at room temperature for 10 minutes. The filter stacks were also submerged in 1 x Trans-Blot Turbo

Transfer Buffer for 10 minutes. Then, the transfer stack was assembled in the following order in a BioRad Trans-Blot® Turbo™ cassette:

+ | Filter paper | Membrane | Gel | Filter paper | -

Air gaps between the gel and membrane were removed using a roller. The cassette was placed in a BioRad Trans-Blot® Turbo™ and transferred at 2.5 A 25 V for 10 minutes.

Following transfer, each membrane was placed in a 50 ml centrifuge tube (Sarstedt) and blocked with 10 ml TBST + 5 % BSA for 2 hours with 30 RPM rolling (Star Lab Tube Roller). The blocking solution was replaced with 5 ml TBST + 5 µl rabbit anti-HA 1 ° antibody (Cell Signalling). The primary antibody was incubated with rolling at room temperature overnight.

The following day, the membrane was then washed with 10 ml TBST for 5 minutes, which was repeated three times. Then 1 µl of the secondary antibody, goat anti-rabbit (Invitrogen) was added to 5 ml TBST, which was then incubated with rolling for an hour. The membranes were washed once again in 10 ml TBST for 5 minutes, repeated three times.

To image the tagged proteins, 500 µl peroxide solution and 500 µl ECL (BioRad) were combined and the membrane was incubated in the mix for 1 minute. The membrane was then imaged via chemiluminescence using the BioRad ChemiDoc™ MP imaging system. Bands were quantified using BioRad Image Lab software.

2.7 DNA Detection Methods

2.7.1 Restriction Digest and Electrophoresis For Southern Blotting

Restriction digests followed by Southern blotting was used to CO/NCO products formed during meiosis. This consisted of a digest, separation via electrophoresis, transfer to a membrane, and then detecting the specific DNA sequence with a labelled probe.

10-20 ml of a timecourse sample was collected and the gDNA was purified (section **2.5.1**). In a 1.5 ml microfuge tube, a digest was set up (section 2.4.8) using XhoI (NEB) to digest 3 µg of DNA(Yun and Kim, 2019). The digest mix was carefully mixed via gentle pipetting and incubated at 37 °C overnight to ensure complete digestion.

Following digestion, 4 µl 6 X purple loading dye (NEB) was added to each reaction. Each sample was then loaded onto a 0.7 % agarose-TAE gel made with 50 µg / ml ethidium bromide. The NEB λ-BstEII digest ladder was also added as a molecular weight standard. The gel was run in a (Thermo Scientific Owl A5) for 16 hours at 60 V (Consort EV243 Power Pack). As the gel had been stained with ethidium bromide, the DNA digestion was checked using a UV transilluminator (BioRad ChemiDoc™ MP imaging system). After imaging, the gel was transferred to a membrane for hybridisation (sections **2.7.3** and **2.7.5**).

2.7.2 Pulsed Field Gel Electrophoresis for Southern Blotting

Pulsed Field Gel Electrophoresis (PFGE) is a technique used to separate large-molecular-weight DNA fragments such as chromosomes. Unlike with a standard agarose gel, the DNA is prepared in an agarose-plug; the method for this plug making was adapted from here (Murakami et al., 2009) . For this study, Contour-Clamped Homogenous Electric Field (CHEF) PFGEs were used.

Between 10 – 20 ml of sporulation culture was taken during a meiotic timecourse and pelleted at 15,500 *xg* (Sigma 1-15P). The pellets were resuspended in 1 ml of 50 mM EDTA pH 8 before being pelleted again at 10,000 *xg.* This wash step was repeated another two times. After washing, the pellets were resuspended in 135 µl 'PFGE Solution 1'.

The samples in 'PFGE Solution 1' was heated up to 55 °C for 10 seconds (Stuart SBH130DC), then 165 µl molten LMP agarose mix was added and carefully homogenised with a pipette. The sample-agarose mix was then added to the PFGE plug mould (BioRad) and left to set at 4 °C for 30 minutes.

Once set, the plugs were expelled into a 2 ml low-bind tube (Eppendorf DNA LoBind) containing 1 ml of 'PFGE Solution 2'. The plugs were incubated at 37 °C (LEEC) for 2 hours with occasional inversion to ensure complete RNA digestion. After this, the 'PFGE Solution 2' was aspirated and replaced with 1 ml 'PFGE Solution 3' which was incubated at 55 °C overnight to allow Proteinase K to digest proteins.

The 'PFGE Solution 3' was then removed and replaced with1 ml 50 mM EDTA to wash the plugs. These were washed at room temperature for 30 minutes on a rotating wheel (Cole Parmer TR-200) set to 6 RPM. The EDTA was the replaced with 1 ml fresh 50 mM EDTA for another 30 minute wash-with-rotation; this washing was repeated three times in total. Once the plugs were washed, they could be used for a PFGE immediately. However, they could also be prepared for storage at -20 °C; this was achieved by replacing the EDTA with 1 ml 'PFGE Storage buffer', equilibrated at room temperature for 30 minutes, then replaced with 1 ml fresh 'PFGE Storage Buffer' and kept at -20 °C for future use.

To prepare the PFGE gel, 150 ml 0.5 x TBE was used to make a 1.3 % agarose gel (SeaKem® Gold) which was boiled then kept at 55 °C so as to remain molten. Whilst the agarose cooled, plugs were cut in half and equilibrated in 1 ml of 0.5 x TBE for 15 minutes with rotation at 6 RPM. Then these ½ a plugs were placed on the PFGE comb alongside a 2 mm disc of λ-PFGE ladder (NEB) was used as a molecular weight standard. These were secured in place with a drop (10-20 µl) molten agarose which was left to set at room temperature for 10 minutes.

Once the samples and ladder had set, the comb was placed into the casting tray and 145 ml of the molten agarose was poured in, then left to set at room temperature for 30 minutes. After this, the comb was removed leaving the samples and ladder embedded in the gel. Then the gaps left from the comb were filled with the remaining molten agarose and left to set for 10 minutes at room temperature.

When fully prepared, the gel was placed into the PFGE running tank (BioRad Electrophoresis Cell) with 0.5 x TBE as the running buffer cooled to 14 °C (BioRad Cooling Module) circulating with a BioRad Variable Speed Pump set to 100. The gel was left to equilibrate in the tank for 15 minutes before initiating 'Program 1' followed by 'Program 2' as described below in Table 2-13 (BioRad Chef Mapper™).

Table 2-13 Program settings for PFGE using the BioRad Chef Mapper™.

	Program 1	**Program 2**
Program Duration	25 hours	4 hours
Initial Switch Time	15 s	45 s
End Switch Time	22 s	45 s
Switch Angle	60 °	60 °
Voltage Gradient	6 V / cm	6 V / cm
Shape	linear (0)	linear (0)

Once the programs were complete, the gel was removed from the tank and stained in a metal tray containing 300 ml ddH_2O with 0.5 µg / ml ethidium bromide. This was incubated with gentle shaking (Stovall Belly Dancer) for 15 minutes. The ethidium bromide was then poured away and replaced with 300 ml fresh ddH_2O to wash the gel for 5 minutes with gentle shaking. The gel was then imaged using a UV transilluminator (BioRad ChemiDoc™ MP imaging system).

2.7.3 PFGE/Digest Gel Transfer Using the Whatman® TurboBlotter System

Once the Southern Blot/PFGE has been run, the gel can be transferred to a membrane so it can be probed for specific DNA sequences. The first step is to shear the large fragments of DNA into smaller pieces to allow for a more efficient transfer to the membrane; this was achieved via acid depurination by soaking the gel in 0.25 M HCl at room temperature for 30 minutes with gentle shaking (Stovall Belly Dancer). Then the acid was poured off, and the gel was washed in ddH_2O for 5 minutes at room temperature with gentle shaking. Then the gel was washed in 'PFGE/SB Denaturing Buffer' to make the DNA single stranded to further aid DNA transfer. This was left to soak for 30 minutes at room temperature with gentle shaking. The old denaturing buffer was then discarded and replaced with fresh 'PFGE/SB Denaturing Buffer' which was incubated for another 30 minutes; this was then repeated meaning that a total of three denaturing washes took place.

Following the denaturation of the DNA, the gel was then soaked in 'PFGE/SB Transfer Buffer' for 15 minutes at room temperature with gentle shaking. Concurrently, a Whatman® Nytran™ SuPerCharge membrane was soaked ddH2O for 15 minutes. Then the Whatman® TurboBlotter transfer stack was assembled as shown below (Figure 2-1). The buffer wick was kept wet with 'PFGE/SB Transfer Buffer' for 2-6 hours to allow the DNA to transfer from the agarose gel onto the membrane.

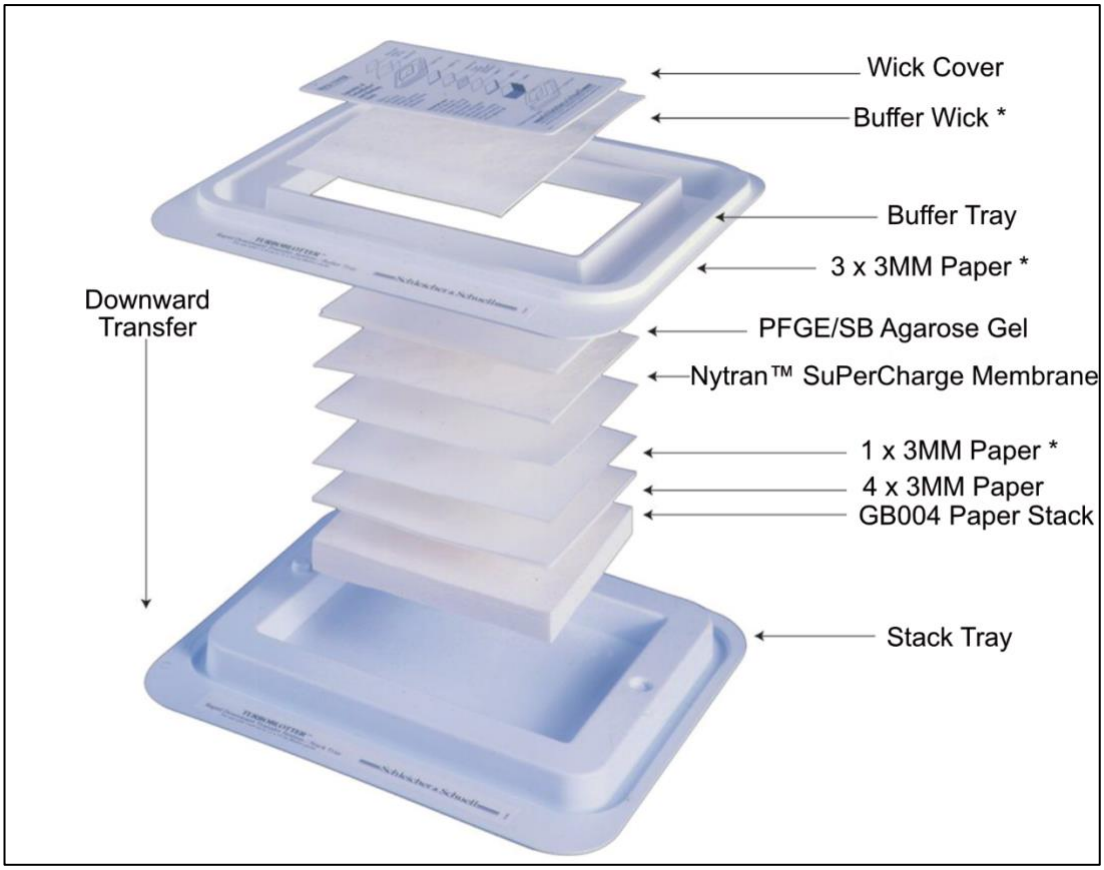

Figure 2-1 The assembly of the Whatman® TurboBlotter transfer system. Papers marked with * are pre-wet in 'PFGE/SB Transfer Buffer'.

When the transfer had completed, the stack was disassembled, the gel discarded and the membrane was soaked in '1 x PFGE/SB Neutralisation Buffer' for 5 minutes at room temperature. Then the membrane was dried using 3MM paper, and the DNA was covalently attached to the membrane using a UV crosslinker (UVP CX-2000) set to 1200 J / m^2. The membrane was subsequently wrapped in cling film and stored at 4 °C until ready for hybridisation.

2.7.4 PFGE/SB Probe Preparation

A 25 µl PCR reaction was set up as described previously (section **2.4.1**) using wildtype gDNA as the template. NEB 6 x Purple Loading Dye was then added to the sample, and the DNA was run on a standard agarose gel (section **2.4.3**). Then the gel was placed onto a UV Illuminator (Syngene) and a P1000 pipette tip was used to 'stab' the band on the gel which corresponded with the probe size. This small piece of DNA-agarose was then added to 250 µl SDW in a 1.5 ml microfuge tube, which was then boiled for 5 minutes (Stuart SBH130DC). Once cooled, four 50 µl PCR reactions were set up as before but with the 250 µl boiled DNA-water as the template; this ensures that only the target sequence acts as the probe, none of the template DNA from the original PCR reaction. The PCR reactions were then checked using a UV transilluminator (BioRad ChemiDoc™ MP Imaging System) and purified via a PCR cleanup step (section **2.4.2**).

2.7.5 PFGE/SB Hybridisation

The ‘Pre-Hyb’ and ‘Hyb’ solutions were prepared in 50 ml centrifuge tubes (Sarstedt) and heated to 65 °C using a microwave (Sharp), and then incubated at 65 °C for 30 minutes in an hybridisation oven (Techne HB-1D) 800 µl of 10 mg / ml salmon sperm DNA was boiled for 5 minutes and added to the ‘Pre-hyb’ solution. The ‘Pre-Hyb’ solution was then added to a pre-warmed hybridisation tube (Techne) and the membrane to be hybridised was inserted into the tube, ensuring it was completely ‘stuck’ to the edges of the tube with no air bubbles. This was allowed to pre-hybridise in the hybridisation oven at 65 °C for 3 hours with rotation.

Whilst the membranes were pre-hybridising, the probes were prepared. A 20 µl DNA-probe mix was prepared by adding 0.1 – 1 µg probe DNA, 1 ng ladder DNA (λ ladder for PFGE, λ-BstEII digest ladder for SB; both made by NEB) in SDW which was then boiled at 100 °C for 5 minutes and kept on ice. This DNA mix was then radio-end-labelled by adding 4 µl High Prime and 2 µl [αP^{32}] dCTP (both Roche) and incubating at 37 °C for 20 minutes in a hot block (Techne DB-2D). After this incubation, the label-incorporated-probe DNA was separated from residual [αP^{32}] dCTP by adding 30 µl TE buffer to the reaction mix, which was then loaded onto a Sephadex G-50 Fine column (Roche) which was centrifuged at 1,250 *xg* (Fisher Scientific accuSpin Micro 17)) for 4 minutes. The flow-through from this spin was then added to 450 µl 10 mg / ml salmon sperm DNA and this whole mix was boiled at 100 °C for 5 minutes in a hot block. Finally the ‘Pre-Hyb’ mix in the tube was poured away, replaced with the ‘Hyb’ solution, and the radio-labelled-probe mix was added to the tubes. These were hybridised overnight at 65 °C with rotation.

Following hybridisation, the membranes were washed twice with 50 ml 65 °C ‘Hyb Wash 1’ solution; both washes for 30 minutes at 65 °C with rotation. Then this double-wash was then repeated in the same fashion with ‘Hyb Wash 2’. Then the membrane was removed from the hybridisation tube, wrapped in clingfilm (Saragold®), placed in a cassette (Fujifilm) with a screen (Fujifilm) to develop for 1-7 days depending on the age of the radiation used. Once developed, the screens were imaged using a Typhoon™ imager (Cytiva). Bands were quantified using BioRad Image Lab software.

Chapter 3: Alternative Removal of Spo11: An Investigation into Tdp1

During meiosis, DSBs are initiated by the Spo11 complex, which then remains covalently bound to the DNA. In order for these DSBs to be repaired, Spo11 must be removed from the DNA. As described earlier (section **1.3.5**), the removal of Spo11 is effected nucleolytically by the MRX complex (section **1.3.6**). However, when the MRX complex has been rendered nucleolytically inactive, either by *rad50S* or *sae2Δ*, alongside a NHEJ-defective *ku70Δ* mutation, meiotic recombinant products are seen. This indicates that Spo11 can be removed by other means (Yun and Kim, 2019). But how is Spo11 being removed?

As outlined in section **1.4.1**,the phosphodiesterase Tdp1 could be responsible for removing Spo11. It is upregulated in meiotic prophase when the MRX complex is compromised (Kugou et al., 2007). It can also remove similar substrates from 5′-DNA ends (Nitiss et al., 2006). To investigate how important Tdp1 is to meiosis, and whether it can remove Spo11 from DNA to produce CO/NCO products, several *in vivo* experiments were performed. To see is Tdp1 is essential to meiosis, sporulation efficiency and spore viability was determined (section **3.1**), the downstream CO/NCO pathway for following-up Spo11 removal in *ku70Δ sae2Δ* was investigated (section **3.2),** the presence of Tdp1 during meiosis was monitored via western blotting (section **3.3)**, utilising an overexpression system to try and generate moreTdp1-catalysed CO/NCO products in a *ku70Δ sae2Δ* (section **3.4)** and DSB dynamics DNA repair was monitored via Southern blotting (sections **3.5** and **3.6).**

3.1 The Effects of *tdp1Δ* on Sporulation

If Tdp1 is responsible for removing Spo11 in the *ku70Δ sae2Δ* background, deleting *tdp1* would remove CO/NCO formation as Spo11 would remain bound, arresting the cells in prophase. As such, a fluorescent reporter strain was utilised to monitor crossovers at a cellular level. These diploid strains, based on previously made strains (Thacker et al., 2011), have heterozygous fluorescent genes on chromosome 8. One chromatid has the mCerulean gene encoding a cyan fluorescent protein from *A. victoria* (Rizzo and Piston, 2005) whilst the homologous chromatid has a tdTomato gene which codes for a red fluorescent protein from the *Discosoma* genus (Shaner et al., 2004). When crossovers occur, it is possible to exchange these fluorescent markers between chromatids. This gives 3 possible tetrad fluorescent options: parental ditype where no COs occur and there are 2 red and 2 cyan spores; a tetratype where 1 CO occurs meaning there is 1 yellow, 1 non-fluorescent, 1 red and 1 cyan spore; or a non-parental ditype where 2 COs occur generating 2 yellow and 2 non-fluorescent spores. A schematic showing the four possible fluorescent spores which can be generated is shown in **Figure 3-1**. Therefore, if *tdp1Δ* removes the ability to remove Spo11 in the *ku70Δ sae2Δ* background, we should see a reduction in COs via fluorescence.

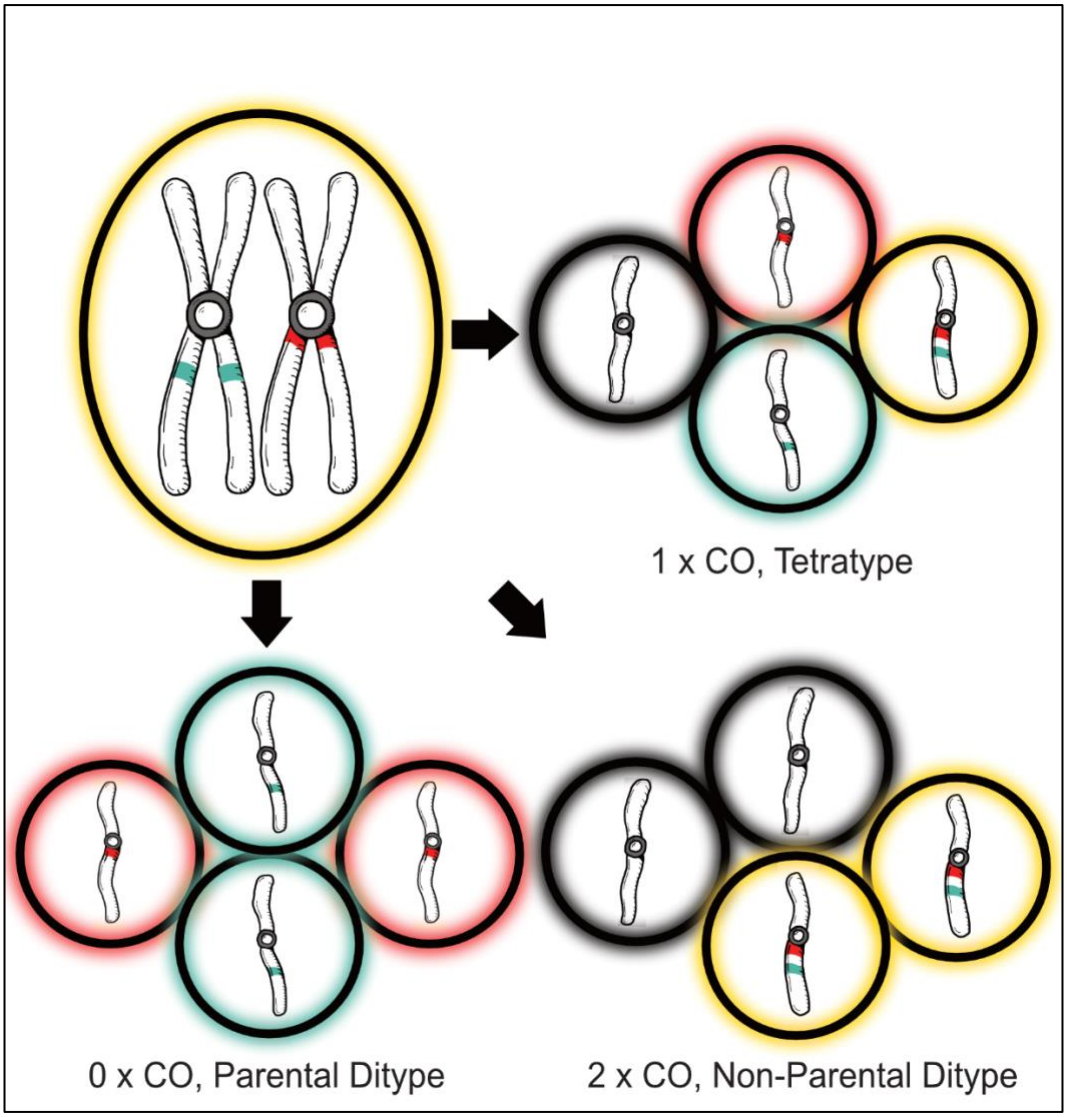

Figure 3-1 Monitoring CO Formation via Fluorescent Markers. CHR VIII contained heterozygous fluorescent markers; one chromatid contained mCerulean, the homolog contained tdTomato. When driven through meiosis, three possible tetrad combinations are possible: tetratype, parental ditype, or non-parental ditype.

Before commencing with fluorescent assays, it was important gauge whether Tdp1 is playing a vital role in meiosis. To see if this is the case, sporulation efficiency experiments were performed. Here, diploid cells were inoculated into sporulation media and grown with shaking at 30 °C for 48 hours, then the percentage of sporulated-to-unsporulated cells were calculated. Further to this, tetrads were dissected into individual spores which are then grown for 2 days to determine spore viability. Taken together; these experiments give an insight to whether a certain genotype affects meiotic completion. As shown in **Figure 3-2 C**,

the removal of tdp1 reduces spore efficiency modestly from 81.8% in wildtype, compared to 76.2% in *tdp1Δ*; whilst the spore viability in **Figure 3-2 A/B** is barely affected: 96.8% in wildtype to 94.9% in *tdp1Δ*. Taken together, Tdp1, in an otherwise wildtype background, does not seem to play an essential role in meiosis when the MRX-Sae2 and NHEJ pathways are fully operational.

When the MRX-Sae2 and NHEJ pathways are compromised, CO/NCO products are observed, indicating that Spo11 is processed and meiosis can continue (Yun and Kim, 2019); it is under these conditions that I hypothesised Tdp1's meiotic function may reveal itself. Ku70 is a protein involved in NHEJ (reviewed here (Emerson and Bertuch, 2016)). As Ku70 preferentially binds to blunt ended DSBs, it was not expected to play a role in Spo11-induced DSBs as they are resected to form a ssDNA end (Foster et al., 2011). **Figure 3-2 C** shows *ku70Δ* leads to a 1 % decrease in sporulation efficiency compared to wildtype The spore viability of *ku70Δ* shown in **Figure 3-2 A** and **B** are slightly higher than wildtype, with 97.9 % viability compared to wildtype 96.8 %. The deletion of *sae2* however has drastic effects on sporulation efficiency, reducing it to 0.77 %, thereby rendering spore viability tests impossible; this was expected as Sae2 is needed to activate MRX, which in-turn removes Spo11 (Neale et al., 2005, Cannavo and Cejka, 2014). Despite CO/NCO products being seen previously in the *sae2Δ ku70Δ* background (Yun and Kim, 2019), sporulation efficiency was reduced to 0.92%, meaning that tetrads could not be dissected to calculate spore viability. The *ku70Δ sae2Δ tdp1Δ* didn't sporulate at all, which could indicate that Tdp1 is required for Spo11 removal in an MRX/NHEJ compromised background, however the difference in sporulation between the *sae2Δ, ku70Δ sae2Δ,* and *ku70Δ sae2Δ tdp1Δ* strains is less than 1 %. Due to the poor levels of sporulation see in these backgrounds, it wasn't possible to monitor crossovers via the fluorescent marker assay described earlier. Therefore, to see if *tdp1Δ* can abolish CO/NCO in the *ku70Δ sae2Δ* background, Southern blotting was utilised (sections **3.5** and **3.6)**

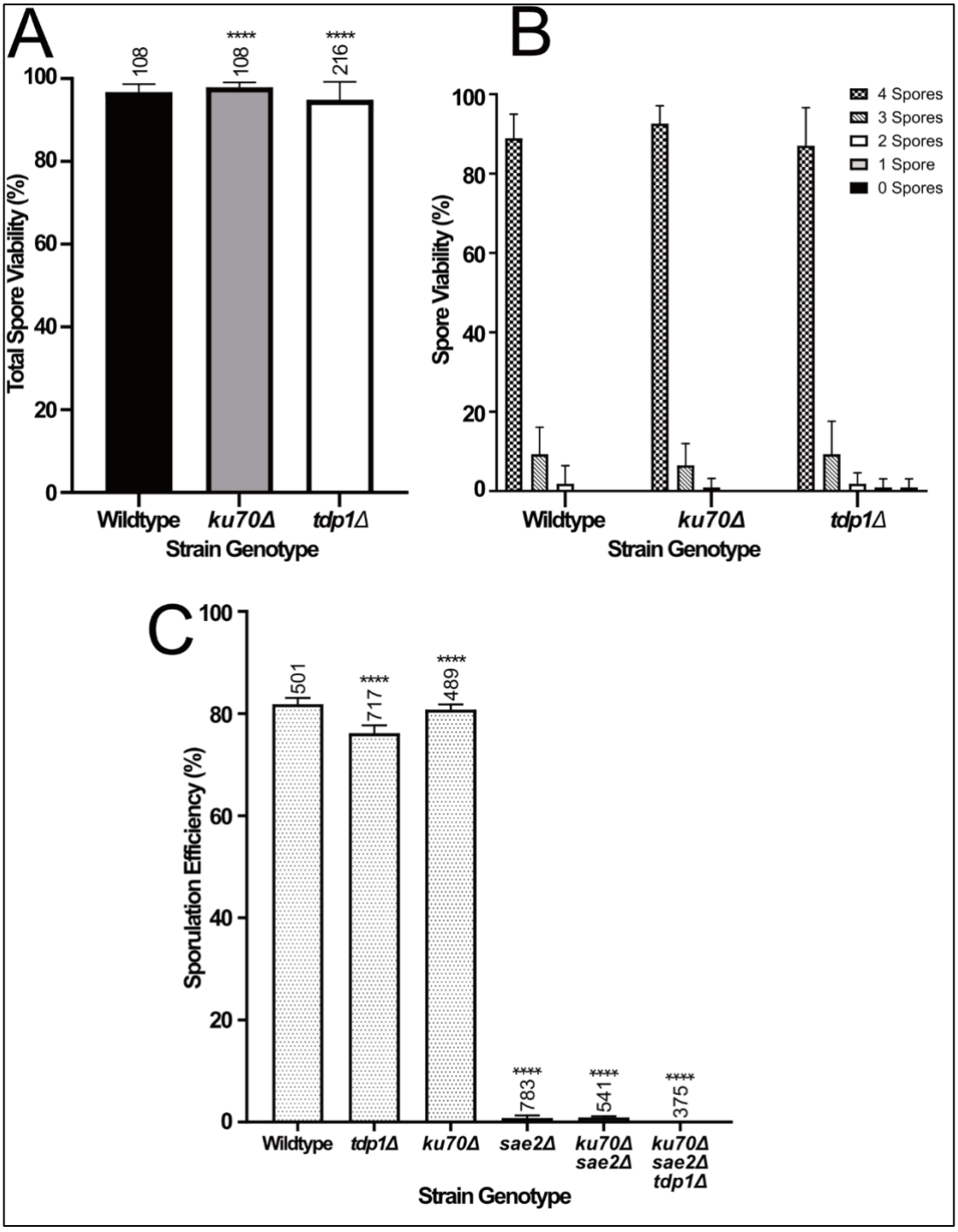

Figure 3-2 The effects that Tdp1, Ku70, and Sae2 have on sporulation. Cultures were inoculated into 2 % potassium acetate to sporulate for 48 hours at 30 °C with shaking. Samples were then counted for sporulation efficiency and, where possible, dissected for spore viability. Strains used: Wildtype = YSG236; *tdp1Δ* = YSG579 & YSG580; *ku70Δ* = YSG566-568; *sae2Δ* = YSG 571; *ku70Δ sae2Δ* = YSG574-576; *ku70Δ sae2Δ tdp1Δ* = YSG554-556. **A)** Overall spore viability of dissected yeast tetrads in wildtype, *ku70Δ* and *tdp1Δ* strains. Number of tetrads dissected shown above error bar. Error bars = 1 SD. **** = $p < 0.0001$, unpaired t test. **B)** Shows the individual spore viabilities per tetrad dissected in

‘A’. **C)** Shows the sporulation efficiency of strains with deletions in *ku70, sae2*, and *tdp1*. The number of cells/spores counted is shown above each bar. Error bars = 1 SD. . **** = p < 0.0001, unpaired t test.

3.2 Investigating Which CO Resolution Pathway is Active When NHEJ and MRX are Disrupted

As well as removing Spo11, there is a CO repair pathway being utilised in *ku70Δ sae2Δ* strains. To investigate this, mutants in structure selective nucleases (SSNs) known to be expressed and playing a role in meiosis were tested for sporulation efficiency and spore viability. These SSNs play vital roles in the different meiotic CO resolution 'classes'. The most well understood JM resolution pathway, often referred to as 'Class I' COs, form from dHJs which are processed nucleolytically into CO products. This is coordinated by Msh4-5, Exo1, and the MutLγ nuclease Mlh1-3 (Zakharyevich et al., 2012, Nishant et al., 2008). As well as CO resolution, Mlh1 also forms a complex with Pms1, Mutlα, which is required for mismatch repair (Manhart and Alani, 2016). An alternative CO pathway involves the XPF-family nuclease Mus81 with Mms4. As well as being able to resolve dHJs, Mus81 is able to cleave nicked HJs as well as flaps; often referred to as 'Class II' CO resolution, this pathway can account for up to 40% of COs seen in S. cerevisiae (Zakharyevich et al., 2012, Hollingsworth and Brill, 2004, de Los Santos et al., 2003). It has also been shown that the SSNs Slx1-4 and Yen1 can also process JMs into COs (Zakharyevich et al., 2012).

Figure 3-3 A shows that the *pms1Δ, slx4Δ*, and *yen1Δ* had modest effects on sporulation efficiency; dropping from 81.8 % in wildtype to 74.6 %, 72.9 %, and 73 % respectively. Despite retaining good sporulation efficiency, the spore viability of the *pms1Δ* strains was very low at 34.9 %, compared to 90.7 % viability for *slx4Δ* and 96.3 % for *yen1Δ* (**Figure 3-3 B/C**). The *mlh1Δ* had a modest effect on sporulation efficiency (68.0 %) but had the largest impact on spore viability, dropping to 23.4 %. Interestingly the *mus81Δ* reduced sporulation efficiency by the most, reducing it to 25.6 %, whilst the spore viability was close to the *pms1Δ* at 34.7 %.

Unfortunately, trying to understand which CO pathway is being utilised in the *ku70Δ sae2Δ* background fluorescently proved impossible as described earlier (section **3.1**) As the

sporulation efficiency across the board was below 1 % when *ku70Δ* and *sae2Δ* mutations were present, there were too few tetrads produced to analyse CO events fluorescently.

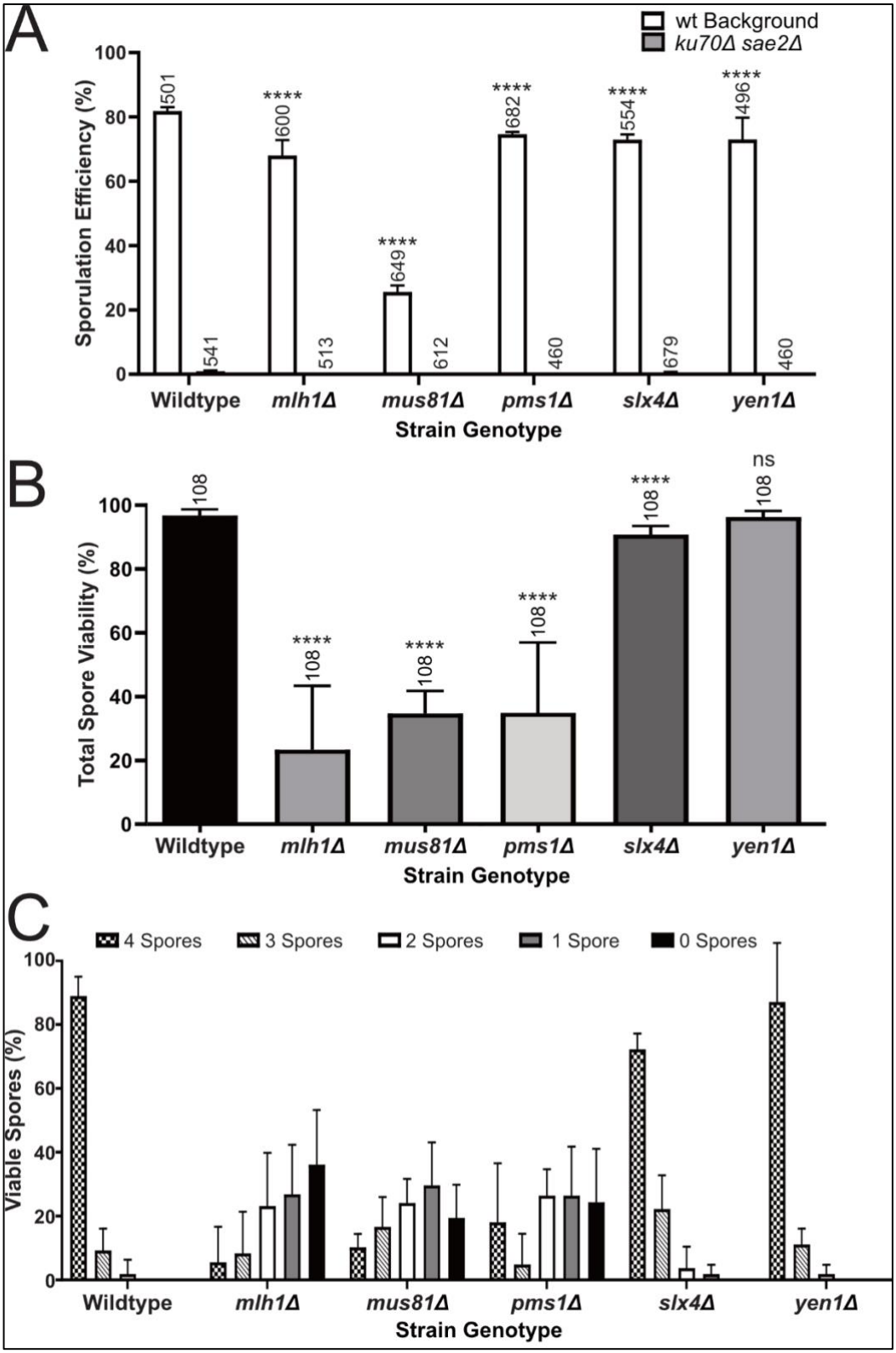

Figure 3-3 The effects that SSN deletions have on sporulation. Cultures were inoculated into 2 % potassium acetate to sporulate for 48 hours. Samples were then counted for sporulation efficiency and, where possible, dissected for spore viability. Strains used:

Wildtype = YSG236; *ku70Δ-sae2Δ* = YSG574-576; *mlh1Δ* = YSG237; *mlh1Δ ku70Δ sae2Δ* = YSG750-752; *mus81Δ* = YSG725-727; *mus81Δ ku70Δ sae2Δ* = YSG753 & YSG 754; *pms1Δ* = YSG728 & YSG729; *pms1Δ ku70Δ sae2Δ* = YSG833-835; *slx4Δ* = YSG730-732; *slx4Δ ku70Δ sae2Δ* = YSG816-818; *yen1Δ* = YSG733-735; *yen1Δ ku70Δ sae2Δ* = YSG821-823. **A)** Shows the sporulation efficiency of strains with SSN deletions in in wildtype and *ku70Δ sae2Δ* backgrounds. The number of cells/spores counted is shown above each bar. Error bars = 1 SD. . **** compares SSNΔ to wildtype, $p < 0.0001$. **B)** Shows overall spore viability of dissected yeast tetrads in wildtype and *SSNΔ* strains. Number of tetrads dissected shown above error bar. Error bars = 1 SD. **** = $p < 0.0001$, unpaired t test. **C)** Shows the individual spore viabilities per tetrad dissected in **'B'**.

3.3 Monitoring Tdp1 Levels During Meiosis

If Tdp1 is playing a role in Spo11 removal, Tdp1 should be detectable during meiosis via western blotting. To investigate this, Tdp1 with N-terminal His_6-HA_3 tags was generated in wildtype, *ku70Δ, sae2Δ,* and *ku70Δ saeΔ* backgrounds.

Before monitoring Tdp1 levels via western blotting, it was important to ascertain whether the addition of His_6-HA_3 affinity tags to the N-terminal of Tdp1 would affect its function. To ensure the tags didn't affect Tdp1 function, we measured the spore viability and sporulation efficiency of the tagged-Tdp1 strains compared to the un-tagged strains.

The presence of a tag on Tdp1 made a minimal impact on sporulation (**Figure 3-4 A**). In the wildtype background, sporulation efficiency dropped from 81.8 % to 80.9 % when a tag was present. In the *ku70Δ* background, the presence of a tag on Tdp1 increased sporulation efficiency, albeit by less than 1% from 80.8 % in un-tagged, to 81.8 % when tagged. The *sae2Δ* and *ku70Δ-sae2Δ* background strains all sporulated incredibly poorly, though the presence of a tag on Tdp1 did increase sporulation efficiency by 2 % in the sae2 % background, and by 1.2 % in the *ku70Δ sae2Δ* background. The Tdp1-tags also had a minimal effect on spore viability, with both the wildtype and *ku70Δ* backgrounds having a spore viability of 98.2 %, both higher than the wildtype un-tagged Tdp1 of 96.8 % spore viability of.

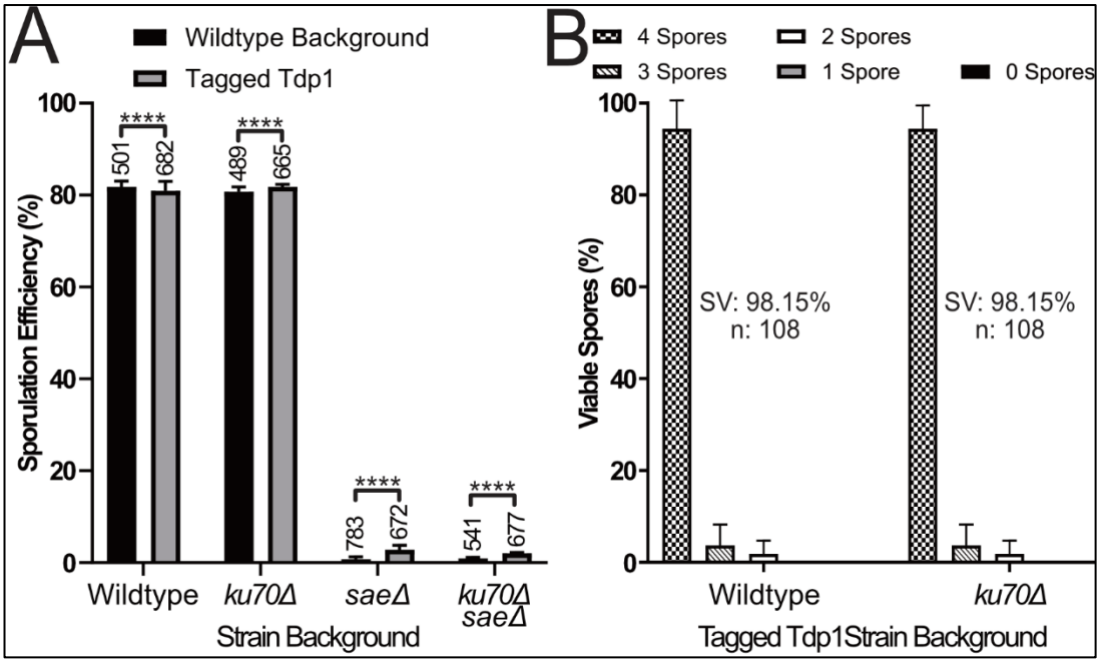

Figure 3-4 The N-terminal affinity tags have a minimal effect on Tdp1 during meiosis. Cultures were inoculated into 2 % potassium acetate to sporulate for 48 hours, cultures were then counted for sporulation efficiency and, where possible, dissected for spore viability. Strains used: Wildtype = YSG236; Wildtype-Tagged-Tdp1 = YSG710 & YSG711; *ku70Δ* = YSG566-568; *ku70Δ*-Tagged-Tdp1 = YSG741 & YSG742; *sae2Δ* = YSG 571; *sae2Δ*-Tagged-Tdp1 = YSG744 & YSG745; *ku70Δ sae2Δ* = YSG574-576; *ku70Δ sae2Δ*-Tagged-Tdp1 = YSG827 & YSG828. **A)** Shows the sporulation efficiency of strains with tagged Tdp1 Vs untagged equivalents in wildtype, *ku70Δ, sae2Δ,* and *ku70Δ-sae2Δ*. The number of cells/spores counted is shown above each bar. Error bars = 1 SD. **** = $p < 0.0001$ unpaired t test. **B)** Spore viability of dissected yeast spores with tagged Tdp1-His_6-HA_3 in wildtype and ku70Δ backgrounds. SV = total spore viability, n = tetrads dissected.

As the presence of a tag on Tdp1 doesn't seem to affect its meiotic function, the levels of Tdp1 during meiosis were monitored via western blotting. Meiotic timecourses were run in wildtype, *ku70Δ, sae2Δ* and *ku70Δ-sae2Δ* backgrounds, with protein samples taken every hour for 8 hours. It is during these first 8 hours of meiosis that we expect DSBs to be initiated and repaired (as confirmed later in section **3.5**), meaning that Spo11 removal is occurring. Untagged-strain controls were used to ensure that only the HA-tags on Tdp1 were being detected, as opposed to non-specific binding. Vegetative samples were also taken to provide a basal-level of Tdp1 abundance with which to compare meiotic levels to.

Furthermore, as TCE was added to the SDS-PAGE gels, the UV-tryptophan fluorescence of the total-soluble-protein could be compared to the chemiluminescence of the western Blot bands, enabling Tdp1-levels could be compared to total-soluble-protein loaded.

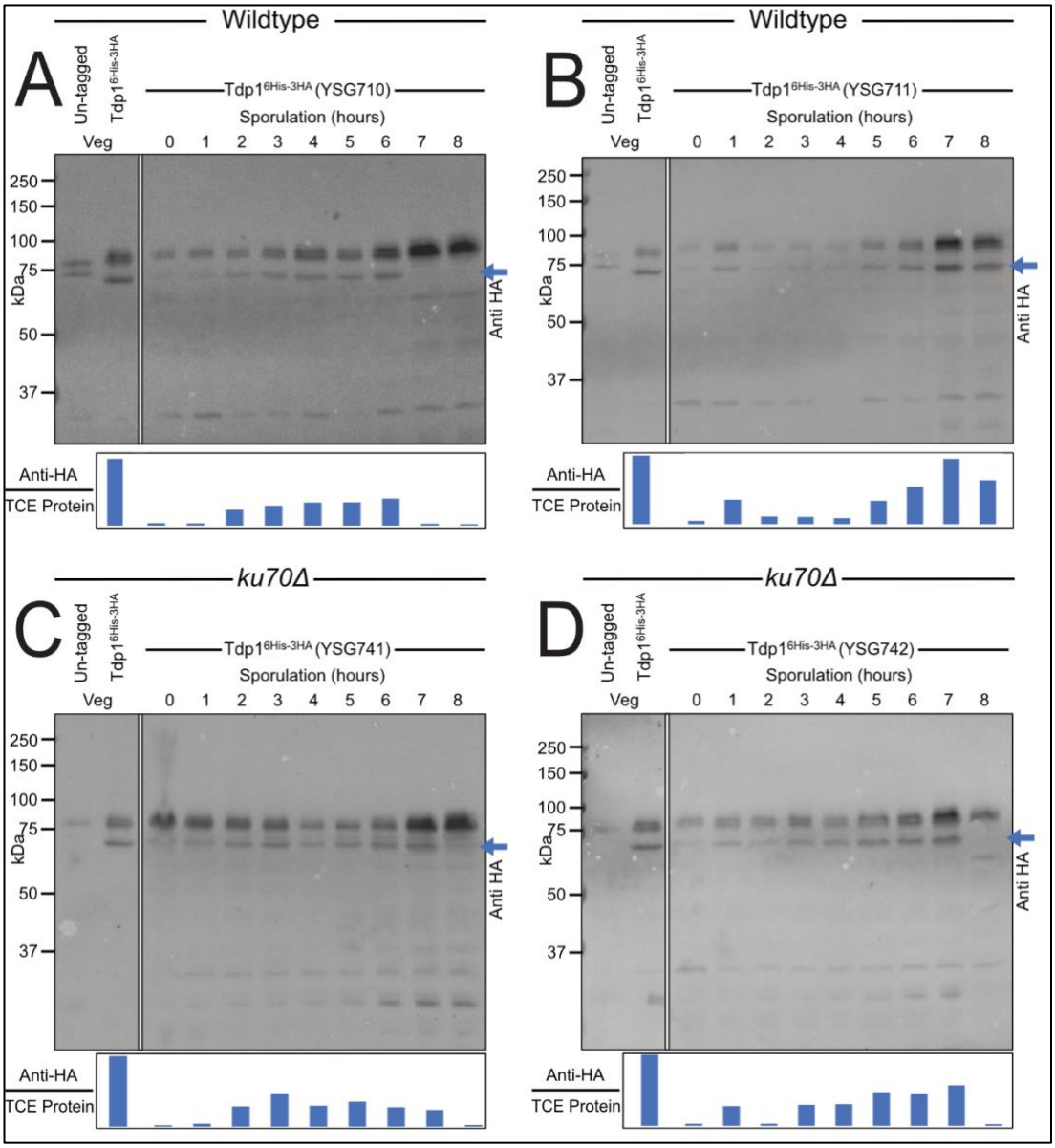

Figure 3-5 Monitoring levels of Tdp1 during meiosis in wildtype and *ku70Δ* backgrounds via western blotting. 20ml of meiotic timecourse culture was harvested at the times shown. Total soluble-protein extracts were run on a 10 % SDS-PAGE gel containing TCE for visualisation via UV. Tdp1-His_6-HA_3 was detected via western blotting, using rabbit-anti-HA 1° antibodies and goat-anti-rabbit 2° antibodies. The blue arrow shows the 67kDa tagged-Tdp1. Bands were quantified using BioRad ImageLab software and levels of Tdp1-His_6-HA_3 were compared to total TCE protein at each time point, represented in the bar charts. **A)** and **B)** show Tdp1-His_6-HA_3 levels in wildtype backgrounds; **C)** and **D)** show

Tdp1-His_6-HA_3 levels in *ku70Δ* backgrounds. Empty lane between the vegetative and meiotic samples were cropped out.

Figure 3-5 and **Figure 3-6** show the levels of Tdp1 protein during the first 8 hours of meiosis in wildtype, *ku70Δ* backgrounds, and *sae2Δ / ku70Δ sae2Δ* backgrounds respectively. In all of the tagged strains, there an anti-HA band corresponding to the 67 kDa of the Tdp1-His_6-HA_3 protein, which was absent in the untagged controls. There was also a non-specific band slightly higher which can be seen in the un-tagged lanes and some of the tagged samples. Though present, meiotic Tdp1 levels never reached vegetative expression levels.

Figure 3-5 A shows Tdp1 levels increasing as meiosis progresses in a wildtype background, with Tdp1 abundance peaking at the 6-hour mark, then rapidly declining. **Figure 3-5 B** also shows wildtype Tdp1 levels, though here Tdp1 levels fluctuate and peak at near-vegetative levels at 7 hours. The *ku70Δ* strains in **Figure 3-5 C / D** show that Tdp1 levels peak at 3 hours and 7 hours respectively. Whilst the anti-HA/TCE-protein ratio do not show any Tdp1-abundance trends, it is clear that Tdp1 is present during meiosis.

Similarly, **Figure 3-6** also shows that Tdp1 is present in meiosis in *sae2Δ* and *ku70Δ sae2Δ* backgrounds. **Figure 3-6 A** shows that in one of the *sae2Δ* backgrounds the levels of Tdp1 remain consistent between 1 to 8 hours, whilst **Figure 3-6 B** shows the levels of Tdp1 increase, peaking at 6 hours, then declining. In the *ku70Δ sae2Δ* backgrounds, **Figure 3-6 C** shows Tdp1 abundance gradually increasing to 7 hours, then decreasing, whilst **Figure 3-6 D** shows Tdp1 levels peaking at 3 hours, then fluctuating slightly before declining sharply at 8 hours.

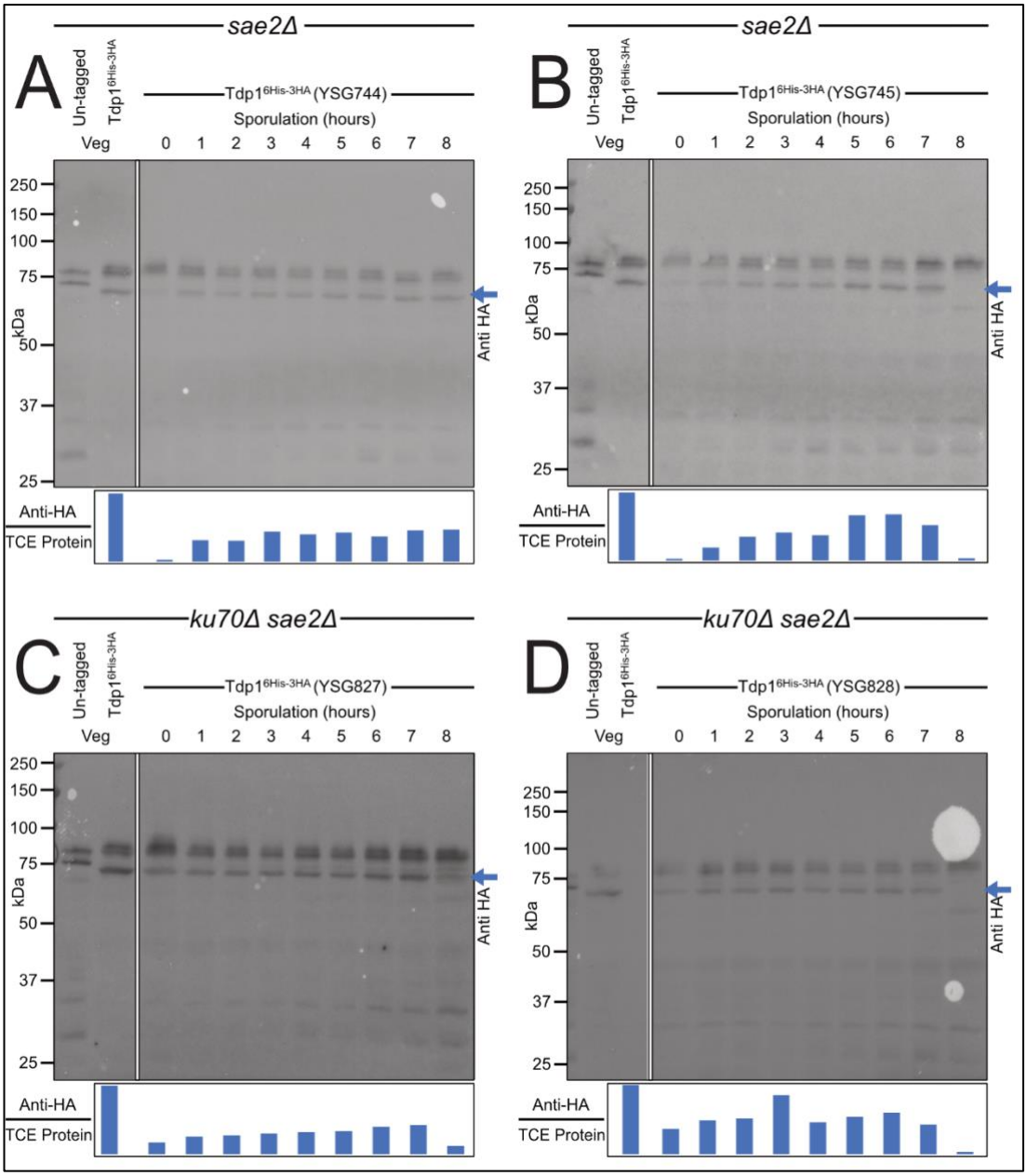

Figure 3-6 Monitoring levels of Tdp1 during meiosis in *sae2Δ* and *ku70Δ sae2Δ* backgrounds via western blotting. 20ml of meiotic timecourse culture was harvested at the times shown. Total soluble-protein extracts were run on a 10 % SDS-PAGE gel containing TCE for visualisation via UV. Tdp1-His_6-HA_3 was detected via western blotting, using rabbit-anti-HA 1° antibodies and goat-anti-rabbit 2° antibodies. Blue arrows point to the 67kDa tagged-Tdp1 protein. Bands were quantified using BioRad ImageLab software and levels of Tdp1-His_6-HA_3 were compared to total TCE protein at each time point, represented in the bar charts. **A)** and **B)** show Tdp1-His_6-HA_3 levels in *sae2Δ* backgrounds; **C)** and **D)** show Tdp1-His_6-HA_3 levels in *ku70Δ sae2Δ* backgrounds. Empty lanes between vegetative controls and meiotic lanes were cropped out.

3.4 Overexpressing Tdp1 Using the P^{CUP1} Promoter

If Tdp1 is able to remove Spo11 in a *sae2Δ-ku70Δ* background, by increasing the level of Tdp1 expression via an inducible promoter could lead to more Spo11 processing via this pathway. By overexpressing Tpd1, we could see how effective this Tdp1-Spo11 pathway can be. The His_6-HA_3-tagged tdp1 gene was placed under the P^{CUP1} copper-inducible promoter (Macreadie et al., 1989). The effectiveness of the copper-induced overexpression was tested via western blotting (**Figure 3-7 A**).

The initial overexpression was carried out in haploid strains to check the effectiveness before making diploid strains via mating. Cultures were grown with or without 25 μM $CuSO_4$ for 2 hours, then cells were harvested, proteins separated via SDS-PAGE and Tdp1 levels measured via western blotting. Despite no obvious bands in the TCE gel, the western blots successfully showed high levels of Tdp1when induced with $CuSO_4$.

Despite the successful overexpression of Tdp1, sporulation was not recovered in the *sae2Δ* or *ku70Δ-sae2Δ* backgrounds as shown in **Figure 3-7 B**. There was less than 0.5 % sporulation seen in both the sae2Δ and the ku70Δ-sae2Δ strains regardless of whether Tdp1 was overexpressed with the addition of $CuSO_4$. Furthermore, in the P^{CUP1}-tdp1, P^{CUP1}-tdp1-ku70Δ, and the tagged-tdp1 only strains, the addition of $CuSO_4$ drastically reduced sporulation by 28.8 %, 26.5 %, and 10.1 % respectively. The Tdp1 upregulation was not enough to improve sporulation, and the $CuSO_4$ used to induce overexpression seemed to hinder sporulation further, exemplified by the sporulation reduction in the tagged-tdp1 strain.

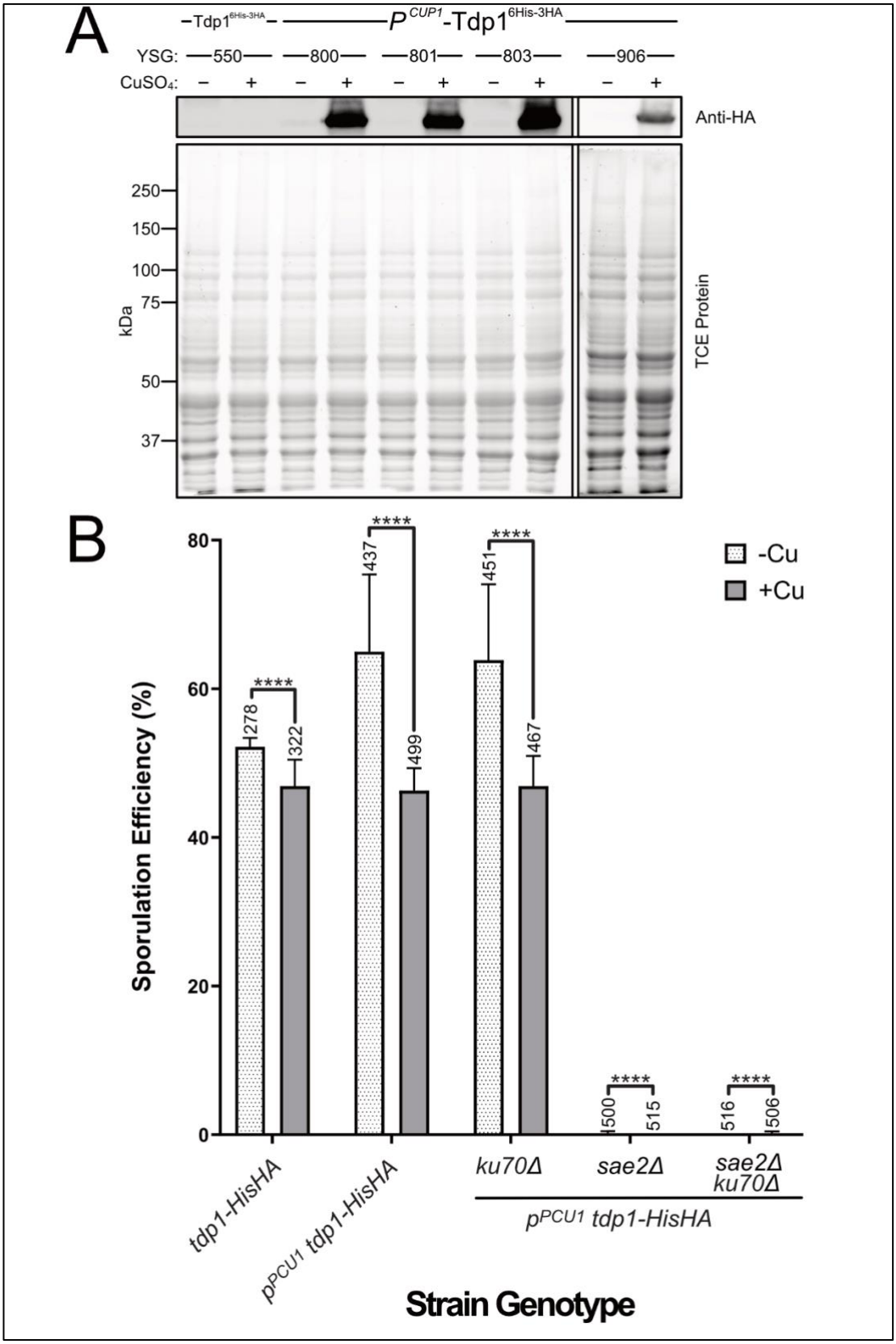

Figure 3-7 Inducing Tdp1 expression via the *P*^{CUP1} promoter. **A)** Shows the pilot overexpression of Tdp1-His$_6$-HA$_3$. Cultures were grown in YPD, then split in half: one

received 25 μM CuSO4 to induce Tdp1 expression, the other received SDW; these were incubated with shaking for 2 hours to allow protein expression before being harvested. Total soluble-protein extracts were run on a 10 % SDS-PAGE gel containing TCE for visualisation via UV. Tdp1-His_6-HA_3 was detected via western blotting, using rabbit-anti-HA 1° antibodies and goat-anti-rabbit 2° antibodies. **B)** Shows the effect of overexpressing Tdp1 using $CuSO_4$. Cultures were inoculated into 2 % potassium acetate, supplemented with either 25 μM $CuSO_4$ or SDW, to sporulate for 48 hours. Spores were counted to measure sporulation efficiency. Number of cells/spores counted is shown above each bar. Error bars = 1 SD. **** = $p < 0.0001$ unpaired t test.

3.5 Tdp1 DSB Dynamics: Whole Chromosome Analysis via PFGE and Southern Blotting

Despite the evidence of Tdp1 being present during meiosis and the previous work showing that the *ku70Δ sae2Δ tdp1Δ* mutants do not produce spores, it is important to determine that meiotic DSBs are still being induced and repaired as expected. Otherwise it could argued be that instead of removing Spo11 to help form CO/NCO meiotic repair products, DSBs aren't forming or being repaired, hence the reason why the *ku70Δ sae2Δ tdp1Δ* mutants did not sporulate. To address this concern, Pulsed Field Gel Electrophoresis (PFGEs) followed by Southern blotting was implemented. With this technique, chromosomal integrity could be analysed as meiosis progresses; as DSBs are induced by Spo11, smaller bands representing broken chromosomes would appear on the blot. These could then persist if Spo11 can't be removed and CO/NCO repair products are unable to form; or the chromosomes are repaired, meaning only the parental bands are visible, and meiosis progresses as usual. A schematic showing meiotic DSBs forming at the chromosomal level and persisting is shown in **Figure 3-8**.

Furthermore, by using PFGEs and Southern blotting, we can compare DSB dynamics in different deletion backgrounds, to see if DSBs are repaired/induced more slowly or more quickly. As meiotic repair products are seen in a *ku70Δ sae2Δ* background, we may be able to see DSBs being repaired as meiosis progresses which may be absent in other backgrounds such as *sae2Δ*.

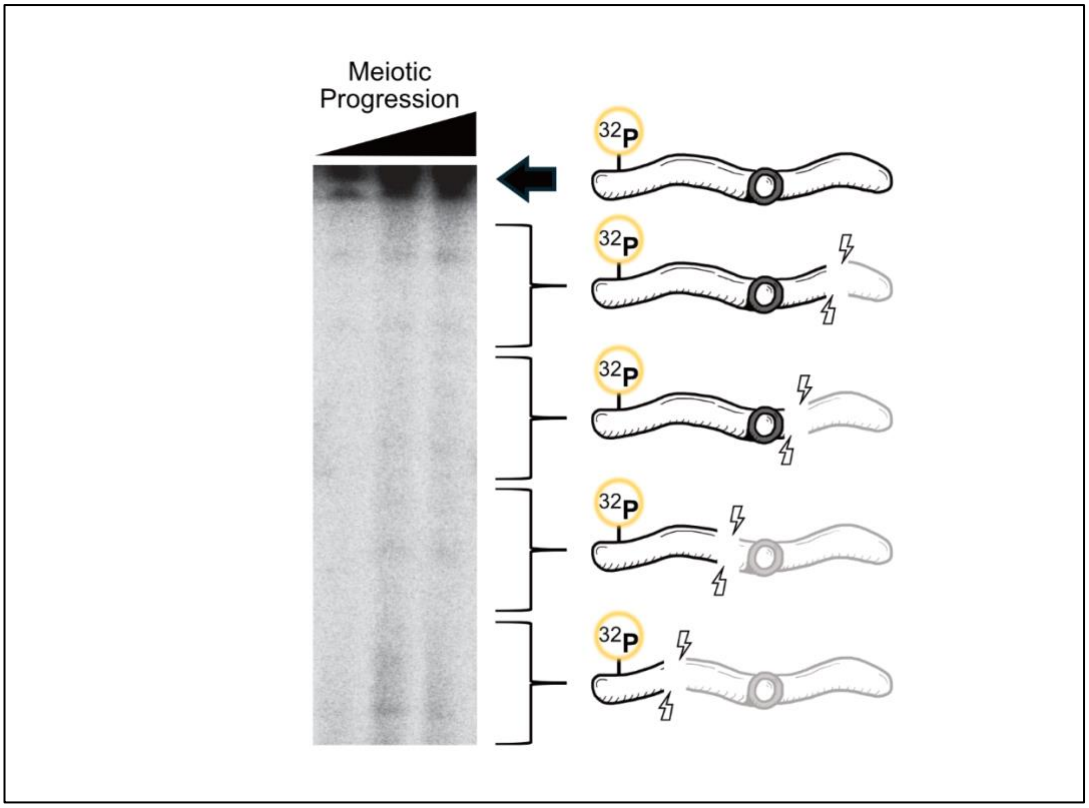

Figure 3-8 Schematic of PFGE being used to view meiotic DSBs at the chromosomal level. Samples were taken from timecourses, made into an agarose 'plug' and the DNA was purified. The large-molecular-weight DNA was subsequently separated on a 1.3 % agarose TBE gel via PFGE for 29 hours. The DNA was then transferred to a nylon membrane and Southern Blotted using ^{32}P-labelled probes for specific chromosomes. Intact chromosomes appear as a large band at the top of the blot. The smaller bands are un-repaired meiotic DSBs representing smaller chromosome fragments.

As expected, the wildtype strains shown in **Figure 3-9** and **Figure 3-10** show DSBs are present in CHR V at 4 hours, and repaired by 8 hours, implying that CO/NCO products have successfully been formed. The *ku70Δ tdp1Δ* strain from **Figure 3-10** resembles the wildtype strains, with DSBs present at 4 hours, then repaired by the 8-hour mark. Interestingly, the *tdp1Δ* strain from **Figure 3-9** shows that these DSBs remain unrepaired at the 8 hour mark, indicating that repair is delayed in this background when compared to wildtype, though by 10 hours they are repaired. All of the strains with *sae2Δ* present show DSBs forming from the 4-hour point, which then remain unrepaired; there is no real difference whether *tdp1Δ* or *ku70Δ* is present alongside the *sae2Δ*. The quantification of these blots may have been skewed by excessive background signal.

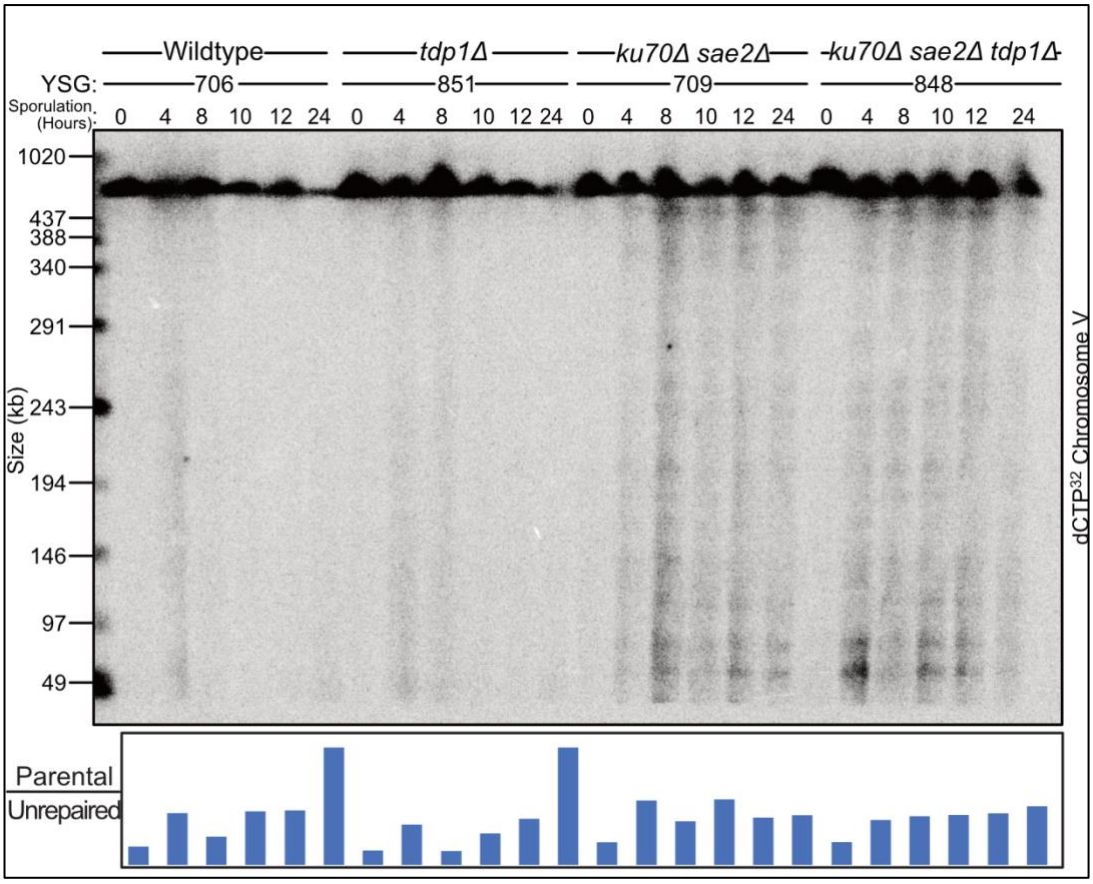

Figure 3-9 CHR V remains unrepaired in *ku70Δ sae2Δ tdp1Δ* strains during meiosis, as detected by PFGE and Southern blotting. Samples were taken from timecourses at the times indicated, made into an agarose 'plug' and the DNA was purified. The large-molecular-weight DNA was subsequently separated on a 1.3 % agarose TBE gel via PFGE for 29 hours. The DNA was then transferred to a nylon membrane and Southern Blotted using ^{32}P-labelled Rmd6 probe for CHRV detection. Large bands at the top of the blot represent intact parental chromosomes. DSBs appear as lower bands, representing smaller chromosomal fragments. Bands were quantified using BioRad ImageLab software.

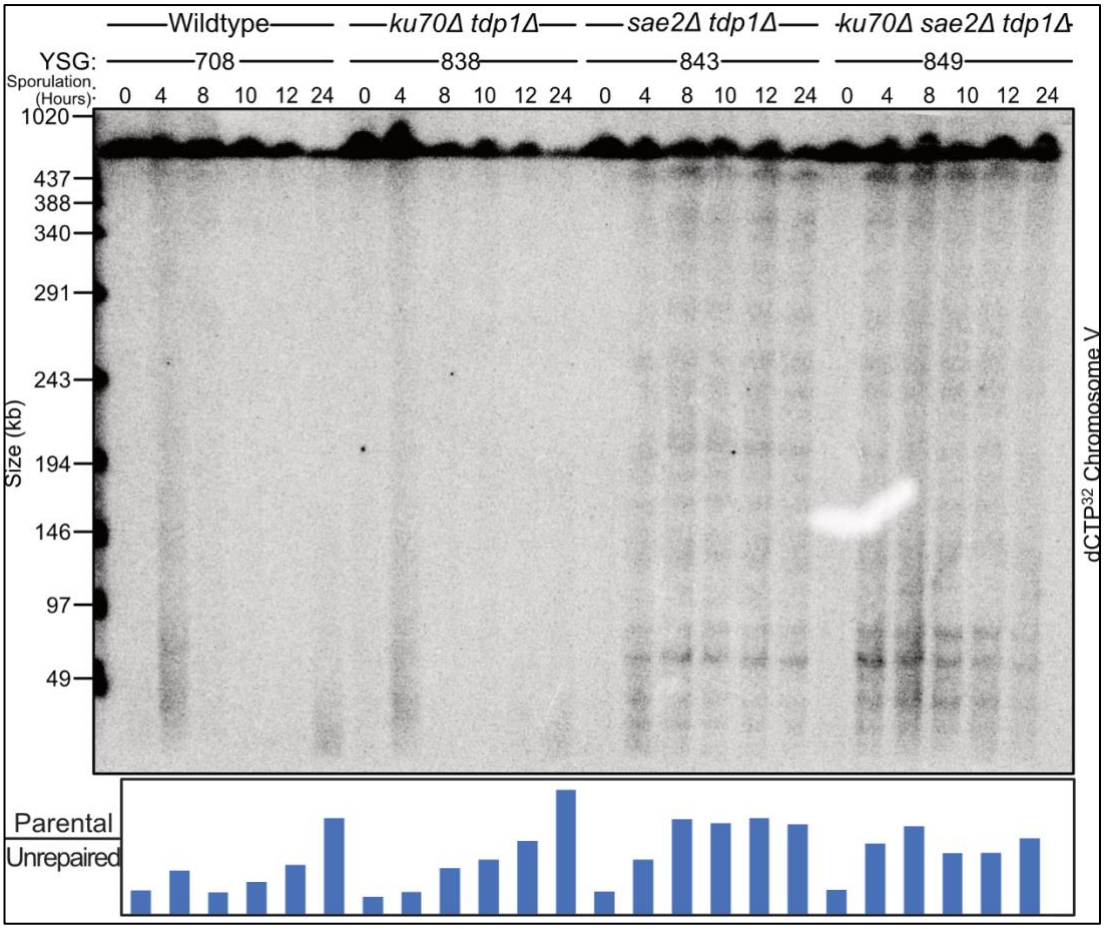

Figure 3-10 A biological repeat showing CHR V remains unrepaired in *ku70Δ sae2Δ tdp1Δ* strains during meiosis, as detected by PFGE and Southern blotting. Samples were taken from timecourses at the times indicated, made into an agarose 'plug' and the DNA was purified. The large-molecular-weight DNA was subsequently separated on a 1.3 % agarose TBE gel via PFGE for 29 hours. The DNA was then transferred to a nylon membrane and Southern Blotted using ^{32}P-labelled Rmd6 probe for CHRV detection. Large bands at the top of the blot represent intact parental chromosomes. DSBs appear as lower bands, representing smaller chromosomal fragments. Bands were quantified using BioRad ImageLab software.

Chromosome XI was also analysed for DSB dynamics, shown in **Figure 3-11** and **Figure 3-12**, which confirm the findings from chromosome V. As previously observed, the wildtype and *ku70Δ tdp1Δ* chromosomes are broken at the 4-hour point, then repaired by hour 8. Tdp1 mutant strains shows a delay in repair, with some faint bands seen from the 49 kb point indicating CHR XI fragments. The absence of Sae2 means that DSBs persist as the majority of Spo11 can't be removed by the MRX complex, meaning that CO/NCO products

can't form. Whilst some DSBs must be being repaired in the *ku70Δ sae2Δ* background to generate the CO/NCO products seen previously (Yun and Kim, 2019), it not enough to see repair at the 12/24-hour timepoints using this technique. There may well be repair in the *ku70Δ sae2Δ* which is absent in the *sae2Δ* and perhaps the *ku70Δ sae2Δ tdp1Δ*, but it is being missed here.

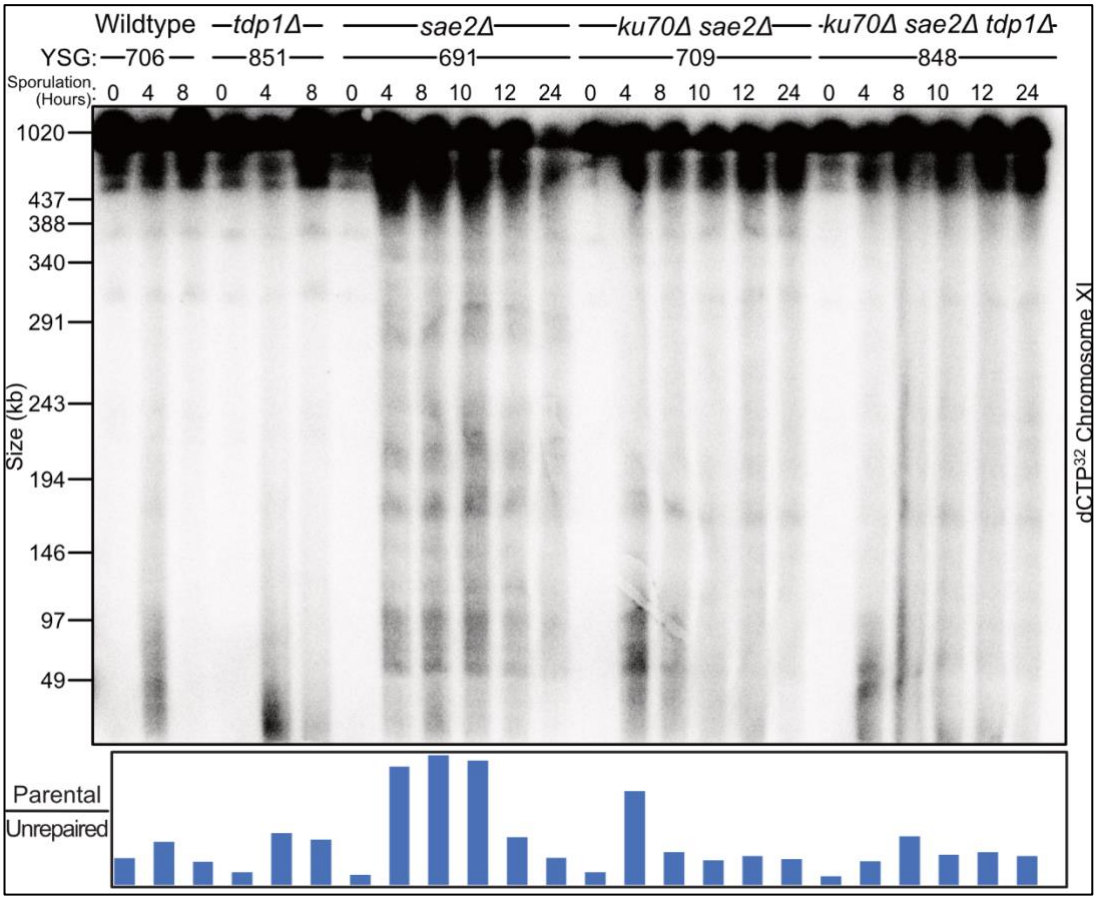

Figure 3-11 CHRXI remains unrepaired in *ku70Δ sae2Δ tdp1Δ* strains during meiosis, as detected by PFGE and Southern blotting. Samples were taken from timecourses at the times indicated, made into an agarose 'plug' and the DNA was purified. The large-molecular-weight DNA was subsequently separated on a 1.3 % agarose TBE gel via PFGE for 29 hours. The DNA was then transferred to a nylon membrane and Southern Blotted using 32P-labelled Jen1 probe for CHRXI detection. Large bands at the top of the blot represent intact parental chromosomes. DSBs appear as lower bands, representing smaller chromosomal fragments. Bands were quantified using BioRad ImageLab software.

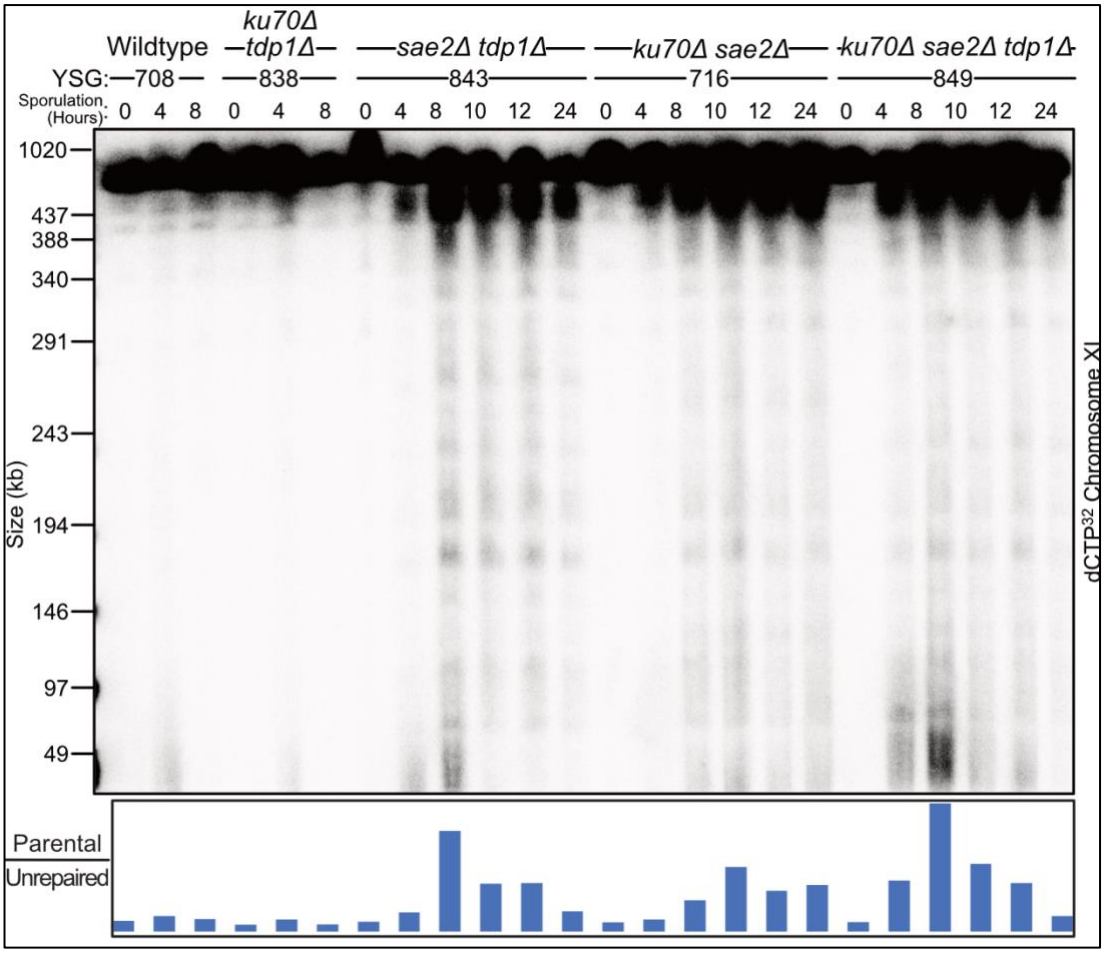

Figure 3-12 A biological repeat showing that CHRXI remains unrepaired in *ku70Δ sae2Δ tdp1Δ* strains during meiosis, as detected by PFGE and Southern blotting. Samples were taken from timecourses at the times indicated, made into an agarose 'plug' and the DNA was purified. The large-molecular-weight DNA was subsequently separated on a 1.3 % agarose TBE gel via PFGE for 29 hours. The DNA was then transferred to a nylon membrane and Southern Blotted using ^{32}P-labelled Jen1 probe for CHRXI detection. Large bands at the top of the blot represent intact parental chromosomes. DSBs appear as lower bands, representing smaller chromosomal fragments. Bands were quantified using BioRad ImageLab software.

Although it wasn't possible to see significant repair in any of the *sae2Δ* strains, the PFGEs of both CHR V and XI showed that in the *tdp1Δ* strain, DSBs are present for longer than in the wildtype and the *ku70Δ-tdp1Δ* strain, highlighting a possible role for Tdp1 in meiotic DSB repair regardless of whether NHEJ and the MXR complexes have been compromised. To address this, timecourses were repeated but with samples taken every hour to define detailed timings of when DSBs are induced, how long they persist, and when

they are fully repaired. Unfortunately, as shown in **Figure 3-13** and **Figure 3-14**, PFGEs and Southern blots didn't show DSBs forming or being repaired in any of the strains which contained the *sae2* gene.

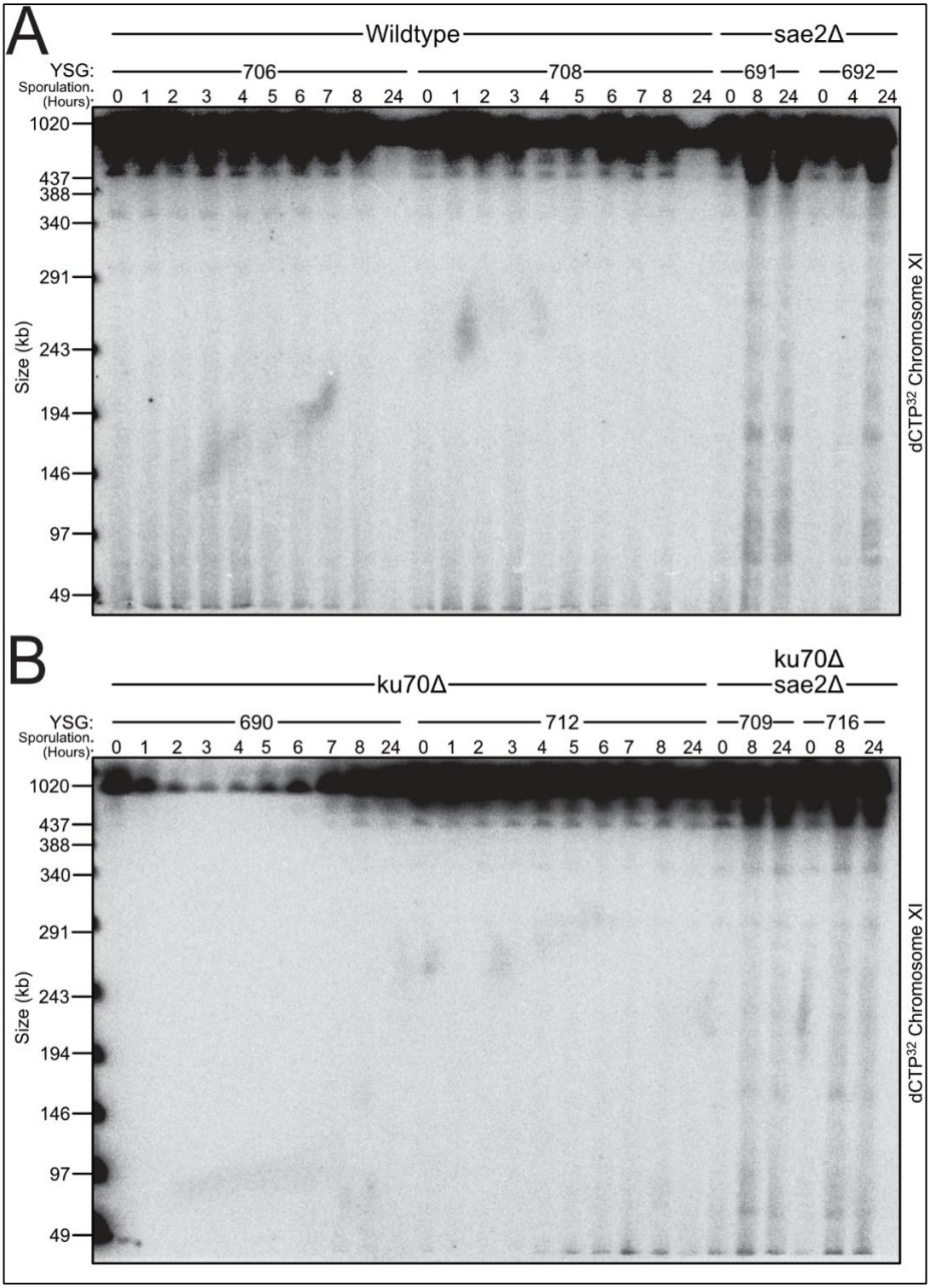

Figure 3-13 Persistent DSBs are seen when *sae2* is deleted in wildtype and *ku70Δ* backgrounds. Samples were taken from timecourses at the times indicated, made into an agarose 'plug' and the DNA was purified. The large-molecular-weight DNA was subsequently separated on a 1.3 % agarose TBE gel via PFGE for 29 hours. The DNA was then transferred to a nylon membrane and Southern Blotted using ^{32}P-labelled Jen1 probe

for CHRXI detection. Large bands at the top of the blot represent intact parental chromosomes. DSBs appear as lower bands, representing smaller chromosomal fragments.

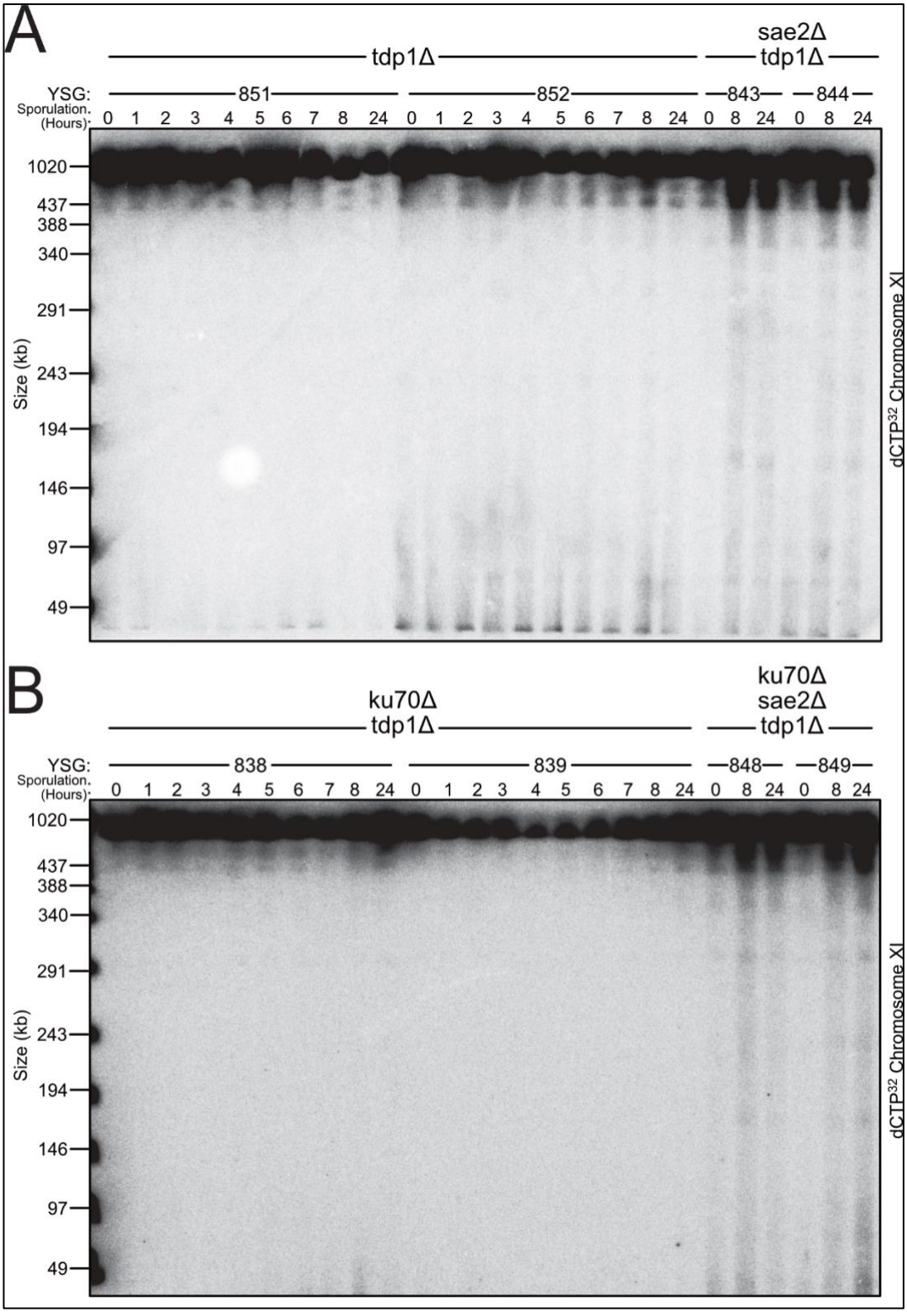

Figure 3-14 Persistent DSBs are seen when *sae2* is deleted in *tdp1Δ* and *ku70Δ tdp1Δ* backgrounds. Samples were taken from timecourses at the times indicated, made into an agarose 'plug' and the DNA was purified. The large-molecular-weight DNA was subsequently separated on a 1.3 % agarose TBE gel via PFGE for 29 hours. The DNA was

then transferred to a nylon membrane and Southern Blotted using ^{32}P-labelled Jen1 probe for CHRXI detection. Large bands at the top of the blot represent intact parental chromosomes. DSBs appear as lower bands, representing smaller chromosomal fragments.

3.6 Analysing Tdp1's Role in Meiotic Recombination Using Restriction Digests and Southern Blotting

As it wasn't possible to ascertain whether Tdp1 could remove Spo11 and allow COs to form via observing fluorescent spores (section **3.1**), a new strategy had to be used. Meiotic recombination can be monitored by digesting DNA samples with specific restriction enzymes, then probing the sequences in the form of a Southern blot. Here, the strains utilised have heterozygous XhoI cut sites on CHRIII, meaning that the different chromatids will produce different-sized bands when digested. These restriction sites flank the *HIS4::LEU2* DSB 'hotspot' (section **1.3.3**), meaning it is likely DSBs will be induced and subsequently repaired at this locus. If any CO/NCO event occurs, 'in-between' sized bands can be produced as the recombinant has a cut-site from one of the parent chromatids, and the second cut-site from the remaining chromatid. It is via this technique that the possibility of a second Spo11-removal pathway was hypothesised (Yun and Kim, 2019). A schematic of the possible Southern-blot products produced by an XhoI digest is shown below in **Figure 3-15**. Samples from meiotic timecourses were taken every two hours for 12 hours, with a final 24 hour sample taken too. The gDNA from each sample was purified, digested with XhoI, run on an agarose gel, and Southern blotted with the MXR2 probe (Gray et al., 2013). It is possible to determine whether the recombination products are CO products or NCO products via additional digests with NgoMIV and BamHI, but this was not performed.

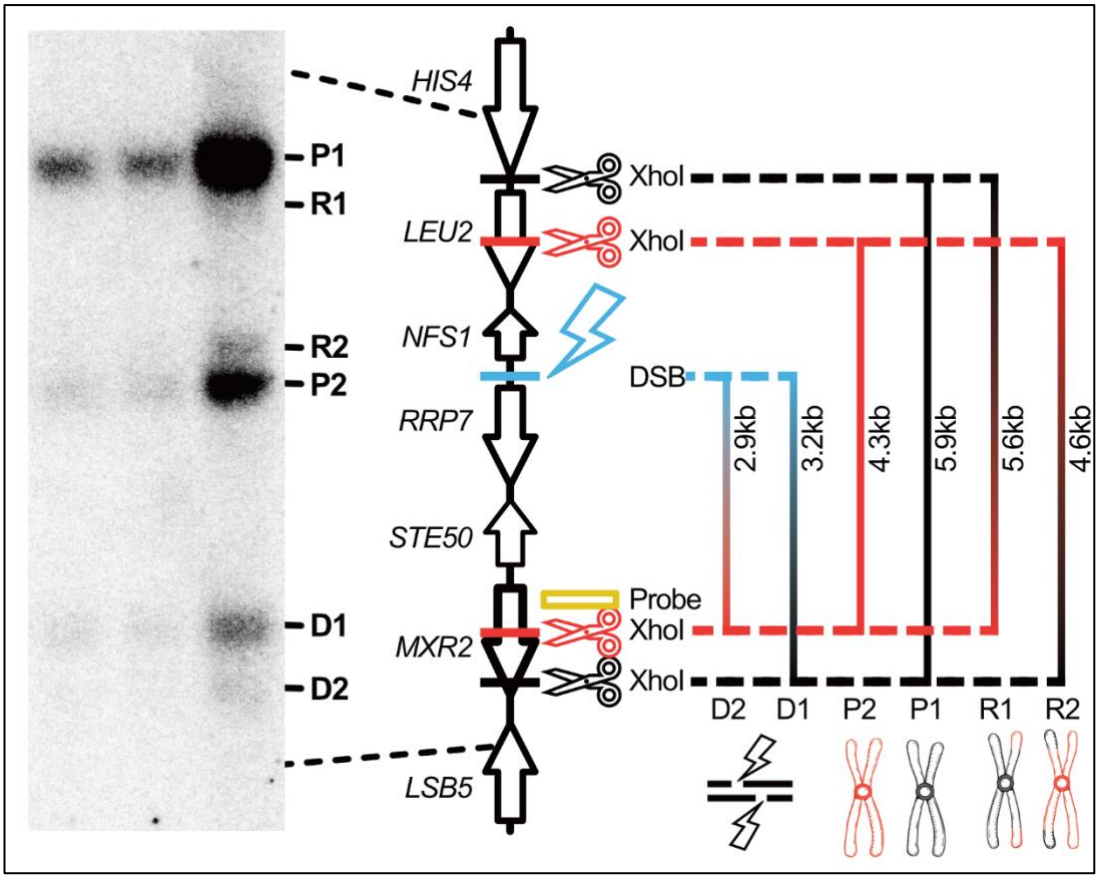

Figure 3-15 Schematic of possible meiotic products generated at the *HIS4::LEU2* locus, detected by restriction digestion and Southern Blotting. Genomic DNA can be digested with XhoI, run on a 0.7 % agarose-TAE, transferred to a nylon membrane and Southern blotted with ^{32}P-labelled MXR2-probe. Depending on whether DSBs occur at the *HIS4::LEU2* hotspot and if these are subsequently repaired via HR, different molecular weight DNA products can be acquired. Relative positions of genes on CHRIII are shown as arrows. Parent 1 only = black lines; Parent 2 only = red lines; DSB affecting both = blue line. D1 / C2 = un-repaired DSBs formed at *HIS4::*LEU2. P1 / P2 = unaffected parental bands. R1 / R2 = recombinant CO/NCO products formed as *HIS4::LEU2* breaks are repaired via meiotic recombination. Figure adapted from (Garcia et al., 2011b).

As to be expected, the wildtype strain in **Figure 3-16** shows recombination products clearly produced from the 6-hour timepoint onwards, predominantly the 'R2' recombinants, with very few un-repaired DSBs visible. The *sae2Δ* strain shows a modest recombinant 'R1' product at 12 hours, meaning that a small amount of Spo11 is being removed to allow HR to progress. Compared to the wildtype, the *sae2Δ* shows persistent DSBs which can't be repaired. This indicates that most, though not all, Spo11 is still covalently attached, thereby

preventing repair. The *sae2Δ tdp1Δ* strain looks very similar to the *sae2Δ*, with a small amount of 'R1' recombinant product visible at 24 hours, showing that in this background, Spo11 can be removed and HR can occur. Once again, persistent DSBs are seen as repair is hindered by Spo11 binding. The *ku70Δ sae2Δ tdp1Δ* triple mutant also showed CO/NCO products, with a clear 'R2' recombinant product visible at 24 hours. Unfortunately, this indicates that Spo11 is being removed in the absence of Tdp1, meaning that it is processed by another protein.

Interestingly, the R1 bands are more faint than the R2 bands. This is also true for the P2 bands being more faint than the P1 bands This could be due to the probe being used which bound to the *MRX2* locus, which is where the XhoI cut-sites are found. This could mean that the probe itself isn't able to bind as easily to this DNA so we could be missing out on CO/NCO signal, therefore it would be useful to re-Southern blot these with a different probe.

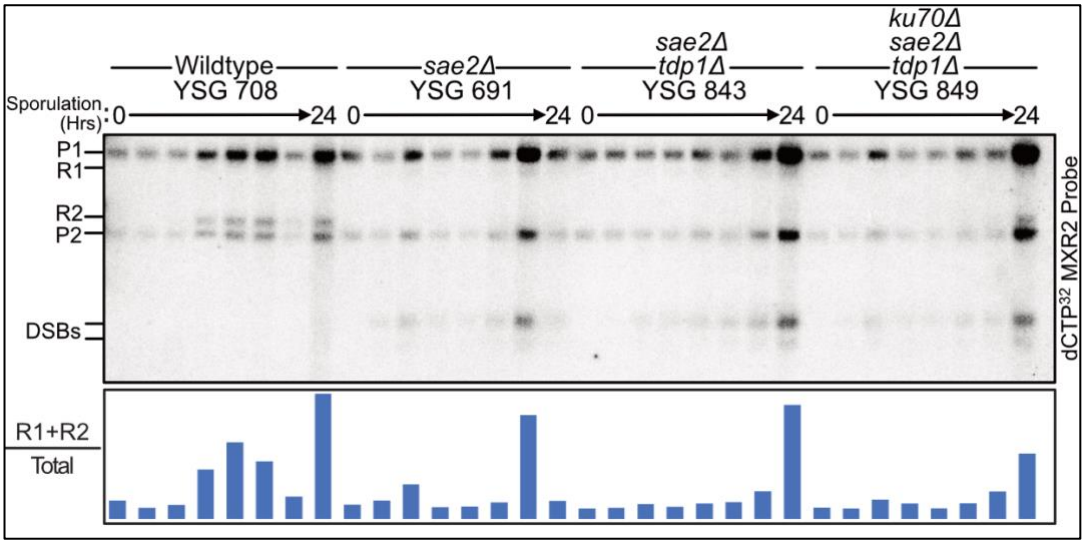

Figure 3-16 Meiotic CO/NCO products can be detected in a *ku70Δ sae2Δ tdp1Δ* background via Southern Blotting. Meiotic timecourses set up, cultures were put into sporulation media at 30 °C with 250 RPM shaking. Samples were taken every 2 hours from 0 to 12 hours, then a final sample at 24 hours. gDNA was extracted and purified, then 3 µg of DNA per sample was digested with XhoI for 16 hours at 37 °C. Digested DNA was run on a 0.7 % agarose-TAE gel at 60 V for 16 hours. DNA was then transferred to a nylon membrane using the Whatman® TurboBlotter system. ^{32}P-labelled MXR2 probe was used to detect DNA between XhoI sites at the *HIS4::LEU2* locus of CHRIII. Southern Blot was

imaged using a Cytiva Typhoon™ imager. Bands were quantified using BioRad ImageLab software. P1 / P2 = unaffected parental DNA. R1 / R2 = CO/NCO products formed by DSBs at *HIS4::LEU2* being repaired by meiotic recombination. DSBs = unrepaired DSBs formed at *HIS4::LEU2*.

This result was confirmed upon further repeats, shown in **Figure 3-17**. As this Southern blot was to confirm previous findings, only the 0 and 24 hour timepoints were analysed per strain. Recombinant 'R2' repair products were produced in wildtype, *tdp1Δ*, *ku70Δ, ku70Δ tdp1Δ,* and *ku70Δ sae2Δ* backgrounds. The 'R1' recombinants were predominantly seen in the *sae2Δ* and *sae2Δ tdp1Δ* strains. The ku70Δ *sae2Δ tdp1Δ* strains once again showed evidence of CO/NCO products being formed, with a faint 'R1' recombination product seen in the YSG848 at 24 hours, indicating that our hypothesis of Spo11 removal by Tdp1 was incorrect.

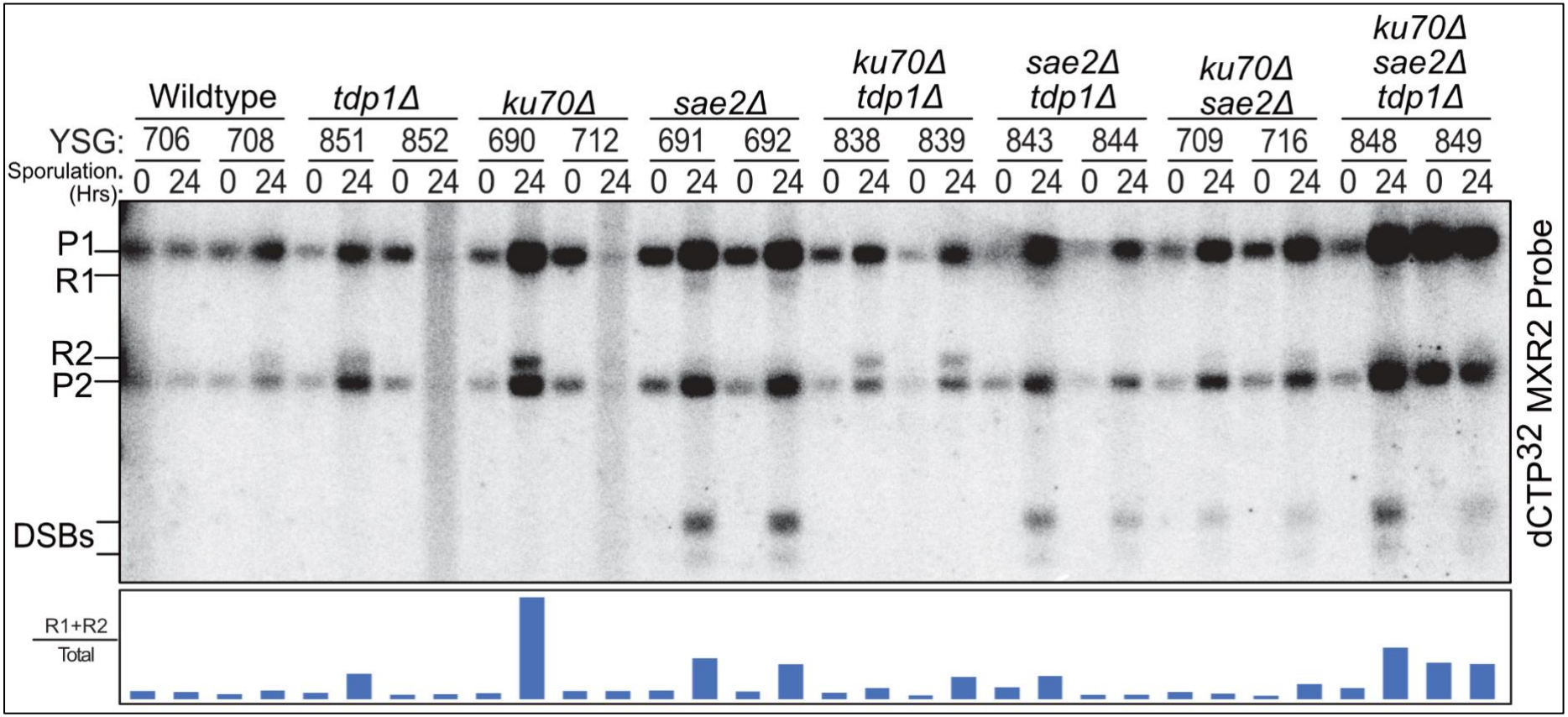

Figure 3-17 Southern Blot confirming that Tdp1 is not responsible for Spo11 processing when NHEJ and MRX are compromised. Meiotic timecourses were set up, cultures were put into sporulation media at 30 °C with 250 RPM shaking. Only the the 0 and 24 hour samples were analysed by Southern Blotting. gDNA was extracted and purified, then 3 µg of DNA per sample was digested with XhoI for 16 hours at 37 °C. Digested DNA was run on a 0.7 % agarose-TAE gel at 60 V for 16 hours. DNA was then transferred to a nylon membrane using the Whatman® TurboBlotter system. ^{32}P-labelled MXR2

probe was used to detect DNA between XhoI sites at the *HIS4::LEU2* locus of CHRIII. Southern Blot was imaged using a Cytiva Typhoon™ imager. Images were quantified using BioRad ImageLab software. P1 / P2 = unaffected parental DNA. R1 / R2 = CO/NCO products formed by DSBs at *HIS4::LEU2* being repaired by meiotic recombination. DSBs = unrepaired DSBs formed at *HIS4::LEU2*.

3.7 Summary of Findings for Chapter 3

The experiments shown in this chapter were performed to test the hypothesis that Tdp1 is able to remove Spo11 from DNA as a alternative pathway for meiosis to progress. It was not possible to determine whether Tdp1 could act on Spo11-DNA by monitoring sporulation as too few spores were produced in the *sae2Δ ku70Δ* mutants (**3.1**), nor was it possible to see whether SSNs were acting on these Spo11-roadblocks for the same reason (**3.2**). Whilst it was determined that Tdp1 is present during meiosis via western blotting (**3.3**), overexpression of tdp1 could not restore sporulation in the *sae2Δ ku70Δ* mutants (**3.4**). PFGEs determined that DSBs are effected and persist in *sae2Δ ku70Δ* strains, it was impossible to tell whether the loss of tdp1 from these strains had an effect on DSB dynamics as the Southern blots were not sensitive enough (**3.5**). The evidence that Spo11 removal is not dependent on Tdp1 in *sae2Δ ku70Δ* mutants came from the restriction digest Southern blots in section **3.6**. There are clearly CO/NCO products being formed in the *sae2Δ ku70Δ tdp1Δ* triple mutants (**Figure 3-16** and **Figure 3-17**) meaning that the mechanism for removing Spo11 from DNA in these strains remains elusive.

Chapter 4: How Are Ectopic Recombinant Products Produced? An Investigation into the Single Strand Annealing Pathway.

Non-allelic homologous recombination, also called ectopic recombination, is where repair occurs at the incorrect loci. This can result in gross chromosomal rearrangements. It has been recently demonstrated that ectopic recombinants are produced in *rad51Δ dmc1Δ* recombinase-deficient strains, yet require short regions of homology (Allison et al., 2023). Furthermore, the deletion of *rad24,* which is known to increase resection length (Shinohara et al., 2003a), increases the frequency of ectopic recombination (Grushcow et al., 1999, Shinohara and Shinohara, 2013). Therefore, it is a recombinase-free, homology-driven pathway which requires end-resection, such as an annealing-based pathway like SSA (section **1.2.5.2**) to generate ectopic recombinants (Allison et al., 2023). As the SSA pathway hasn't been characterised in *S. cerevisiae* in a meiotic context, it is important to determine whether this pathway is active during meiosis as a first step.

To see whether the SSA pathway is active during meiosis, the abundances of Rad1, Rad10, Rad52, and Rad59 were observed via western blotting. His_6-HA_3 affinity tags were added onto the C-terminus of SSA proteins as these tags have been previously utilised without affecting enzymatic functions (Eichmiller et al., 2018, Seol et al., 2018, Moore et al., 2009, Davis and Symington, 2001, Lisby et al., 2001). As with the Tdp1 investigation previously described (Section **3.3**) meiotic timecourses were run with 20 ml protein samples collected every hour for 8 hours. Unlike before, the strain backgrounds utilised were wildtype and *rad24Δ.* This was to see the abundance of the SSA pathway proteins when the 911-clamp is unable to be loaded, compromising the DNA damage repair checkpoint (DDC)

pathway and therefore Mec1 signalling. If these proteins are present during meiosis, and specifically more abundant in the *rad24Δ* background, it raises the possibility that the SSA pathway is being utilised for producing ectopic recombination products. Untagged-strain controls were used to ensure that only the HA_3-tags on the SSA proteins were being detected by the anti-HA primary antibodies as opposed to non-specific protein-binding. Vegetative samples were run on the gels to compare SSA protein levels in meiosis against basal levels. TCE was once again added to the SDS-PAGE gels to compare western blot chemiluminescent signal to the UV fluorescence from the total-soluble-protein loaded.

Figure 4-1 shows the levels of Rad1 during the first 8 hours of meiosis in wildtype and *rad24Δ* backgrounds. In each tagged sample there was a visible band from the western blot corresponding to the 131 kDa Rad1-His_6-HA_3 protein. In three of the four timecourses analysed the levels of Rad1 during meiosis exceeded vegetative levels. **Figure 4-1 A** shows Rad1 levels in a wildtype background. The levels of Rad1 peak at the 0-hour point and stay high for the next two hours. Then the levels of Rad1 steadily decrease, reaching basal levels at 5-6 hours before declining further. Similarly, **Figure 4-1 B** also shows Rad1 in a wildtype background, also peaking at the 0-hour timepoint. Unlike in **A**, the levels stay higher than vegetative levels throughout. **Figure 4-1 C** shows levels of Rad1 in a *rad24Δ* background. As with the Rad1 levels seen in **B**, Rad1 is most abundant at the start of meiosis, with Rad1 remaining at above-vegetative-levels throughout the timecourse. **Figure 4-1 D** also shows Rad1 in a *rad24Δ* background. Unlike the other three timecourses, the Rad1 levels seen at the start of meiosis were the same as vegetative levels. Rad1 then gradually declined throughout the 8-hour timecourse. As Rad1 was seen in all the samples, with 3 of the 4 timecourses showing Rad1 being more abundant than during a vegetative state, it seems that Rad1 could be playing an active role during meiosis. There is also some Rad1-tag seen in the wildtype backgrounds, but this is likely due to a loading error that Rad1-tag being present in these samples due to how faint the bands are and the absence in the *rad24Δ* blots. When comparing intensity values between wildtype and *rad24Δ* backgrounds, the highest level of Rad1 / TCE Protein was seen in the *rad24Δ* **D** blot at 26.3 arbitrary units. The intensities of the wildtype **A** and **B** (18.9 and 18 respectively) and were roughly double the maximum intensity seen in the *rad24Δ* **C** blot (9.5).

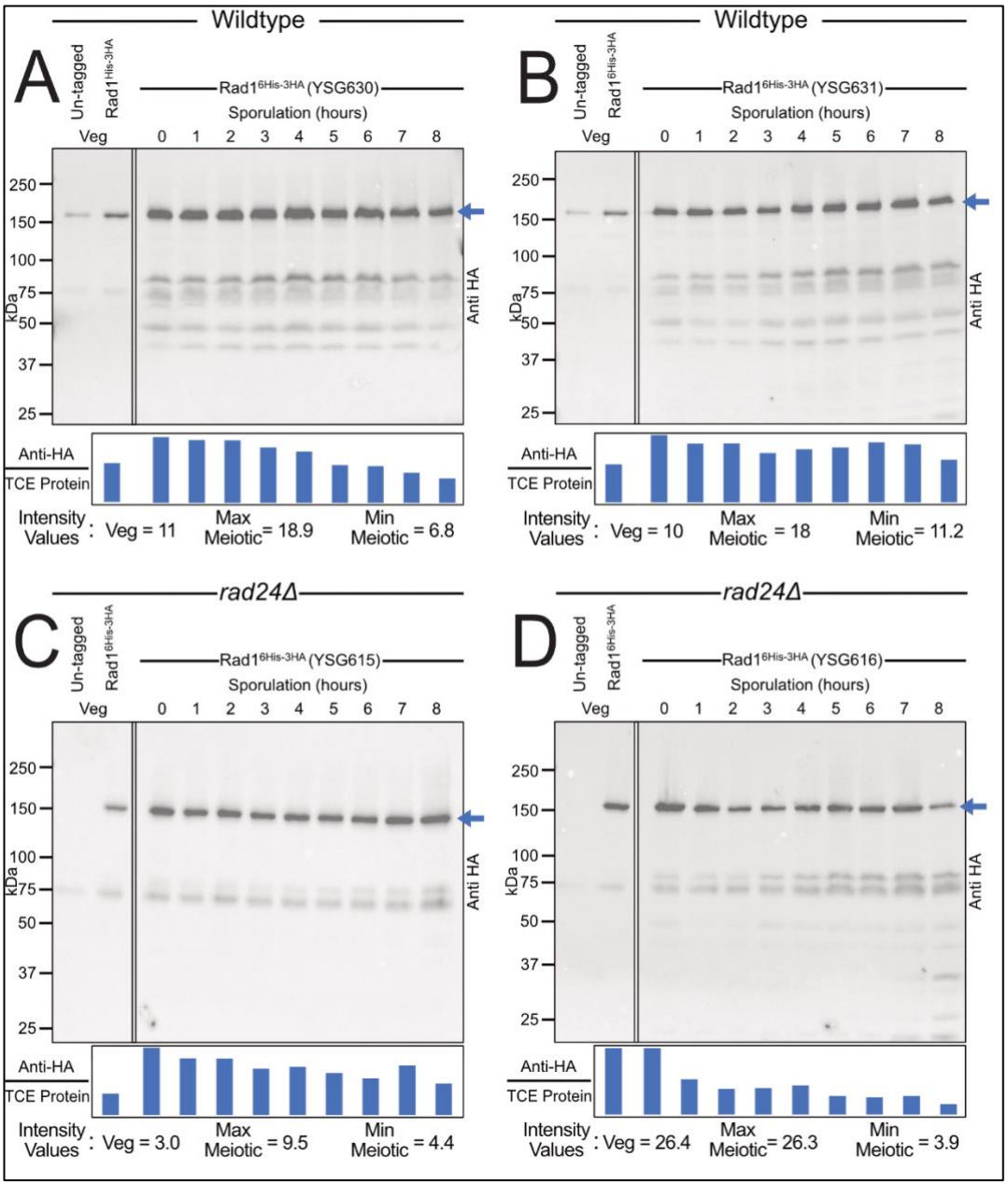

Figure 4-1 Monitoring levels of Rad1 during meiosis in wildtype and *rad24Δ* backgrounds via western blotting. 20ml of meiotic timecourse culture was harvested at the times shown. Total soluble-protein extracts were run on a 7.5 % SDS-PAGE gel containing TCE for visualisation via UV. Rad1-His_6-HA_3 was detected via western blotting, using rabbit-anti-HA 1° antibodies and goat-anti-rabbit 2° antibodies. Blue band represents the 132 kDa tagged-Rad1 proteins. Bands were quantified using BioRad ImageLab software and levels of Rad1-His_6-HA_3 were compared to total TCE protein at each time point, represented in the bar charts and 'Intensity values'. **A)** and **B)** show Rad1-His_6-HA_3 levels in

wildtype backgrounds; **C)** and **D)** show Rad1-His_6-HA_3 levels in *rad24Δ* backgrounds. Empty lanes between vegetative controls and meiotic samples were cropped out.

Figure 4-2 Shows the levels of Rad10 during the first 8 hours of meiosis in wildtype and *rad24Δ* backgrounds. Each tagged sample collected had a band on the western blot at 29 kDa, which matches the molecular mass of Rad10-His_6-HA_3. The levels of Rad10 seen in the **Figure 4-2 A** wildtype samples are lower during meiosis than when in a vegetative state. They peak at 0 hours, reaching around 50 % of vegetative levels, then decrease steadily for the next 8 hours. Whilst **Figure 4-2 B** is also a wildtype background, the levels of Rad10 during meiosis actually exceed vegetative levels. The abundance of Rad10 peaks at the 1-hour timepoint, remaining around vegetative levels until the 3 hour timepoint, before decreasing. **Figure 4-2 C** and **D** show Rad10 levels in a *rad24Δ* background: Rad10 quantities hover around vegetative levels throughout meiosis in **C**; whereas in **D** they reach double vegetative levels at the 0-hour mark and then steadily decline. Although the levels of Rad10 aren't as consistently high as Rad1 during meiosis, they are still present and indicate a potential meiotic role. The intensity values of the wildtype background vary greatly, with **A** showing a relative abundance of Rad10 of 7 at the maximum meiotic point, whilst **B** peaked at 15.9. The *rad24Δ* were much lower than **A**, with **D** showing a relative Rad10 abundance similar to A of 7.9, whilst **C** had the lowest abundance of 5.6. On average, the abundance of Rad10 was lower in the *rad24Δ* background when compared to wildtype.

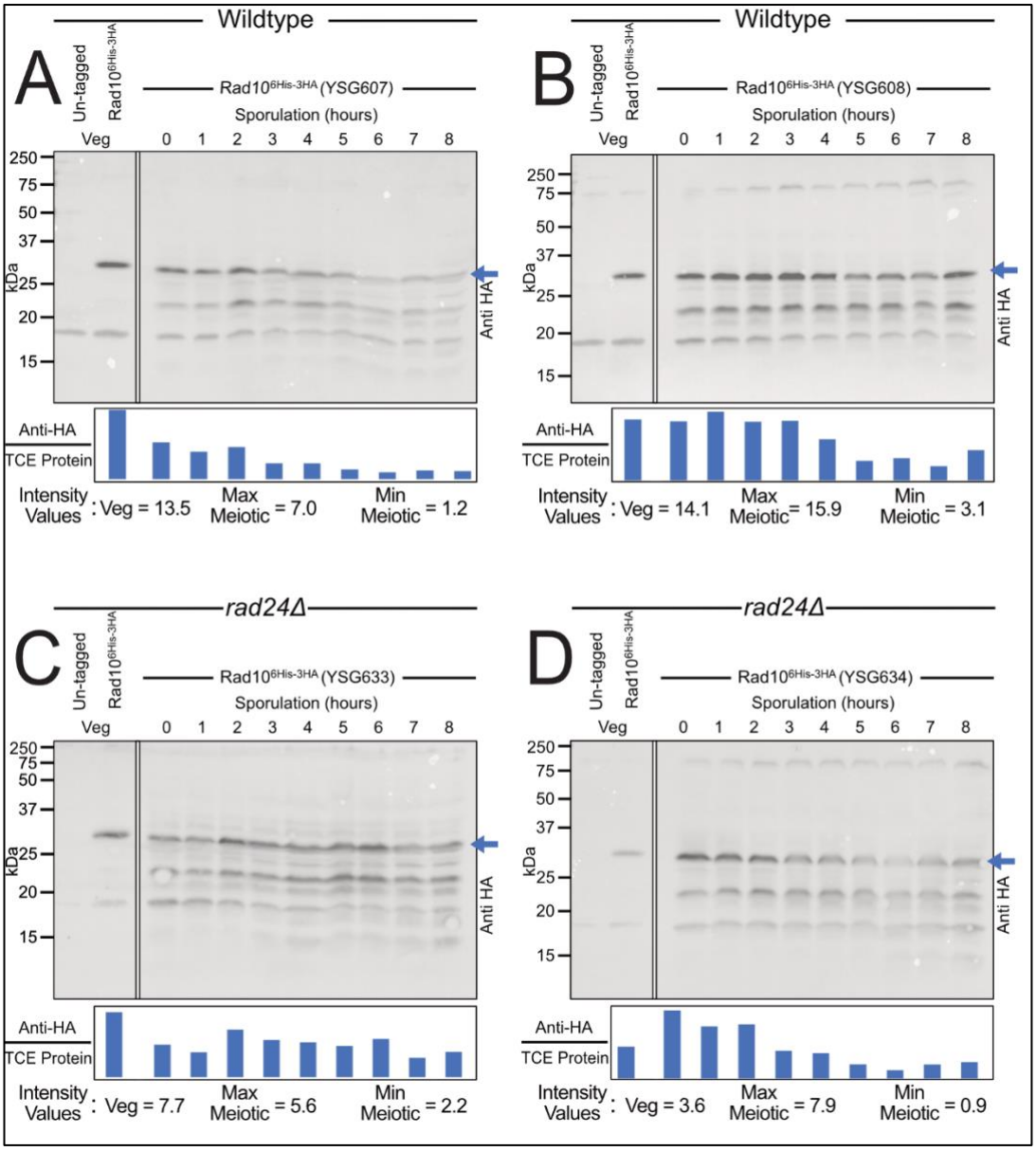

Figure 4-2 Monitoring levels of Rad10 during meiosis in wildtype and *rad24Δ* backgrounds via western blotting. 20ml of meiotic timecourse culture was harvested at the times shown. Total soluble-protein extracts were run on a 15 % SDS-PAGE gel containing TCE for visualisation via UV. Rad10-His_6-HA_3 was detected via western blotting, using rabbit-anti-HA 1° antibodies and goat-anti-rabbit 2° antibodies. Blue arrow represents the 29 kDa band corresponding to tagged-Rad10 Bands were quantified using BioRad ImageLab software and levels of Rad10-His_6-HA_3 were compared to total TCE protein at each time point, represented in the bar charts and 'intensity values'. **A)** and **B)** show Rad10-His_6-HA_3 levels in wildtype backgrounds; **C)** and **D)** show Rad10-His_6-HA_3 levels in *rad24Δ* backgrounds. Empty lanes between the vegetative controls and the meiotic samples were cropped out.

Figure 4-3 Shows that a 57 kDa band signifying Rad52 was present during meiosis. In wildtype and in *rad24Δ* backgrounds the levels of Rad52 were higher during meiosis that when in a vegetative state. The wildtype timecourse in **Figure 4-3 A** shows that Rad52 levels

steadily increase from 0 to 3 hours, peaking at around double vegetative levels, before declining for the next 5 hours. **Figure 4-3 B** also shows wildtype levels of Rad52 during meiosis, but this time the peak at the start, then level-out near vegetative levels for 2 hours, before declining steadily. The *rad24Δ* timecourse in **Figure 4-3 C** show the levels fluctuating throughout the first 8 hours of meiosis, with three timepoints displaying higher-than-vegetative Rad52 levels. The *rad24Δ* repeat in **Figure 4-3 D** has Rad52 levels peaking at the 0 hour mark, then rapidly declining to lower-than-vegetative levels and remaining low for the next 8 hours. Given that Rad52 has been implicated in meiotic recombination, it is unsurprising to see it is present during meiosis. Much like with the Rad10 intensity values, the Rad52 wildtype abundances varied from a maximum of 17.9 in **B**, to 7.4 in **A**. The *rad24Δ* Rad52 intensity values were similar to the wildtype shown in **A**, with 7.1 and 9.5 for **C** and **D** respectively. Again, on average the relative abundance of Rad52 is higher in wildtype than in *rad24Δ*, but this is largely due to the data from **B**.

The final SSA protein investigated for meiotic abundance was Rad59. **Figure 4-4** demonstrates that a 32 kDa band matching the mass of Rad59 was present in all tagged samples, with meiotic levels exceeding vegetative levels in both repeats of wildtype and *rad24Δ* backgrounds. **Figure 4-4 A** and **B** show that in wildtype backgrounds, Rad59 levels peak at the onset of meiosis, then gradually decrease as meiosis progresses. The *rad24Δ* timecourses show slightly different Rad59 profiles. **Figure 4-4 C** shows levels starting high, then decreasing, before peaking at 7 / 8 hours. **Figure 4-4 D** shows the Rad59 levels peaking at 1 hour, then steadily declining. As with the other SSA proteins monitored, the levels of Rad59 are significant during meiosis, indicating an active role. Unlike with the other SSA proteins, the intensity values here indicate that Rad59 is more relatively abundant in *rad24Δ* backgrounds compared to wildtype. The wildtype intensities peak at 11.3 and 9.4 for **A** and **B** respectively, whereas the intensities for the *rad24Δ* are 9.1 in **C** and 16.8 in **D**.

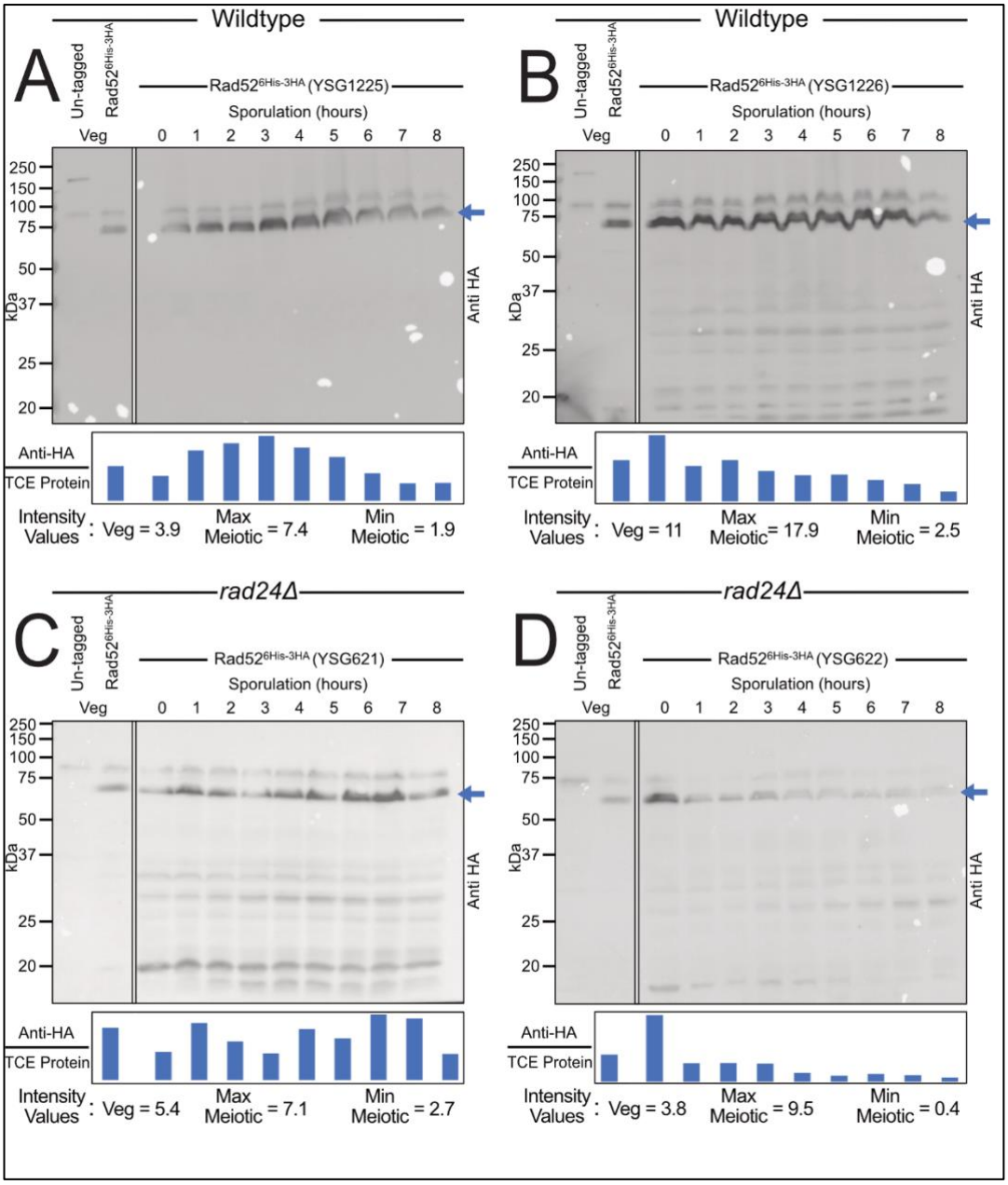

Figure 4-3 Monitoring levels of Rad52 during meiosis in wildtype and *rad24Δ* backgrounds via western blotting. 20ml of meiotic timecourse culture was harvested at the times shown. Total soluble-protein extracts were run on a 12 % SDS-PAGE gel containing TCE for visualisation via UV. Rad52-His_6-HA_3 was detected via western blotting, using rabbit-anti-HA 1° antibodies and goat-anti-rabbit 2° antibodies. Blue arrow points to the 56 kDa bands corresponding to tagged-Rad52. Bands were quantified using BioRad ImageLab software and levels of Rad52-His_6-HA_3 were compared to total TCE protein at each time point, represented in the bar charts and 'intensity values'. **A)** and **B)** show Rad52-His_6-HA_3 levels in wildtype backgrounds; **C)** and **D)** show Rad52-His_6-HA_3 levels in *rad24Δ* backgrounds. Empty lanes between vegetative controls and meiotic samples were cropped out.

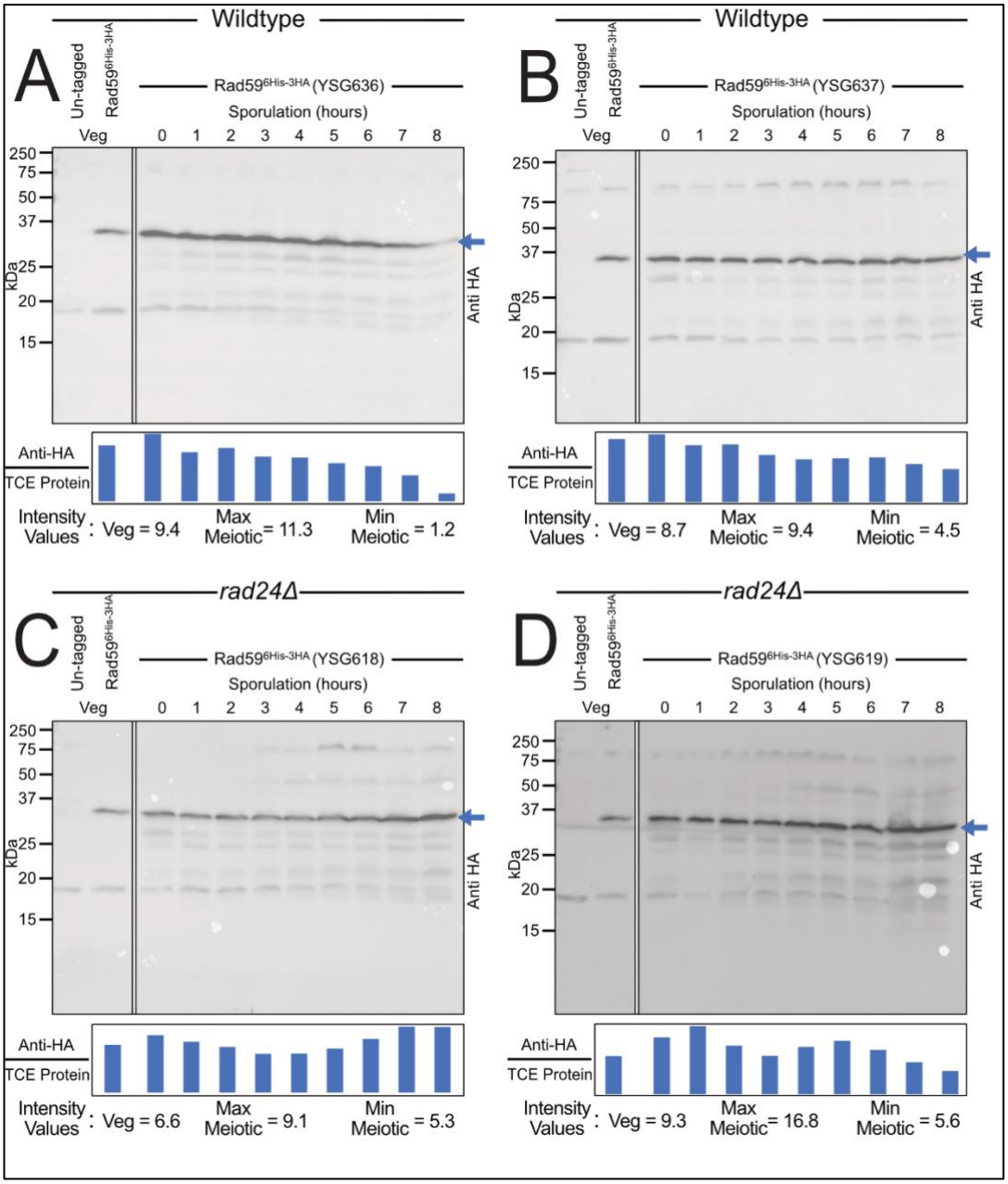

Figure 4-4 Monitoring levels of Rad59 during meiosis in wildtype and *rad24Δ* backgrounds via western blotting. 20ml of meiotic timecourse culture was harvested at the times shown. Total soluble-protein extracts were run on a 15 % SDS-PAGE gel containing TCE for visualisation via UV. Rad59-His_6-HA_3 was detected via western blotting, using rabbit-anti-HA 1° antibodies and goat-anti-rabbit 2° antibodies. Blue arrow points to the 32 kDa bands corresponding to tagged-Rad59. Bands were quantified using BioRad ImageLab software and levels of Rad59-His_6-HA_3 were compared to total TCE protein at each time point, represented in the bar charts and 'intensity values'. A) and B) show Rad59-His_6-HA_3 levels in wildtype backgrounds; C) and D) show Rad59-His_6-HA_3 levels in *rad24Δ* backgrounds. Empty lanes between vegetative controls and meiotic samples were cropped out.

Overall, the SSA proteins Rad1, Rad10, Rad52, and Rad59 are present during meiosis in both wildtype and *rad24Δ* backgrounds. This is very promising for our hypothesis that the SSA pathway is actively driving ectopic recombination during meiosis. When comparing levels of SSA proteins in wildtype and *rad24Δ* backgrounds, Rad1, Rad10, and Rad52 are more relatively abundant in wildtype. However, Rad59 is more relatively abundant in the *rad24Δ* background when compared to wildtype.

Chapter 5: Discussion

5.1 Spo11 Can Still Be Removed in *tdp1Δ* Strains

In meiotic recombination, Spo11 initiates DSBs and remains covalently attached to the DNA. The MRX-Sae2 complex is the main pathway for removing Spo11, doing so nucleolytically releasing Spo11-oligo molecules in the process. However, it is possible to remove Spo11 independently of the MRX complex when NHEJ has also been compromised (Yun and Kim, 2019). The mechanism behind this Spo11 remains elusive, so how is Spo11 removed under these circumstances?

One of the aims of this project was to investigate whether the phosphodiesterase Tdp1 can remove Spo11 from DNA in a *ku70Δ sae2Δ* background. Unfortunately, as shown in **Figure 3-16** and **Figure 3-17**, meiotic recombination products can be produced independently of Tdp1 in a *ku70Δ sae2Δ* background. This means that the mechanism for how Spo11 is removed when NHEJ and MRX-Sae2 nucleolytic cleavage have been compromised remains elusive.

The investigation started by using fluorescent marker strains to monitor CO products visually (section **3.1**). However, this proved impossible due to *ku70Δ sae2Δ* strains not being able to sporulate efficiently. Although the lack of sporulation is likely due to the strain genotypes being investigated, sporulation was inconsistent throughout this project. Despite changing media, potassium acetate brand, water used, glassware, shaking speed, and culture volumes, sporulation would sometimes not occur, even in control wildtype strains. This issue resolved itself once a new incubator was acquired in May of 2024, as a result of this most of the results from this project are from May-August of 2024. Whilst the sporulation-inconsistency issue did not prevent proving that Tdp1 cannot remove Spo11, it may have prevented finding out whether a structure selective nuclease (SSN) can remove Spo11.

In section **3.2**, the SSN / SSN-accessory proteins Mlh1, Mus81, Pms1, Slx4, and Yen1 deleted to try and determine which pathway is responsible for producing CO / NCO products. For these experiments to work, it required the strains to undergo meiosis successfully and spores to be produced. Whilst single deletions in any of the SSNs did allow spores to form, when in a *ku70Δ sae2Δ* background sporulation was almost entirely prevented. However, some spores were formed, or at least partial division indicating progression from prophase I and therefore Spo11 removal. The fluorescent investigation involving *tdp1Δ* (section **3.1**) also poor led to sporulation when coupled with *ku70Δ sae2Δ*, seemingly much like the *SSNΔ* strains. However, when looking down the fluorescent microscope, it was noticed that the *ku70Δ sae2Δ tdp1Δ* strains did not divide at all, indicating prophase arrest due to Spo11 remaining bound (Brealey, 2022). Therefore, at this stage it was decided to focus completely on Tdp1 and stop investigating the SSN strains.

Whilst it was determined that Tdp1 is present during meiosis via western blotting (section **3.3**), these results have some major caveats. The first is that non-meiotic controls were taken from vegetative cells rather than actively growing cultures. As meiosis involves replication and division, it may have been better to compare meiotic cultures to mitotically growing cultures rather than stationary-phase cultures. Another major caveat is the lack of positive control for meiosis. Whilst it was determined that meiosis was occurring by counting spores after the western blot cultures were taken, by having a positive meiotic control like a tagged-Ndt80 would be able to line-up Tdp1 abundance with how meiosis is progressing. A final issue with these blots is the Tdp1 levels shown as relative abundance are not consistent between biological repeats. A third repeat could help to rectify this to see if there is a trend in Tdp1 levels.

When looking as CO/NCO products via restriction digest followed by Southern blotting (section **3.6**) it was possible to yield meiotic repair products, even in the *ku70Δ sae2Δ* background. This is likely due to a combination of factors. The first is a reliable method for sporulating by using the new incubator. The second is that using Southern blotting doesn't require the full MI-MII divisions, it just shows CO / NCO repair, thereby isolating the stage of meiosis required to see Spo11 removal. It could be possible that CO /

NCO products were being formed in these backgrounds, but due to mutations or improper meiotic signalling, the meiotic divisions could not be completed. The third is that Southern blotting with radiation is incredibly sensitive, especially compared to manually viewing tetrads using a fluorescent microscope. Therefore, it could be worth investigating whether these SSNs can actually remove Spo11 from DNA by using the *HIS4::LEU2* digest Southern blot protocol from section **3.6**. It's been shown that Rad1-Rad10 can remove Top1cc from DNA in *S. cerevisiae* when Tdp1 isn't functional (Vance and Wilson, 2002), so perhaps Rad1-Rad10, Mus81, Mlh1, Slx4 or Yen1 may be able to remove Spo11 by using flap-endonuclease activity.

If repeating these Southern blots, it would be a good idea to use different radioactive probes and combine data from them to determine what is a true CO/NCO product and not just a DSB. This is important because the MRX2 probe used here binds to where the DNA is digested by XhoI, meaning that we are losing a lot of probe signal due to binding issues. This was determined by the faint R1 and P2 bands throughout. There are additional probes which could be used to target the *HIS4::LEU2* locus which shouldn't be affected by the XhoI digests. Another issue with these Southern blots is that the band intensities don't seem to line up with what is seen with the CO/NCO bands. This is due to the program used detecting bands automatically and there is spill over between where one band begins and another ends. This is prevalent when there is lots of parental signal spilling into 'CO/NCO' bands. This could be rectified by consistent DNA loading of 3 µg (as was attempted) so there is a clear separation between bands. Another caveat with these Southern blots is that the strains used in the original study were *rad50S* whereas I used *sae2Δ*. Theoretically, these ought to be phenotypically the same as they both prevent Sae2 from binding and activating Rad50, but it would be a good idea to include a *rad50S* strain alongside a *sae2Δ* strain to ensure that these both have the same phenotype. Whilst they both show CO/NCO products forming, the Yun and Kim, 2019 data shows much clearer CO/NCO bands in the *rad50S* than my *sae2Δ* produced, though again this could be due to probe issues.

If Spo11 isn't removed by Tdp1 or SSNs, it could potentially be the work of a metalloprotease. Some metalloproteases are able to remove TOPcc complexes by

proteolytically degrading them. In humans, Sprtn has been shown to remove Top1ccs in tumours (Maskey et al., 2017). The yeast homolog Wss1 has also been implicated in removing TOPccs (Deng et al., 2005), so it could be removing Spo11 by proteolytic degradation. The wss1 gene has been shown to be transcribed during meiotic prophase, potentially playing an active role (Kugou et al., 2007). Therefore it could be worth investigating Wss1 using restriction-digest Southern blotting such as in section **3.6**.

Despite showing that Tdp1 cannot remove Spo11 to allow for meiotic recombination to take place, Tdp1 could still be playing a role in meiosis. If it is playing a role, it must be non-essential due to the low impact the *tdp1Δ* had on sporulation efficiency and spore viability (**Figure 3-2**). As discussed earlier, Tdp1 is present during meiosis as detected by western blotting. This aligns with published data showing that *tdp1* is actively expressed during meiotic prophase (Kugou et al., 2007). But what role could Tdp1 be playing? **Figure 3-9** and **Figure 3-11** show that in a *tdp1Δ* strain, there are DSBs which persist longer than in wildtype, indicating some sort of delay in DSB formation and or repair. Unfortunately, when attempting to repeat this finding but more frequent samples, the PFGE signal was far too weak to monitor DSB formation and repair (**Figure 3-13** and **Figure 3-14**). If this could be repeated and the delay is once again present, it demonstrates that Tdp1 is playing some role in meiotic DSB formation and/or repair. Perhaps Tdp1 acts as a Spo11 'recycler', removing the oligo tails from Spo11. By removing the oligos from Spo11, Tdp1 could be allowing Spo11 to initiate more DSBs. Ergo, when Tdp1 isn't present, there is a slight delay in DSB formation and repair as the pool of enzymatically active Spo11 is reduced due to Spo11-oligos persisting. This mechanism may not be necessary in *S. cerevisiae* where only a minority of Spo11 engages in DSB formation (Neale et al., 2005), Spo11 is an ancient and well-conserved protein so it could have implications in other organisms (Bloomfield, 2016). This means that if an alternative pathway for Spo11 removal can be found in *S. cerevisiae*, it could be potentially useful for creating novel therapies for fertility issues and even cancers (Cheng et al., 2022).

This Spo11-recycling hypothesis could be tested both *in vivo* and *in vitro*. To look at this *in vivo*, a meiotic timecourse could be run in wildtype and *tdp1Δ* backgrounds with

tagged Spo11. Samples could be taken and Spo11 isolated utilising the affinity tags for immunoprecipitation (Neale and Keeney, 2009). Then the ratio of Spo11 : Spo11-oligos could be compared in the wildtype and *tdp1Δ* backgrounds, hopefully showing that there are more Spo11-oligos in the *tdp1Δ* background as each Spo11 can only be used for one DSB. If this was successful, this function could be tested *in vitro* too by using electromobility shift assay (EMSA) style 'shift-western blots' (Harbers, 2015). First, Tdp1 would need to be purified, either using *E. coli* or *S. cerevisiae* to overexpress the protein. Spo11-oligos would also need to be either purified (Claeys Bouuaert et al., 2021b) or obtained through immunoprecipitation (Neale and Keeney, 2009). Then Tdp1 could be precipitated into a reaction mix containing the Spo11-oligos and run on a gel, which could be transferred to a membrane and visualised by western blotting. If Tdp1 can remove the oligos from the Spo11, there would be a shift in molecular weight. To follow this experiment up, Tdp1 mutants could be utilised. A H182A mutation would render the Tdp1 hydrolytically dead (Liu et al., 2004), which when titrated into the Spo11 oligo mix should result in no shift. A second mutant in the general-acid-base histidine, H432A (He et al., 2007, Comeaux et al., 2015), would make a Tdp1 which can form an intermediate with the Spo11-oligo, but not be released, thereby making a higher molecular-weight species visible on the shift-western blot.

Another interesting point is the effect that $CuSO_4$ has on sporulation. As shown in **Figure 3-7** the addition of $CuSO_4$ to sporulation media causes a reduction in sporulation efficiency, regardless of whether the P^{CUP1} promoter is being used to overexpress Tdp1 or not. $CuSO_4$ does have fungicidal properties (Yasokawa et al., 2008), which could be causing this reduction in sporulation efficiency; therefore it may be worth re-examining the concentration of $CuSO_4$ added, lowering it from 25 µM (a concentration used in previous experiments (Bhagwat et al., 2021)) to try and avoid these toxic effects whilst retaining protein overexpression. Alternatively, another promoter could be used like the P^{GAL} promoter which can be activated with β-oestradiol (Gray et al., 2013).

Aside from experimental findings, this part of the project served as a method-development exercise. As the first student in a brand-new lab, several techniques had to be developed. Methods optimised include running PFGEs, which involved adjusting the

programs on the power-pack and repairing the PFGE tank due to a faulty electrode. The transfer process was also optimised, with acid-depurination followed by alkaline transfer yielding the best results. Southern blot digests were optimised by using 3 µg DNA, whilst hybridisation protocols from two lab groups were merged with much trial-and-error to allow for visualising probed DNA.

5.2 Is the Single Strand Annealing Pathway Producing Ectopic Recombinant Products

Non-allelic recombination, or ectopic recombination, is where DNA repair uses the incorrect loci as a template, often resulting in gross chromosomal rearrangements. These ectopic recombinant products are seen around 1 % of the time in wildtype *S. cerevisiae* (Grushcow et al., 1999). It was shown recently that the pathway which produces these ectopic products does not require the recombinases Rad51 or Dmc1, and that ectopic recombination is supressed by Rad24 (Allison et al., 2023). This evidence points towards annealing-based DSB repair, such as the single strand annealing pathway (SSA), but this pathway hasn't been investigated in a meiotic context. Is the SSA pathway responsible for ectopic recombination during meiosis?

This part of the project aimed to see whether the SSA pathway is responsible for producing ectopic recombinant products as recently hypothesised (Allison et al., 2023). The first step was to monitor Rad1, Rad10, Rad52, and Rad59 proteins via western blotting in wildtype, *rad24Δ*, and *rad24Δ-dmc1Δ* backgrounds. This was to see if these proteins were present in strains where ectopic recombinant products are produced around 1 % of the time (wildtype) (Grushcow et al., 1999), where increased ectopic recombination occurs (*rad24Δ*), and where ectopic recombinants are overproduced in a recombinase-lacking background (*rad24Δ-dmc1Δ*). **Chapter 4**:shows that each SSA protein is present during meiosis in wildtype and *rad24Δ* backgrounds, indicating that they may be playing an active meiotic role. However the *rad24Δ-dmc1Δ* background strains were not tested as the un-tagged control strain could not be made in time.

Whilst is it promising that these proteins are present in the *rad24Δ* background where interhomolog bias is compromised and resection lengths are longer (Carballo et al., 2008, Shinohara et al., 2003a) it is not surprising that they are present in wildtype. Rad52 has a role in helping Rad51/Dmc1 load onto filaments by removing RPA (Joo et al., 2024). Rad1-Rad10 have also been implicated in meiosis (Kirkpatrick, 1999). Rad1, Rad10 and Rad52 (**Figure 4-1, Figure 4-2, Figure 4-3** respectively) all had higher relative abundances

in wildtype than in *rad24Δ*, perhaps due to these already-characterised meiotic roles. Rad59 (**Figure 4-4**) however was more relatively abundant in the *rad24Δ* background, so perhaps the SSA pathway is active when ectopic recombination is occurring. However, as discussed in the previous section (**5.1**), the relative abundances shown do not display a trend; therefore it may be a good idea to use these 'relative abundances' as a rough guide to proteins being present rather than a timeline of expression, which would be better shown by qPCR for example. Once again, a meiotic positive control such as a tagged-Ndt80 would be useful for monitoring meiotic progression.

What needs to be proven is that these proteins are working together as a part of a single pathway, this could be investigated through yeast-2-hybrid (Y2H) reactions. It is possible to implement Y2H experiments during meiosis (Arora et al., 2004), so it would be interesting to see if these proteins interact together during meiosis. The vectors for this have been made, so with more time they could be performed.

The most pressing experiment to complete is restriction-digest Southern blotting strains with *rad1Δ, rad10Δ, rad52Δ, and rad59Δ* deletions in wildtype, *rad24Δ*, and *rad24Δ dmc1Δ* backgrounds. Several of the *SSAΔ* strains were made in the *rad24Δ dmc1Δ* backgrounds, but due to time constraints they were not used in this study. By using Southern blotting around the *HIS4::LEU2* and *leu2::hisG* loci on CHR III, it is possible to view ectopic recombination products (Allison et al., 2023). It is vital to see if ectopic recombination is suppressed when SSA proteins are knocked out, to either confirm or reject the hypothesis of SSA producing ectopic recombination products. Timecourses have been completed in many of these required strains, but the Southern blots were not performed due to a lack of time.

If the western blots in the *rad24Δ dmc1Δ* background show the SSA proteins are present, and the Southern blots show that eliminating SSA proteins prevents ectopic recombinants forming, it is vital to rule-out Break Induced Replication as a potential pathway (section **1.2.3**). BIR can produce gross chromosomal rearrangements like SSA, it can be recombinase independent, and relies on Rad52 and Rad59 (Signon et al., 2001, Malkova et al., 2005). Therefore, it is important to see if ectopic recombinant products can be produced

in a *pif1Δ* background. Pif1 is the helicase which is essential for BIR (Saini et al., 2013), but not required for SSA, so if ectopic recombinant products can be made in a *pif1Δ* or a BIR-deficient *pif1M40A* mutant background (Malone et al., 2022), but not in *rad1Δ, rad10Δ, rad52Δ,* and *rad59Δ*, it would prove that the single strand annealing pathway is indeed responsible for producing ectopic recombinants during meiosis.

If the SSA pathway is confirmed as the pathway for producing ectopic recombinants, it could be interesting to see whether site directed mutagenesis (SDM) could allow for SSA-specific mutations to prevent ectopic products forming without hindering secondary protein functions. Whilst knocking out SSA proteins will disrupt SSA, it will also disrupt many other DNA repair pathways, as well as eliminating secondary / structural roles these proteins may play. By making specific mutations which target SSA activities of these proteins, it makes the argument that SSA is producing ectopic recombinants more convincing. Rad1 with the nuclease mutation D825A has been shown to be SSA-null (Eichmiller et al., 2018, Li et al., 2013). Likewise Rad52 with R37 mutated to K or A is deficient in SSA (Shi et al., 2009, Yan et al., 2019), whilst Rad59 F180A is also SSA-null (Pannunzio et al., 2010). These constructs have been made and some have been transformed into the endogenous loci of *S. cerevisiae*.

Furthermore, SDM can be used to see the effects that phosphorylation has upon SSA activity. These mutants aim to either mimic phosphorylation (phosphor-mimetic) by replacing the serine/threonine of interest with an aspartic acid, or nullify the phosphate site (phosphor-mutant) by replacing the S/T with an alanine. This aims to shed some light on how post-translational modifications affect the function of SSA proteins, and may demonstrate these as additional targets of known meiotic kinases such as Mec1 and Tel1 (section **1.3.7**). Several Rad1 phosphorylation mutants in positions S613, S1071, and T1072 (Holt et al., 2009) have been made in plasmid form, but so far none have been transformed into yeast.

Acknowledgements

First and foremost thanks to Stephen for letting me join his lab. Thanks to Harriet, Mahari, Tom, Nadia, Laura and especially Kate for being great to work alongside. Thanks to everyone from the Allers lab: Thorsten, Laura (again), Anna, Cath, Callum, Vicky. Thanks to the Bolt lab past and present, especially: Ed, Tom K, Anna (again), Liv, Buckley, Andy, Tabi, He, Alice, and Emily S. Thanks to the Friel labs and Alan Huett too. Thanks to Harry, Chris, Jack, Igor, Josh, Paulina, Morgan, Rory, and Alex.

Thanks to my parents for always looking out for me. Thanks to Amandine for making my brother grow up. I suppose thanks to Luke for growing up. Thanks to the Beavises, the Burnleys and the Parkers for inviting me to your weddings.

Thanks to the following critters: Baymax, Ossie, Gary, Big Chungus, Bluebell, Magic (RIP), Ben (RIP), Yim (RIP), the Seamonkeys (RIP).

Bibliography

ACQUAVIVA, L., SZÉKVÖLGYI, L., DICHTL, B., DICHTL, B. S., DE LA ROCHE SAINT ANDRÉ, C., NICOLAS, A. & GÉLI, V. 2013. The COMPASS subunit Spp1 links histone methylation to initiation of meiotic recombination. *Science,* 339**,** 215-218.

AGASHE, S., JOSEPH, C. R., REYES, T. A. C., MENOLFI, D., GIANNATTASIO, M., WAIZENEGGER, A., SZAKAL, B. & BRANZEI, D. 2021. Smc5/6 functions with Sgs1-Top3-Rmi1 to complete chromosome replication at natural pause sites. *Nat Commun,* 12**,** 2111.

ALANI, E., PADMORE, R. & KLECKNER, N. 1990. Analysis of Wild-Type and rad50 Mutants of Yeast Suggests an Intimate Relationship between Meiotic Chromosome Synapsis and Recombination. *Cell,* 61**,** 419-436.

ALBERTS, B., JOHNSON, A., LEWIS, J., RAFF, M., ROBERTS, K. & WALTER, P. 2002. *Molecular Biology of the Cell,* USA, Garland Science.

ALLERS, T. & LICHTEN, M. 2001. Differential timing and control of noncrossover and crossover recombination during meiosis. *Cell,* 106**,** 47-57.

ALLISON, R. M., JOHNSON, D. J., NEALE, M. J. & GRAY, S. 2023. Recombinase-independent chromosomal rearrangements between dispersed inverted repeats in *Saccharomyces cerevisiae* meiosis. *Nucleic Acids Res,* 51**,** 9703-9715.

ALTMANNOVA, V., ECKERT-BOULET, N., ARNERIC, M., KOLESAR, P., CHALOUPKOVA, R., DAMBORSKY, J., SUNG, P., ZHAO, X., LISBY, M. & KREJCI, L. 2010. Rad52 SUMOylation affects the efficiency of the DNA repair. *Nucleic Acids Res,* 38**,** 4708-21.

ALTMANNOVA, V., FIRLEJ, M., MULLER, F., JANNING, P., RAULEDER, R., ROUSOVA, D., SCHAFFLER, A., BANGE, T. & WEIR, J. R. 2023. Biochemical characterisation of Mer3 helicase interactions and the protection of meiotic recombination intermediates. *Nucleic Acids Res,* 51**,** 4363-4384.

ANDERSON, J. & PARKER, R. 1998. The 3' to 5' degradation of yeast mRNAs is a general mechanism for mRNA turnover that requires the SK12 DEVH box protein and 3' to 5' exonucleases of the exosome complex. *EMBO J,* 17**,** 1497-1506.

ANTONY, E., TOMKO, E. J., XIAO, Q., KREJCI, L., LOHMAN, T. M. & ELLENBERGER, T. 2009. Srs2 disassembles Rad51 filaments by a protein-protein interaction triggering ATP turnover and dissociation of Rad51 from DNA. *Mol Cell,* 35**,** 105-15.

ARAVIND, L. & KOONIN, E. V. 1998. The HORMA domain, a common structural denominator in mitotic checkpoints, synapsis and DNA repair. *Trends Biochem Sci.,* 98**,** 284-286.

ARORA, C., KEE, K., MALEKI, S. & KEENEY, S. 2004. Antiviral protein Ski8 is a direct partner of Spo11 in meiotic DNA break formation, independent of its cytoplasmic role in RNA metabolism. *Mol Cell,* 13**,** 549-559.

ATCHESON, C., DI DOMENICO, B., FRACKMAN, S., ESPOSITO, R. & ELDER, R. 1987. Isolation, DNA sequence, and regulation of a meiosis-specific eukaryotic recombination gene. *Proc Natl Acad Sci U S A,* 84**,** 8035-8039.

AURICHE, C., DI DOMENICO, E. G. & ASCENZIONI, F. 2008. Budding yeast with human telomeres: a puzzling structure. *Biochimie,* 90**,** 108-15.

AYLON, Y., LIEFSHITZ, B. & KUPIEC, M. 2004. The CDK regulates repair of double-strand breaks by homologous recombination during the cell cycle. *EMBO J,* 23**,** 4868-75.

BAI, Y. & SYMINGTON, L. 1996. A Rad52 homolog is required for RAD51-independent mitotic recombination in Saccharomyces cerevisiae. . *Genes Dev,* 10**,** 2025-2037.

BALESTRINI, A., RISTIC, D., DIONNE, I., LIU, XIAO Z., WYMAN, C., WELLINGER, RAYMUND J. & PETRINI, JOHN H. J. 2013. The Ku Heterodimer and the Metabolism of Single-Ended DNA Double-Strand Breaks. *Cell Reports,* 3**,** 2033-2045.

BANTELE, S. C., FERREIRA, P., GRITENAITE, D., BOOS, D. & PFANDER, B. 2017. Targeting of the Fun30 nucleosome remodeller by the Dpb11 scaffold facilitates cell cycle-regulated DNA end resection. *Elife,* 6.

BARDWELL, J., BARDWELL, L., TOMKINSON, A. E. & FRIEDBERG, E. C. 1994. Specific cleavage of model recombination and repair intermediates by the yeast Rad1-Rad10 DNA endonuclease. *Science,* 265**,** 2082-2085.
BAUDAT, F. & NICOLAS, A. 1997. Clustering of meiotic double-strand breaks on yeast chromosome III. *Proc Natl Acad Sci U S A,* 94**,** 5213-5218.
BEBENEK, K., GARCIA-DIAZ, M., PATISHALL, S. R. & KUNKEL, T. A. 2005. Biochemical properties of Saccharomyces cerevisiae DNA polymerase IV. *J Biol Chem,* 280**,** 20051-8.
BERCHOWITZ, L. E., HANLON, S. E., LIEB, J. D. & COPENHAVER, G. P. 2009. A positive but complex association between meiotic double-strand break hotspots and open chromatin in *Saccharomyces cerevisiae*. *Genome Res,* 19**,** 2245-57.
BERGERAT, A., DE MASSYT, B., GADELLE, D., VAROUTAST, P.-C., NICOLAST, A. & FORTERRE, P. 1997. An atypical topoisomerase II from Archaea with implications for meiotic recombination. *Nature,* 386**,** 414-417.
BERNSTEIN, K. A., REID, R. J., SUNJEVARIC, I., DEMUTH, K., BURGESS, R. C. & ROTHSTEIN, R. 2011. The Shu complex, which contains Rad51 paralogues, promotes DNA repair through inhibition of the Srs2 anti-recombinase. *Mol Biol Cell,* 22**,** 1599-607.
BHAGWAT, N. R., OWENS, S. N., ITO, M., BOINAPALLI, J. V., POA, P., DITZEL, A., KOPPARAPU, S., MAHALAWAT, M., DAVIES, O. R., COLLINS, S. R., JOHNSON, J. R., KROGAN, N. J. & HUNTER, N. 2021. SUMO is a pervasive regulator of meiosis. *Elife,* 10.
BHARGAVA, R., ONYANGO, D. O. & STARK, J. M. 2016. Regulation of Single-Strand Annealing and its Role in Genome Maintenance. *Trends Genet,* 32**,** 566-575.
BISHOP, D. K. 1994. RecA homologs Dmc1 and Rad51 interact to form multiple nuclear complexes prior to meiotic chromosome synapsis. *Cell,* 79**,** 1081-1092.
BISHOP, D. K., PARK, D., XU, L. & N., K. 1992. DMC1: A Meiosis-Specific Yeast Homolog of E. coli recA Required for Recombination, Synaptonemal Complex Formation, and Cell Cycle Progression. *Cell,* 69**,** 439-456.
BIZARD, A. H. & HICKSON, I. D. 2014. The dissolution of double Holliday junctions. *Cold Spring Harb Perspect Biol,* 1;6(7):a016477.
BJORNSTI, M. A. & KAUFMANN, S. H. 2019. Topoisomerases and cancer chemotherapy: recent advances and unanswered questions. *F1000Res,* 8.
BLAT, Y., PROTACIO, R. U., HUNTER, N. & KLECKNER, N. 2002. Physical and functional interactions among basic chromosome organizational features govern early steps of meiotic chiasma formation. *Cell,* 6**,** 791-802.
BLOOM, K. & COSTANZO, V. 2017. Centromere Structure and Function. *Prog Mol Subcell Biol,* 56**,** 515-539.
BLOOMFIELD, G. 2016. Atypical ploidy cycles, Spo11, and the evolution of meiosis. *Semin Cell Dev Biol,* 54**,** 158-64.
BODENMILLER, B., CAMPBELL, D., GERRITIS, B., LAM, H., JOVANOVIC, M., PICOTTI, P., SCHLAPBACH, R. & AEBERSOLD, R. 2008. PhosphoPep--a database of protein phosphorylation sites in model organisms. *Nat Biotechnol,* 26**,** 1339-1340.
BODENMILLER, B., WANKA, S., KRAFT, C., URBAN, J., CAMPBELL, D., PEDRIOLI, P. G., GERRITS, B., PICOTTI, P., LAM, H. & VITEK, O. 2010. Phosphoproteomic Analysis Reveals InterconnectedSystem-Wide Responses to Perturbationsof Kinases and Phosphatases in Yeast. *Sci Signal,* 3**,** rs4.
BONETTI, D., VILLA, M., GOBBINI, E., CASSANI, C., TEDESCHI, G. & LONGHESE, M. P. 2015. Escape of Sgs1 from Rad9 inhibition reduces the requirement for Sae2 and functional MRX in DNA end resection. *EMBO Rep,* 16**,** 351-61.
BORDE, V., GOLDMAN, A. S. & LICHTEN, M. 2000. Direct coupling between meiotic DNA replication and recombination initiation. *Science,* 290**,** 806-809.
BÖRNER, G. V., KLECKNER, N. & HUNTER, N. 2004. Crossover/Noncrossover Differentiation, Synaptonemal Complex Formation, and Regulatory Surveillance at the Leptotene/Zygotene Transition of Meiosis. *Cell,* 117**,** 29-45.
BREALEY, J. 2022. *Tyrosyl-DNA phosphodiesterase 1 participates in a novel Mre11-independent mechanism of Spo11 cleavage during meiosis in Saccharomyces cerevisiae.* MSc, University of Nottingham.

BRILL, S. & STILLMAN, B. 1991. Replication factor-A from *Saccharomyces cerevisiae* is encoded by three essential genes coordinately expressed at S phase. *Genes Dev,* 5**,** 1589-1600.
BROWN, G. B. B., GITTENS, W. H., ALLISON, R. M., OLIVER, A. W. & NEALE, M. J. 2024. CC-seq: Nucleotide-Resolution Mapping of Spo11 Double-Strand Breaks in *S. cerevisiae* Cells. *Methods Mol Biol,* 2818**,** 3-22.
BROWN, M. S. & BISHOP, D. K. 2014. DNA strand exchange and RecA homologs in meiosis. *Cold Spring Harb Perspect Biol,* 7**,** a016659.
BROWN, M. S., GRUBB, J., ZHANG, A., RUST, M. J. & BISHOP, D. K. 2015. Small Rad51 and Dmc1 Complexes Often Co-occupy Both Ends of a Meiotic DNA Double Strand Break. *PLoS Genet,* 11**,** e1005653.
BUHLER, C., BORDE, V. & LICHTEN, M. 2007. Mapping meiotic single-strand DNA reveals a new landscape of DNA double-strand breaks in *Saccharomyces cerevisiae*. *PLoS Biol,* 5**,** e324.
BURGESS, R. C., RAHMAN, S., LISBY, M., ROTHSTEIN, R. & ZHAO, X. 2007. The Slx5-Slx8 complex affects sumoylation of DNA repair proteins and negatively regulates recombination. *Mol Cell Biol,* 27**,** 6153-62.
BZYMEK, M., THAYER, N. H., OH, S. D., KLECKNER, N. & HUNTER, N. 2010. Double Holliday junctions are intermediates of DNA break repair. *Nature,* 464**,** 937-41.
CALLENDER, T. L., LAUREAU, R., WAN, L., CHEN, X., SANDHU, R., LALJEE, S., ZHOU, S., SUHANDYNATA, R. T., PRUGAR, E., GAINES, W. A., KWON, Y., BORNER, G. V., NICOLAS, A., NEIMAN, A. M. & HOLLINGSWORTH, N. M. 2016. Mek1 Down Regulates Rad51 Activity during Yeast Meiosis by Phosphorylation of Hed1. *PLoS Genet,* 12**,** e1006226.
CANNAVO, E. & CEJKA, P. 2014. Sae2 promotes dsDNA endonuclease activity within Mre11-Rad50-Xrs2 to resect DNA breaks. *Nature,* 514**,** 122-5.
CANNAVO, E., JOHNSON, D., ANDRES, S. N., KISSLING, V. M., REINERT, J. K., GARCIA, V., ERIE, D. A., HESS, D., THOMA, N. H., ENCHEV, R. I., PETER, M., WILLIAMS, R. S., NEALE, M. J. & CEJKA, P. 2018. Regulatory control of DNA end resection by Sae2 phosphorylation. *Nat Commun,* 9**,** 4016.
CAO, L., E., A. & KLECKNER, N. 1990a. A pathway for generation and processing of double-strand breaks during meiotic recombination in *S. cerevisiae*. *Cell,* 6**,** 1089-1101.
CAO, L., E., A. & KLECKNER, N. 1990b. A pathway for generation and processing of double-strand breaks during meiotic recombination in S. cerevisiae. *Cell,* 61**,** 1089-1101.
CARBALLO, J. A., JOHNSON, A. L., SEDGWICK, S. G. & CHA, R. S. 2008. Phosphorylation of the axial element protein Hop1 by Mec1/Tel1 ensures meiotic interhomolog recombination. *Cell,* 132**,** 758-70.
CARBALLO, J. A., PANIZZA, S., SERRENTINO, M. E., JOHNSON, A. L., GEYMONAT, M., BORDE, V., KLEIN, F. & CHA, R. S. 2013. Budding yeast ATM/ATR control meiotic double-strand break (DSB) levels by down-regulating Rec114, an essential component of the DSB-machinery. *PLoS Genet,* 9**,** e1003545.
CARREIRA, R., AGUADO, F. J., HURTADO-NIEVES, V. & BLANCO, M. G. 2022. Canonical and novel non-canonical activities of the Holliday junction resolvase Yen1. *Nucleic Acids Res,* 50**,** 259-280.
CASSANI, C., GOBBINI, E., WANG, W., NIU, H., CLERICI, M., SUNG, P. & LONGHESE, M. P. 2016. Tel1 and Rif2 Regulate MRX Functions in End-Tethering and Repair of DNA Double-Strand Breaks. *PLoS Biol,* 14**,** e1002387.
CEJKA, P. & KOWALCZYKOWSKI, S. C. 2010. The full-length *Saccharomyces cerevisiae* Sgs1 protein is a vigorous DNA helicase that preferentially unwinds holliday junctions. *J Biol Chem,* 285**,** 8290-301.
CEJKA, P., PLANK, J. L., BACHRATI, C. Z., HICKSON, I. D. & KOWALCZYKOWSKI, S. C. 2010. Rmi1 stimulates decatenation of double Holliday junctions during dissolution by Sgs1-Top3. *Nat Struct Mol Biol,* 17**,** 1377-82.
CHALISSERY, J., JALAL, D., AL-NATOUR, Z. & HASSAN, A. H. 2017. Repair of Oxidative DNA Damage in Saccharomyces cerevisiae. *DNA Repair (Amst),* 51**,** 2-13.
CHAN, Y. L., BROWN, M. S., QIN, D., HANDA, N. & BISHOP, D. K. 2014. The third exon of the budding yeast meiotic recombination gene HOP2 is required for calcium-

dependent and recombinase Dmc1-specific stimulation of homologous strand assimilation. *J Biol Chem,* 289**,** 18076-86.
CHAN, Y. L., ZHANG, A., WEISSMAN, B. P. & BISHOP, D. K. 2019. RPA resolves conflicting activities of accessory proteins during reconstitution of Dmc1-mediated meiotic recombination. *Nucleic Acids Res,* 47**,** 747-761.
CHEN, X., CUI, D., PAPUSHA, A., ZHANG, X., CHU, C. D., TANG, J., CHEN, K., PAN, X. & IRA, G. 2012. The Fun30 nucleosome remodeller promotes resection of DNA double-strand break ends. *Nature,* 489**,** 576-80.
CHEN, X. & TOMKINSON, A. E. 2011. Yeast Nej1 is a key participant in the initial end binding and final ligation steps of nonhomologous end joining. *J Biol Chem,* 286**,** 4931-40.
CHENG, H., SHANG, D. & ZHOU, R. 2022. Germline stem cells in human. *Signal Transduct Target Ther,* 7**,** 345.
CHOU, K. Y., LEE, J. Y., KIM, K. B., KIM, E., LEE, H. S. & RYU, H. Y. 2023. Histone modification in *Saccharomyces cerevisiae*: A review of the current status. *Comput Struct Biotechnol J,* 21**,** 1843-1850.
CLAEYS BOUUAERT, C., PU, S., WANG, J., OGER, C., DACCACHE, D., XIE, W., PATEL, D. J. & KEENEY, S. 2021a. DNA-driven condensation assembles the meiotic DNA break machinery. *Nature,* 592**,** 144-149.
CLAEYS BOUUAERT, C., TISCHFIELD, S. E., PU, S., MIMITOU, E. P., ARIAS-PALOMO, E., BERGER, J. M. & KEENEY, S. 2021b. Structural and functional characterization of the Spo11 core complex. *Nat Struct Mol Biol,* 28**,** 92-102.
CLERICI, M., TROVESI, C., GALBIATI, A., LUCCHINI, G. & LONGHESE, M. P. 2014. Mec1/ATR regulates the generation of single-stranded DNA that attenuates Tel1/ATM signaling at DNA ends. *EMBO J,* 33**,** 198-216.
CLOUD, V., CHAN, Y. L., GRUBB, J., BUDKE, B. & BISHOP, D. K. 2012. Rad51 is an accessory factor for Dmc1-mediated joint molecule formation during meiosis. *Science,* 337**,** 1222-1226.
COLOMBO, C. V., GNUGNOLI, M., GOBBINI, E. & LONGHESE, M. P. 2020. How do cells sense DNA lesions? *Biochemical Society Transactions,* 48**,** 677-691.
COMEAUX, E. Q., CUYA, S. M., KOJIMA, K., JAFARI, N., WANZECK, K. C., MOBLEY, J. A., BJORNSTI, M. A. & VAN WAARDENBURG, R. C. 2015. Tyrosyl-DNA phosphodiesterase I catalytic mutants reveal an alternative nucleophile that can catalyze substrate cleavage. *J Biol Chem,* 290**,** 6203-14.
COMSTOCK, W., SANFORD, E., NAVARRO, M. & SMOLKA, M. B. 2024. Profiling Tel1 Signaling Reveals a Non-Canonical Motif Targeting DNA Repair and Telomere Control Machineries. *bioRxiv*.
CONSTANTINOU, A., CHEN, X. B., MCGOWAN, C. H. & WEST, S. C. 2002. Holliday junction resolution in human cells, two junction endonucleases with distinct substrate specificities. *EMBO J,* 21**,** 5577-5585.
CORBETT, K. D., BENEDETTI, P. & BERGER, J. M. 2007. Holoenzyme assembly and ATP-mediated conformational dynamics of topoisomerase VI. *Nat Struct Mol Biol,* 14**,** 611-9.
CORTES LEDESMA, F., EL KHAMISY, S. F., ZUMA, M. C., OSBORN, K. & CALDECOTT, K. W. 2009. A human 5'-tyrosyl DNA phosphodiesterase that repairs topoisomerase-mediated DNA damage. *Nature,* 461**,** 674-8.
CRICK, F. H. 1958. On Protein Synthesis. *Symp Soc Exp Biol***,** 138-163.
DALEY, J. & WILSON, T. 2008. Evidence that base stacking potential in annealed 3' overhangs determines polymerase utilization in yeast nonhomologous end joining. *DNA Repair (Amst),* 1**,** 67-76.
DASH, S., JOSHI, S., PANKAJAM, A. V., SHINOHARA, A. & NISHANT, K. T. 2024. Heterozygosity alters Msh5 binding to meiotic chromosomes in the baker's yeast. *Genetics,* 226.
DAVIS, A. P. & SYMINGTON, L. S. 2001. The Yeast Recombinational Repair Protein Rad59 Interacts with Rad52 and stimulates SSA. . *Genetics,* 155**,** 515-525.
DAVIS, A. P. & SYMINGTON, L. S. 2023. RAD51-Dependent Break-Induced Replication in Yeast. *Molecular and Cellular Biology,* 24**,** 2344-2351.

DE LA TORRE-RUIZ, M.-A. & LOWNDES, N. F. 2000. The *Saccharomyces cerevisiae* DNA damage checkpoint is required for efficient repair of double strand breaks by non-homologous end joining. *FEBS Letters,* 467**,** 311-315.
DE LOS SANTOS, T., HUNTER, N., LEE, C. S., LARKIN, B., LOIDL, J. & HOLLINGSWORTH, N. M. 2003. The Mus81-Mms4 endonuclease acts independently of dHJ resolution to promote a distinct subset of Crossovers during meiosis in budding yeast. *Genetics,* 164**,** 81-94.
DE MUYT, A., JESSOP, L., KOLAR, E., SOURIRAJAN, A., CHEN, J., DAYANI, Y. & LICHTEN, M. 2012. BLM helicase ortholog Sgs1 is a central regulator of meiotic recombination intermediate metabolism. *Mol Cell,* 46**,** 43-53.
DENG, C., BROWN, J. A., YOU, D. & BROWN, J. M. 2005. Multiple endonucleases function to repair covalent topoisomerase I complexes in *Saccharomyces cerevisiae*. *Genetics,* 170**,** 591-600.
DENG, S. K., GIBB, B., DE ALMEIDA, M. J., GREENE, E. C. & SYMINGTON, L. S. 2014. RPA antagonizes microhomology-mediated repair of DNA double-strand breaks. *Nat Struct Mol Biol,* 21**,** 405-12.
DESHPANDE, I., SEEBER, A., SHIMADA, K., KEUSCH, J. J., GUT, H. & GASSER, S. M. 2017. Structural Basis of Mec1-Ddc2-RPA Assembly and Activation on Single-Stranded DNA at Sites of Damage. *Mol Cell,* 68**,** 431-445 e5.
DESHPANDE, R. & WILSON, T. 2007. Modes of interaction among yeast Nej1, Lif1 and Dnl4 proteins and comparison to human XLF, XRCC4 and Lig4. *DNA Repair (Amst),* 10**,** 1507-1516.
DIAZ-RUIZ, R., RIGOULET, M. & DEVIN, A. 2011. The Warburg and Crabtree effects: On the origin of cancer cell energy metabolism and of yeast glucose repression. *Biochim Biophys Acta,* 1807**,** 568-76.
DIBITETTO, D., FERRARI, M., RAWAL, C. C., BALINT, A., KIM, T., ZHANG, Z., SMOLKA, M. B., BROWN, G. W., MARINI, F. & PELLICIOLI, A. 2016. Slx4 and Rtt107 control checkpoint signalling and DNA resection at double-strand breaks. *Nucleic Acids Res,* 44**,** 669-82.
DONNIANNI, R. A. & SYMINGTON, L. S. 2013. Break-induced replication occurs by conservative DNA synthesis. *Proc Natl Acad Sci U S A,* 110**,** 13475-80.
DUBRANA, K., VAN ATTIKUM, H., HEDIGER, F. & GASSER, S. M. 2007. The processing of double-strand breaks and binding of single-strand-binding proteins RPA and Rad51 modulate the formation of ATR-kinase foci in yeast. *J Cell Sci,* 120**,** 4209-20.
DUROC, Y., KUMAR, R., RANJHA, L., ADAM, C., GUEROIS, R., MD MUNTAZ, K., MARSOLIER-KERGOAT, M. C., DINGLI, F., LAUREAU, R., LOEW, D., LLORENTE, B., CHARBONNIER, J. B., CEJKA, P. & BORDE, V. 2017. Concerted action of the MutLbeta heterodimer and Mer3 helicase regulates the global extent of meiotic gene conversion. *Elife,* 6.
EHMSEN, K. T. & HEYER, W. D. 2008. Saccharomyces cerevisiae Mus81-Mms4 is a catalytic, DNA structure-selective endonuclease. *Nucleic Acids Res,* 36**,** 2182-95.
EICHMILLER, R., MEDINA-RIVERA, M., DESANTO, R., MINCA, E., KIM, C., HOLLAND, C., SEOL, J. H., SCHMIT, M., ORAMUS, D., SMITH, J., GALLARDO, I. F., FINKELSTEIN, I. J., LEE, S. E. & SURTEES, J. A. 2018. Coordination of Rad1-Rad10 interactions with Msh2-Msh3, Saw1 and RPA is essential for functional 3' non-homologous tail removal. *Nucleic Acids Res,* 46**,** 5075-5096.
ELANGO, R., SHENG, Z., JACKSON, J., DECATA, J., IBRAHIM, Y., PHAM, N. T., LIANG, D. H., SAKOFSKY, C. J., VINDIGNI, A., LOBACHEV, K. S., IRA, G. & MALKOVA, A. 2017. Break-induced replication promotes formation of lethal joint molecules dissolved by Srs2. *Nat Commun,* 8**,** 1790.
ELLENBERGER, T. & TOMKINSON, A. E. 2008. Eukaryotic DNA ligases: structural and functional insights. *Annu Rev Biochem,* 77**,** 313-38.
EMERSON, C. H. & BERTUCH, A. A. 2016. Consider the workhorse: Nonhomologous end-joining in budding yeast. *Biochem Cell Biol,* 94**,** 396-406.
ENGEBRECHT, J. A., VOELKEL-MEIMAN, K. & ROEDER, G. S. 1991. Meiosis-specific RNA splicing in yeast. *Cell,* 66**,** 1257-1268.
ENSERINK, J. M. & KOLODNER, R. D. 2010. An overview of Cdk1-controlled targets and processes. *Cell Div,* 5**,** 11.

FALK, J. E., CHAN, A. C., HOFFMANN, E. & HOCHWAGEN, A. 2010. A Mec1- and PP4-dependent checkpoint couples centromere pairing to meiotic recombination. *Dev Cell,* 19**,** 599-611.
FASCHING, C. L., CEJKA, P., KOWALCZYKOWSKI, S. C. & HEYER, W. D. 2015. Top3-Rmi1 dissolve Rad51-mediated D loops by a topoisomerase-based mechanism. *Mol Cell,* 57**,** 595-606.
FERGUSON, D. O., SEKIGUCHI, J. M., CHANG, S., FRANK, M. K., GAO, Y., DEPINHO, R. A. & ALT, F. W. 2000. The NHEJpathway of DNA repair is required for genomic stability and the suppression of translocations. *Proc Natl Acad Sci U S A,* 97**,** 6630-6333.
FERRARI, S. R., GRUBB, J. & BISHOP, D. K. 2009. The Mei5-Sae3 protein complex mediates Dmc1 activity in *Saccharomyces cerevisiae*. *J Biol Chem,* 284**,** 11766-70.
FINLEY, D., ULRICH, H. D., SOMMER, T. & KAISER, P. 2012. The ubiquitin-proteasome system of *Saccharomyces cerevisiae*. *Genetics,* 192**,** 319-60.
FISHMAN-LOBELL, J., RUDIN, N. & HABER, J. E. 1992. Two alternative pathways of DSB repair that are kinetically separable and independently modulated. *Mol Cell Biol,* 12**,** 1292-1393.
FITCH, W. M. 1964. The probable sequence of nucleotides in some codons. *Proc Natl Acad Sci U S A,* 2.
FLOTT, S., ALABERT, C., TOH, G. W., TOTH, R., SUGAWARA, N., CAMPBELL, D. G., HABER, J. E., PASERO, P. & ROUSE, J. 2007. Phosphorylation of Slx4 by Mec1 and Tel1 regulates the single-strand annealing mode of DNA repair in budding yeast. *Mol Cell Biol,* 27**,** 6433-45.
FOSTER, S. S., BALESTRINI, A. & PETRINI, J. H. 2011. Functional interplay of the Mre11 nuclease and Ku in the response to replication-associated DNA damage. *Mol Cell Biol,* 31**,** 4379-89.
FUKUNAGA, K., KWON, Y., SUNG, P. & SUGIMOTO, K. 2011. Activation of protein kinase Tel1 through recognition of protein-bound DNA ends. *Mol Cell Biol,* 31**,** 1959-71.
GADGIL, R. Y., ROMER, E. J., GOODMAN, C. C., RIDER, S. D., JR., DAMEWOOD, F. J., BARTHELEMY, J. R., SHIN-YA, K., HANENBERG, H. & LEFFAK, M. 2020. Replication stress at microsatellites causes DNA double-strand breaks and break-induced replication. *J Biol Chem,* 295**,** 15378-15397.
GAO, J. & COLAIACOVO, M. P. 2018. Zipping and Unzipping: Protein Modifications Regulating Synaptonemal Complex Dynamics. *Trends Genet,* 34**,** 232-245.
GARCIA, V., PHELPS, S. E., GRAY, S. & NEALE, M. J. 2011a. Bidirectional resection of DNA double-strand breaks by Mre11 and Exo1. *Nature,* 479**,** 241-4.
GARCIA, V., PHELPS, S. E., GRAY, S. & NEALE, M. J. 2011b. Bidirectional resection of DNA double-strand breaks by Mre11 and Exo1 (Supplemental materials). *Nature,* 479.
GARDINER, J. M., BULLARD, S. A., CHROME, C. & MALONE, R. E. 1997. Molecular and genetic analysis of REC103, an early meiotic recombination gene in yeast. *Genetics,* 146.
GIAEVER, G. & NISLOW, C. 2014. The yeast deletion collection: a decade of functional genomics. *Genetics,* 197**,** 451-65.
GIETZ, R. D. 2014. Yeast transformation by the LiAc/SS carrier DNA/PEG method. *Methods Mol Biol,* 1205**,** 1-12.
GOBBINI, E., CASARI, E., COLOMBO, C. V., BONETTI, D. & LONGHESE, M. P. 2020. The 9-1-1 Complex Controls Mre11 Nuclease and Checkpoint Activation during Short-Range Resection of DNA Double-Strand Breaks. *Cell Rep,* 33**,** 108287.
GOBBINI, E., CASSANI, C., VERTEMARA, J., WANG, W., MAMBRETTI, F., CASARI, E., SUNG, P., TISI, R., ZAMPELLA, G. & LONGHESE, M. P. 2018. The MRX complex regulates Exo1 resection activity by altering DNA end structure. *EMBO J,* 37.
GOBBINI, E., CASSANI, C., VILLA, M., BONETTI, D. & LONGHESE, M. P. 2016. Functions and regulation of the MRX complex at DNA double-strand breaks. *Microb Cell,* 3**,** 329-337.
GOFFEAU, A., BARRELL, B. G., BUSSEY, H., DAVIS, R. W., DUJON, B., FELDMAN, H., GALIBERT, F., HOHEISEL, D., JACQ, C., JOHNSTON, M., LOIUS, E. J., MEWES, H. W., MURAKAMI, Y., PHILIPPSEN, P., TETTELIN, H. & OLIVER, S. G. 1996. Life with 6000 genes. *Science,* 274**,** 546-567.

GOLDSTEIN, G., SCHEID, M., HAMMERLING, D. H., NIALL, H. D. & BOYSE, E. A. 1975. Isolation of a polypeptide that has lymphocyte-differentiating properties and is probably represented universally in living cells. *Proc Natl Acad Sci U S A,* 1**,** 11-15.
GRAILLE, M., CLADIERE, L., DURAND, D., LECOINTE, F., GADELLE, D., QUEVILLON-CHERUEL, S., VACHETTE, P., FORTERRE, P. & VAN TILBEURGH, H. 2008. Crystal structure of an intact type II DNA topoisomerase: insights into DNA transfer mechanisms. *Structure,* 16**,** 360-70.
GRAY, S., ALLISON, R. M., GARCIA, V., GOLDMAN, A. S. & NEALE, M. J. 2013. Positive regulation of meiotic DNA double-strand break formation by activation of the DNA damage checkpoint kinase Mec1(ATR). *Open Biol,* 3**,** 130019.
GRAY, S. & COHEN, P. E. 2016. Control of Meiotic Crossovers: From Double-Strand Break Formation to Designation. *Annu Rev Genet,* 50**,** 175-210.
GRENON, M., COSTELLOE, T., JIMENO, S., O'SHAUGHNESSY, A., FITZGERALD, J., ZGHEIB, O., DEGERTH, L. & LOWNDES, N. F. 2007. Docking onto chromatin via the *Saccharomyces cerevisia*e Rad9 Tudor domain. *Yeast,* 24**,** 105-19.
GREY, C. & DE MASSY, B. 2022. Coupling crossover and synaptonemal complex in meiosis. *Genes Dev,* 34**,** 4-6.
GRIGAITIS, R., RANJHA, L., WILD, P., KASACIUNAITE, K., CEPPI, I., KISSLING, V., HENGGELER, A., SUSPERREGUI, A., PETER, M., SEIDEL, R., CEJKA, P. & MATOS, J. 2020. Phosphorylation of the RecQ Helicase Sgs1/BLM Controls Its DNA Unwinding Activity during Meiosis and Mitosis. *Dev Cell,* 53**,** 706-723 e5.
GRUSHCOW, J. M., HOLZEN, T. M., PARK, K. J., WEINERT, T., LICHTEN, M. & BISHOP, D. K. 1999. Saccharomyces cerevisiae Checkpoint Genes MEC1, RAD17 and RAD24 Are Required for Normal Meiotic Recombination Partner Choice. *Genetics,* 153**,** 607-620.
HALBACH, F., REICHELT, P., RODE, M. & CONTI, E. 2013. The yeast ski complex: crystal structure and RNA channeling to the exosome complex. *Cell,* 154**,** 814-26.
HALDANE, J. B. S. 1919. The combination of linkage values, and the calculation of distances between the loci of linked factors. *Journal of Genetics,* 8**,** 299-309.
HARBERS, M. 2015. Shift-Western Blotting: Separate Analysis of Protein and DNA from Protein-DNA Complexes. *Methods Mol Biol,* 2015;1312:355-73.
HASTINGS, P. J., IRA, G. & LUPSKI, J. R. 2009. A microhomology-mediated break-induced replication model for the origin of human copy number variation. *PLoS Genet,* 5**,** e1000327.
HAYASE, A., TAKAGI, M., MIYAZAKI, T., OSHIUMI, H., SHINOHARA, M. & SHINOHARA, A. 2004. A protein complex containing Mei5 and Sae3 promotes the assembly of the meiosis-specific RecA homolog Dmc1. *Cell,* 119**,** 927-40.
HE, W., VERHEES, G. F., BHAGWAT, N., YANG, Y., KULKARNI, D. S., LOMBARDO, Z., LAHIRI, S., ROY, P., ZHUO, J., DANG, B., SNYDER, A., SHASTRY, S., MOEZPOOR, M., ALOCOZY, L., LEE, K. G., PAINTER, D., MUKERJI, I. & HUNTER, N. 2021. SUMO fosters assembly and functionality of the MutSgamma complex to facilitate meiotic crossing over. *Dev Cell,* 56**,** 2073-2088 e3.
HE, X., VAN WAARDENBURG, R., BABAOGLU, K., PRICE, A. C., NITISS, K. C., NITISS, J. L., BJORNSTI, M. A. & WHITE, S. W. 2007. Mutation of a conserved active site residue converts tyrosyl-DNA phosphodiesterase I into a DNA topoisomerase I-dependent poison. *J Mol Biol,* 372**,** 1070-1081.
HENDERSON, K. A., KEE, K., MALEKI, S., SANTINI, P. A. & KEENEY, S. 2006. Cyclin-dependent kinase directly regulates initiation of meiotic recombination. *Cell,* 125**,** 1321-1332.
HEPWORTH, S., FRIESEN, H. & SEGALL, J. 1998. NDT80 and the Meiotic Recombination Checkpoint Regulate Expression of Middle Sporulation-Specific Genes in *Saccharomyces cerevisiae*. *Molecular and Cellular Biology,* 18**,** 5750-5761.
HOHL, M., KWON, Y., GALVÁN, S. M., XUE, X., TOUS, C., AGUILERA, A., SUNG, P. & PETRINI, J. H. J. 2011. The Rad50 coiled-coil domain is indispensable for Mre11 complex functions. *Nature Structural & Molecular Biology,* 18**,** 1124-1131.
HOLLINGSWORTH, N. M. 2016. Mek1/Mre4 is a master regulator of meiotic recombination in budding yeast. *Microb Cell,* 3**,** 129-131.
HOLLINGSWORTH, N. M. & BRILL, S. J. 2004. The Mus81 solution to resolution: generating meiotic crossovers without Holliday junctions. *Genes Dev,* 18**,** 117-25.

HOLT, L. J., TUCH, B. B., VILLEN, J., JOHNSON, A. D., GYGI, S. P. & MORGAN, D. O. 2009. Global analysis of Cdk1 substrate phosphorylation sites provides insights into evolution. *Science,* 325**,** 1682-6.
HONG, E. L., SHINOHARA, A. & BISHOP, D. K. 2001. *Saccharomyces cerevisiae* Dmc1 protein promotes renaturation of single-strand DNA (ssDNA) and assimilation of ssDNA into homologous super-coiled duplex DNA. *J Biol Chem,* 276**,** 41906-12.
HOPFNER, K. P., CRAIG, L., MONCALIAN, G., ZINKEL, R. A., USUI, T., OWEN, B. A. L., KARCHER, A., HENDERSON, B., BODMER, J., MCMURRAY, C. T., CARNEY, J. P., PETRINI, J. H. & TAINER, J. A. 2002. The Rad50 zinc-hook is a structure joining Mre11 complexes in DNA recombination and repair. *Nature,* 418**,** 562-566.
HOPFNER, K. P., KARCHER, A., CRAIG, L., WOO, T. T., CARNEY, J. P. & TAINER, J. A. 2001. Structural biochemistry and interaction architecture of the DNA double-strand break repair Mre11 nuclease and Rad50-ATPase. *Cell,* 4**,** 473-485.
HUERTAS, P., CORTES-LEDESMA, F., SARTORI, A. A., AGUILERA, A. & JACKSON, S. P. 2008. CDK targets Sae2 to control DNA-end resection and homologous recombination. *Nature,* 455**,** 689-92.
HUNTER, N. 2015. Meiotic Recombination: The Essence of Heredity. *Cold Spring Harb Perspect Biol,* 7.
HUNTER, N. & KLECKNER, N. 2001. The single-end invasion, an asymmetric intermediate at the DSB to double-holliday junction transition of meiotic recombination. *Cell,* 106**,** 59-70.
IMHOF, A. & BECKER, P. B. 2001. Modifications of the histone N-terminal domains. Evidence for an "epigenetic code"? *Mol Biotechnol,* 17**,** 1-13.
IP, S. C., RASS, U., BLANCO, M. G., FLYNN, H. R., SKEHEL, J. M. & WEST, S. C. 2008. Identification of Holliday junction resolvases from humans and yeast. *Nature,* 456**,** 357-61.
IRA, G., PELLICIOLI, A., BALIJJA, A., WANG, X., FIORANI, S., CAROTENUTO, W., LIBERI, G., BRESSAN, D., WAN, L., HOLLINGSWORTH, N. M., HABER, J. E. & FOIANI, M. 2004. DNA end resection, homologous recombination and DNA damage checkpoint activation require CDK1. *Nature,* 431**,** 1011-7.
ITO, M., KUGOU, K., FAWCETT, J. A., MURA, S., IKEDA, S., INNAN, H. & OHTA, K. 2014. Meiotic recombination cold spots in chromosomal cohesion sites. *Genes Cells,* 19**,** 359-73.
IVANOV, D. & NASMYTH, K. 2005. A topological interaction between cohesin rings and a circular minichromosome. *Cell,* 122**,** 849-60.
IVANOV, E. L., SUGAWARA, N., FISHMAN-LOBELL, J. & HABER, J. E. 1996. Genetic requirements for the SSA pathway of DSB repair in *S. cerevisiae*. *Genetics,* 142**,** 693-704.
JIA, X., WEINERT, T. & LYDALL, D. 2004. Mec1 and Rad53 inhibit formation of single-stranded DNA at telomeres of *Saccharomyces cerevisiae* cdc13-1 mutants. *Genetics,* 166**,** 753-764.
JOHNSON, D., ALLISON, R. M., CANNAVO, E., CEJKA, P., HARPER, J. A. & NEALE, M. J. 2024. Exploring the removal of Spo11 and topoisomerases from DNA breaks in S. cerevisiae by human Tyrosyl DNA Phosphodiesterase 2. *DNA Repair (Amst),* 142**,** 103757.
JOHNSON, D., CRAWFORD, M., COOPER, T., CLAEYS BOUUAERT, C., KEENEY, S., LLORENTE, B., GARCIA, V. & NEALE, M. J. 2021. Concerted cutting by Spo11 illuminates meiotic DNA break mechanics. *Nature,* 594**,** 572-576.
JONES, G. H. 1984. The control of chiasma distribution. *Symp Soc Exp Biol,* 38**,** 293-320.
JOO, J. H., HONG, S., HIGASHIDE, M. T., CHOI, E. H., YOON, S., LEE, M. S., KANG, H. A., SHINOHARA, A., KLECKNER, N. & KIM, K. P. 2024. RPA interacts with Rad52 to promote meiotic crossover and noncrossover recombination. *Nucleic Acids Res,* 52**,** 3794-3809.
KARLIN, J. & FISCHHABER, P. L. 2013. Rad51 ATP binding but not hydrolysis is required to recruit Rad10 in synthesis-dependent strand annealing sites in S. cerevisiae. *Adv Biol Chem,* 3**,** 295-303.
KATO, R. & H., O. 1994. An essential gene, ESR1, is required for mitotic cell growth, DNA repair and meiotic recombination in *Saccharomyces cerevisiae*. *Nucleic Acids Res,* 22**,** 3104-3112.

KEE, K., PROTACIO, R. U., ARORA, C. & KEENEY, S. 2004. Spatial organization and dynamics of the association of Rec102 and Rec104 with meiotic chromosomes. *EMBO J,* 23**,** 1815-24.
KEENEY, S., GIROUX, C. N. & KLECKNER, N. 1997. Meiosis-specific DNA double-strand breaks are catalyzed by Spo11, a member of a widely conserved protein family. *Cell,* 88**,** 375-384.
KIM, C., SNYDER, R. O. & WOLD, M. S. 1992. Binding properties of replication protein A from human and yeast cells. *Mol Cell Biol,* 12**,** 3050-3059.
KIM, T. & BURATOWSKI, S. 2009. Dimethylation of H3K4 by Set1 recruits the Set3 histone deacetylase complex to 5' transcribed regions. *Cell,* 137**,** 259-72.
KIRKPATRICK, D. T. 1999. Roles of the DNA mismatch repair and nucleotide excision repair proteins during meiosis. *Cell Mol Life Sci.,* 3**,** 437-449.
KLECKNER, N. 2006. Chiasma formation: chromatin/axis interplay and the role(s) of the synaptonemal complex. *Chromosoma,* 115**,** 175-94.
KLEIN, F., MAHR, P., GALOVA, M., BUONOMO, S. B. C., MICHAELIS, C., NAIRZ, K. & NASMYTH, K. 1999. A Central Role for Cohesins in Sister Chromatid Cohesion, Formation of Axial Elements, and Recombination during Yeast Meiosis. *Cell,* 98**,** 91-103.
KREJCI, L., VAN KOMEN, S., LI, Y., VILLEMAIN, J., REDDY, M. S., KLEIN, H., ELLENBERGER, T. & SUNG, P. 2003. DNA helicase Srs2 disrupts the Rad51 presynaptic filament. *Nature,* 423**,** 305-309.
KROKAN, H. E. & BJORAS, M. 2013. Base excision repair. *Cold Spring Harb Perspect Biol,* 5**,** a012583.
KUGOU, K., SASANUMA, H., MATSUMOTO, K., SHIRAHIGE, K. & OHTA, K. 2007. Mre11 mediates gene regulation in yeast spore development. *Genes Genet. Syst.,* 82**,** 21-33.
KUPER, J. & KISKER, C. 2023. At the core of nucleotide excision repair. *Curr Opin Struct Biol,* 80**,** 102605.
KUPIEC, M. 2014. Biology of telomeres: lessons from budding yeast. *FEMS Microbiol Rev,* 38**,** 144-71.
KWON, Y., SEONG, C., CHI, P., GREENE, E. C., KLEIN, H. & SUNG, P. 2008. ATP-dependent chromatin remodeling by the Saccharomyces cerevisiae homologous recombination factor Rdh54. *J Biol Chem,* 283**,** 10445-52.
LADNER, C. L., YANG, J., TURNER, R. J. & EDWARDS, R. A. 2004. Visible fluorescent detection of proteins in polyacrylamide gels without staining. *Anal Biochem,* 326**,** 13-20.
LAM, I. & KEENEY, S. 2014. Mechanism and regulation of meiotic recombination initiation. *Cold Spring Harb Perspect Biol,* 7**,** a016634.
LAO, J. P., CLOUD, V., HUANG, C. C., GRUBB, J., THACKER, D., LEE, C. Y., DRESSER, M. E., HUNTER, N. & BISHOP, D. K. 2013. Meiotic crossover control by concerted action of Rad51-Dmc1 in homolog template bias and robust homeostatic regulation. *PLoS Genet,* 9**,** e1003978.
LAUWERS, E., JACOB, C. & ANDRE, B. 2009. K63-linked ubiquitin chains as a specific signal for protein sorting into the multivesicular body pathway. *J Cell Biol,* 185**,** 493-502.
LEE, C.-S., LEE, K., LEGUBE, G. & HABER, J. E. 2013. Dynamics of yeast histone H2A and H2B phosphorylation in response to a double-strand break. *Nature Structural & Molecular Biology,* 21**,** 103-109.
LEE, J. Y., TERAKAWA, T., QI, Z., STEINFELD, J. B., REDDING, S., KWON, Y., GAINES, W. A., ZHAO, W., SUNG, P. & GREENE, E. C. 2015. DNA RECOMBINATION. Base triplet stepping by the Rad51/RecA family of recombinases. *Science,* 349**,** 977-81.
LEE, K., JI, J. H., YOON, K., CHE, J., SEOL, J. H., LEE, S. E. & SHIM, E. Y. 2019. Microhomology Selection for Microhomology Mediated End Joining in *Saccharomyces cerevisiae*. *Genes (Basel),* 10.
LEE, K. & LEE, S. E. 2007. *Saccharomyces cerevisiae* Sae2- and Tel1-dependent single-strand DNA formation at DNA break promotes microhomology-mediated end joining. *Genetics,* 176**,** 2003-14.

LEE, M. S., HIGASHIDE, M. T., CHOI, H., LI, K., HONG, S., LEE, K., SHINOHARA, A., SHINOHARA, M. & KIM, K. P. 2021. The synaptonemal complex central region modulates crossover pathways and feedback control of meiotic double-strand break formation. *Nucleic Acids Res,* 49**,** 7537-7553.
LEE, S. E., PÂQUES, F., SYLVAN, J. & HABER, J. E. 1999. Role of yeast SIR genes and mating type in directing DNA double-strand breaks to homologous and non-homologous repair paths. *Curr Biol,* 9**,** 767-770.
LEE, S. Y. & RUSSELL, P. 2013. Brc1 links replication stress response and centromere function. *Cell Cycle,* 12**,** 1665-71.
LEUTERT, M., BARENTE, A. S., FUKUDA, N. K., RODRIGUEZ-MIAS, R. A. & VILLEN, J. 2023. The regulatory landscape of the yeast phosphoproteome. *Nat Struct Mol Biol,* 30**,** 1761-1773.
LI, F., DONG, J., EICHMILLER, R., HOLLAND, C., MINCA, E., PRAKASH, R., SUNG, P., YONG SHIM, E., SURTEES, J. A. & EUN LEE, S. 2013. Role of Saw1 in Rad1/Rad10 complex assembly at recombination intermediates in budding yeast. *EMBO J,* 32**,** 461-72.
LI, J., HOOKER, G. W. & ROEDER, G. S. 2006. *Saccharomyces cerevisiae* Mer2, Mei4 and Rec114 form a complex required for meiotic double-strand break formation. *Genetics,* 173**,** 1969-81.
LISBY, M., ROTHSTEIN, R. & MORTENSEN, U. H. 2001. Rad52 forms DNA repair and recombination centers during S phase. *Proc Natl Acad Sci U S A,* 98**,** 8276-8282.
LIU, C., POULIOT, J. J. & NASH, H. A. 2004. The role of TDP1 from budding yeast in the repair of DNA damage. *DNA Repair (Amst),* 3**,** 593-601.
LIU, J., EDE, C., WRIGHT, W. D., GORE, S. K., JENKINS, S. S., FREUDENTHAL, B. D., TODD WASHINGTON, M., VEAUTE, X. & HEYER, W.-D. 2017. Srs2 promotes synthesis-dependent strand annealing by disrupting DNA polymerase δ-extending D-loops. *eLife,* 6.
LIU, J., RENAULT, L., VEAUTE, X., FABRE, F., STAHLBERG, H. & HEYER, W. D. 2011. Rad51 paralogues Rad55-Rad57 balance the antirecombinase Srs2 in Rad51 filament formation. *Nature,* 479**,** 245-8.
LIU, P., GAN, W., SU, S., HAUENSTEIN, A. V., FU, T., BRASHER, B., SCHWERDTFEGER, C., LIANG, A. C., XU, M. & WEI, W. 2018. K63-linked polyubiquitin chains bind to DNA to facilitate DNA damage repair. *Sci Signal,* 11**,** eaar8133.
LIU, S., MINE-HATTAB, J., VILLEMEUR, M., GUEROIS, R., PINHOLT, H. D., MIRNY, L. A. & TADDEI, A. 2023. In vivo tracking of functionally tagged Rad51 unveils a robust strategy of homology search. *Nat Struct Mol Biol*.
LIU, Y., SUNG, S., KIM, Y., LI, F., GWON, G., JO, A., KIM, A. K., KIM, T., SONG, O. K., LEE, S. E. & CHO, Y. 2016. ATP-dependent DNA binding, unwinding, and resection by the Mre11/Rad50 complex. *EMBO J,* 35**,** 743-58.
LYDEARD, J. R., JAIN, S., YAMAGUCHI, M. & HABER, J. E. 2007. Break-induced replication and telomerase-independent telomere maintenance require Pol32. *Nature,* 448**,** 820-3.
MA, J.-L., KIM, E. M., HABER, J. E. & LEE, S. E. 2003. Yeast Mre11 and Rad1 Proteins Define a Ku-Independent Mechanism To Repair Double-Strand Breaks Lacking Overlapping End Sequences. *Molecular and Cellular Biology,* 23**,** 8820-8828.
MACHEREY-NAGEL. 2021a. *NucleoSpin Gel and PCR Clean-up, Mini kit for gel extraction and PCR clean up* [Online]. Available: https://www.mn-net.com/nucleospin-gel-and-pcr-clean-up-mini-kit-for-gel-extraction-and-pcr-clean-up-740609.50 [Accessed].
MACHEREY-NAGEL. 2021b. *NucleoSpin Plasmid, Mini kit for plasmid DNA* [Online]. Available: https://www.mn-net.com/nucleospin-plasmid-mini-kit-for-plasmid-dna-740588.50 [Accessed].
MACREADIE, I. G., JAGADISH, M. N., AZAD, A. A. & VAUGHAN, P. R. 1989. Versatile cassettes designed for the copper inducible expression of proteins in yeast. *Plasmid*.
MADRONA, A. Y. & WILSON, D. K. 2004. The structure of Ski8p, a protein regulating mRNA degradation: Implications for WD protein structure. *Protein Sci,* 13**,** 1557-65.
MAJKA, J. & BURGERS, P. M. 2003. Yeast Rad17/Mec3/Ddc1: a sliding clamp for the DNA damage checkpoint. *Proc Natl Acad Sci U S A,* 100**,** 2249-54.

MAJKA, J., NIEDZIELA-MAJKA, A. & BURGERS, P. M. 2006. The checkpoint clamp activates Mec1 kinase during initiation of the DNA damage checkpoint. *Mol Cell,* 24**,** 891-901.
MALEKI, S., NEALE, M. J., ARORA, C., HENDERSON, K. A. & KEENEY, S. 2007. Interactions between Mei4, Rec114, and other proteins required for meiotic DSB formation in *S. cerevisiae*. *Chromosoma,* 116**,** 471-486.
MALKOVA, A., NAYLOR, M. L., YAMAGUCHI, M., IRA, G. & HABER, J. E. 2005. RAD51-dependent break-induced replication differs in kinetics and checkpoint responses from RAD51-mediated gene conversion. *Mol Cell Biol,* 25**,** 933-44.
MALONE, E. G., THOMPSON, M. D. & BYRD, A. K. 2022. Role and Regulation of Pif1 Family Helicases at the Replication Fork. *Int J Mol Sci,* 23.
MALUMBRES, M. 2014. Cyclin-dependent kinases. *Genome Biol.,* 15(6):122.
MANHART, C. M. & ALANI, E. 2016. Roles for mismatch repair family proteins in promoting meiotic crossing over. *DNA Repair (Amst),* 38**,** 84-93.
MANTIERO, D., CLERICI, M., LUCCHINI, G. & LONGHESE, M. P. 2007. Dual role for *Saccharomyces cerevisiae* Tel1 in the checkpoint response to double-strand breaks. *EMBO Rep,* 8**,** 380-7.
MARINI, V., NIKULENKOV, F., SAMADDER, P., JUUL, S., KNUDSEN, B. R. & KREJCI, L. 2023. MUS81 cleaves TOP1-derived lesions and other DNA-protein cross-links. *BMC Biol,* 21**,** 110.
MARTINI, E., DIAZ, R., HUNTER, N. & KEENEY, S. 2006. Crossover homeostasis in yeast meiosis. *Cell,* 126**,** 285-295.
MARYON, E. & CARROLL, D. 1991. Characterization of recombination intermediates from DNA injected into *X. laevis* oocytes evidence for a nonconservative HR. *Mol Cell Biol,* 11**,** 3278-3287.
MASKEY, R. S., FLATTEN, K. S., SIEBEN, C. J., PETERSON, K. L., BAKER, D. J., NAM, H. J., KIM, M. S., SMYRK, T. C., KOJIMA, Y., MACHIDA, Y., SANTIAGO, A., VAN DEURSEN, J. M., KAUFMANN, S. H. & MACHIDA, Y. J. 2017. Spartan deficiency causes accumulation of Topoisomerase 1 cleavage complexes and tumorigenesis. *Nucleic Acids Res,* 45**,** 4564-4576.
MATELLAN, L. & MONJE-CASAS, F. 2020. Regulation of Mitotic Exit by Cell Cycle Checkpoints: Lessons From *Saccharomyces cerevisiae*. *Genes (Basel),* 11.
MATHIASEN, D. P. & LISBY, M. 2014. Cell cycle regulation of homologous recombination in Saccharomyces cerevisiae. *FEMS Microbiol Rev,* 38**,** 172-84.
MAZINA, O. M., MAZIN, A. V., NAKAGAWA, T., KOLODNER, R. D. & KOWALCZYKOWSKI, S. C. 2004. *Saccharomyces cerevisiae* Mer3 helicase stimulates 3'-5' heteroduplex extension by Rad51; implications for Crossover control in meiotic recombination. *Cell,* 117**,** 47-56.
MCVEY, M. 2014. RPA puts the brakes on MMEJ. *Nat Struct Mol Biol,* 21**,** 348-9.
MEHTA, A. & HABER, J. E. 2014. Sources of DNA double-strand breaks and models of recombinational DNA repair. *Cold Spring Harb Perspect Biol,* 6**,** a016428.
MENEES, T. M., ROSS-MACDONALD, P. B. & ROEDER, G. S. 1992. MEI4, a meiosis-specific yeast gene required for chromosome synapsis. *Mol Biol Cell,* 12**,** 1340-1351.
MERKER, J. D., DOMINSKA, M. & PETES, T. D. 2003. Patterns of heteroduplex formation associated with the initiation of meiotic recombination in *S. cerevisiae*. *Genetics,* 17**,** 1377-1382.
MIMITOU, E. P. & SYMINGTON, L. S. 2010. Ku prevents Exo1 and Sgs1-dependent resection of DNA ends in the absence of a functional MRX complex or Sae2. *EMBO J,* 29**,** 3358-69.
MOCKEL, C., LAMMENS, K., SCHELE, A. & HOPFNER, K. P. 2012. ATP driven structural changes of the bacterial Mre11:Rad50 catalytic head complex. *Nucleic Acids Res,* 40**,** 914-27.
MOORE, D. M., KARLIN, J., GONZALEZ-BARRERA, S., MARDIROS, A., LISBY, M., DOUGHTY, A., GILLEY, J., ROTHSTEIN, R., FRIEDBERG, E. C. & FISCHHABER, P. L. 2009. Rad10 exhibits lesion-dependent genetic requirements for recruitment to DNA double-strand breaks in *Saccharomyces cerevisiae*. *Nucleic Acids Res,* 37**,** 6429-38.

MORIN, I., NGO, H. P., GREENALL, A., ZUBKO, M. K., MORRICE, N. & LYDALL, D. 2008. Checkpoint-dependent phosphorylation of Exo1 modulates the DNA damage response. *EMBO J,* 27**,** 2400-10.
MULLEN, J. R., NALLASETH, F. S., LAN, Y. Q., SLAGLE, C. E. & BRILL, S. J. 2005. Yeast Rmi1/Nce4 controls genome stability as a subunit of the Sgs1-Top3 complex. *Mol Cell Biol,* 25**,** 4476-87.
MULLER, H., SCOLARI, V. F., AGIER, N., PIAZZA, A., THIERRY, A., MERCY, G., DESCORPS-DECLERE, S., LAZAR-STEFANITA, L., ESPELI, O., LLORENTE, B., FISCHER, G., MOZZICONACCI, J. & KOSZUL, R. 2018. Characterizing meiotic chromosomes' structure and pairing using a designer sequence optimized for Hi-C. *Mol Syst Biol,* 14**,** e8293.
MURAKAMI, H., BORDE, V., NICOLAS, A. & KEENEY, S. 2009. Gel electrophoresis assays for analyzing DNA double-strand breaks in *Saccharomyces cerevisiae* at various spatial resolutions. *Methods Mol Biol,* 557**,** 117-142.
NAKADA, D., MATSUMOTO, K. & SUGIMOTO, K. 2003. ATM-related Tel1 associates with double-strand breaks through an Xrs2-dependent mechanism. *Genes Dev,* 17**,** 1957-62.
NEALE, M. J. & KEENEY, S. 2009. End-labeling and analysis of Spo11-oligonucleotide complexes in *Saccharomyces cerevisiae*. *Methods Mol Biol,* 557**,** 183-195.
NEALE, M. J., PAN, J. & KEENEY, S. 2005. Endonucleolytic processing of covalent protein-linked DNA double-strand breaks. Nature. . *Nature,* 436**,** 1053-1057.
NEB. 2021. *NEBaseChanger® v. 1.3.3* [Online]. Available: https://nebasechanger.neb.com/ [Accessed].
NEB. 2022. *NEBuilder® Assembly Tool v. 2.6.1* [Online]. Available: https://nebuilder.neb.com/#!/ [Accessed].
NIMONKAR, A. V., DOMBROWSKI, C. C., SIINO, J. S., STASIAK, A. Z., STASIAK, A. & KOWALCZYKOWSKI, S. C. 2012. *Saccharomyces cerevisiae* Dmc1 and Rad51 proteins preferentially function with Tid1 and Rad54 proteins, respectively, to promote DNA strand invasion during genetic recombination. *J Biol Chem,* 287**,** 28727-37.
NIMONKAR, A. V., SICA, R. A. & KOWALCZYKOWSKI, S. C. 2008. Rad52 promotes second-end DNA capture in double-stranded break repair to form complement-stabilized joint molecules. *Proc Natl Acad Sci U S A,* 106**,** 3077-3082.
NISHANT, K. T., PLYS, A. J. & ALANI, E. 2008. A mutation in the putative MLH3 endonuclease domain confers a defect in both mismatch repair and meiosis in *Saccharomyces cerevisiae*. *Genetics,* 179**,** 747-55.
NITISS, K. C., MALIK, M., HE, X., WHITE, S. W. & NITISS, J. L. 2006. Tyrosyl-DNA phosphodiesterase (Tdp1) participates in the repair of Top2-mediated DNA damage. *Proc Natl Acad Sci U S A,* 103**,** 8953-8.
NIU, H., WAN, L., BAUMGARTNER, B., SCHAEFER, D., LOIDL, J. & HOLLINGSWORTH, N. M. 2005. Partner choice during meiosis is regulated by Hop1-promoted dimerization of Mek1. *Mol Biol Cell,* 12**,** 5804-5818.
NIU, H., WAN, L., BUSYGINA, V., KWON, Y., ALLEN, J. A., LI, X., KUNZ, R. C., KUBOTA, K., WANG, B., SUNG, P., SHOKAT, K. M., GYGI, S. P. & HOLLINGSWORTH, N. M. 2009. Regulation of meiotic recombination via Mek1-mediated Rad54 phosphorylation. *Mol Cell,* 36**,** 393-404.
OH, J., AL-ZAIN, A., CANNAVO, E., CEJKA, P. & SYMINGTON, L. S. 2016. Xrs2 Dependent and Independent Functions of the Mre11-Rad50 Complex. *Mol Cell,* 64**,** 405-415.
OH, J., LEE, S. J., ROTHSTEIN, R. & SYMINGTON, L. S. 2018. Xrs2 and Tel1 Independently Contribute to MR-Mediated DNA Tethering and Replisome Stability. *Cell Rep,* 25**,** 1681-1692 e4.
OH, S. D., LAO, J. P., HWANG, P. Y., TAYLOR, A. F., SMITH, G. R. & HUNTER, N. 2007. BLM ortholog, Sgs1, prevents aberrant crossing-over by suppressing formation of multichromatid joint molecules. *Cell,* 2**,** 259-272.
OLBY, R. 1974. DNA before Watson--Crick. *Nature,* 248**,** 782-785.
PALMER, S., SCHILDKRAUT, E., LAZARIN, R., NGUYEN, J. & NICKOLOFF, J. A. 2003. Gene conversion tracts in *Saccharomyces cerevisiae* can be extremely short and highly directional. *Nucleic Acids Res,* 31**,** 1164-73.

PAN, J., SASAKI, M., KNIEWEL, R., MURAKAMI, H., BLITZBLAU, H. G., TISCHFIELD, S. E., ZHU, X., NEALE, M. J., JASIN, M., SOCCI, N. D., HOCHWAGEN, A. & KEENEY, S. 2011. A hierarchical combination of factors shapes the genome-wide topography of yeast meiotic recombination initiation. *Cell,* 144**,** 719-31.
PANNUNZIO, N. R., MANTHEY, G. M. & BAILIS, A. M. 2010. RAD59 and RAD1 cooperate in translocation formation by single-strand annealing in *Saccharomyces cerevisiae*. *Curr Genet,* 56**,** 87-100.
PÂQUES, F. & HABER, J. E. 1997. Two pathways for removal of nonhomologous DNA ends during double-strand break repair in *Saccharomyces cerevisiae*. *Mol Cell Biol,* 17**,** 6765-6771.
PAULL, T. T. & GELLERT, M. 1998. The 3' to 5' exonuclease activity of Mre11 facilitates repair of DNA double-strand breaks. *Mol Cell,* 1**,** 969-979.
PAYEN, C., KOSZUL, R., DUJON, B. & FISCHER, G. 2008. Segmental duplications arise from Pol32-dependent repair of broken forks through two alternative replication-based mechanisms. *PLoS Genet,* 4**,** e1000175.
PENKNER, A., PORTIK-DOBOS, Z., TANG, L., SCHNABEL, R., NOVATCHKOVA, M., JANTSCH, V. & LOIDL, J. 2007. A conserved function for a Caenorhabditis elegans Com1/Sae2/CtIP protein homolog in meiotic recombination. *EMBO J,* 26**,** 5071-82.
PETERS, J. M. 2006. The anaphase promoting complex/cyclosome: a machine designed to destroy. *Nat Rev Mol Cell Biol,* 7**,** 644-56.
PETUKHOVA, G., VAN KOMEN, S., VERGANO, S., KLEIN, H. & SUNG, P. 1999. Yeast Rad54 promotes Rad51-dependent homologous DNA pairing via ATP hydrolysis-driven change in DNA double helix conformation. *J Biol Chem,* 274**,** 29453-62.
PEZZA, R. J., CAMERINI-OTERO, R. D. & BIANCO, P. R. 2010. Hop2-Mnd1 condenses DNA to stimulate the synapsis phase of DNA strand exchange. *Biophys J,* 99**,** 3763-72.
PFANDER, B. & DIFFLEY, J. F. 2011. Dpb11 coordinates Mec1 kinase activation with cell cycle-regulated Rad9 recruitment. *EMBO J,* 30**,** 4897-907.
PICKART, C. M. 1997. Targeting of substrates to the 26S proteasome. *FASEB J,* 11**,** 1055-66.
PITTMAN, D., LU, W. & MALONE, R. E. 1993. Genetic and molecular analysis of REC114, an early meiotic recombination gene in yeast. *Curr Genet,* 23**,** 295-304.
PIZZUL, P., CASARI, E., GNUGNOLI, M., RINALDI, C., CORALLO, F. & LONGHESE, M. P. 2022. The DNA damage checkpoint: A tale from budding yeast. *Front Genet,* 13**,** 995163.
POMMIER, Y., SUN, Y., HUANG, S. N. & NITISS, J. L. 2016. Roles of eukaryotic topoisomerases in transcription, replication and genomic stability. *Nat Rev Mol Cell Biol,* 17**,** 703-721.
POULIOT, J. J., YAO, K. C., ROBERTSON, C. A. & NASH, H. A. 1999. Yeast gene for a Tyr-DNA phosphodiesterase that repairs topoisomerase I complexes. *Science,* 286**,** 552-5.
PRAKASH, R., SATORY, D., DRAY, E., PAPUSHA, A., SCHELLER, J., KRAMER, W., KREJCI, L., KLEIN, H., HABER, J. E., SUNG, P. & IRA, G. 2009. Yeast Mph1 helicase dissociates Rad51-made D-loops: implications for crossover control in mitotic recombination. *Genes Dev,* 23**,** 67-79.
PRASAD, T. K., ROBERTSON, R. B., VISNAPUU, M. L., CHI, P., SUNG, P. & GREENE, E. C. 2007. A DNA-translocating Snf2 molecular motor: *Saccharomyces cerevisiae* Rdh54 displays processive translocation and extrudes DNA loops. *J Mol Biol,* 369**,** 940-53.
PRIELER, S., CHEN, D., HUANG, L., MAYRHOFER, E., ZSOTER, S., VESELY, M., MBOGNING, J. & KLEIN, F. 2021. Spo11 generates gaps through concerted cuts at sites of topological stress. *Nature,* 594**,** 577-582.
PRIELER, S., PENKNER, A., BORDE, V. & KLEIN, F. 2005. The control of Spo11's interaction with meiotic recombination hotspots. *Genes Dev,* 19**,** 255-69.
PUDDU, F., GRANATA, M., DI NOLA, L., BALESTRINI, A., PIERGIOVANNI, G., LAZZARO, F., GIANNATTASIO, M., PLEVANI, P. & MUZI-FALCONI, M. 2008. Phosphorylation of the budding yeast 9-1-1 complex is required for Dpb11 function in the full activation of the UV-induced DNA damage checkpoint. *Mol Cell Biol,* 28**,** 4782-93.

PYATNITSKAYA, A., ANDREANI, J., GUEROIS, R., DE MUYT, A. & BORDE, V. 2022. The Zip4 protein directly couples meiotic crossover formation to synaptonemal complex assembly. *Genes Dev,* 36**,** 53-69.
PYATNITSKAYA, A., BORDE, V. & DE MUYT, A. 2019. Crossing and zipping: molecular duties of the ZMM proteins in meiosis. *Chromosoma,* 128**,** 181-198.
QI, Z., REDDING, S., LEE, J. Y., GIBB, B., KWON, Y., NIU, H., GAINES, W. A., SUNG, P. & GREENE, E. C. 2015. DNA sequence alignment by microhomology sampling during homologous recombination. *Cell,* 160**,** 856-869.
RAMOS, W., LIU, G., GIROUX, C. & TOMKINSON, A. 1998. Biochemical and genetic characterization of the DNA ligase encoded by *Saccharomyces cerevisiae* open reading frame YOR005c, a homolog of mammalian DNA ligase IV. *Nucleic Acids Res,* 24**,** 5676-5683.
RIBES-ZAMORA, A., MIHALEK, I., LICHTARGE, O. & BERTUCH, A. A. 2007. Distinct faces of the Ku heterodimer mediate DNA repair and telomeric functions. *Nat Struct Mol Biol,* 14**,** 301-7.
RICH, T., ALLEN, R. & WYLLIE, A. 2000. Defying death after DNA damage. *Nature,* 407**,** 777-783.
RIZVI, S. M. A., PRAJAPATI, H. K. & GHOSH, S. K. 2018. The 2 micron plasmid: a selfish genetic element with an optimized survival strategy within *Saccharomyces cerevisiae*. *Curr Genet,* 64**,** 25-42.
RIZZO, M. A. & PISTON, D. W. 2005. High-contrast imaging of fluorescent protein FRET by fluorescence polarization microscopy. *Biophys J,* 88**,** L14-6.
ROSS-MACDONALD, P. B. & ROEDER, G. S. 1994. Mutation of a meiosis-specific MutS homolog decreases crossing over but not mismatch correction. *Cell,* 79**,** 1069-1080.
ROUSOVA, D., NIVSARKAR, V., ALTMANNOVA, V., RAINA, V. B., FUNK, S. K., LIEDTKE, D., JANNING, P., MULLER, F., REICHLE, H., VADER, G. & WEIR, J. R. 2021. Novel mechanistic insights into the role of Mer2 as the keystone of meiotic DNA break formation. *Elife,* 10.
SAINI, N., RAMAKRISHNAN, S., ELANGO, R., AYYAR, S., ZHANG, Y., DEEM, A., IRA, G., HABER, J. E., LOBACHEV, K. S. & MALKOVA, A. 2013. Migrating bubble during break-induced replication drives conservative DNA synthesis. *Nature,* 502**,** 389-392.
SAKOFSKY, C. J., AYYAR, S., DEEM, A. K., CHUNG, W. H., IRA, G. & MALKOVA, A. 2015. Translesion Polymerases Drive Microhomology-Mediated Break-Induced Replication Leading to Complex Chromosomal Rearrangements. *Mol Cell,* 60**,** 860-72.
SALEM, L., WALTER, N. & MALONE, R. 1999. Suppressor analysis of the Saccharomyces cerevisiae gene REC104 reveals a genetic interaction with REC102. *Genetics,* 151**,** 1261-1272.
SAN FILIPPO, J., SUNG, P. & KLEIN, H. 2008. Mechanism of eukaryotic homologous recombination. *Annu Rev Biochem,* 77**,** 229-57.
SASANUMA, H., TAWARAMOTO, M. S., LAO, J. P., HOSAKA, H., SANDA, E., SUZUKI, M., YAMASHITA, E., HUNTER, N., SHINOHARA, M., NAKAGAWA, A. & SHINOHARA, A. 2013. A new protein complex promoting the assembly of Rad51 filaments. *Nat Commun,* 4**,** 1676.
SCHALBETTER, S. A., FUDENBERG, G., BAXTER, J., POLLARD, K. S. & NEALE, M. J. 2019. Principles of meiotic chromosome assembly revealed in *S. cerevisiae*. *Nat Commun,* 10**,** 4795.
SCHWACHA, A. & KLECKNER, N. 1995. Identification of double Holliday junctions as intermediates in meiotic recombination. *Cell,* 83**,** 783-791.
SCHWARTZ, E. K. & HEYER, W. D. 2011. Processing of joint molecule intermediates by structure-selective endonucleases during homologous recombination in eukaryotes. *Chromosoma,* 120**,** 109-27.
SEIFERT, F. U., LAMMENS, K., STOEHR, G., KESSLER, B. & HOPFNER, K. P. 2016. Structural mechanism of ATP-dependent DNA binding and DNA end bridging by eukaryotic Rad50. *EMBO J,* 35**,** 759-72.
SENGUPTA, S. & PICK, E. 2023. The Ubiquitin-like Proteins of *Saccharomyces cerevisiae*. *Biomolecules,* 13.
SEOL, J. H., HOLLAND, C., LI, X., KIM, C., LI, F., MEDINA-RIVERA, M., EICHMILLER, R., GALLARDO, I. F., FINKELSTEIN, I. J., HASTY, P., SHIM, E. Y., SURTEES, J. A. &

LEE, S. E. 2018. Distinct roles of XPF-ERCC1 and Rad1-Rad10-Saw1 in replication-coupled and uncoupled inter-strand crosslink repair. *Nat Commun,* 9**,** 2025.
SFEIR, A. & SYMINGTON, L. S. 2015. Microhomology-Mediated End Joining: A Back-up Survival Mechanism or Dedicated Pathway? *Trends in Biochemical Sciences,* 40**,** 701-714.
SHALTZ, S. & JINKS-ROBERTSON, S. 2023. Genetic control of the error-prone repair of a chromosomal double-strand break with 5' overhangs in yeast. *Genetics,* 225.
SHANER, N. C., CAMPBELL, R. E., STEINBACH, P. A., GIEPMANS, B. N., PALMER, A. E. & TSIEN, R. Y. 2004. Improved monomeric red, orange and yellow fluorescent proteins derived from Discosoma sp. red fluorescent protein. *Nat Biotechnol,* 22**,** 1567-72.
SHARPLES, G. J. & LEACH, D. R. 1995. Structural and functional similarities between the SbcCD proteins of *Escherichia coli* and the RAD50 and MRE11 (RAD32) recombination and repair proteins of yeast. *Mol Microbiol,* 17**,** 1215-1220.
SHI, I., HALLWYL, S. C., SEONG, C., MORTENSEN, U., ROTHSTEIN, R. & SUNG, P. 2009. Role of the Rad52 amino-terminal DNA binding activity in DNA strand capture in homologous recombination. *J Biol Chem,* 284**,** 33275-84.
SHINOHARA, A., SHINOHARA, M., OHTA, T., MATSUDA, S. & OGAWA, T. 1998. Rad52 forms ring structures and co-operates with RPA in single-strand DNA annealing. *Genes to Cells,* 3**,** 145-156.
SHINOHARA, M., OH, S. D., HUNTER, N. & SHINOHARA, A. 2008. Crossover assurance and crossover interference are distinctly regulated by the ZMM proteins during yeast meiosis. *Nat Genet,* 40**,** 299-309.
SHINOHARA, M., SAKAI, K., OGAWA, T. & SHINOHARA, A. 2003a. The mitotic DNA damage checkpoint proteins Rad17 and Rad24 are required for repair of double-strand breaks during meiosis in yeast. *Genetics,* 3**,** 855-865.
SHINOHARA, M., SAKAI, K., SHINOHARA, A. & BISHOP, D. K. 2003b. Crossover interference in *Saccharomyces cerevisiae* requires a TID1 and DMC1-dependent pathway. *Genetics,* 163**,** 1273-1286.
SHINOHARA, M. & SHINOHARA, A. 2013. Multiple pathways suppress non-allelic homologous recombination during meiosis in *Saccharomyces cerevisiae*. *PLoS One,* 8**,** e63144.
SIGNON, L., MALKOVA, A., NAYLOR, M. L., KLEIN, H. & HABER, J. E. 2001. Genetic requirements for RAD51- and RAD54-independent break-induced replication repair of a chromosomal double-strand break. *Mol Cell Biol,* 21**,** 2048-56.
SOLLIER, J., LIN, W., SOUSTELLE, C., SUHRE, K., NICOLAS, A., GELI, V. & DE LA ROCHE SAINT-ANDRE, C. 2004. Set1 is required for meiotic S-phase onset, double-strand break formation and middle gene expression. *EMBO J,* 23**,** 1957-67.
SOURIRAJAN, A. & LICHTEN, M. 2008. Polo-like kinase Cdc5 drives exit from pachytene during budding yeast meiosis. *Genes Dev,* 22**,** 2627-32.
SPIES, J., WAIZENEGGER, A., BARTON, O., SURDER, M., WRIGHT, W. D., HEYER, W. D. & LOBRICH, M. 2016. Nek1 Regulates Rad54 to Orchestrate Homologous Recombination and Replication Fork Stability. *Mol Cell,* 62**,** 903-917.
SUGAWARA, N., IRA, G. & HABER, J. E. 2000. DNA length dependence of the SSA pathway and the role of *S. cerevisiae* RAD59 in double-strand break repair. *Mol Biol Cell,* 20**,** 5300-5309.
SUGIYAMA, T., KANTAKE, N., WU, Y. & KOWALCZYKOWSKI, S. C. 2006. Rad52-mediated DNA annealing after Rad51-mediated DNA strand exchange promotes second ssDNA capture. *EMBO J,* 25**,** 5539-48.
SUGIYAMA, T. & KOWALCZYKOWSKI, S. C. 2002. Rad52 protein associates with replication protein A (RPA)-single-stranded DNA to accelerate Rad51-mediated displacement of RPA and presynaptic complex formation. *J Biol Chem,* 277**,** 31663-72.
SUN, X., HUANG, L., MARKOWITZ, T. E., BLITZBLAU, H. G., CHEN, D., KLEIN, F. & HOCHWAGEN, A. 2015. Transcription dynamically patterns the meiotic chromosome-axis interface. *Elife,* 4.

SUNG, P. 1997. Yeast Rad55 and Rad57 proteins form a heterodimer that functions with RPA to promote DNA strand exchange by Rad51 recombinase. *Genes Dev,* 11**,** 1111-1121.
SUNG, P. & STRATTON, S. A. 1996. Yeast Rad51 recombinase mediates polar DNA strand exchange in the absence of ATP hydrolysis. *J Biol Chem,* 271**,** 27983-6.
SYM, M., ENGEBRECHT, J. A. & ROEDER, G. S. 1993. ZIP1 is a synaptonemal complex protein required for meiotic chromosome synapsis. Cell. *Cell,* 72**,** 365-378.
SZOSTAK, J. W., ORR-WEAVER, T. L., ROTHSTEIN, R. J. & STAHL, F. W. 1983. The double-strand-break repair model for recombination. *Cell,* 33**,** 25-35.
TANG, S., WU, M. K. Y., ZHANG, R. & HUNTER, N. 2015. Pervasive and essential roles of the Top3-Rmi1 decatenase orchestrate recombination and facilitate chromosome segregation in meiosis. *Mol Cell,* 57**,** 607-621.
TAVARES, E. M., WRIGHT, W. D., HEYER, W. D., LE CAM, E. & DUPAIGNE, P. 2019. In vitro role of Rad54 in Rad51-ssDNA filament-dependent homology search and synaptic complexes formation. *Nat Commun,* 10**,** 4058.
TEO, S. H. & JACKSON, S. P. 1997. Identification of *Saccharomyces cerevisiae* DNA ligase IV, involvement in DNA double-strand break repair. *EMBO J,* 16**,** 4788-4795.
TERASAWA, M., OGAWA, T., TSUKAMOTO, Y. & OGAWA, H. 2008. Sae2p phosphorylation is crucial for cooperation with Mre11p for resection of DNA double-strand break end during meiotic recombination in *Saccharomyces cerevisiae*. *Genes Genet. Syst.,* 83**,** 209-217.
THACKER, D., LAM, I., KNOP, M. & KEENEY, S. 2011. Exploiting spore-autonomous fluorescent protein expression to quantify meiotic chromosome behaviors in Saccharomyces cerevisiae. *Genetics,* 189**,** 423-39.
THERMO-SCIENTIFIC. 2012. *General Recommendations for DNA Electrophoresis* [Online]. Available: https://assets.thermofisher.com/TFS-Assets/LSG/manuals/MAN0012614_Gen_Recommend_DNA_Electrophoresis_UG.pdf [Accessed].
TISCHFIELD, S. E. & KEENEY, S. 2012. Scale matters: the spatial correlation of yeast meiotic DNA breaks with histone H3 trimethylation is driven largely by independent colocalization at promoters. *Cell Cycle,* 11**,** 1496-503.
TOH, G. W., O'SHAUGHNESSY, A. M., JIMENO, S., DOBBIE, I. M., GRENON, M., MAFFINI, S., O'RORKE, A. & LOWNDES, N. F. 2006. Histone H2A phosphorylation and H3 methylation are required for a novel Rad9 DSB repair function following checkpoint activation. *DNA Repair (Amst),* 5**,** 693-703.
TOH, G. W., SUGAWARA, N., DONG, J., TOTH, R., LEE, S. E., HABER, J. E. & ROUSE, J. 2010. Mec1/Tel1-dependent phosphorylation of Slx4 stimulates Rad1-Rad10-dependent cleavage of non-homologous DNA tails. *DNA Repair (Amst),* 9**,** 718-26.
TRAN, P. T., ERDENIZ, N., DUDLEY, S. & LISKAY, R. M. 2002. Characterization of nuclease-dependent functions of Exo1p in *Saccharomyces cerevisiae*. *DNA Repair (Amst)***,** 895-912.
TRECO, D. & WINSTON, F. 2008. Growth and manipulation of yeast. *Curr Protoc Mol Biol.,* 82.
TRUJILLO, K. M. & SUNG, P. 2001. DNA structure-specific nuclease activities in the *Saccharomyces cerevisiae* Rad50-Mre11 complex. *J Biol Chem,* 276**,** 35458-64.
TSUBOUCHI, H. & ROEDER, G. S. 2006. Budding yeast Hed1 down-regulates the mitotic recombination machinery when meiotic recombination is impaired. *Genes Dev,* 20**,** 1766-75.
TSUKAMOTO, Y., MITSUOKA, C., TERASAWA, M., OGAWA, H. & O'GAWA, T. 2005. Xrs2- regulates Mre11p translocation to the nucleus and plays a role in telomere elongation and meiotic recombination. *Molecular Biology of the Cell,* 16**,** 597-608.
TUNG, K. S. & ROEDER, G. S. 1998. Meiotic chromosome morphology and behavior in zip1 mutants of *Saccharomyces cerevisiae*. *Proc Natl Acad Sci U S A,* 97**,** 12187-12192.
USUI, T. & SHINOHARA, A. 2021. Rad9, a 53BP1 Ortholog of Budding Yeast, Is Insensitive to Spo11-Induced Double-Strand Breaks During Meiosis. *Front Cell Dev Biol,* 9**,** 635383.
VANCE, J. R. & WILSON, T. E. 2002. Yeast Tdp1 and Rad1-Rad10 function as redundant pathways for repairing Top1 replicative damage. *Proc Natl Acad Sci U S A,* 99**,** 13669-74.

VASIANOVICH, Y., HARRINGTON, L. A. & MAKOVETS, S. 2014. Break-induced replication requires DNA damage-induced phosphorylation of Pif1 and leads to telomere lengthening. *PLoS Genet,* 10**,** e1004679.
VEAUTE, X., JEUSSET, J., SOUSTELLE, C., KOWALCZYKOWSKI, S. C., LE CAM, E. & FABRE, F. 2003. The Srs2 helicase prevents recombination by disrupting Rad51 nucleoprotein filaments. *Nature,* 423**,** 305-9.
VOELKEL-MEIMAN, K., LIDDLE, J. C., BALSBAUGH, J. L. & MACQUEEN, A. J. 2024. Proximity labeling reveals new functional relationships between meiotic recombination proteins in *S. cerevisiae*. *PLoS Genet,* 20**,** e1011432.
VRIELYNCK, N., CHAMBON, A., VEZON, D., PEREIRA, L., CHELYSHEVA, L., DE MUYT, A., MÉZARD, C., MAYER, C. & GRELON, M. 2016. A DNA topoisomerase VI-like complex initiates meiotic recombination. *Science,* 351**,** 939-943.
WALKER, J., CORPINA, R. & GOLDBERG, J. 2001. Structure of the Ku heterodimer bound to DNA and its implications for double-strand break repair. *Nature,* 412**,** 607-614.
WAN, L., NIU, H., FUTCHER, B., ZHANG, C., SHOKAT, K. M., BOULTON, S. J. & HOLLINGSWORTH, N. M. 2008. Cdc28-Clb5 (CDK-S) and Cdc7-Dbf4 (DDK) collaborate to initiate meiotic recombination in yeast. *Genes Dev,* 22**,** 386-97.
WANG, S., ZICKLER, D., KLECKNER, N. & ZHANG, L. 2015. Meiotic crossover patterns: obligatory crossover, interference and homeostasis in a single process. *Cell Cycle,* 14**,** 305-14.
WANG, X., IRA, G., TERCERO, J. A., HOLMES, A. M., DIFFLEY, J. F. X. & HABER, J. E. 2004. Role of DNA Replication Proteins in Double-Strand Break-Induced Recombination in *Saccharomyces cerevisiae*. *Molecular and Cellular Biology,* 24**,** 6891-6899.
WATSON, J. D. & CRICK, F. H. 1953. Genetical implications of the structure of deoxyribonucleic acid. *Nature,* 171**,** 964-967.
WEST, A. M., ROSENBERG, S. C., UR, S. N., LEHMER, M. K., YE, Q., HAGEMANN, G., CABALLERO, I., USON, I., MACQUEEN, A. J., HERZOG, F. & CORBETT, K. D. 2019. A conserved filamentous assembly underlies the structure of the meiotic chromosome axis. *Elife,* 8.
WILD, P., SUSPERREGUI, A., PIAZZA, I., DORIG, C., OKE, A., ARTER, M., YAMAGUCHI, M., HILDITCH, A. T., VUINA, K., CHAN, K. C., GROMOVA, T., HABER, J. E., FUNG, J. C., PICOTTI, P. & MATOS, J. 2019. Network Rewiring of Homologous Recombination Enzymes during Mitotic Proliferation and Meiosis. *Mol Cell,* 75**,** 859-874 e4.
WILLIAMS, R. S., MONCALIAN, G., WILLIAMS, J. S., YAMADA, Y., LIMBO, O., SHIN, D. S., GROOCOCK, L. M., CAHILL, D., HITOMI, C., GUENTHER, G., MOIANI, D., CARNEY, J. P., RUSSELL, P. & TAINER, J. A. 2008. Mre11 dimers coordinate DNA end bridging and nuclease processing in double-strand-break repair. *Cell,* 135**,** 97-109.
WILLIAMSON, W. D. & PINTO, I. 2012. Histones and genome integrity. *Front Biosci,* 3**,** 984-995.
WILSON, T., GRAWUNDER, U. & LIEBER, M. 1997. Yeast DNA ligase IV mediates non-homologous DNA end joining. *Nature,* 388**,** 495-498.
WU, Y., KANTAKE, N., SUGIYAMA, T. & KOWALCZYKOWSKI, S. C. 2008. Rad51 protein controls Rad52-mediated DNA annealing. *J Biol Chem,* 283**,** 14883-92.
XIN, J., XU, Z., WANG, X., TIAN, Y., ZHANG, Z. & CAI, G. 2019. Structural basis of allosteric regulation of Tel1/ATM kinase. *Cell Res,* 29**,** 655-665.
XU, L., AJIMURA, M., PADMORE, R., KLEIN, C. & N., K. 1995. NDT80, a meiosis-specific gene required for exit from pachytene in *Saccharomyces cerevisiae*. *Mol Cell Biol,* 15**,** 6572-6581.
XU, X., WANG, M., SUN, J., YU, Z., LI, G., YANG, N. & XU, R. M. 2021. Structure specific DNA recognition by the SLX1-SLX4 endonuclease complex. *Nucleic Acids Res,* 49**,** 7740-7752.
YADAV, V. K. & CLAEYS BOUUAERT, C. 2021. Mechanism and Control of Meiotic DNA Double-Strand Break Formation in *S. cerevisiae*. *Front Cell Dev Biol,* 9**,** 642737.
YAN, Z., XUE, C., KUMAR, S., CRICKARD, J. B., YU, Y., WANG, W., PHAM, N., LI, Y., NIU, H., SUNG, P., GREENE, E. C. & IRA, G. 2019. Rad52 Restrains Resection at DNA Double-Strand Break Ends in Yeast. *Mol Cell,* 76**,** 699-711 e6.

YANG, S. W., BURGIN, A. B., HUIZENGA, B. N., ROBERTSON, C. A., YAO, K. C. & NASH, H. A. 1996. A eukaryotic enzyme that can disjoin dead-end ccs between DNA and type I topoisomerases. *Proc Natl Acad Sci U S A,* 93**,** 11534-11539.
YASOKAWA, D., MURATA, S., KITAGAWA, E., IWAHASHI, Y., NAKAGAWA, R., HASHIDO, T. & IWAHASHI, H. 2008. Mechanisms of copper toxicity in *Saccharomyces cerevisiae* determined by microarray analysis. *Environ Toxicol,* 23**,** 599-606.
YOON, S. W., LEE, M. S., XAVER, M., ZHANG, L., HONG, S. G., KONG, Y. J., CHO, H. R., KLECKNER, N. & KIM, K. P. 2016. Meiotic prophase roles of Rec8 in crossover recombination and chromosome structure. *Nucleic Acids Res,* 44**,** 9296-9314.
YUN, H. & KIM, K. 2019. Ku complex suppresses recombination in the absence of MRX activity during budding yeast meiosis. *BMB Reports,* 52**,** 607-612.
ZAKHARYEVICH, K., TANG, S., MA, Y. & HUNTER, N. 2012. Delineation of joint molecule resolution pathways in meiosis identifies a crossover-specific resolvase. *Cell,* 149**,** 334-47.
ZHANG, F., KHAJAVI, M., CONNOLLY, A. M., TOWNE, C. F., BATISH, S. D. & LUPSKI, J. R. 2009. The DNA replication FoSTeS/MMBIR mechanism can generate genomic, genic and exonic complex rearrangements in humans. *Nat Genet,* 41**,** 849-53.
ZHU, Z., CHUNG, W. H., SHIM, E. Y., LEE, S. E. & IRA, G. 2008. Sgs1 helicase and two nucleases Dna2 and Exo1 resect DNA double-strand break ends. *Cell,* 134**,** 981-94.